

"Preparation and characterization of different metal complexes of amino hydroxy-9,10-anthraquinones: Computational, spectroscopic, electrochemical and biophysical studies"

**Thesis submitted for the degree of
Doctor of Philosophy (Science) of
Jadavpur University**

Under the supervision of

Prof. Saurabh Das & Dr. Partha Sarathi Guin

by

SOMENATH BANERJEE



**Department of Chemistry
Jadavpur University
Raja S. C. Mullick Road
Kolkata- 700 032
West Bengal, INDIA**

**Department of Chemistry
Shibpur Dinobundhoo Institution (College)
412/1 G.T. Road
Howrah- 711 102
West Bengal, INDIA**

2022

যাদবপুর বিশ্ববিদ্যালয়
কলকাতা-৭০০ ০৩২, ভারত



*JADAVPUR UNIVERSITY
KOLKATA-700032, INDIA

FACULTY OF SCIENCE : DEPARTMENT OF CHEMISTRY : INORGANIC CHEMISTRY SECTION

CERTIFICATE FROM THE SUPERVISOR

This is to certify that the thesis entitled “**Preparation and characterization of different metal complexes of amino hydroxy-9,10-anthraquinones: Computational, spectroscopic, electrochemical and biophysical studies**” submitted by Sri. **Somenath Banerjee** who got his name registered on **28th October, 2015** for the award of Ph.D.(Science) degree of Jadavpur University is based on his own work, performed partially under my supervision at the **Department of Chemistry, Jadavpur University, Kolkata-700032** and that neither this thesis nor any part of it was submitted for any degree or diploma or for any other academic award anywhere before.

Saurabh Das 27.12.2022
(Signature of Supervisor and date with official seal)

Dr. Saurabh Das
Professor
Department of Chemistry
Jadavpur University
Kolkata - 700 032

*Established on and from 24th December, 1955 vide Notification No. 10986-Edn/IU-42/55 dated 6th December, 1955 under Jadavpur University Act, 1955 (West Bengal Act XXXIII of 1955) followed by Jadavpur University Act, 1981 (West Bengal Act XXIV of 1981)

দুরভাষ : ২৪১৪-৬৬৬৬/৩১২৪/৬৬৪৩/৬৪৪৩ প্রদারণ : ২৪৬৯
দুরবার্তা : (৯১)-০৩৩-২৪১৪-৬৪১৪/৬২১০/২৪১৩-৭১২১

Website : www.jadavpur.edu

Phone : 2414-6666/6194/6643/6495/6443 Extn. 2469

E-mail : registrar@admin.jdvu.ac.in

Fax : (91)-033-2414-6414/6210/2413-7121

CERTIFICATE FROM THE SUPERVISOR

This to certify that the thesis entitled “**Preparation and characterization of different metal complexes of amino hydroxy-9,10-anthraquinones: Computational, spectroscopic, electrochemical and biophysical studies**” submitted by Sri. **Somenath Banerjee** who got his name registered on **28th October, 2015** for the award of Ph.D. (Science) degree of Jadavpur University is absolutely based on his own work, performed partially under my supervision at the **Department of Chemistry, Shibpur Dinobundhoo Institution (College), Howrah-711102** and that neither this thesis nor any part of it was submitted for any degree or diploma or for any other academic award anywhere before.

Partha Sarathi Guin 27/12/2022
(Signature of Supervisor and date with official seal)

Dr. Partha Sarathi Guin
Associate Professor
Department of Chemistry
Shibpur Dinobundhoo Institution (College)



JADAVPUR UNIVERSITY
KOLKATA-700 032
MARK SHEET

NO. PHCW/1701/

(For Ph.D Course Work)

Results of the	PH.D. COURSE WORK EXAMINATION, 2016
In	SCIENCE held in NOVEMBER, 2016
Name	SOMENATH RANERJEE
Examination Roll No.	PHDCHEM16233

Course Name / Subject	Credit Hr.(c)	Marks	Grade
COMPULSORY UNITS :: EX/CHEM/PHD/A & B RESEARCH METHODOLOGY & REVIEW OF RESEARCH WORK	4	79	A
ELECTIVE UNITS :: EX/CHEM/PHD/I-1 :: APPLICATION OF SPECTROSCOPIC STUDIES IN CHEMICAL RESEARCH EX/CHEM/PHD/I-2 :: MATERIALS, CATELYSES & ELECTROCHEMICAL STUDIES EX/CHEM/PHD/I-3 :: METALS IN LIFE & REACTION DYNAMICS EX/CHEM/PHD/O-4 :: BIO-ORGANIC CHEMISTRY	4	72	B

Total Marks : 151 (out of 200)

SGPA: 9.50

Remarks: P

Prepared by :

Checked by :

Date of issue : 07-02-2017

Controller of Examinations

Declaration

I do, hereby declare, that the work embodied in the thesis entitled “**Preparation and characterization of different metal complexes of amino hydroxy-9,10-anthraquinones: Computational, spectroscopic, electrochemical and biophysical studies**” submitted for the award of Doctor of Philosophy (Ph. D.) in Science, is the completion of studies carried out by me under the supervision of Dr. Saurabh Das at the Department of Chemistry, Jadavpur University and Dr. Partha Sarathi Guin at the Department of Chemistry, Shibpur Dinobundhu Institution (College), Shibpur, Howrah. The work is original and has not been submitted in part or full for any equivalent degree/diploma or any other academic award elsewhere.

In keeping with the general practice of reporting scientific observations, due acknowledgements have been made wherever the work described was done taking active assistance of a laboratory that has an expertise in that particular field of investigation.

Somenath Banerjee
27/12/2022
Somenath Banerjee
Research Scholar

Department of Chemistry
Inorganic Chemistry Section
Jadavpur University
Raja S. C. Mullick Road
Kolkata- 700032
West Bengal, INDIA

Department of Chemistry
Shibpur Dinobundhoo Institution (College)
412/1 G.T. Road
Howrah- 711102
West Bengal, INDIA

श्रद्धावान् लभते ज्ञानं तत्परः संयतेन्द्रियः ।
ज्ञानं लब्ध्वा परां शान्तिमचिरेणाधिगच्छति ॥

Dedicated
to
my parents, my teachers
and
the Indian Army

**गुरु ब्रम्हा गुरु विष्णु गुरुः देवो महेश्वरा
गुरु शाक्षात परब्रम्हा तस्मै श्री गुरुवे नमः**

Acknowledgement

The past seven years have become one of the most important and memorable chapters in my life. By that time, there are so many people those deserve my heartfelt gratitude. At the outset, I am happy to utilize the opportunity to express my deep sense of gratitude and regards to my supervisors, Prof. Saurabh Das and Dr. Partha Sarathi Guin for their constant guidance, advice and valuable suggestions. Above all and the most needed, they provided me unflinching encouragement and support in various ways. Their intuition on several issues has provided me a constant oasis of ideas and a passion for science, which exceptionally inspired and enriched my desires in research. Their training, guidance and suggestions made this work possible. I am indebted to them for what I have learnt from them particularly with respect to various techniques of data analysis that formed an important part of the work.

I am grateful to Prof. Subenoy Chakraborty, Dean, Faculty of Science, Jadavpur University for an opportunity to use all facilities available at the science faculty.

I express my sincere gratitude to Prof. Swapan Kumar Bhattacharya, Head, Department of Chemistry and Prof. Saurabh Das, Section-in-Charge, Inorganic Chemistry Section, Jadavpur University for their keen interest and constant encouragement.

I am grateful to Ashis Kumar Das, Dr. Arup Datta, Dr. Arpita Biswas, Dr. Srimanta Kundu of the Department of Chemistry, Shibpur Dinobundhoo Institution (College) for their support in completing my research and for giving me the opportunity to use all departmental facilities.

I am thankful to Dr. Sanjay Roy, Head & Associate Professor, Department of Chemistry, Netaji Subhas Open University, Kolkata for academic and experimental help and encouragement.

I am thankful to Prof. Suman Das, Prof. Shouvik Chattopadhyay, Dr. Saubhik Halder and Prof. Kausikisankar Pramanik for their help and encouragement. Assistance from Mr. Raju Biswas for recording NMR spectra is acknowledged.

I am thankful to Prof. Debasis Das of the Department of Chemistry, University of Burdwan, Dr. Chandan Adhikary, Department of Education, University of Burdwan for help received in different forms.

I am thankful to Dr. Subhas Chandra Bhat, Assistant Professor in Chemistry (WBES), Govt. College of Education, Banipur, North 24 Paraganas, Dr. Anup Kumar Sikdar, Emeritus Professor of Biotechnology & Academic Advisor, The Bhowbanipur Education Society College, Kolkata, Dr. Arnab Halder, Department of Chemistry, Presidency University, Kolkata, Dr. Sarat Chandra Patra, State Aided College Teacher of Department of Chemistry, Muralidhar Girl's College for valuable suggestions and continuous motivation.

I am thankful to ex-H.M. Sri Shovan Kumar Bera and ex-A.T. Sk. Abbas Ali (Chemistry Teacher) of Howrah Vivekananda Institution from where I completed my schooling. I am very grateful to ex-H.M. of Shibpur Dinobundhoo Institution (Branch) Dr. Arun Kumar Maity for his continuous encouragement from the beginning of my research career.

I am grateful to Sri Bikash Kumar Bag, ex-H.M., Banharishpur High Madrasah attached Primary School and Smt. Pampa Mukherjee, H.M. Sri Ramkrishana Sikhalaya who gave me the opportunity to persuade my research career while in service at the above mentioned places.

I would like to thank Dr. Palash Mondal, Assistant Professor, Department of Chemistry, Vivekananda Mahavidyalaya, Burdwan, West Bengal for collaborative support on theoretical and computational studies.

I am grateful to Prof. Asoke Prasun Chattopadhyay, Department of Chemistry, University of Kalyani, for his valuable suggestions and continuous inspiration.

I am thankful to Prof. Dhanasekaran Dharumadurai, Department of Microbiology, (School of Life Sciences, Bharathidasan University, Tiruchirappalli, Tamil Nadu) and his scholars for collaborative studies in various experimental aspects of biology.

I am grateful to lab mates Dr. Ramesh Chandra Santra, Dr. Durba Ganguly, Dr. Mouli Saha, Ms. Promita Nandy, Mr. Tanmoy Saha and friends in days of research, Dr. Saikat Gayen,

Mr. Sagnik Jana, Ms. Pameli Ghosh, Mr. Rakesh Debnath, Mr. Monotosh Bhattacharjee of Jadavpur University and Sk. Imran of the Department of Chemistry, Shibpur Dinobundhoo Institution (College) for their ungrudging suggestions, cooperation and help.

Besides, I have been gifted with some good friends like Rajdip, Subhrakanti, Priyabrata, Tamal, Dilip, Sujoy, Alope, Subhojit, Nintyananda, Abhijit, Suvra, Krishnendu, Arko, S. Chandra for their support during my research period.

Word is not enough to express the influence of my parents. It is the time; I want to share my happiness with my parents. Since childhood days, my parents have done lots of sacrifice for me. Words cannot express my gratitude to my father Late Sri Lokenath Banerjee, whose ambition, strength and passion for excellence inspired me always in every moment of my life. I want to express my heartiest feelings for my mother, Smt. Pampa Banerjee who has continuously supported me during this journey. She has devoted her total life to make me a proper human being. I would like to acknowledge my wife who constantly inspired me towards completing this very important milestone in life.

Somenath Banerjee
27/11/2022
Somenath Banerjee

*Department of Chemistry
Inorganic Chemistry Section
Jadavpur University
Raja S. C. Mullick Road
Kolkata- 700032
West Bengal, India,*

*Department of Chemistry
Shibpur Dinobundhoo Institution(College)
412/1 G.T. Road
Howrah- 711102
West Bengal, India,*

List of Abbreviations used

ACN	:	Acetonitrile
AdSWV	:	Adsorptive Square-Wave Voltammetry
AQ	:	2-Amino-3-hydroxy-9,10-anthraquinone
AO/EB	:	Acridine orange /Ethidium bromide
AR	:	Analytical Research
AQSH	:	Sodium 3-amino-2-hydroxy-9,10-anthraquinone-1-sulphonate
CC	:	Coupled-Cluster
CD	:	Circular Dichroism
CI	:	Configuration Interaction
CMC	:	Critical Micelle Concentration
CoQ10	:	Coenzyme Q10
COSY	:	<i>Correlated Spectroscopy</i>
CPE	:	Carbon paste electrode
CTAB	:	Cetyltrimethylammonium bromide
DFT	:	Density Functional Theory
DMEM	:	Dulbecco's Modified Eagle Medium
DMF	:	Dimethyl formamide
DMSO	:	Dimethyl sulfoxide
DNA	:	Deoxyribonucleic acid
DOX	:	Doxorubicin
DTAB	:	Dodecyltrimethylammonium bromide
ECE	:	Electron transfer-Chemical reaction-Electron transfer
EPR	:	Electron paramagnetic Resonance
ESMS	:	Electrospray mass spectrometry
EXSY	:	Exchange Spectroscopy
FMO	:	Frontier Molecular Orbital Theory
FTIR	:	Fourier Transform Infrared
GC	:	Glassy Carbon
HDME	:	Hanging drop mercury electrode

HF	:	Hartree-Fock
Hg(Ag)FE	:	Silver-amalgam film electrode
HOMO	:	Highest Occupied Molecular Orbital
Ln	:	Lanthanides
LSV	:	Linear Sweep Voltammetry
LUMO	:	Lowest Un-occupied Molecular Orbital
MBPT	:	Many-body perturbation theory
MDR	:	Multidrug-resistance
MOs	:	Molecular orbitals
NADPH	:	Reduced nicotinamide adenine dinucleotide phosphate
NMR	:	Nuclear Magnetic Resonance
PBE	:	Perdue Burke Ernzerhof
PED	:	Potential Energy Distribution
PXRD	:	Powder X-ray Diffraction
QH	:	1-amino-4-hydroxy-9,10-anthraquinone
RNA	:	Ribonucleic acid
ROS	:	Reactive Oxygen Species
SCE	:	Saturated calomel Electrode
SDS	:	Sodium Dodecyl Sulfate
SWV	:	Square-Wave Voltammetry
TBAB	:	Tetrabutyl ammonium bromide
TDDFT	:	Time-dependent DFT
TOCSY	:	<i>Total Correlation Spectroscopy</i>
UV-VIS	:	Ultraviolet–Visible
VEDA	:	Vibrational Energy Distribution Analysis

CONTENTS

	Pages
Abstract	
1. Introduction	1-6
2. Studies on Anthracyclines and their analogues	7-62
2.1. Anthracyclines and their analogues as anticancer agents	7
2.2. Metal complexes of anthracyclines and their analogues	14
2.3. Electrochemical behavior of anthracyclines and their analogues	23
2.4. Theoretical studies on anthracyclines and anthraquinones	34
2.5 Interaction of anthracyclines and anthraquinones with surfactant micelles	35
References	42
3. Genesis and scope of the Research	63-70
4. Experimental	71-84
4.1. Introduction	71
4.2. Materials	72
4.3. Methods	73
4.3.1. Instruments	73
4.3.2. Preparation and characterization of sodium 3-amino-2-hydroxyanthraquinone-1-sulphonate (AQSH)	74
4.3.3. Synthesis of Cu^{II} complex of sodium 3-amino-2-hydroxy-9,10-anthraquinone-1-sulphonate $[\text{Cu}(\text{AQS})_2]$	75
4.3.4. Synthesis of Ni^{II} complex of sodium 3-amino-2-hydroxy-9,10-anthraquinone-1-sulphonate $[\text{Ni}(\text{AQS})\text{Cl}_2(\text{H}_2\text{O})_2]$	75
4.3.5. Synthesis of Co^{III} complex of 1-amino-4-hydroxy-9,10-anthraquinone (CoQ_3)	76
4.3.6: Preparation of solutions of complexes of $\text{Cu}^{\text{II}}-(\text{AQS})_2$, $\text{Ni}^{\text{II}}-(\text{AQS})\text{Cl}_2 \cdot 2\text{H}_2\text{O}$, CoQ_3 and surfactants	76
4.3.7: Computational studies	78

4.3.8: Spectroscopic studies	78
4.3.9: Electrochemical studies	79
4.3.10: Studies on the interaction of compounds with surfactant micelles	80
4.3.11. Determination of critical micelle concentration	80
4.3.12. Cell Culture	81
4.3.13. Cell Viability Assay	81
4.3.14. Acridine orange and ethidium bromide (AO/EB) staining	82
4.3.15. Hoechst 33528 staining	82
4.3.16. Mitochondrial membrane potential assessment by JC1 staining	83
References	83
5. Solubilization of sodium 3-amino-2-hydroxyanthraquinone-1-sulphonate in SDS micelles explains its permeation in A549 human lung cancer cell.	85-106
6. Formation and characterization of a Cu^{II} complex of sodium 2-amino-3-hydroxy-9,10-anthraquinone-1-sulphonate and studies on its electrochemical behavior, interaction with SDS micelles and nucleation in A549 human lung cancer cells.	107-128
7. Studies on synthesis and characterization of a Ni^{II} complex of sodium 2-amino-3-hydroxy-9,10-anthraquinone-1-sulphonate, its electrochemical behavior and interaction with SDS micelles and A549 human lung cancer cells.	129-149
8. A Co^{III} Complex of 1-Amino-4-hydroxy-9,10-anthraquinone Exhibits Apoptotic Action against MCF-7 Human Breast Cancer Cells.	150-172
9. Summary and Conclusion	173-176

Appendices

Abstract

Title

Preparation and characterization of different metal complexes of amino hydroxy-9,10-anthraquinones: Computational, spectroscopic, electrochemical and biophysical studies

Submitted by
Somenath Banerjee
27/11/2022
Somenath Banerjee

Anthracyclines and their analogues, that includes metal-complexes exhibit extra-ordinary role as chemotherapeutic agents in the treatment of various forms of human cancers. The presence of a planar anthraquinone ring with a sugar residue was identified to play a significant role in healing ovarian, bladder, Hodgkin's and non-Hodgkin's lymphomas, Wilms's tumour and neuroblastoma. Although anticancer features and drug functioning mechanism of such anthracyclines and their derivatives including those of metal complexes are well investigated, some ambiguity exists owing to high price and severe cardio-toxic features with an unexpected multi-drug resistance (MDR) that restrict frequent use by oncologists. To overcome such limitations, various attempts have been made by several research groups to arrive at suitable alternatives of anthracyclines, particularly those that have low cardiotoxicity and other side effects either through structural modification or synthesis of metal-anthracyclines complexes.

In the present study, sodium 3-amino-2-hydroxy-9,10-anthraquinone-1-sulphonate (AQSH) was initially prepared and characterized. Its Cu^{II} and Ni^{II} complexes and a Co^{III} complex of 1-amino-4-hydroxy-9,10-anthraquinone were prepared. These were characterized by elemental analysis, UV-Vis spectroscopy, fluorescence spectroscopy, FTIR spectroscopy, mass spectrometry, PXRD and theoretical studies, with the help of which their binding to metal ions were identified and compared with that reported for standard anthracyclines.

Cu^{II} forms 1:2 and Ni^{II} forms 1:1 metal-ligand complexes with 3-amino-2-hydroxy-9,10-anthraquinone-1-sulphonate while Co^{III} forms a ternary (1:3) complex with 1-amino-4-hydroxy-9,10-anthraquinone.

In the current study, different methods were employed to obtain single crystals of metal complexes taking different compositions of solvents. However, all efforts to obtain an appropriate single crystal failed; the planarity of the anthraquinone unit in these complexes could possibly be a hindrance in procuring single crystals. For this reason, an effort was made to characterize the 1:3 Co^{III} complex of 1-amino-4-hydroxy-9,10-anthraquinone theoretically using density functional theory (DFT) based on experimental evidence obtained like elemental analysis, IR spectroscopy, mass spectrometry, powder X-ray diffraction, molecular spectroscopy and electrochemistry. DFT helped to generate energy optimized structures. Various essential parameters of the complex were obtained from such theoretical studies.

Electrochemical studies on the chosen analogues and their metal complexes in aqueous and organic solvents having different polarity were performed using cyclic voltammetry. Several electrochemical parameters were evaluated to find out the actual mechanism of electrochemical reduction. These were then compared with those of the different standard drugs. This is crucial for determining the biochemical and biophysical action of chosen molecules. Electrochemical behavior indicates that experimental compounds mimic action of standard anthracycline drugs. To see whether such molecules permeate biological membranes, studies on interaction with surfactant micelles were performed. Mode of interaction whether it is hydrophilic or hydrophobic, were evaluated. The study suggests that chosen analogues and their corresponding metal complexes might easily penetrate cell membranes in an encapsulated form without any form of degradation. Partition coefficients, binding constants and other thermodynamic parameters were evaluated that confirmed that such drug-micelle interactions were thermodynamically favorable with adequate negative value of the Gibb's free energy, under the experimental conditions.

Finally, the chosen amino-anthraquinone ligands and their prepared complexes were tested on different human cancer cell lines to see whether they initiate apoptosis. IC_{50} of different compounds chosen for experiments were estimated by employing a cell viability assay. Apoptosis was characterized by cellular morphological changes observed during the process of cell death which was analyzed by the dual staining method of acridine orange (AO) and ethidium bromide (EB). Results of this study show that chosen molecules may be considered as less costly alternatives of anthracyclines that are already in use.

Saurabh Das 27.12, 2022

Dr. Saurabh Das
Professor
Department of Chemistry
Jadavpur University
Kolkata - 700 032

Partha Sarathi Guin 27/12/2022

Dr. Partha Sarathi Guin
Associate Professor
Department of Chemistry
Shibpur Dinobundhoo Institution

CHAPTER 1

Introduction

Introduction

Earth is a unique planet in our solar system because conditions that are favorable to support life are found here. The biosphere in which we live has oxygen, nitrogen, carbon dioxide, argon and water vapor in a balanced ratio that ensures a healthy life. However, with the advancement of civilization we are creating several forms of trouble in the environment either with or without a proper knowledge about it. The air, the land and the water are getting polluted increasingly creating several hazards to environment and to our health. The environment is constantly being polluted as a result of various forms of pollution due to poisonous gases and particulate matter, accumulation of toxic wastes, food additives and contaminants. Water and air pollution due to automobile exhaust emissions and other combustion products is another area of concern in an increasingly expanding population. Application of insecticides and pesticides in agriculture and use of different chemical compounds at each stage of our lives also increase risks that we face from the environment. Industrial wastes containing different species of arsenic, antimony, chromium, cadmium, lead etc. and various forms of organic matter are responsible for different types of cancer [1-3]. The increasing use of nitrates in agriculture and in food is also considered a reason for cancer [4-6]. Other reactive nitrogen and oxygen species cause what is known as oxidative stress-induced cancers [7]. Enormous use of chlorofluorocarbons cause depletion of the ozone layer thereby increasing the penetration of UV-radiation at the ground level. Increasing doses of UV-B ray causes skin cancer, cataract of the eyes, damage to immune system in animals and in humans having an adverse impact on the growth of plants making cancer the most furious threat to mankind. It is therefore a great challenge to prevent and combat cancer.

For the last few decades, a lot of efforts has been on to augment our knowledge on various aspects of cancer through studies on its initiation, its propagation and a possible mechanism leading to rapid growth of cells, the possible approaches to check proliferation by different modes of action using either drugs or radiation or a combination of both. Although considerable progress has been made in this area, however a lot remains to be achieved. Till date the most important approach in treating cancer is chemotherapy and radiotherapy in conjunction with surgery. A relatively new technique like photodynamic therapy experienced a huge upsurge in research activity over the last two decades. However, most of such approaches excepting surgery have several serious side effects. It has been observed that most often an affected patient dies not of the disease but more because of various forms of side effects during treatment. This is very alarming and there is a growing need to think of new ways of treating cancer that takes care of the aspect of side effects during treatment.

Anthracycline drugs like adriamycin (doxorubicin), daunorubicin, carminomycin, aclacinomycin, nogalamycin, etc., are some of the important chemotherapeutic agents used to treat of various forms of human cancers [8]. Long term cardiac damage is a major adverse side effect of these drugs that limits effectiveness of these drugs [9]. Experimental evidence indicates *in vivo* formation of semiquinone free radical intermediate by one-electron reduction of the quinone moiety present in these drugs being a requirement both for chemotherapeutic efficiency as well as toxicity. Both therapeutic efficiency and toxicity are seen to be associated with redox properties and electrochemical parameters play an important role in determining structure-activity relationship of such molecules. Upon complex formation with certain metal ions the 9,10-anthraquinone moiety of anthracyclines is modified and this considerably decreases any form of toxicity of such drugs. A number of metal complexes of anthracyclines were tried for

treatment of cancer. Use of such metal complexes explored a growing body of interest on the role of metal ions in these compounds [10-12].

Deciphering structure–activity relationship may lead to introduction of new medicines for a good number of diseases. Thus attempts have been made through earlier studies [13-15] so as to lead to a proper understanding regarding structure–selectivity relationship of anthracyclines that lead to bringing up a novel chemotherapeutic agent for treatment of cancer. Computational and spectroscopic measurements were performed to understand the electronic state of the molecules [16-19].

Though several mechanisms of drug action due to these molecules were been proposed, the intercalation of such molecules into the DNA backbone has been established as the dominating mode of their drug action [20, 21, 22]. In addition, mechanism of drug action is related to the interaction of a drug molecule with biological tissues by means of its binding to membranes at the molecular level [23–25]. Micellar systems possess the ability to solubilize hydrophobic drugs [26-28] thereby increasing bioavailability and thus it can be used as a model system for bio-membranes, as well as drug carriers in numerous drug delivery and drug targeting systems [29–31]. The physicochemical interactions of drugs with surfactant micelles can be visualized as an approximation for their interactions with biological membranes. This provides an insight into more complex biological processes like the passage of drugs through cell membranes.

Studies on anthracyclines and their analogues carried out in the last few decades are briefly reviewed in *Chapter 2*. Aspects of anthracyclines and their analogues as anticancer agents have been reviewed in *Section 2.1 (Chapter- 2)*. *Section 2.2 (Chapter-2)* deals with a review on complex formation of anthracyclines and their analogues with metal ions. In *Section 2.3*,

electrochemical behavior of such molecules and some other quinones in different solvents are described. *Section 2.4* deals with aspects of theoretical studies that are reviewed in brief. *Section 2.5* describes interaction of molecules with surfactant micelles.

References

1. F. F. Álvarez, M. T. Rodríguez, A. J. F. Espinosa, A. Gutiérrez Dabán, *Anal. Chim. Acta* 524 (2004) 33-40.
2. A. Levina, P. A. Lay, N. E. Dixon, *Chem. Res. Toxicol.* 14 (8) (2001) 946-950.
3. B.-C. Han, W.-L. Jeng, T.-C. Hung, Y.-C. Ling, M.-J. Shieh, L.-C. Chien, *Environ. Pollut.* 109 (2000) 147-156.
4. F. P. de Andrade Jr., A. L. S. de Cabral, J. M. D. de Araújo, L. V. Cordeiro, M. de B. Cândido, A. P. da Silva, B. T. de M. Lima, B. B. Dantas, *Rev. Colomb. Cienc.Quím.Farm.* 50(1) (2021) 269-291.
5. M. H. Ward, *Rev. Environ. Health.* 24 (4) (2009) 357-363.
6. E. Chazelas, F. Pierre, N. Druesne-Pecollo, Y. Esseddik, F. S. de Edelenyi, C. Agaesse, A. De Sa, R. Lutchia, S. Gigandet, B. Srour, C. Debras, I. Huybrechts, C. Julia, E. Kesse-Guyot, B. Alle`s, P. Galan, S. Hercberg, M. Deschasaux-Tanguy, M. Touvier, *Int. J.Epidemiol.* 51 (4) (2022) 1106-1119.
7. M. Valko, C. J. Rhodes, J. Moncol, M. Izakovic, M. Mazur, *Chem. Biol. Interact.* 160 (1) (2006) 1-40.
8. J. G. Hardman, A. G. Gilman, L. E. Limbird, Goodman and Gilman's *The Pharmacological Basis of Therapeutics*, 9thedn., McGraw-Hill Companies, 1996.
9. P. K. Singal, N. Iliskovic, *N. Engl. J. Med.* 339 (13) (1998) 900-905.
10. M. M. L. Fiallo, A. Garnier-Suillerot, B. Matzanke, H. Kozlowski, *J. Inorg. Biochem.* 75 (2) (1999) 105-115.
11. N. Nikolis, C. Methenitis, G. Pneumatikakis, *J. Inorg. Biochem.* 95 (2003) 177-193.

12. C. Menidiatis, C. Methenitis, N. Nikolis, G. Pneumatikakis, J. Inorg. Biochem. 98 (11) (2004) 1795-1805.
13. M. B. Martins-Teixeira, I. Carvalho, ChemMedChem. 15 (11) (2020) 933-948.
14. P. Taneja, P. Labhasetwar, P. Nagarnaik, J. H. J. Ensink, J. Water Health. 15 (4) (2017) 602–614
15. J. Marinello, M. Delcuratolo, G. Capranico, Int. J. Mol. Sci. 19(11) (2018) 3480.
16. P. Mondal, S. Roy, G. Loganathan, B. Mandal, D. Dharumadurai, Md. A. Akbarsha, P. S. Sengupta, S. Chattopadhyay, P. S. Guin, Biochem. Biophys. Rep.4 (2015) 312–323.
17. A. Das, S. Roy, P. Mondal, A. Datta, K. Mahali, G. Loganathan, D. Dharumadurai, P. S. Sengupta, Md. A. Akbarsha, P. S. Guin, RSC Adv.6 (2016) 28200–28212.
18. S. Roy, P. Mondal, P. S. Sengupta, D. Dhak, R. C. Santra, S. Das, P. S. Guin, Dalton Trans. 44 (2015) 5428-5440.
19. S. Roy, P. S. Sengupta, P. S. Guin, Chem. Phys. Lett. 694 (2018) 7–13.
20. J. Nadas, D. Sun, Exp. Opin. Drug Discov.1 (6) (2006) 549-568.
21. M. Binaschi, M. Bigioni, A. Cipollone, C. Rossi, C. Goso, C. A. Maggi, G. Capranico, F. Animati, Curr. Med. Chem. 1 (2) (2001) 113-130.
22. G. Minotti, P. Menna, E. Salvatorelli, G. Cario, L. Giani, Pharmacol. Rev.56 (2) (2004) 185-229.
23. G. P. Van Balen, C. M. Martinet, G. Caron, G. Bouchard, M. Reist, P. A. Carrupt, R. Fruttero, A. Gasco, B. Testa, Med. Res. Rev. 24 (2004) 299-324.
24. R. Pignatello, T. Musumeci, L. Basile, C. Carbone, G. Puglisi, J. Pharm. Bio Allied Sci. 3 (1) (2011) 4-14.
25. A. M. Seddon, D. Casey, R.V. Law, A. Gee, R. H. Templer, O. Ces, Chem. Soc. Rev. 38 (9) (2009) 2509-2519.
26. J. Xi, R. Guo, J. Pharm. Biomed. Anal. 43 (1) (2007) 111-118.
27. N. Erdinc, S. Gokturk, M. Tuncay, J. Pharm. Sci. 93 (2004) 1566-1575.
28. W. Sun, C. K. Larive, M. Z. Southard, J. Pharm. Sci. 92 (2003) 424-435.

29. M. E. Dalmora, S. L. Dalmora, A. G. Oliveira, *Int. J. Pharm.* 222 (2001) 45-55.

30. M. C. Jones, J. C. Leroux, *Eur. J. Pharm. Biopharm.* 48 (2) (1999) 101-111.

31. C. O. Rangel-Yagui, H.W. L. Hsu, A. I. Pessoa Jr, L. C. Tavares, *Braz. J. Pharm. Sci.* 41(2005) 237-246.

CHAPTER 2

Studies on anthracyclines and their analogues

Anthracyclines form a broad category of anticancer drugs. Following decades of their discovery, biological features of such molecules were investigated by several workers to recognize mechanism of drug action. In spite of their growing consciousness in the field of oncology, mechanism of drug action is not clearly recognized as yet. Since anthracycline drugs are expensive and also have several adverse effects including multidrug-resistance (MDR), a number of attempts were made to find suitable alternatives to overcome several limitations. Similar chemical and biological features are exhibited by simple and inexpensive hydroxy-9,10-anthraquinones, para-quinones and their analogues. The current chapter is dedicated to compounds having structures similar to anthracyclines for whom mechanism of action on biological targets are similar. The main purpose of this chapter is to provide a concise review on anticancer activity of anthracyclines and analogous compounds including metal complexes, their electrochemical behaviour in different solvents, interaction with different surfactant molecules to understand membrane permeability and interaction with cancer cells.

2.1. Anthracyclines and their analogues as anticancer agents

Nowadays cancer is one of the major diseases responsible for death globally and is characterized by uncontrolled and unlimited growth of cells accompanied with unusual cell transformation resulting untamed proliferation and circumvention from normal cell growth. Although anthracyclines were discovered in the last century, its systematic isolation and separation was made in 1950s with identification of daunorubicin, that was well documented in the early 1960s for its successful performance against acute leukemias and lymphomas [1]. Daunorubicin was cultivated from *Streptomyces peucetius* [2] and later in the same decade another more efficient anticancer agent, a derivative of daunorubicin, 14-hydroxydaunomycin or

adriamycin [doxorubicin (DOX)] was isolated from cultivation of *Streptomyces coeruleorubidus*, a modified strain of the original mould. These anticancer agents showed extraordinary antineoplastic activity than their predecessors [3, 4] against different types of cancer [5, 6]. Later a good number of anthracyclines were introduced that were found to be extremely promising as anticancer agents. Epirubicin is highly effective in treating stomach, breast and urinary tract carcinomas [7], daunorubicin is a dependable agent in treating acute leukemia, idarubicin shows its effectiveness in dealing myelogenous leukemia [8] and valrubicin shows its efficacy in treating bladder cancer [9]. Mitoxantrone, an amino-hydroxy-9,10-anthraquinone, a simple analogue of anthracycline drugs has been used effectively in treating prostate or breast cancer, non-Hodgkin's lymphoma and acute myeloid leukemia [10]. Introduction of anthracyclines as anticancer drugs has reduced pre-mature death due to various types of human cancer and therefore created a revolution in the area of contemporary oncology. However, in spite of various applications, their use as anticancer drugs are restricted to some extent due to high cost, strong cardiotoxic nature [11,12], multidrug-resistance [13,14] and other related side effects. Thus efforts are being made worldwide to overcome such issues. Recently anthracyclines are being introduced in human physiology in combined form of two or more drugs instead of a single one which reduce toxicities significantly [6, 15] resulting in better therapeutic efficacy [16-20].

Introduction of anthracycline anticancer drugs led to a breakthrough in the history of oncology. However, exact mechanism of drug action and toxicities yet remain debated. Previous studies show that mode of drug action is a combination of a group of mechanisms like oxidative stress, binding to cellular DNA through intercalation and interaction with Topoisomerase II [21, 22]. Topoisomerase II causes a change in the topology of DNA without any change in the

structure or sequence of DNA. Topoisomerase I and Topoisomerase II play important roles during replication of DNA. The planar anthraquinone unit of anthracyclines intercalate between DNA base pairs through hydrophobic and π - π stacking interactions in which the long axis of the anthraquinone becomes almost perpendicular to the axis of DNA double helix. It has been found that amino sugar residues remain as the non-intercalating portion of the anthracycline and that it helps to stabilize the anthracycline-DNA-Topoisomerase II ternary complex through interacting with negatively charged phosphate groups in the DNA major groove [23, 24]. Along with this H-bonding between adjacent base pairs of DNA and drug molecule plays a vital role in drug-DNA interaction stabilizing the adduct [25,26]. In case of daunomycin drug-DNA adduct gets additional stability due to greater electrostatic force caused by the presence of the uni-positive charge on daunomycin. Adriamycin and daunomycin were found to form aggregation with chromosomal DNA exclusively within the cellular nuclei [27, 28]. Intercalation of a drug molecule into DNA results in distortion in the DNA double helix thereby hampering replication and transcription of DNA and RNA respectively [25, 29, 30]. However, drug-DNA interaction is insufficient to justify the actual mechanism of drug action.

DNA and protein (mainly Histone) combine to form chromatin [31] in the nucleus. Chromatin undergoes unfolding and conglomeration upon interaction with anthracyclines thereby leading to structural and functional changes of chromatin [32, 33]. A number of metabolic processes of cellular DNA like DNA replication and transcription were severely interrupted by structural deformation of chromatin due to such antitumor drugs in living cells [32, 33].

Though aspects of cardiotoxicity caused by anthracycline drugs are complicated two theories like formation of Reactive Oxygen Species (ROS) and mitochondrial damages are

mainly considered to explain this. Formation of Reactive Oxygen Species (ROS) in cardiomyocytes is an accepted theory [34, 35, 36] where ROS are predominantly generated in presence of various cellular oxidoreductases [37] through different redox cycles catalyzed by anthracyclines. In the presence of the reduced form of nicotinamide adenine dinucleotide phosphate (NADPH), anthracycline reacts with cytochrome reductase producing semiquinone free-radical that undergoes many redox reactions, finally generating superoxide ($O_2^{\cdot-}$), hydroxyl radical (OH^{\cdot}) and hydrogen peroxide (H_2O_2) [38, 39]. Such radicals are dangerous to human physiology and damage DNA, brings about peroxidation of lipid of the cell membrane [40-43] and oxidation of nuclear bases, thiols and amines. Heart tissues are devoid of glutathione peroxidase which is an enzyme catalysing the conversion of superoxide radicals into oxygen [44, 45]. Thus heart tissues are easily affected by such radicals produced by anthracyclines and this is the reason why they exhibit cardiotoxicity. Another theory in explaining cardiotoxicity due to anthracyclines is the mitochondrial damage they cause. By affecting the bioenergetics of mitochondria and mitochondrial DNA [46-48], disturbing mitochondrial homeostasis of Ca^{2+} [49], attacking sarcoplasmic reticulum, motivating programmed cell death [50,51] and causing many related consequences, anthracyclines cause strong cardiotoxic action [52-59]. However, cardiotoxicity is also dependent on the nature of the drug used, extent of dose applied [60, 61], condition, age [62] and gender of patients suffering from cancer. During the course of treatment using anthracyclines, one should be careful about the dose of the drug used, time table for delivering the drug, route of its action, choice of one or more drug(s) applied, etc. to reduce effects of such toxicity. Further, during treatment one must be cautious about whether there is any prior cardiovascular dysfunction, abnormalities in metabolic processes and over sensitivity to the drugs applied to the suffering person. Beside their deadlier action on different cancer cells,

sometimes normal tissue systems of the patient were found to be affected by the dose used leading to variety of side effects like myelosuppression, neutropenia, nausea, hematopoietic, mutagenesis, vomiting along with secondary tumors. Cardiotoxicity of anthracycline is related considerably to age and it increases with olden [62]. Earlier studies showed that in case of a dose of doxorubicin reaching to a maximum value of 400 mg/m^2 , probability of heart failure of a patient with age more than 65 years is more than two times compared to a patient with age below 65 years [63]. Patients suffering from pre-existing cardiac abnormalities like hypertension, diabetes, obesity, hyperthyroidism and obstructive lung disease have a threefold greater consequences of cardiotoxicity than patients with no pre-existing cardiac abnormalities [64]. Apoptosis and cardiotoxicity induced by doxorubicin became more enthralling when sexual distinction was observed in different case studies. Male patients were found to be suffering from congestive heart failure and other cardiovascular diseases in large number in comparison to female patients of similar age [65,66]. This indicates the existence of sexual distinction in case of cardio protection. Substantial secretion of female sex hormone estrogen and increasing activity of telomerase [67, 68] accelerate tissue revival capability [69] and consequently brings about sexual divergence.

Different *in vitro* studies showed anthracyclines damage cellular respiration and cause cell death by lowering energy level and oxygen deficiency [34-36,70]. Cellular respiratory tract was damaged indirectly by anthracycline drugs when it attacked the sarcoplasmic reticulum [34] by using either destruction of pre-mature cell or by means of programmed cell death [35, 36]. Semiquinone free radicals produced by cellular reduction of the quinone in anthracycline drugs are responsible in damaging mitochondria [6, 70].

To improve their antineoplastic functionality and reducing cardiotoxicity more than 2000 modified anthracycline analogues were introduced [71-74]. Many of them have better clinical activity [72-74]. Though such a huge number of anthracycline analogues have been tested for clinical purpose only epirubicin [75] and idarubicin [76] were approved for medical use. Mitoxantrone, an analogue of anthracycline, developed in 1980 received approval in 1987. It is superior in antitumor efficiency and has less toxic side effects over that of adriamycin [19]. Mitoxantrone hinders the function of Topoisomerase II and produces small number of reactive free-radicals in comparison to other anthracycline drugs [77]. It is a milestone as an anticancer agent in the treatment of various types of human cancer like breast cancer, prostate cancer, blood cancer and lymphoma. It exhibits extra-ordinary performance for the condensation of segregated chromatin [78], rupture of protein correlated DNA molecule [79] and plays a crucial role as an inhibitor during DNA and RNA synthesis in malignant cancerous cells [80]. It is well known for prolonged DNA damaging mechanism. Idarubicin (4-demethoxydaunorubicin), another analogue of daunorubicin with similar morphology, lacking a methoxy group in its C-4 position, is more lipophilic compared to daunorubicin with a higher affinity of accumulation in leukaemic cells. When myeloid leukaemic cells are treated with idarubicin, it was found that inhibition of cell proliferation takes place ten-folds stronger than daunorubicin [20]. It has been found that idarubicin is absorbed by tumor cells at a faster rate in comparison to daunorubicin and that the former binds with cellular DNA more tightly than the later. Idarubicin also exhibits less cardiotoxic action than daunorubicin because it forms less free radicals during the course of its action. This is why idarubicin shows a wide range of antitumor activity than daunorubicin and it was suggested to be administered into patients orally [20]. Epirubicin, an analogue of doxorubicin, shows 30% less cardiotoxicity than doxorubicin, administrated intravenously to

patients suffering from breast cancer. It inhibits DNA synthesis [81]. Iododoxorubicin, an iodine substituted analogue of doxorubicin, exhibits higher cardiotoxicity than doxorubicin, yet it was suggested to be an excellent anticancer drug in the treatment of human myeloma, ovarian and colon cancer [82, 83].

To reduce cardiotoxicity several metal-anthracycline complexes have been prepared. It directs a new series of anticancer drugs [84, 85] with reduced cardiotoxicity. Metal complex formation results in a modification of the electrochemical properties of the original drug thereby reducing its cardiotoxic property [86, 87]. It also changes the polarity of the drug molecule which affects interaction of such modified structures with different cellular components such as cell membranes and nucleic acids [88,89]. Due to inclusion of the positive charge due to the metal ion, the metal-drug complex binds DNA more efficiently in comparison to that of parent drug [90]. Fe^{III} -carminomycin (1:3) and Pd^{II} complexes of adriamycin and daunorubicin were found to inhibit growth of P388 leukemia cells in a way similar to that of free drug molecules. Electrochemical properties of such free drug molecules were found to be changed following complex formation with metal ions. The metal-drug complexes were incapable of exhibiting catalytic activity due to flow of electrons in presence of NADH dehydrogenase from NADH to molecular oxygen. This reduces the chance of formation of superoxide radical anion by metal complexes compared to free drugs [91]. The *in vivo and in vitro* studies on Cu^{II} complexes of anthraquinone-1,5-disulphonic acid and carminic acid [92] showed complexes possess an excellent growth inhibiting performance in sarcoma180 and L1210 leukemic cells compared to free anthraquinone molecules [93].

2.2. Metal Complexes of anthracyclines and their analogues

Nature has selected many metal ions [94] as important cellular component in a wide variety of proteins and enzymes. Metals play vital roles in catalysis and are involved in swapping of electrons to catalysts [95]. In human physiology, many metal ions like gallium, zinc, strontium, manganese, cobalt, silver, vanadium, copper, etc., in macro or micro concentrations are essential for growth and other biological processes. A deficiency in a particular metal ion or presence in excess in our body causes different abnormalities and toxic side effects. Metals like mercury, lead, nickel, arsenic, cadmium, chromium, are carcinogenic and have less contribution in the body. Although introduction of anthracyclines as anticancer agents convey a dramatic change in treatment of different human cancers but its acute and chronic toxicities are a major drawback of using them. Therapeutic as well as cardiotoxic properties of anthracyclines were found to be inter-related with various metal ions [96, 97]. Thus cardiotoxicities of these drugs throw a challenge to investigators for synthesis of non-cardiotoxic and more sensitive anticancer drugs which are efficient in showing antiproliferative property against malignant cells selectively. Reduction in cardiotoxicity can be made through modification of the aglycon portion of the molecules through complex formation with suitable metal ions. This generates a new class of antineoplastic drugs with much lower toxicity. Numerous studies established that when metal ions are combined with anthracyclines therapeutic efficiency and other biological actions increase considerably [90, 98-107]. During complex formation, pH and other solution features act as a referee to decide whether single or both doubly bonded oxygen atoms of the aglycon moiety amalgamate with metal ions. Different spectroscopic and potentiometric methods were employed by researchers to monitor complex formation of anthracycline with metal ions in solid

state as well as in solution followed by calculation of stoichiometry and formation constants of such complexes [92,108-110].

Among several metals, Cu is one of the requisite cellular elements which is involved in different biological process and acts as a co-factor in different enzyme catalytic process [111]. Thus many Cu^{II} complexes of anthracyclines were prepared and characterized [111]. The complex formation between anthracyclines and other metals has also been reported [90,112-114] where metal ions preferably exhibited their site of binding with the C5-, C12- carbonyl and C6-, C11- phenolate oxygen. Beraldo *et al.* reported complex formation between adriamycin and Cu^{II} [99]. They showed 1:1 and 1:2 Cu^{II} adriamycin complexes were formed at two different pH and calculated their corresponding stability constants $(1.8 \pm 0.7) \times 10^{12}$ and $(4.6 \pm 1.1) \times 10^{16}$, respectively. The 1:1 complex comprises of an extended polymeric chain and observed at higher pH (=7.2), whereas the binary complex is found distinctly at a comparatively lower pH (=5.2). Chelation within such 1:1 and bis complexes arise due to preferential bonding opportunity of Cu^{II} with the aglycon ketonic oxygen and neighboring β -ketophenolate moieties established by Resonance Raman spectroscopy. An analogous binding pattern were also observed between Cu^{II} and adriamycin during their complex formation [115] recommended by a parallel EPR study. The pH of the solution plays a crucial role in explaining the stability of 1:2 Cu-adriamycin complex. A similar study was carried out by a group of workers [101] who used Resonance Raman spectroscopy to conclude that 1:2 Cu-adriamycin complex shows its existence permanently in solution till pH 12 and that no alteration was found in Raman spectroscopy of the metal-ligand mixture after studying at a variety of pH. Change in such spectra was observed beyond pH 12 which was supposed to be a continuous transformation of the binary complex into

a polymeric species. This study [101] contradicts the study carried out by Beraldo and his coworkers [99] (mentioned above). Formation of a tris (1:3) Fe^{II} -adriamycin complex was reported at pH 7 by Feng *et. al.*[116]. A detailed study on magneto and other spectroscopic properties of Cu-anthracycline complex was studied by Greenway and Dabrowiak [117]. They suggested the simultaneous formation of two water soluble 1:1 and 1:2 Cu-adriamycin complexes in a particular range of pH (5.5 – 8.0) in which 1:1 complex shows its supremacy at lower pH (=6) whereas 1:2 complex was predominant in the pH range of 6.0 – 8.5. If such 1:1 and 1:2 metal-drug mixtures were brought into solution, an insoluble 1:1 complex is separated out. Formation of a similar species was also observed in ethanolic media.

Anthracycline also forms very stable complexes with Pd^{II} of both 1:2 and 2:2 (dimeric form of 1:1 complex) stoichiometry [102]. Such complexes were found to intercalate between base pairs of DNA acting as excellent antineoplastic agents against P388 Leukemia cells in comparison to free drugs. It was found that Pd^{II} -anthracycline bis complex has mode of binding analogous to Cu^{II} . In the dimeric structure of 1:1 complex β -ketophenolate moiety of 1st anthracycline and amino nitrogen of the sugar part of 2nd anthracycline molecule exposed as preferential binding sites for each Pd^{II} ions of two mutually interacting anthracycline [Figure 1] instead of a polymeric appearance.

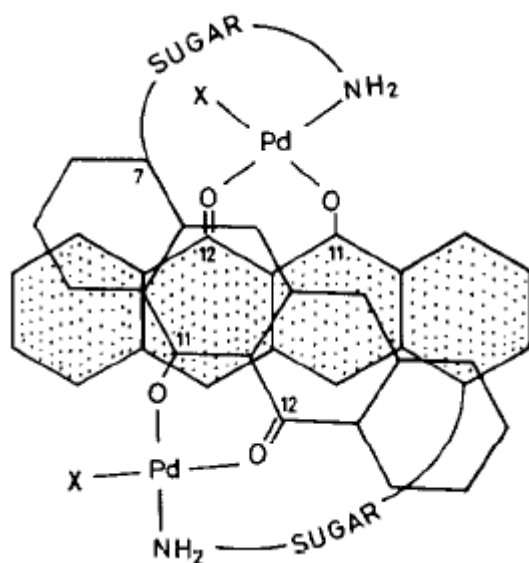


Figure 1: Dimeric form of 1:1 Pd(II)-Adriamycin complex

Iron is an important element extremely necessary in all living cells and plays a vital role in many biological systems, including oxygen delivery, energy metabolism, cell proliferation, metabolism of xenobiotics and it also participates in immune reactions and anabolic processes. The most abundant form of iron in our body is metalloproteins (e.g., hemoglobin, myoglobin, cytochromes). A lot of iron chelators were synthesized [118,119] that reduce participation of Fe^{II} and Fe^{III} in free-radical producing reactions and plays a beneficial role in treatment of ischemia reperfusion injury [120,121], neurodegenerative diseases [122,123] and inflammation [124] conditions. From the middle of the previous century numerous attempts were enlisted on interaction between Fe^{III} and anthracyclines to obtain Fe-anthracycline chelated compounds [84, 90, 91, 112, 125-127] that can display their pharmacological activity. Absorption and fluorescence spectroscopy, ⁵⁷Fe Mössbauer, EPR, X-ray absorption spectroscopy, CD, magnetic susceptibility measurements, etc. were used to characterize the formation of mononuclear, dinuclear and polynuclear Fe^{III}-anthracycline complexes. The first trinuclear Fe-doxorubicin chelate complex

is quelamycin [84]; it was found to diminish the cardiotoxic effect of doxorubicin [125]. Many other researchers put their efforts to characterize various Fe^{III} -doxorubicin and Fe^{III} -daunorubicin complexes [90, 91,112,126,127]. Formation of ternary complexes of Fe^{III} with doxorubicin and daunorubicin were also reported [90] and in such cases each molecule of the drug releases one proton from phenolic $-\text{OH}$ at C_{11} . Magnetic susceptibility measurements [90] revealed complexes were in a high-spin state with 5 unpaired electrons and one Fe^{III} atom is coordinated with six oxygen atoms from three neighboring β -ketophenolate moiety of three anthracycline molecules [Figure 2]. Two analogues of adriamycin such as 11-deoxyadriamycin and aclacinomycin [128], lacking of phenolic $-\text{OH}$ group at C_{11} , were found to be incapable to form hexagonal chelate firmly with Fe^{III} . This suggests coordination of Fe^{III} with anthracycline involves the C_{12} carbonyl and C_{11} -phenolate oxygen atoms respectively. Bachur *et al.* [125] published another parallel explanation that complex formation between Fe^{III} and doxorubicin gives rise to two compounds, a monomer with 1:1 stoichiometry and an oligomer (or a polymer) formed due to interaction between two or more monomeric fragments. ^{57}Fe Mössbauer and EPR studies were performed to investigate interactions between Fe^{III} and anthracyclines that established in aqueous solution such monomeric species get stabilized by a large excess of anthracycline [105,129]. 5-Iminodaunorubicin, a semi-synthetic analogue of anthracyclines with a modified benzoquinone moiety was investigated to confirm whether any alternation of the quinone moiety produces a new drug with low cytotoxic effect than adriamycin. Therefore, complex formation between Fe^{III} and 5-iminodaunorubicin provides a golden opportunity to study impact of alternations in the quinone geometry on the formation and biochemistry of such complexes. Fe^{III} forms a 1:3 chelate complex with 5-iminodaunomycin at physiological pH. The complex yields less hydroxyl free radical (OH^\bullet) than that of doxorubicin. Formation of hydroxyl

free radicals was found to be reduced considerably at high 5-iminodaunorubicin/ Fe^{III} ratio. Coordination between idarubicin and Fe^{III} were also of growing interest and this was well studied by Fiallo and co-workers [90] with the help of absorption, CD, Mössbauer and EPR spectroscopy. They suggested formation of two Fe^{III} -idarubicin complexes having 2:1 and 1:1 stoichiometry with a very fair value of stability constants of $(5.3 \times 10^{24}) \text{ M}^{-2}$ and $(4.8 \times 10^{11}) \text{ M}^{-1}$ respectively. During formation of 2:1 Fe^{III} -idarubicin complex, the ligand utilizes both of its β -ketophenolate portions towards the metal ions as binding sites for co-ordination.

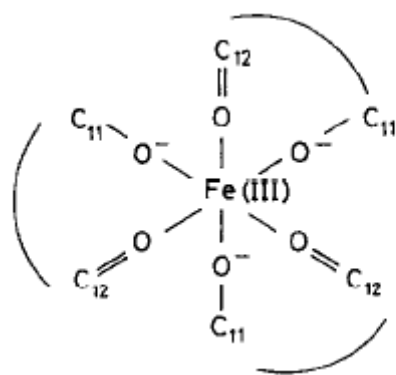


Figure 2: Binding pattern of 1:3 Fe^{III} -Adriamycin complex

Complex formation of Uranyl (+6) ion (UO_2^{2+}) with adriamycin and daunorubicin were well studied by using circular dichroism, fluorescence, absorption and NMR spectroscopy and these complexes depend strongly on dielectric constant of the solvent, the metal-to-ligand ratio and pH of the solution [130]. Both the above mentioned drugs form two complexes with uranyl ion in which the first complex is formed in aqueous solution with a 1:2 metal to ligand stoichiometry at pH 6.5. The formation of second complex involved with drug molecules bridging two metal ions and forming oligomeric or polymeric structures [Figure 3] in aqueous solution of pH above 7. The chelation of 1:2 complex involved coordination of the metal ion to $[\text{C}(11)-\text{O}^-, \text{C}(12)=\text{O}]$ chelating site, while the second complex (**II**) involves coordination to

[C(6)-O⁻, C(5)=O] site. CD and NMR studies suggest concomitant formation of both complexes in methanolic solution.

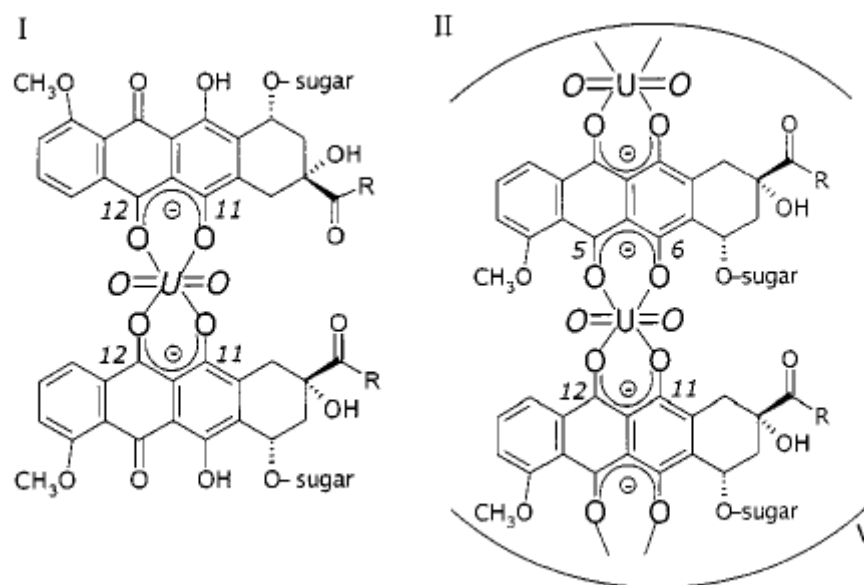


Figure 3: The proposed structures of the complexes formed upon interaction of UO_2^{2+} with adriamycin (I) and daunomycin (II) [130].

Qualitative analysis by several researchers [131-134] suggest Al^{III} undergoes complex formation with anthracyclines that are very useful in fluorescence labeling microscopy and DNA cytochemistry. $\text{Al}(\text{III})$ forms 1:1 tetrahedral complex at $\text{pH} > 5$ with adriamycin and its analogues in which metal ion is attached with the ligand via anthracyclenic oxygen atoms which was confirmed by potentiometric and spectroscopic analysis. Two OH^- groups complete the coordination sphere. Although complexes are comparatively stable formation of $[\text{Al}(\text{OH})_2]^-$ at $\text{pH} > 8.5$ excludes adriamycin from the metal ion co-ordination sites.

Both adriamycin and daunorubicin have also been seen to form significantly stable chelate complexes with various lanthanide ions. Due to wide optical, chemical and magnetic

properties [135-138], lanthanide ions were considered to be useful equipment in exploring such drug systems. Currently introduction of Ln^{3+} ions in the biochemical processes operating in cellular membranes, organelles and cytoplasm have been studied by using several modern techniques. As Ln^{3+} ions have strong affinity towards oxygen-rich ligands analogous to alkaline earth metals, they get chelated with the β -ketophenolate moiety of anthracyclines and as a result Ln^{3+} ions impart better alternative for alkaline earth metals in anthracycline- metal binding atmosphere of biomolecules [137,138]. Complexes of lanthanides as therapeutic agents could not be implemented in the last century much impressively although a few successful applications of radioactive lanthanide complexes were made in identifying and healing of cancer [139]. Some lanthanide complexes show antitumor efficacy with significant toxicity [140] when a higher dose is delivered [139]. The complex formation between different lanthanide ions with adriamycin and daunorubicin was studied by performing optical and 2D NMR (COSY, TOCSY, and EXSY) techniques in aqueous as well as methanolic solution. Studies on NMR suggested that the predominant formation of 1:1 Yb^{3+} - anthracycline complex in aqueous solution at the pH range 4 – 5 when metal to drug ratio was less than 10. Formation of three different Yb^{3+} - drug complexes with the stoichiometry 1:2, 1:3 (both with the aid of a base) and 2:1 (when metal to drug ratio higher than 25) were also reported [141]. Metalation with anthracyclines was observed at 11, 12- β -ketophenolate in all complexes. The metalation of 2:1 metal- ligand complex was also seen at 5, 6- β -ketophenolate region [142]. Electrochemical, spectroscopic and NMR studies showed other lanthanide ions like Pr^{3+} , Eu^{3+} and Dy^{3+} exhibit analogous binding pattern both in aqueous and methanolic solution like Yb^{3+} to anthracyclines in accordance with same coordination model [142,143]. As complexation of Ln^{3+} - drug followed the same binding protocol with other

metal-anthracycline complexes [142] hence these Ln^{3+} -daunomycin complexes can present a model system for understanding of other metal-anthracycline systems.

As hydroxy anthraquinones show pharmacological and pharmacokinetic activity like known anthracycline drugs, several metal complexes of different hydroxy-9,10-anthraquinones like anthracyclines. Complexation of Fe^{III} and Al^{III} with 1,4-dihydroxy-9,10-anthraquinone were characterized in many studies [144-147]. On the other hand formation of long chain polymeric compounds of Cu^{II} with 1,4-dihydroxy-9,10-anthraquinone was obtained [148]. Transition metal complexes of Cu^{II} , Ni^{II} , Mn^{II} and Zn^{II} with 1,4-dihydroxy -9,10-anthraquinone were reported [149, 150] . The studies [149,150] showed that complexes of Cu^{II} and Ni^{II} are found in both monomeric and dimeric form whereas Mn^{II} and Zn^{II} are formed only monomeric complexes. Formation and characterization of such complexes were studied in aqueous solution and in solid states [151]. Complex formation of Pb^{II} with 1,2,5,8 -tetrahydroxy -9,10-anthraquinone (quinalizarin) was reported though the actual structure of such complex was not clear [141]. Binary compounds of Cu^{II} and Ce^{II} are formed with anthracycline analogue mitoxantrone in 2:1 stoichiometry [152,153].

The metal-anthracycline and metal-dihydroxy anthraquinone complexes are mostly devoid of three dimensional structural informations due to some intrinsic difficulties in obtaining suitable single crystal which is probably because of planarity of the aglycon moiety [154].

Beside metal complex formation of hydroxy anthraquinones, metal complex formation of amino-hydroxy anthraquinones was studied along with corresponding metal complexes in aqueous media and in solid states [154-160].

2.3. Electrochemical behavior of anthracyclines and their analogues

Quinone/hydroquinone couple is common in chemistry for their unique redox features. This is very significant from both biochemical and medicinal point of view. There is a direct relationship between pharmacological action and toxicity of anthracyclines (a category of anthraquinones drugs) with redox properties demonstrated by numerous studies [161-168]. Several living systems [169–171] are enriched pharmaceutically through the multistep redox behaviour of quinones [172-174]. This led to the electrochemical study on quinones to be an emerging field of research in medical science. Quinone derivatives are well studied electrochemically for quite a long period [175–178] to investigate their redox machinery. The electrochemical features of quinones are found to have direct connection with equilibrium and kinetics of electron and proton transfer processes thereby providing precious information related to molecular structure, mode of interaction and the atmosphere of the electrochemical processes of quinones [172]. Some category of quinones, like naphthaquinones are very much popular for their anti-inflammatory, antibacterial, topoisomerase inhibition and antitumor activity and also used successfully in the treatment of laceration [179-181]. Anthraquinones and their derivatives are essential and elementary structural units of different electro-active molecules having biological significance [172,37,182,161]. Anthracycline drugs have been found to have cardiotoxicity and chromosome damaging activity which has reduced their efficacy in the field of oncology. During the formulation of vitamin K, naphthaquinone moiety acts as a fundamental constituent. In addition to this another fat soluble quinone, having similarities with vitamin, Coenzyme Q10 (2,3-dimethoxy-5-methyl-6-decaprenyl-1,4-benzoquinone, CoQ10) commonly known as ubiquinone or ubidecarenone (CoQ10) [183,184], a kind of electronic receptor [185], serves versatile role in biological systems and respiratory chains of mitochondria [186,187]

,existing in humans, most mammals and other edible vegetable soil [189–191] , participate in electron and proton transfers [192–194], photosynthetic reaction [195–198], undergoes oxidation and reduction by forming a free-radical intermediate [199,200], etc. On the other hand para-quinones undergo induced reduction to semiquinones catalysed by mitochondrial NADH dehydrogenase [201, 202] and as well as attached covalently to a large number of bio-active molecules to prevent the mobility of the system and generate ROS [203] and thereby exhibits comparable redox functioning as anthraquinones.

Electrochemical, electron spin resonance and pulse radiolysis techniques were performed earlier [172,203,204] in studying the redox chemistry of quinones to investigate role of several factors in the reaction pathway and in biological and chemical environments. By applying solvents of different polarity under different reaction conditions polarography, cyclic voltammetry, and square wave voltammetry were carried out [172] to investigate the effect of these factors on the redox chemistry of quinones. Effect of several other important factors like pH of the media [205], nature of supporting electrolytes, intramolecular/intermolecular hydrogen bonding, stability of the semiquinone and quinone dianion [172], stereochemistry, diffusion, solubility, partition coefficient, oxygen content in the electrochemical cell and more were also examined by electrochemical studies [172,164].

2.3.1. Electrochemical properties in buffered aqueous media

The quinone-hydroquinone couple is the most well known example of single step two-electron redox system where potentials are affected by various factors such as pH of the media, concentration of the electrolytes and other species present in the media [205]. Existence of numerous redox and protonated species in such solution as a function of their corresponding pK_a values and their redox property [178, 206-210] could be explained by means of the Pourbaix or

potential- pH diagrams, a graphical illustration of equilibrium in solution. Studies on cyclic voltammetry has shown a single reversible reduction wave associated with anthraquinones and other para-quinones in buffered aqueous media. In acidic media such reduction has been found to be two-electron two-proton processes forming hydroquinone [Figure 5] [211-221] while in alkaline medium proton independent two-electron reduction [221-225] has been seen leading to the formation of quinone dianion [Figure 6]. On the other hand two-electron one-proton or proton free two-electron reduction process is well documented in neutral pH [221-225]. In acidic and neutral solution some anthracyclines and hydroxy-9,10-anthraquinones undergo irreversible two-electron reduction which has been shown by cyclic voltammetric experiments [211].

The wide electro-analytical behavior of adriamycin, daunorubicin and doxorubicin has been studied by several researchers since the last century [211-232] as the electrochemical aspects of these molecules were seen to be related with their drug action and cardiotoxicity [211,233,234]. Rao [211] and Molinier-Jumel *et al.* [212] investigated the electrochemistry of daunorubicin and adriamycin in terms of two-electron reduction process by using a hanging drop mercury electrode (HDME) and they established a relationship between pharmaceutical efficacy of the drug with their practical redox identity. Both observations were well characterized by two significant reduction signals in which the first one was mounted with -0.6 V vs saturated calomel electrode (SCE) corresponding to a reversible reduction of quinone to hydroquinone with the aid of two-electron reduction, whereas the second one is completely irreversible in nature exhibiting much more negative potentials leading to the irreversible reduction of side chain contiguous to planer aglycone moiety of Adriamycin. An analogous electrochemical reduction on adsorbed adriamycin was performed by Chaney and Baldwin at carbon paste electrode (CPE) which was absolutely qualitative in nature [214].

Redox mechanism of adriamycin and quinizarin were investigated electrochemically at hanging drop mercury electrode surface by Kano and co-workers by using the theory of cyclic a.c. and d.c. voltammetry for a two-step surface redox reaction proposed by Kakutani and Senda [235] at pH 4.5 and concluded that such electrochemical redox reaction is dominated extremely through adsorption of adriamycin whereas contribution of diffusion was observed insignificantly and both processes characterized as a function of their respective current value. In presence of acetate buffer cyclic d.c. voltammetry of adriamycin has been enriched with two important reduction peaks, one remarkable peak functioned reversibly at -0.45 V while another irreversible peak at -1.13 V under the experimental pH of 4.5. Almost an identical couple of reduction peaks have also been observed in the cyclic d.c. voltammetry of quinizarin namely one reversible peak at -0.416 V and another irreversible peak at -1.095 V, respectively. Kano has shown that an analogous peak of unique nature was observed when same condition was applied for a.c. voltammetry like d.c. Electrochemical reduction of adriamycin has a relation with the thermodynamic and kinetic properties of the reduction. The study has also shown a dislocation of second reduction potential by about 0.050 V when the scan rate increases in a span of 0.01 to 0.5 V/s. The effect of increasing temperature on peak current has also been studied. Appearance of the second irreversible reduction peak is the supportive documents for the catalytic evolution of hydrogen catalyzed by two -OH groups adjacent to benzene rings. A drop in irreversible peak or its complete disappearances can be visualized when adequate amount of dimethyl formamide (DMF) or alkali was added. Kano and his co-workers thus suggested that this instability of reduction peak is due to the catalytic evolution of hydrogen caused by two -OH groups adjacent benzene rings of the planer quinone molecule [215].

Interesting redox behaviour was also exhibited by doxorubicin hydrochloride (adriamycin) in aqueous solution. Hahn and his groups [218] examined the redox property of doxorubicin hydrochloride by applying cyclic voltammetry and square wave voltammetry in the presence of acetate buffer under different pH at the surface of hanging drop mercury electrode. Studies showed that electro-chemical reduction of doxorubicin hydrochloride is quasi-reversible in nature and associated with two-electron and two-proton at the hanging drop mercury electrode surface under acidic pH. It has been observed that peak current maintains linearity with doxorubicin concentration and concentration of many specimens under investigation has been measured by applying this linearity principle with high accuracy [218]. Redox mechanism of adriamycin could be explained in terms of surfactant interaction by Zhang and his group members [219] at carbon paste electrode (CPE) by using a cationic surfactant Cetyltrimethylammonium bromide (CTAB) as standard in which adriamycin gets adsorbed appreciably at the electrode surface induced by CTAB. This leads to shifting of reduction peak resulting in a change of peak current and redox potential values and ultimately reaching irreversibly to a sensitive reductive wave value of -0.50 V [219]. Another endeavor has been made by Hu and his co-researchers [220] on electro-analytical behaviour of adriamycin by means of linear sweep voltammetry (LSV) using glassy carbon (GC) electrode and Ni-ion.

Redox behaviour of doxorubicin was also implanted glassy carbon electrode (Ni/GC) in the presence of supporting electrolyte acetic acid-sodium acetate buffer under acidic pH 4.5. In this case [220] the reduction of adriamycin at ion-implanted is well characterized by an impressive quasi-reversible reduction peak of -0.55 V (vs SCE). It is evident from this study that cathodic peak current is linearly dependent on the scan rate and they have concluded that the reduction of adriamycin was entirely diffusion-controlled and independent of adsorption at the

electrode surface. Characterized and measured voltammetrically using first time with a renewable silver-amalgam film electrode (Hg(Ag)FE) by direct cathodic square-wave voltammetry (SWV) and by highly sensitive adsorptive square-wave voltammetry (AdSWV) in the presence of well buffered aqueous solution of Britton-Robinson buffer as supporting electrolyte in the pH range 2–8 [236]. The Hg(Ag)FE electrode was monitored in the potential range between -0.20 and -0.80. The reversible reduction process was explained by assuming as two-electron and two-proton reduction [Figure 4]. On implementation of this adsorptive technique sensitivity of the system was increased 50 folds more compared to the direct cathodic determination.

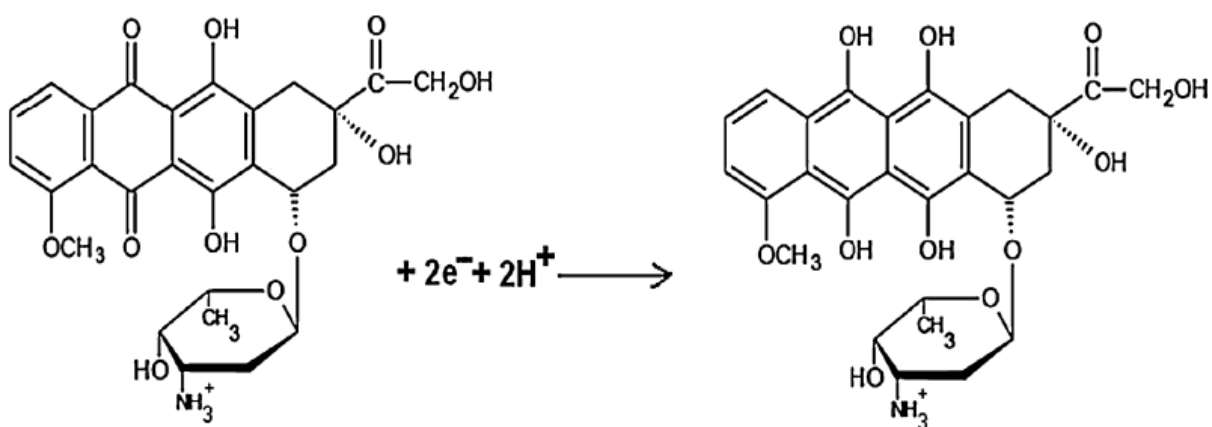


Figure 4: Tentative reduction mechanism of DOX on Hg(Ag)FE at pH 6.0.

Thus spiked human urine sample containing doxorubicin can be estimated by using silver-amalgam film electrode Hg(Ag)FE coupled with AdSWV technique under appropriate condition to determine the concentration of doxorubicin upto nanogram level [236]. Redox behaviour of daunomycin has also been illustrated by adsorption at hanging mercury drop electrode (HMDE) under aqueous pH of 9.18 assuming two-electron reduction followed by ECE route [221] and the results obtained corroborated well with earlier outcome [222].

Aqueous electrochemistry of a lot of anthracycline was studied [231-237] in aqueous buffer by cyclic voltammetry using a variety of anthraquinones and its versatile analogues to confirm their function as an alternative of novel anthraquinone. Owing to poor solubility in water anthraquinone preferentially derivatives of anthraquinone having sufficient water solubility was selected as model compound during experiments. Potential- pH diagrams were formulated for each of the individual compounds. Spectrophotometric studies have also been made to obtain pK values for a few cases because pK values are important to understand the stability of reduced species. Redox behaviour of anthraquinone-2-sulphonate in alkaline pH were studied individually by Gill [223] and Furman [224] with their respective co-workers and described the two-electron one-proton reduction of anthraquinone-2-sulphonate to form de-protonated dihydroxy-anthracene, characterized by well-developed polarographic wave under alkaline pH. Two-electron two-proton reduction was also found for disodium anthraquinone-2,6-sulphonate, disodium anthraquinone-2,7-sulphonate, sodium anthraquinone-1-sulphonate, sodium anthraquinone-2-sulphonate, disodium anthraquinone-1,5-sulphonate, sodium anthraquinone-1-amino-2-sulphonate, etc., under acidic pH in the presence of acetate buffer [226]. Reduction of quinizarin in acidic pH also involved two-electron two-proton process in the presence of acetate buffer as supporting electrolyte [237, 238]. Wipf *et al.* [207] showed that in alkaline pH anthraquinone, sodium anthraquinone-2-sulphonate and disodium anthraquinone-2,6-sulphonate undergo exclusively two-electron reduction and thereby forming dianionic species. In spite of some disputation they suggested that such electro-chemical reduction involved two reduction waves in which the amplitude of first one is linearly dependent with the square root of the scan rate indicating diffusion controlled event. On the other hand the second wave was found at more negative potential with non-linear dependence on square root of scan rate indicates the reduction

to be adsorption controlled at the surface of the electrode [207]. A negative slope of -0.060V/pH in Pourbaix diagram confirmed that anthraquinone and its derivatives undergo similar type of two-electron two-proton reduction under acidic condition [215] and thus a relation between number of participating electrons required for reducible quinone, cathodic peak potential and half width potential can be calculated by the following equation- (1).

$$|E_{Pc} - E_{Pc/2}| = 90.6/n \quad (1)$$

Where E_{Pc} is the cathodic peak potential, $E_{Pc/2}$ is potential at half width of the cathodic peak and n is the number of participating electrons involved in the reduction process.

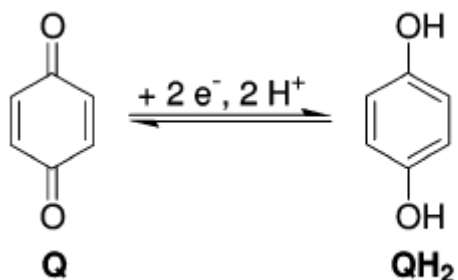


Figure 5: Two-electron two-proton reduction of quinone in aqueous buffer [219-229]

2.3.2. Electrochemical properties in unbuffered aqueous media

Although numerous studies were witnessed of electrochemical behaviour of quinones in well buffered aqueous solution only a few cases under unbuffered medium has been reported [178,208,228-232]. It was assumed that either quinones exhibit analogous behaviour in aqueous solution both in buffered and unbuffered condition or unbuffered electrochemistry of quinones possesses ambiguity in aqueous phase which is difficult to explain. A detailed voltammetric inspection on quinhydrone (a 1:1 complex of benzoquinone and benzohydroquinone) has been studied by Müller *et al.* [239] who suggested that electrochemical study must be carried out in the

presence of well buffered condition. This was later supported by Kolthoff and Lingane [240] and they confirmed the difficulties of interpretation of polarographic studies on quinones in unbuffered or diluted buffer solution through their investigation. Although some controversial cases on unbuffered aqueous electrochemistry of quinone has been reported [239,241,242,209,243-245,228-230] experimental results and its elucidation were differed from each other. When the proton concentration is almost equal with quinone concentration two sensitive voltammetric waves were characterized. The reversible peak was characterized by two-electron two-proton reduction while their reversible wave at more negative potential was explained in terms of protons coming from either water or hydroquinone [239,241-243]. A parallel investigation was made by Shim and Park [245,230] and they explained the same through the formation of quinone radical anion by single electron reduction. Wang and co-workers [229] claimed that quinone dianion is formed due to two-electron reduction. Later Forster and Kelly [228] proposed a theory of adsorption of quinone monolayers on Hg electrodes. Thus from the overall studies it has been concluded that electrochemical reduction of quinone in unbuffered aqueous solution is associated with a two electron-reduction leading to the formation of strongly hydrogen-bonded quinone dianion that is present in solution as an equilibrium mixture with other protonated species depending on their respective pK_a values.

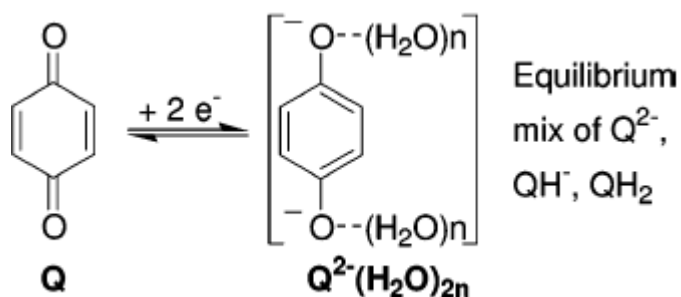


Figure 6: Two-electron reduction of quinone in aqueous buffer [229-233]

2.3.3. Electrochemical Properties in Non-Aqueous Media

Reduction of *para*-quinones including 9,10-anthraquinones in non-aqueous medium like acetonitrile or dimethyl sulfoxide, etc., involves two consecutive one-electron reductions leading to formation of short living semiquinone radical ($Q^{\cdot-}$) reversibly followed by formation of quinone dianion (Q^{2-}), through quasi-reversible process in succession [177, 246-251] [Figure 7]. By introducing conventional scan rates it was observed this transient species, i.e., semiquinone radical ($Q^{\cdot-}$) smoothly disproportionate [178, 208] into a quinone and its corresponding dianion. Moreover, reduction is controlled through diffusion [246, 247, 251, 252] as peak currents of first and second electrochemical reductions [172] vary linearly with square root of traditional scan rate. This two sequential reduction potentials were found to be influenced remarkably by several auxiliary factors like solvent polarity [157, 159, 172, 177, 207, 237, 253-256], ion-pair formation [237, 238, 257-259], nature of supportive electrolyte [237, 238, 248], protonation–deprotonation equilibria [177, 255, 256, 259-261], intra- and intermolecular hydrogen bonding [177, 260-263], different additive acidic or alkaline species [172, 177, 256, 257, 260, 261, 265] etc. Beside these other significant processes such as disproportionation [178, 208], comproportionation, [172,177,246,266-268] and dimerization [251] also affect the general electrochemical behavior of quinones in non-aqueous media.

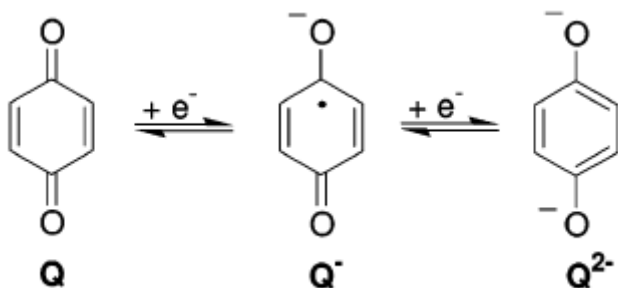
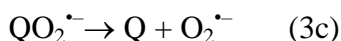
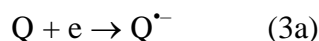


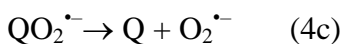
Figure 7: Two consecutive one-electron reductions in non-aqueous media [177,246-251]

2.3.4. Electrochemical behaviour of quinones in oxygen mediated non-aqueous media

Anticancer property of anthraquinone and its derivatives are closely related to formation of electro-active superoxide radical anion and other reactive oxygen species in solution that are produced through one-electron reduction of molecular oxygen. Voltammetric studies suggest such mono-electronic reduction in non-aqueous oxygenated atmosphere can be explained by introducing the following mechanism where the first step involved formation of semiquinone through one-electron reduction of the original quinone (Q) followed by further oxidation of semiquinone $Q^{\bullet-}$ (formed in the first step) by molecular oxygen leading to the formation of a certain complex ($QO_2^{\bullet-}$) that ultimately disproportionate to parent anthraquinone along with superoxide anion radical ($O_2^{\bullet-}$) [269, 270]. The overall mechanism can be expressed as follows:



On the other hand, a second mechanism [271,272] also brought into consideration along with the first one to explain such behaviour wherein the first step was accompanied with adduct formation through an active participation of singlet oxygen and anthraquinone while the second step was associated with one-electron reduction of such adduct to disproportionate into anthraquinone and superoxide radical anion as follows:



2.4. Theoretical studies on anthracyclines and anthraquinones

Theoretical studies play a significant role in justifying experimental findings on structure, energetics and spectroscopic behavior of anthracyclines and their analogues. Computational chemistry is an important area of theoretical chemistry that acts in solving several chemical problems through computer simulation. Quantum mechanical methods can be divided as *ab-initio* and *semi-empirical* methods in which *ab-initio* method encompasses with Hartree-Fock(HF), configuration interaction (CI), many-body perturbation theory (MBPT), coupled-cluster(CC) theory, and other approaches [273-276], whereas *semi-empirical* method follows quantum mechanical laws strictly containing few empirical parameters to patch things up. Although Density functional theory (DFT) [277] is a quantum mechanical approach it is very difficult to categorize this as *ab-initio* or *semi-empirical* method since some DFT methods are free from empirical parameters, while others depend strictly on calibration with experiment. Thus the current trend in DFT research is to employ increasing number of empirical factors, making recent DFT techniques semi-empirical. In studying various molecules theoretically these methods are highly imperative.

Deciphering structure–activity relationship may lead to introduction of new medicines for a lot of diseases. Attempts were made in many earlier studies [278-280] so as to lead to a proper understanding of structure–selectivity relationship of anthracyclines that may lead to bringing up a novel chemotherapeutic agent for treatment of cancer. Thus computational and spectroscopic measurements were performed to understand the electronic state of the molecules and to draw knowledge on hydrogen bonding [155]. In this context, it is interesting to note that three-dimensional structures are known only for a few anthracyclines and 1-amino-4-hydroxy- 9,10-anthraquinone [155,281,282]. It is worth mentioning that although several metal complexes of

adriamycin, daunorubicin, mitoxantrone and their analogues with Fe^{III} , Al^{III} , Cu^{II} , Ni^{II} , Pd^{II} and Tb^{III} were prepared and characterized [85, 108, 116, 144-146, 154, 283-295], a comprehensive knowledge on structures of these metal complexes is lacking due to inherent difficulties in obtaining single crystals for X-ray diffraction studies. Single-crystal X-ray diffraction structures of only a few hydroxy-9,10-anthraquinone complexes have been reported so far [293, 296, 297]. Thus in many studies, the optimized molecular structures with corresponding energy values and various parameters like bond angle, bond length, etc., of some hydroxy and hydroxy- and amino-9,10-anthraquinones and their metal complexes were estimated using HF, B3LYP and PBEPBE [154,155,160,298]. In such studies, VEDA [299] with PED analysis has been carried out to characterize vibrational spectra of the molecules. Various molecular orbitals were characterized theoretically to explain and analyze the electronic transitions involved in the molecular spectra of such molecules.

2.5. Interaction of anthracyclines and anthraquinones with surfactant micelles

Surfactant chemistry is now of growing interest to all, the world over, due to their unique amphipathic features in solution [156, 252, 300, 301]. This is similar to a lipid molecule. The presence of a polar head group along with concomitant existence of non-polar hydrophobic moiety is responsible to exhibit such amphiphilic nature. Aggregation of such surfactant molecules in solution occurred above a certain concentration, the critical micelle concentration (CMC), leading to rapid formation of colloidal-sized clusters micelles, an extremely energetic arrangement that exist within an equilibrium mixture between its monomeric and polymeric architecture. Nowadays micelles are thought to be a simple and mimicking model to biological membranes. Micelle plays an imperative role in a number of impressive processes in both

fundamental and applied sciences through their amphiphilic nature [156, 252, 300, 301]. Numerous studies are on to investigate drug binding features from different perspective of therapeutic categories to model and natural membranes (micelles of surfactants, phospholipid bilayers, erythrocyte ghosts, etc.) [302-306]. Since it has already been established that biological membranes are composed of tremendous multi-functional network and thus nowadays surfactant micelles with less complicacy are extensively used as a standard model to explain bilayer properties and functions [300,307] of bio-membrane. From the last century studies on drug-surfactant interaction have drawn an emerging attention to the researches all over the world due to their excellent capability in solubilizing hydrophobic drugs. This ensures extensive application of surfactant micelles in pharmaceutical field [300, 308-310].

It has been assumed that micellization process involves several steps that was characterized with several equilibria and corresponding equilibrium constants or as a phase separation (all or none) process. Once a critical concentration (the critical micellar concentration, cmc) is reached, further addition of the surfactant would result in aggregation [307]. Depending on the nature of the polarity of the head group these amphiphilic surfactant molecules are classified as anionic such as sodium dodecyl sulfate (SDS), cationic such as dodecyltrimethylammonium bromide (DTAB) and Cetyltrimethylammonium bromide (CTAB) and nonionic like n-dodecyl tetra (ethylene oxide) ($C_{12}E_4$) and zwitterionic surfactants like dioctanoyl phosphatidylcholine (C_8 -lecithin)(Figure 8) along with a characteristic long chain hydrocarbon residue or sometimes a halogenated or oxygenated hydrocarbon or siloxane chain [311, 312] as tail.

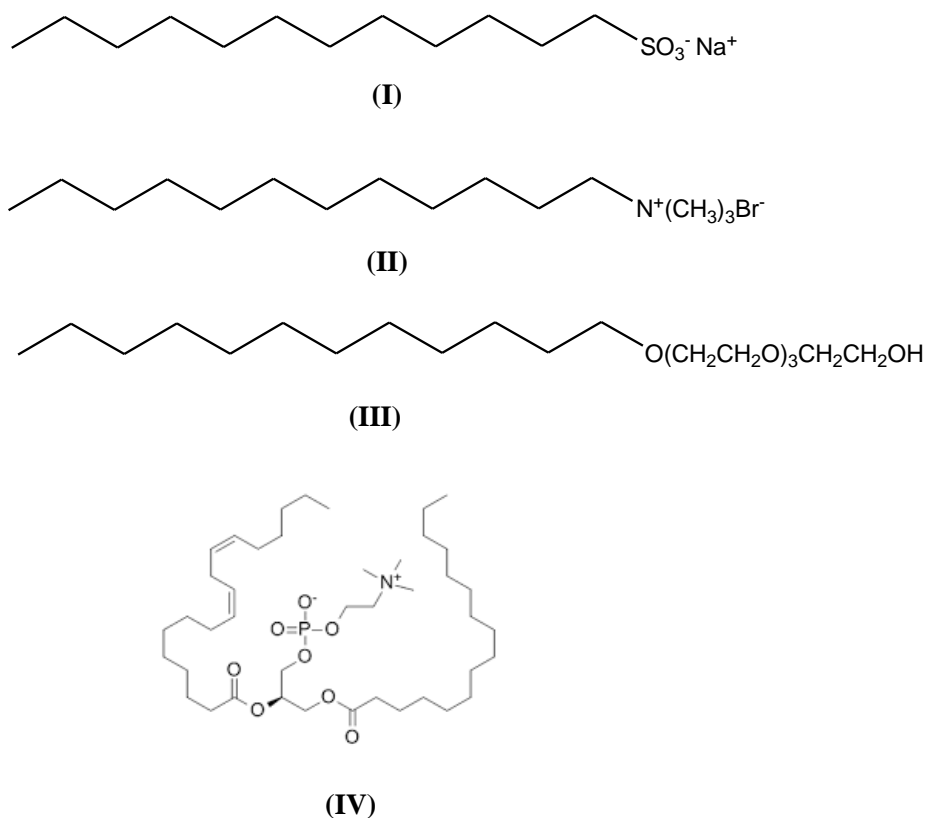


Figure 8: (I): anionic (SDS), (II): cationic (CTAB), (III): nonionic (C_{12}E_4) and (IV) zwitterionic surfactant (C8-lecithin).

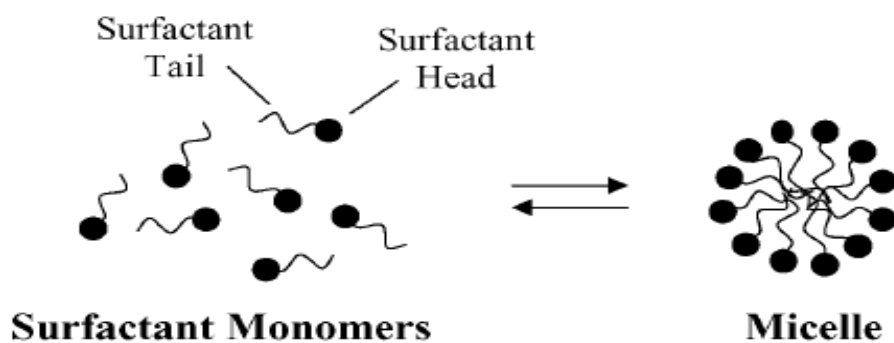


Figure 9: Schematic illustration of the reversible monomer-micelle thermodynamic equilibrium. The black circles represent the surfactant head (hydrophilic moieties) and the black curved lines represent the surfactant tail (hydrophobic moieties). [252]

Energetics of micellization and different physicochemical parameters defining the characteristic of micelles have been reported by a lot of studies [313-319]. Inside the cell when incoming drug molecule approaches towards the targeting DNA it must pass through the cellular and nuclear membranes. Predominance of lipid content as a building block in the biomembrane, asymmetric nature of lipid molecules, versatility in lipid ingredients, coexistence of different phases along with carbohydrate and protein molecules reduce the permeability of cell-membrane. This provides a dynamic and complicated membrane structure which throws a challenge to penetrate and interact for a bio-active molecule across the cell-membrane and functioning in its desired site. Since inner core of the membrane is hydrophobic [320] in nature smooth penetration and interaction of polar molecule through the cell-membrane is hindered. Thus anti-cancer agents demand a suitable drug-membrane interaction mechanism to illustrate their chemotherapeutic actions in their required operating location through the cell-membrane. Ionizable membrane surfaces or corresponding hydrophobic territory of membranes are very much susceptible for most of the significant biological incidents where drug molecules are get attached with cell membrane indicating interaction of drug molecules at molecular levels with biological tissues and thus provide an idea about drug functioning mechanism. Valuable information related to nature of drug-membrane interaction was estimated when a parallel study of drug interaction was performed with different types of surfactants [300, 302, 321]. Hydrophilic external portion along with hydrophobic inner core of micelles exhibit similarities with cell membrane and thus used as a standard model to investigate the action of different factors on the binding of the drug molecules [304]. Simple chemistry, poor toxicity, permeable size distribution, longer life time in the system, elevated bioavailability as well as improved stability of drug due to encapsulation into micelles made the process more superior over the

application of conventional liposomes and soluble polymers [322,323]. Most of the anticancer drugs are less soluble in aqueous media due to their hydrophobicity and therefore these should be water soluble for administration to the patients those who are suffering from cancer. Micelles increase the rate of water solubility of such water repellent drugs leading to the enhancement in bioavailability and thus developed better therapeutic efficient drugs to reduce drug degradation and damage, to suppress deadlier side effects when these are acted in enveloped mode by micelles from site of application to its specific domains which is under consideration [252].

Insertion of drug molecules through the bio-membrane covering with surfactant molecules is very much analogous with the launching of satellites into space by means of thermally insulated rocket by preventing the frictional forces contributed by earth atmosphere. Non-polar drugs get solubilized in the bulk of the micelle while drug molecules having intermediate polarity get distributed along the certain intermediate sites of surfactant molecules [259, 302, 304] .

Drug transport mechanism currently has become very much popular in medicinal field due to their paramount drug loading skill and extra-ordinary selective action on desired site in the tissue system [324-326]. When loaded drugs are encapsulated within drug transporters then their disposition throughout the body is predominantly dependent on surface activity and particle size of the drug carrying agent which plays a phenomenal role in regulated drug delivery system and it is almost independent on the features of loaded drugs [327, 328].

The mechanism of drug action is also related to the interaction of a drug molecule with biological tissues by means of its binding to membranes at the molecular level [329-331]. Many biological processes occur at the ionizable surface of the membranes or along their hydrophobic region which makes a comparative study on the interaction of the drug with cationic, zwitterionic,

anionic and neutral surfactants to be imperative [332,333]. This provides useful information on the nature of drug–membrane interaction. The studies on the drug–surfactant interactions have been done by several workers using various techniques as it has widespread applications in pharmaceutical field. Micellar systems possess the ability to solubilize hydrophobic drugs [306, 310, 311] thereby increasing their bioavailability and thus it can be used as a model system for bio-membrane, as well as drug carriers in numerous drug delivery and drug targeting systems [334, 335]. The physicochemical interactions of drugs with surfactant micelles can be visualized as an approximation for their interactions with biological membranes. This provides an insight into more complex biological processes like the passage of drugs through cell membrane.

Keeping these aspects in mind various studies on drug–surfactant interaction including anthracycline molecules have been carried out by different researchers [248, 336, 156, 158] .

An exclusive study of drug-surfactant interaction was performed with anthracycline anticancer antibiotic daunomycin by Dignam *et al.* [337] using sodium dodecyl sulfate (SDS) and Triton X-100 micelles as model instance to investigate hydrophobic interaction with membranes. Insertion of anthracycline ring in the inner core of SDS and Triton X-100 micelles brings a sharp change in absorbance, fluorescence intensity followed by a characteristic hypsochromic shift in emission spectrum which confirmed the hydrophobic nature of the drug-micelle interaction.

Enache *et al.* [338] has investigated drug-surfactant interaction with the anthracycline anticancer drug mitoxantrone and anionic surfactant SDS under the influence of phosphate buffer in physiological pH (=7.4) using UV–Vis spectroscopy and electrochemical methods. The partition coefficient for the distribution of mitoxantrone between aqueous phase and SDS micelles was calculated and has indicated that it is strongly dependent on the drug concentration.

Both absorption and cyclic voltammetry has revealed that depending on surfactant concentration two different drug-surfactant interactions were operated between mitoxantrone and SDS in which process I is associated with in premicellar range, assigned to the electrostatic interaction between the positively charged groups of the drug and the negatively charged surfactant group leading to the formation of mitoxantrone-SDS complex with a defined stoichiometry while process II was accompanied with micellar range when the surfactant micelles were formed and the drug is encapsulated in micelles in monomer form.

Toader et al. studied [339] drug-surfactant interaction by absorption spectroscopic and conductometric methods with quinizarin, an analogue of anthracycline anticancer drugs and anionic SDS micelles in 0.1 M phosphate buffer under pH 7.4 in the temperature range of 293.15–323.15 K. Value of binding constant for the quinizarin-SDS micelle interaction has also been compared with the binding constant values of mitoxantrone-SDS [340, 341] and epirubicin – SDS interactions [303] at 293.15 K. Both binding and partition processes have been found to be entirely entropy controlled over the range of experimental temperatures and the hydrophobic interactions are dominant evident.

A typical drug-surfactant interaction was studied by Roy *et al.* [158] with 1-amino-4-hydroxy-9,10-anthraquinone, a simple analogue of anthracycline anticancer drugs and cationic surfactant cetyltrimethylammoniumbromide (CTAB) in aqueous solution at physiological pH (= 7.4) using cyclic voltammetry and UV-Vis spectroscopy. Using a series of fitting models intrinsic binding constant, partition coefficient and stoichiometry was computed and compared with earlier studies with analogous anthracycline drug mitoxantrone [342, 343]. Result of the above investigation established a significant participation of hydrophobic mode of interaction of the molecule. Another drug-surfactant interaction was studied by Das et al. [160] with 2-amino-

3-hydroxy anthraquinone with anionic surfactant SDS and cationic surfactant CTAB respectively, under physiological pH (7.4) in aqueous solution by UV-Vis spectroscopy. The binding constant, partition coefficient and Gibbs free energy for binding and distribution of AQ between bulk aqueous solution and surfactant micelles were determined for AQ–surfactant interactions. It was found that encapsulation of AQ into bulk of SDS and CTAB predominantly monitored by hydrophobic and hydrophilic interaction respectively resulted in smooth distribution of AQ between surfactant micelle–water phases. Successful permeation across cell membrane of investigating drug without any degradation was revealed. Another drug–surfactant interaction was studied by Roy et al. [156] using a Cu^{II} complex of 1-amino-4-hydroxy-9,10-anthraquinone and SDS and CTAB separately in aqueous solution at physiological pH (= 7.4).

References

1. C. Tan, H. Tasaka, K. P. Yu, M. L. Murphy, D. A. Karnofsky, *Cancer* 20 (1967) 333–353.
2. A. DiMarco, G. Cassinelli, F. Arcamone, *Cancer Treat. Rep.* 65 (Suppl. 4) (1981) 3–8.
3. F. Arcamone, G. Cassinelli, G. Fantini, et al. *Biotechnol. Bioeng.* 11 (1969) 1101–1110.
4. A. DiMarco, M. Gaetani, B. Scarpinato, *Cancer Chemother. Rep.* 53 (1969) 33–37.
5. C. E. Myers, E. G. Mimnaugh, G. C. Yeh, B. K. Sinha, Biochemical mechanisms of tumor cell kill by the anthracyclines, In: J. W. Lown, (editor), *Anthracycline and Anthracenedione-based anticancer agents*, Elsevier, Amsterdam, (1988) pp 527-569.
6. L. Gianni, B. Corden, C. E. Myers, The biochemical bases of anthracycline toxicity and antitumor action. In: E. Hodgson, J. R. Bend, R. M. Philipot, (editors), *Rev. BiochemToxicol*, Vol.5, Elsevier, Amsterdam, (1983) pp 1-82.
7. V. Bonfante, G. Bonadonna, F. Villani, A. Martini, *Recent Results Cancer Res.* 74 (1980) 192–199.

8. V. Bonfante, L. Ferrari, F. Villani, G. Bonadonna, *Invest New Drugs*. 1 (1983) 161–168.
9. A. Vecchi, F. Spreafico, M. Sironi, M. Cairo, S. Garattini, *Eur. J. Cancer*. 16 (1980) 1289–1296.
10. T. J. Powles. *Eur. J. Cancer Care, (Engl)* 6 (1997) 1–3.
11. T. Šimůnek, M. Štěřba, O. Popelová, M. Adamcová, R. Hrdina, V. Geršl, *Pharmacol. Rep.* 61 (2009) 154–171.
12. E. Hefti, J. G. Blanco, *Cardiovasc. Toxicol.* 16 (2016) 5–13.
13. W. Priebe, R. Perez-Soler, *Pharmacol. Ther.* 60 (1993) 215–234.
14. H. M. Abdallah, A. M. Al-Abd, R. S. El-Dine, A. M. El-Halawany, *J. Adv. Res.*, 6 (2015) 45–62.
15. F. D. Umov, *Ann NY Acad Sci* 983 (1) (2003) 5-21.
16. F. Meyer-Losic, J. Quinonero, V. Dubois, B. Alluis, M. Dechambre, M. Michel, F. Cailler, A. -M. Fernandez, A. Trouet, J. Kearsey, *J. Med. Chem.* 49 (2006) 6908-6916.
17. J. Nadas, D. Sun, *Expert Opin. Drug Discov.* 1(6) (2006) 549-568.
18. K. Reszka, P. Kolodziejczyk, J. A. Hartley, W. D. Wilson, J. W. Lown, *Anthracycline and Anthracenedione-based anticancer agents*, Elsevier Press , Amsterdam, (1998), pp. 401-405.
19. J. Blasiak, E. Gloc, M. Warszawski, *Acta Biochim. Polonica* 49 (1) (2002) 145-155.
20. D. Patel, P. Pouna, S. Bonoron-Adele, J. Robert, *Anticancer Drugs* 10 (7) (1999) 671-676.
21. G. Minotti, P. Menna, E. Salvatorelli, G. Cairo, L. Gianni, *Pharmacol. Rev.* 56 (2) (2004) 185-229.
22. D. A. Gewirtz, *Biochem. Pharmacol.* 57 (7) (1999) 727-741.
23. G. E. Kellogg, J. N. Scarsdale, F. A. Fornari, *Nucleic Acids Res.* 26 (20) (1998) 4721-4732.
24. H. M. Zhang, N.Q. Li, *J. Pharm. Biomed. Anal.* 22 (1) (2000) 67-73.

25. J. B. Chaires, Molecular recognition of DNA, in: *Advances in DNA Sequence-specific agents*, L. H. Hurley, J. B. Chaires, (editors), Greenwich, CT: JAI press, Vol 2, (1996) pp 141-167.
26. A. H.-J. Wang, Structure-activity studies of anthracycline –DNA complexes. In: *Molecular Aspects of Anticancer Drug-DNA Interactions*, S. Neidle, M. Waring,(editors) Vol 1, Boca Raton, FL: CRC Press, (1993) pp 32-53.
27. M. Gigli, S. M. Doglia, J. M. Millet, L. Valentini, M. Manfait, *Biochim. Biophys. Acta* 950(1) (1988) 13-20.
28. F. Belloc, F. Lacombe, P. Dumain, F. Lopez, P. Bernard, M. R. Boisseau, J. Reifers *Cytometry* 13 (8) (1992) 880-885.
29. K. Studzian, M. Wasowska, M. K. Piestrzeniewicz, D. Wilmanska, L. Szmigiero, *Neoplasma* 48 (5) (2001) 412-418.
30. F. Leng, G. H. Leno, *J. Cell. Biochem.* 64 (3) (1997) 476-491.
31. K. E. van Holde, *Chromatin*, Springer-Verlag, New York, 1988.
32. A. Rabbani, M. Iskandar, J. Ausio, *J. Biol. Chem.* 274 (26) (1999) 18401-18406.
33. T. K. Lee, T. C. Lau, I. O. Ng, *Cancer Chemother. Pharmacol.* 49 (2002) 78-86.
34. J. Raju, P. Coralie, W. Hung-Yi, *J. Biol. Chem.* 272 (9) (1997) 5828-5832.
35. B. Kalyanaraman, J. Joseph, S. Kalivendi, S. Wang, E. Konorev, S. Kotamraju, *Mol. Cell. Biochem.* 234 (2002) 119-124.
36. B. Kalyanaraman, K. M. Morehouse, R. P. Mason, *Arch. Biochem. Biophys.* 286 (1) (1991) 164-170.
37. J.V.McGowan, R. Chung, A. Maulik, I. Piotrowska, J. M. Walker, D. M. Yellon, *Cardiovasc. Drugs.Ther.* 31 (2017) 63–75.
38. R. Abraham, R. L. Bassar, M. D. Green, *Drug Saf.* 15 (6) (1996) 406-429.
39. G. P. Stathopoulos, N. A. Malamos, I. Dontas, G. Deliconstantinos, D. Perra-Kotsarelis, P. E. Karayannacos, *Anticancer Res.* 18 (6A) (1998) 4387-4392.

40. G. Bonadonna, S. Monfardini, M. De Lena, F. Fossati-Bellani, G. Beretta. *Cancer Res.* 30 (1970) 2572–2582.
41. D. T. Vincent, Y. F. Ibrahim, M. G. Espey, Y. J. Suzuki, *Cancer Chemother. Pharmacol.* 72 (2013) 1157–1168.
42. M. Štěrba, O. Popelová, A. Vávrová, E. Jirkovský, P. Kovaříková, V. Geršl, T. Šimůnek, *Antioxid. Redox Signaling*, 18 (2013) 899–929.
43. J. S. Dickey, V. A. Rao, *Curr. Mol. Med.* 12 (2012) 763–771.
44. G. Falcone, W. Filippelli, B. Mazzeola, R. Tufano, P. Mastronardi, A. Filippelli, L. Berrino, F. Rossi, *Life Sci.* 63 (17) (1998) 1525–1532.
45. G. F. Samelis, G. P. Stathopoulos, D. Kotsarelis, I. Dontas, C. Frangia, P. E. Karayannacos, *Anticancer Res.* 18 (5A) (1998) 3305–3309.
46. K. B. Wallace, *Cardiovasc. Toxicol.* 7 (2007) 101–107.
47. A. Mordente, E. Meucci, A. Silvestrini, G. E. Martorana, B. Giardina, *Adv. Exp. Med. Biol.* 942 (2012) 385–419.
48. P. Menna, O. Gonzalez Paz, M. Chello, E. Covino, E. Salvatorelli, G. Minotti, *Expert Opin. Drug Saf.* 11 (1) (2012) S21–S36.
49. F. Zorzato, G. Salviati, T. Facchinetti, P. Volpe, *J. Biol. Chem.* 260 (12) (1985) 7349–7355.
50. C. Ferraro, L. Quemeneur, A. F. Prigent, C. Taverne, J. P. Revillard, N. Bonnefoy-Berard, *Cancer Res.* 60 (7) (2000) 1901–1907.
51. N. Maestre, T. R. Tritton, G. Laurent, J. P. Jaffrezou, *Cancer Res.* 61 (6) (2001) 2558–2561.
52. L. Wojnowski, B. Kulle, M. Schirmer, G. Schlüter, A. Schmidt, A. Rosenberger, S. Vonhof, H. Bickeböller, M. R. Toliat, E.-K. Suk, M. Tzvetkov, A. Kruger, S. Seifert, M. Kloess, H. Hahn, M. Loeffler, P. Nürnberg, M. Pfreundschuh, L. Trümper, J. Brockmöller, G. Hassenfuss, *Circulation*, 112 (2005) 3754–3762.

53. R. Kizek, V. Adam, J. Hrabeta, T. Eckschlager, S. Smutny, J. V. Burda, E. Frei, M. Stiborova, *Pharmacol. Ther.* 133 (2012) 26–39.
54. A. Mordente, E. Meucci, A. Silvestrini, G. E. Martorana, B. Giardina, *Curr. Med. Chem.* 16 (2009) 1656–1672.
55. E. Barry, J. A. Alvarez, R. E. Scully, T. L. Miller, S. E. Lipshultz, *Expert Opin. Pharmacother.* 8 (2007) 1039–1058.
56. F. S. Carvalho, A. Burgeiro, R. Garcia, A. J. Moreno, R. A. Carvalho, P. J. Oliveira, *Med. Res. Rev.* 34 (1) (2014) 106-135.
57. Y. Octavia, C. G. Tocchetti, K. L. Gabrielson, S. Janssens, H. J. Crijns, A. L. Moens, J. *Mol. Cell. Cardiol.* 52(6) (2012) 1213-1225.
58. Y.W.Zhang, J. J. Shi, Y. J. Li, L. Wei, *Arch. Immunol. Ther. Exp.*, 57 (6) (2009) 435-445.
59. K. Renu, V. G. Abilash, P. B. T. Pichiah, *Eur. J. Pharmacol.* 818 (2018) 241-253.
60. K. Nysom, K. Holm, S. R. Lipsitz, S. M. Mone, S. D. Colan, E. J. Orav, S. E. Sallan, J. H. Olsen, H. Hertz, J. R. Jacobsen, S. E. Lipshultz, *J. Clin. Oncol.* 16 (2) (1998) 545–550.
61. S. E. Lipshultz, M. J. Adams, *J. Clin. Oncol.* 28 (2010) 1276–1281.
62. D. D. Von Hoff, M.W. Layard, P. Basa, H. L. Davis Jr., A .L. Von Hoff, M. Rozenzweig, F. M. Muggia, *Ann. Intern. Med.* 91(1979) 710-717.
63. S. M. Swain, F. S. Whaley, M. S. Ewer, *Cancer* 97 (11) (2003) 2869-2879.
64. M. Ryberg, D. Nielsen, G. Cortese, G. Nielsen, P. K. Andersen, *J. Natl. Cancer Inst.* 100 (2008) 1058-1067.
65. F. A. Babiker, L. J. De Windt, M. van Eickels, C. Grohe, R. Meyer, P. A. Doevendans, *Cardiovas. Res.* 53 (3) (2002) 709-719.
66. C. S. Hayward, R. P. Kelly, P. Collins, *Cardiovas. Res.* 46 (1) (2000) 28-49.
67. D. Camper-Kirby, S. Welch, A. Walker, I. Shiraishi, K. D. Setchell, E. Schaefer, J. Kajstura, P. Anversa, M. A. Sussman, *Circ. Res.* 88 (10) (2001) 1020-1027.

68. T. Pelzer, M. Schumann, M. Neumann, T. de Jager, M. Stimpel, E. Serfling, L. Neyses, *Biochem. Biophys. Res. Commun.* 268 (1) (2000) 192-200.
69. A. Leri, A. Malhotra, C. C. Liew, J. Kajstura, P. Anversa, *J. Mol. Cell Cardiol.* 32 (3) (2000) 385-390.
70. K. J. Davis, J. H. Doroshov, *J. Biol. Chem.* 261 (7) (1986) 3060-3067.
71. R. B. Weiss, *Semin.Oncol.* 119 (6) (1992) 670-686.
72. A. M. Casazza, *Cancer Treat. Rep.* 70 (1986) 43-49.
73. S. Wadler, J. Z. Fuks, P. H. Wiernik, *J. Clin. Pharmacol.* 26 (1986) 491- 509.
74. F. Arcamone, S. Penco, *Gann. Monograph. on Canc. Res.* 36 (1989) 81-94.
75. C. J. Poole, H. M. Earl, L. Hiller, J. A. Dunn, S. Bathers, R. J. Grieve, D. A. Spooner, R. K. Agrawal, I. N. Fernando, A.M. Brunt, S. M. O'Reilly, S. M. Crawford, D.W. Rea, P. Simmonds, J. L. Mansi, A. Stanley, P. Harvey, K. McADam, L. Foster, R. C. Leonard, C. J. Twelves, *N. Eng. J. Med.* 355 (2006) 1851–1862.
76. X. Li, S. Xu, Y. Tan, J. Chen, *Cochrane Database Sys. Rev.* 6 (2015) CD010432.
77. C. Linassier, C. Barin, G. Calais, S. Letortorec, J. L. Bremond, M. Delain, A. Petit, M. T. Georget, G. Cartron, N. Raban, L. Benboubker, R. Leloup, C. Binet, J. P. Lamagnere, P. Colombat, *Ann. Oncol.* 11 (10) (2000) 1289-1294.
78. J. Kapuscinski, Z. Daizynkiewicz, *Proc. Natl. Acad. Sci. USA* 83 (17) (1986) 6302-6306.
79. A. L. Elus, J. K. Randolph, B. R. Conway, D. A. Gewirtz, *Biochem. Pharmacol.* 39 (10) (1990) 1549-1556.
80. N. Chegini, A. R. Safa, *Cancer Lett.* 37 (3) (1987) 327-336.
81. O. Cantoni, P. Sestili, F. Cattabeni, C. Geroni, F.C Giuliani, *Cancer Chemother. Pharmacol.* 27 (1990) 47-51.
82. J. E. Schwartz, S. E. Salmon. *Invest New Drugs* 5 (1987) 231-234.
83. F. Arcamone, *Cancer Res.* 45 (1985) 5995-5999.
84. M. Gosalvez, M. F. Blanco, C. Vivero, F. Valles, *Eur. J. Cancer*, 14 (11) (1978) 1185-1190.

85. P. Kolodziejczyk, A. Garnier-Suillerot, *Biochim. Biophys. Acta*, 926 (3) (1987) 249-257.
86. A. Kumbhar, S. Padhye, D. Ross, *BioMetals*, 9 (1995) 235–240.
87. A. Bartoszek, *Acta Biochim. Pol.* 49 (2002) 323–331.
88. B. Szachowicz-Petelska, Z. Figaszewski, W. Lewandowski, *Int. J. Pharm.* 222 (2001) 169–182.
89. A. Jabłońska-Trypuć, G. Świdorski, R. Krętowski, W. Lewandowski, *Molecules* 22 (7) (2017) 1106.
90. H. Beraldo, A. Garnier-Suillerot, L. Tosi, F. Lavelle, *Biochem.* 24 (2) (1985) 284-289.
91. M. M. L. Fiallo, A. Garnier-Suillerot, *Biochim. et Biophys. Acta* 840 (1) (1985) 91-98.
92. P. Das, C. K. Jain, S. Roychoudhury, H. K. Majumder, S. Das, *Chemistry Select* 1 (2016) 6623 – 6631.
93. T.-S. Ko, H. Y. Meang, M.-K. Park, I. -H. Park, I.-S. Park, B.-S. Kim, *Bull. Korean Chem. Soc.* 15 (5) (1994) 364-368.
94. S. Norn, H. Permin, E. Kruse, P. R. Kruse, *Dan Medicinhist Årboq.* 36 (2008) 21–40.
95. V. J. Ferrans, *Cancer Treat. Rep.* 62 (6) (1978) 955-961.
96. M. Frezza, S. Hindo, D. Chen, A. Davenport, S. Schmitt, D. Tomco, Q. P. Dou, *Curr. Pharm. Des.* 16 (16) (2010) 1813–1825.
97. P. Bruijninx, P. Sadler, *Curr. Opin. Chem. Biol.* 12 (12) (2008) 197–206.
98. R. kiraly, R. B. Martin, *Inorg. Chim. Acta* 67 (1982) 13-18.
99. H. Beraldo, A. Garnier-Suillerot, L. Tosi, *Inorg. Chem.* 22 (26) (1983) 4117-4124.
100. I. J. Mclellan, R. E. Lenkiski, *J. Am. Chem. Soc.* 106 (23) (1984) 6905-6909.
101. P. K. Dutta, J. A. Hutt, *Biochemistry* 25 (3) (1986) 691-695.
102. M. M. L. Fiallo, A. Garnier-Suillerot, *Biochemistry* 25 (4) (1986) 924-930.
103. T. Allman, R. E. Lenkiski, *J. Inorg. Biochem.* 30 (1) (1987) 35-43.
104. A. Pasini, *Inorg. Chim. Acta* 137 (1987) 123-124.

105. F. Capolongo, M. Giomini, A. M. Giuliani, B. Matzanke, U. Russo, A. Silvestri, A. Trautwein, R. Barbieri, *J. Inorg. Biochem.* 65 (2) (1997) 115-122.
106. M. M. Fiallo, H. Drechsel, A. Garnier-Suillerot, B. Matzanke, H. Kozlowski, *J. Med. Chem.* 42 (15) (1999) 2844-2851.
107. M. M. Fiallo, A. Garnier-Suillerot, B. Matzanke, H. Kozlowski, *J. Inorg. Biochem.* 75 (2) (1999) 105-115.
108. P.S. Guin, S. Das, P.C. Mandal, *J. Inorg. Biochem.* 103 (12) (2009) 1702–1710.
109. P.S. Guin, P.C. Mandal, S. Das. *J. Coord. Chem.* 65(4) (2012) 705-721.
110. S. Mukherjee Chatterjee, C. K. Jain, S. Singha, P. Das, S. Roychoudhury, H. K. Majumder, S. Das, *ACS Omega* 3 (2018) 10255–10266.
111. C. Santini, M. Pellei, V. Gandin, M. Porchia, F. Tisato, C. Marzano, *Chem. Rev.* 114(1) (2014) 815–862.
112. E. Fantine, A. Garnier-Suillerot, *Biochim. Biophys. Acta* 856 (1) (1986) 130-136.
113. E. Gammella, F. Maccarinelli, P. Buratti, S.-Recalcati, G.-Cairo, *Front. Pharmacol.* 5 (2014) 25, doi.org/10.3389/fphar.2014.00025
114. M. Tachibana, M. Iwaizumi, S. Tero-kubota, *J. Inorg. Biochem.* 28 (1987) 131-138.
115. M. Tachibana, M. Iwaizumi, S. Tero-Kubota, *J. Inorg. Biochem.* 30 (2) (1987) 133-140.
116. M. Feng, Y. Yang, P. He, Y. Fang, *Spectrochim. Acta Part A* 56 (3) (2000) 581-587.
117. F. T. Greenway, J. C. Dabrowiak, *J. Inorg. Biochem.* 16 (2) (1982) 91-107.
118. T. B. Chaston, D. R. Richardson, *Am. J. Hematol.* 73(2003) 200-210.
119. J. L. Buss, M. Hermes-Lima, P. Ponka, Pyridoxal isonicotinoyl hydrazone and its analogues. In *Iron Chelating Therapy*. C. Hershko, (Ed.), Plenum Press: New York, 2002.
120. B. R. Reddy, R. A. Kloner, K. Przyklenk, *Free Rad. Biol. Med.* 7 (1989) 45-52.
121. P. A. Ward, J. S. Warren, G. O. Till, J. Varani, K. J. Johnson, *Bailliere's Clin. Haematol.* 2 (1989) 391-402.
122. K. J. Thompson, S. Shoham, J. R. Connor, *Brain Res. Bull.* 55 (2001) 155-164.

123. M. Gassen, M. B. Youdim, *Pharmacol. Toxicol.* 80(1997) 159-166.
124. P. Biemond, A. J. Swaak, H. G. van Eijk, J. F. Koster, *Free Rad. Biol. Med.* 4 (1988) 185-198.
125. N. Bachur, R. D. Friedman, R. G. Hollenbeck, *cancer Chemother. Pharmacol.* 12 (1984) 5-9.
126. C. E. Myers, L. Gianni, C. B. Simone, R. Klecker, R. Green, *Biochemistry* 21 (8) (1982) 1707-1712.
127. E. Gelvan, A. Samuni, *Cancer Res.* 48 (20) (1988) 5645-5649.
128. J. R. F. Muindi, B. K. Sinha, L. Gianni, C. E. Myers, *FEBS Lett.* 172 (2) (1984) 226-230.
129. B. F. Matzanke, E. Bill, C. Butzlaff, A.X. Trauwein, H. Winkler, C. Hermes, H.-F. Nolting, R. Barbieri, U. Russo, *Eur. J. Biochem.* 207 (2) (1992) 747-755.
130. A. Papakyriakou, A. Anagnostopoulou, A. Garnier-Suillerot, N. Katsaros, *Eur. J. Inorg. Chem.* (2002) 1146-1154.
131. P. Del Castillo, E. R. Llorente, A. Gomez, J. Gosalvez, V. J. Goyanes, J. C. Stockert, *Analyt. Quant. Cytol. Histol.* 12 (1) (1990) 11-20.
132. A. R. Llorente, P. Del Castillo, J. C. Stockert, *J. Microsc.* 155 (2) (1989) 227-230.
133. J. C. Stockert, A. R. Llorente, P. Del Castillo, A. Gomez, *Stain. Technol.* 65 (6) (1990) 299-302.
134. A. Juarranz, A. Villanueva, M. Cañete, S. Polo, V. Dominguez, J. C. Stockert, *Histochem. J.* 31 (1999) 201-208.
135. L.-J. Ming, *Paramagnetic Lanthanide(III) Ions as NMR Probes for Biomolecular Structure and Function.* In *Nuclear Magnetic Resonance of Paramagnetic Molecules*, G. N. La Mar, (Ed.), NATOASI, Kluwer: Dordrecht, The Netherlands, (1995).
136. L.-J. Ming, *Magn. Reson. Chem.* 31 (1993) S104-S109.
137. J.-C. G. Bunzli, G. R. Choppin, (Ed.), *Lanthanide Probes in Life, Chemical and Earth Science*, Elsevier, Amsterdam, (1989) pp 432
138. C. H. Evans, *Biochemistry of the Lanthanides*, Plenum Press, New York, (1990).

139. R. Lewin, K. G. Stern, D. M. Ekstein, L. Woidowsky, D. J. Laszlo, *J. Natl. Cancer Inst.* 14 (1953) 45-56.
140. J. Luo, J. Bethune, *Medical Univ.* 17 (1991) 137.
141. W. Xiangdong, Li-. J. Ming, *Inorg. Chem.* 37 (1998) 2255-2262.
142. X. Wei, L.-J. Ming, *Inorg. Chem.* 37 (1998) 2255-2262.
143. L.-J. Ming, X. Wei, *Inorg. Chem.* 33 (21) (1994) 4617-4618.
144. E. Pereira, M. M. Fiallo, A. Garnier-Suillerot, T. Kiss, H. Kozlowski, *J. Chem. Soc., Dalton Trans.* (Issue 3) (1993) 455-459.
145. M. J. Maroney, R. O. Day, T. Psyris, L. M. Fleury, J. Whitehead, *Inorg. Chem.* 28 (1989) 173-175.
146. S. S. Massoud, R. B. Jordan, *Inorg. Chem.* 30 (1991) 4851-4856.
147. E. G. Kiel, P. M. Heertjes, *J. Soc. Dyers Color.* 79 (1) (1963) 21-27.
148. H. D. Coble, H. F. Holtzclaw, *J. Inorg. Nucl.Chem.* 36 (5) (1974) 1049-1053.
149. C. A. Tsipis, E. G. Bakalbassis, *Can. J. Chem.* 60 (19) (1982) 2477-2483.
150. V. Y. Fain, B. E. Zaitsev, M. A. Ryabov, *Russian J. Coord. Chem.* 30 (2004) 360-364.
151. S. das, A. Saha, P. C. Mandal, *Talanta* 43 (1) (1996) 95-102.
152. P. Yang, H. Wang, F. Gao, B. Yang, *J. Inorg. Biochem.* 62 (2) (1996) 137-145.
153. H. Wang, P. Yang, Y. Tian, Z. Zbang, C. Zhao, *J. Inorg. Biochem.* 68 (2) (1996) 117-121.
154. S. Roy, P. Mondal, P. S. Sengupta, D. Dhak, R. C. Santra, S. Das, P. S. Guin, *Dalton Trans.* 44 (2015) 5428-5440.
155. P. Mondal, S. Roy, G. Loganathan, B. Manda, D. Dharumadurai, Md. A. Akbarsha, P. S. Sengupta, S. Chattopadhyay, P. S. Guin, *Biochem. Biophys. Rep.* 4 (2015) 312-323.
156. S. Roy, G. Loganathan, D. Dharumadurai, Md. A. Akbarsha, P. S. Guin, *J. Coord. Chem.* 70 (12) (2017) 2128-2147.
157. S. Roy, P. S. Guin, *J. Electrochem. Soc.* 162 (3) (2015) H124-H131.

158. S. Roy, P. S. Guin, *J. Mol. Liq.* 211 (2015) 846–853.
159. S. Banerjee, S. Roy, D. Dharumadurai, B. Perumalsamy, R. Thirumurugan, S. Das, A. P. Chattopadhyay, P. S. Guin, *ACS Omega* 7 (2022) 1428–1436.
160. A. Das, S. Roy, P. Mondal, A. Datta, K. Mahali, G. Loganathan, D. Dharumadurai, P. S. Sengupta, Md A. Akbarsha, P. S. Guin, *RSC Adv.* 6 (2016) 28200-28212.
161. E. Bachmann, E. Weber, G. Zbinder, *Agents Actions* 5 (4) (1975) 383-393.
162. D. Barasch, O. Zipori, I. Ringel, I. Ginsburg, A. Samuni, J. Katzhendler, *Eur. J. Med. Chem.* 34 (1999) 597-615.
163. Y. Kawakami, A. J. Hopfinger, *Chem. Res. Toxicol.* 3 (1990) 244-247.
164. F. C. de Abreu, P. A. de Ferraz, M. O. F. Goulart, *J. Brazilian Chem. Soc.* 13 (1) (2002) 19-35.
165. J. W. Lown, H. Chen, J. A. Plambeck, E. M. Acton, *Biochem. Pharmacol.* 31 (4) (1982) 575-581.
166. R. L. Blankespoor, E. L. Kusters, A. J. Post, D. P. Van Meurs, *J. Org. Chem.* 56 (4) (1991) 1609-1614.
167. A. Kumbhar, S. Padhye, D. Ross, *Biometals* 9 (3) (1996) 235-240.
168. A. Bartoszek, *Acta Biochim. Polonica* 49 (2) (2002) 323-331.
169. M. Uchimiya, A.T. Stone, *Chemosphere*.77 (2009) 451–458.
170. E. R. Price, S. C. Johnson, *Quinones: Occurrence, medicinal uses and physiological importance*, Nova Science Publishers, Inc., 2013.
171. E. A. Hillard, F.C. De Abreu, D.C.M. Ferreira, G. Jaouen, M.O.F. Goulart, C. Amatore, *Chem. Commun. (Issue 23)* (2008) 2612–2628.
172. P. S. Guin, S. Das, P. C. Mandal, *Inter. J. Electrochem.* 2011 (a review article) ID816202 [doi:10.4061/2011/816202].
173. R. A. Morton, Ed., *Biochemistry of Quinones*, Academic Press, New York, NY, USA, 1965.
174. M. Y. Okamura, G. Feher, *Ann. Rev. Biochem.* 61 (1992) 861–896.

175. J. A. Bautista-Martínez, I. González, M. Aguilar-Martínez, J. Electroanal. Chem. 573 (2) (2004) 289–298.
176. M.W. Lehmann, D.H. Evans, J. Electroanal. Chem. 500 (1) (2001) 12–20.
177. N. Gupta, H. Linschitz, J. Am. Chem. Soc. 119 (27) (1997) 6384–6391.
178. J. Q. Chambers, Electrochemistry of quinones, Quinonoid Compd.1 (1988) 719–757, 2010<https://doi.org/10.1002/9780470772119>.
179. V.P. Papageorgiou, A.N. Assimopoulou, E. A. Couladouros, D. Hepworth, K.C. Nicolaou, Angew. Chem. Int. Ed. 38 (1999) 270–300.
180. Z. F. Plyta, T. Li, V. P. Papageorgiou, A. S. Mellidis, A. N. Assimopoulou, E. N. Pitsinos, E. A. Couladouros, Bioorg. Med. Chem. Lett. 8 (1998) 3385–3390.
181. J. Chen, J. Xie, Z. Jiang, B. Wang, Y. Wang, X. Hu, Oncogene. 30 (2011) 4297–4306.
182. M. Volkova, R. Russell, Curr. Cardiol. Rev. 7 (2012) 214–220.
183. K. Kawamukai, J. Biosci. Bioeng. 95 (2002) 511–517.
184. M.Abe,A.Kubo,S.Yamamoto,Y.Hatoh,M.Murai,Y.Hattori,H.Makabe,T.Nishioka,H.Miyoshi,Biochemistry 47 (2008) 6260–6266.
185. S. Michalkiewicz, Bioelectrochemistry 73 (2008) 30–36.
186. A. Ausili, A. Torrecillas, F. Aranda, A. de Godos, S. Sánchez-Bautista, S. Corbalán-García, J. C. Gómez-Fernández, J. Phys. Chem. B112 (2008) 12696–12701.
187. A.Sharma, G. M. Soliman, N. Al-Hajaj, R. Sharma, D. Maysinger, A. Kakkar, Biomacromolecules 13 (1) (2012) 239–252.
188. F. Q. Alali, X. X. Liu, J. L. McLaughlin, J. Nat. Prod. 62 (1999) 504–540.
189. W. Ma, D. W. Li, T. C. Sutherland, Y. Li, Y. T. Long, H. Y. Chen, J. Am. Chem. Soc. 133 (2011) 12366–12369.
190. B. H. Lipshutz, T. Butler, A. Lower, J. Servesko, Org. Lett. 9 (2007) 3737–3740.
191. G. E. W. Wolstenholme, C. M. O'Connor, Science 134 (1961) 1064.
192. C. Costentin, M. Robert, J. M. Savéant, Chem. Rev. 110 (2010) PR1-PR40.

193. C. Léger, P. Bertrand, *Chem. Rev.* 108 (2008) 2379–2438.
194. Z. Y. Zhu, M. R. Gunner, *Biochemistry* 44 (2004) 82–96.
195. A. W. Rutherford, P. Faller, *Trends Biochem. Sci.* 26 (2001) 341–344.
196. P. Fromme, P. Jordan, N. Krauss, *Biochim. Biophys. Acta* 1507 (2001) 5–31.
197. W. A. Cramer, D. B. Knaff, in *Energy Transduction in Biological Membranes* (Ed.: C. R. Cantor), chap. 4, Springer, New York, NY, USA, 1990.
198. T. J. Monks, S. S. Lau, *Chem. Res. Toxicol.* 10 (1997) 1296–1313.
199. T. H. Porter, F. S. Skelton, K. Folkers, *J. Med. Chem.* 14 (1971) 1029–1033.
200. J. W. Lown, in *Reactive Oxygen Species in Chemistry, Biology and Medicine* (Ed.: A. Quintanilha), Plenum Press, New York, NY, USA (1988) 167–185.
201. E. Khadem, *Anthracycline Antibiotics*, Academic Press, New York, NY, USA, 1982.
202. G. Powis, *Free Radical Biol. Med.* 6 (1989) 63–101.
203. E. J. Land, C. A. Ramsden, P. A. Riley, *J. Photochem. Photobiol. B Biol.* 64 (2001) 123–135.
204. D. Schweinfurth, M. Zalibera, M. Kathan, C. Shen, M. Mazzolini, N. Trapp, J. Crassous, G. Gescheidt, F. Diederich, *J. Am. Chem. Soc.* 136 (2014) 13045–13052.
205. G. J. Gordillo, D.J. Schiffrin, *Faraday Discuss.* 116 (2000) 89–107.
206. R.L. Blankespoor, R. Hsung, D.L. Schutt, *J. Org. Chem.* 53 (1988) 3032–3035.
207. D.O. Wipf, K.R. Wehmeyer, R.M. Wightman, *J. Org. Chem.* 51 (1986) 4760–4764.
208. J. Q. Chambers, “Electrochemistry of Quinones,” in *The Chemistry of Quinonoid Compounds*, S. Patai, Z. Rappoport, Eds., Vol. 1, Ch. 14, Wiley, New York, NY, USA, 1974, pp. 737–791.
209. S.I. Bailey, I.M. Ritchie, *Electrochim. Acta* 30 (1985) 3–12.
210. S.I. Bailey, I.M. Ritchie, *J. Chem. Soc., Perkin Trans. 2* (5) (1983) 545.
211. G.M. Rao, J.W. Lown, J.A. Plambeck, *J. Electrochem. Soc.* 125 (4) (1978) 534–539.

-
212. C. Molinier-Jumel, B. Malfoy, J.A. Reynaud, G. Aubel-Sadron, *Biochem. Biophys. Res. Commun.* 84 (1978) 441–449.
213. R.P. Baldwin, D. Packett, T.M. Woodcock, *Anal. Chem.* 53 (1981) 540–542.
214. E.N. Chaney Jr., R.P. Baldwin, *Anal. Chem.* 54 (1982) 2556–2560.
215. K. Kano, T. Konse, N. Nishimura, T. Kubota, *Bull. Chem. Soc. Jpn.* 57 (9) (1984) 2383-2390.
216. S. G. Mairanovskii, “Catalytic Waves in Polarography“ B. M. Fabus and P. Zuman, translators, Plenum Press, New York, pp. 241-285, 1968.
217. I. Tachi, *Polarography*, Iswanami, Tokyo, pp. 357- 362, 1954.
218. Y. Hahn, H.Y. Lee, *Arch. Pharm. Res.* 27 (1) (2004) 31-34.
219. S. Zhang, K. Wu, S. Hu, *Anal. Sci.* 18 (10) (2002) 1089-1092.
220. J. Hu, Q. Li, *Anal. Sci.* 15 (1999) 1215-1218.
221. V. Kertesz, J. Q. Chambers, A. N. Mullenix, *Electrochim. Acta* 45 (7) (1999) 1095-1104.
222. C. Yi, M. Gratzl, *Biophys. J.* 75 (5) (1998) 2255-2261.
223. R. Gill, H. I. Stonehill, *J. Chem. Soc.* (1952) 1845-1857.
224. N. H. Furman, K. G. Stone, *J. Am. Chem. Soc.* 70 (9) (1948) 3055-3061.
225. F. C. Anson, B. Epstein, *J. Electrochem. Soc.* 115 (11) (1968) 1155-1158.
226. P. He, R. M. Crooks, L. R. Faulkner, *J. Phys. Chem.* 94 (3) (1990) 1135-1141.
227. A. J. Bird, L. R. Faulkner, *Electrochemical methods*, 2nd ed., Wiley, New York, 2001.
228. R. J. Froster, J. P. O’ Kelly, *J. Electroanal. Chem.* 498 (2001) 127-135.
229. Y. Tang, Y. Wu, Z. Wang, *J. Electrochem. Soc.* 148 (4) (2001) E133-E138.
230. H. Park, M. S.-M. Won, C. Cheong, Y.-B.Shim, *Electroanalysis* 14 (21) (2002) 1501-1507.
231. M. Quan, D. Sanchez, M. F. Wasylkiw, D. K. Smith, *J. Am. Chem. Soc.* 129 (42) (2007) 12847-12856.

232. G. March, S. Reisberg, B. Piro, M.-C. Pham, M. Delamar, V. Noel, K. Odenthal, D. B. Hibbert, J. J. Gooding, *J. Electroanal. Chem.* 622 (1) (2008) 37-43.
233. F. Cai, M. A. F. Luis, X. Lin, M. Wang, L. Cai, C. Cen, E. Biskup, *Mol. Clin. Oncol.* (11) (2019) 15-23.
234. E. Barry, J. A. Alvarez, R. E. Scully, T. L. Miller, S. E. Lipshultz, *Expert Opin. Pharmacother.* 8 (8) (2007) 1039-1058.
235. T. Kakutani, M. Senda, *Bull. Chem. Soc. Jpn.* 53 (1980) 1942-1948.
236. O. Vajdle, J. Zbiljić, B. Tasić, D. Jović, V. Guzsvány, A. Djordjevic, *Electrochimica Acta* 132 (2014) 49–57.
237. D. Pletcher, H. Thompson, *J. Chem. Soc., Faraday Trans.* 94 (1998) 3445-3450.
238. M. E. Peover, J. D. Davies, *J. Electroanal. Chem.* 6 (1963) 46-53.
239. O. H. Müller, *J. Am. Chem. Soc.* 62 (1940) 2434-2441.
240. I. M. Kolthoff, J. J. Lingane, *Polarography*; Interscience: New York, p344, 1941.
241. I. M. Kolthoff, E. F. Orlemann, *J. Am. Chem. Soc.* 63(1941) 664-667.
242. J. C. Abbott, J. W. Collat, *Anal. Chem.* 35 (1963) 859-863.
243. R. T. Robertson, B. D. Pendley, *J. Electroanal. Chem.* 374 (1994) 173-177.
244. Y. Sato, M. Fujita, F. Mizutani, K. Uosaki, *J. Electroanal. Chem.* 409(1996) 145-154.
245. Y.-B. Shim, S.-M. Park, *J. Electroanal. Chem.* 425 (1997) 201-207.
246. M. F. Marcus, M. D. Hawley, *Biochim. Biophys. Acta* 222 (1) (1970) 163-173.
247. A. Ashnagar, J. M. Bruce, P. L. Dutton, R. C. Prince, *Biochim. Biophys. Acta* 801(3) (1984) 351-359.
248. M. Oyama, F. Marken, R. D. Webster, J. A. Cooper, R. G. Compton, S. Okajaki, *J. Electroanal. Chem.* 451 (1998) 193–201.
249. M. Aguilar-Martínez, G. Cuevas, M. Jiménez-Estrada, I. González, B. Lotina-Hennsen, N. Macías-Ruvalcaba, *J. Organomet. Chem.* 64 (10) (1999) 3684-3694.

250. M. Shamsipur, A. Siroueinejad, B. Hemmateenejad, A. Abbaspour, H. Sharghi, K. Alizadeh, S. Arshadi, *J. Electroanal. Chem.* 600 (2) (2007) 345-358.
251. M. W. Lehmann, D. H. Evans, *J. Electroanal. Chem.* 500 (2001) 12-20.
252. T. D. Chung, D. Choi, S. K. Kang, S. K. Lee, S.-K. Chang, H. Kim, *J. Electroanal. Chem.* 396 (1995) 431-439.
253. D. Ajloo, B. Yoonesi, A. Soleymanpour, *Int. J. Electrochem. Sci.* 5 (2010) 459 – 477.
254. J.V. Milić, T. Schneeberger, M. Zalibera, F. Diederich, C. Boudon, L. Ruhlmann, *Electrochim. Acta* 313 (2019) 544-560.
255. B. R. Eggins, J.Q. Chambers, *J. Electrochem. Soc.* 117 (2) (1970) 186-192.
256. M. Quan, D. Sanchez, M. F. Wasylkiw, D. K. Smith, *J. Am. Chem. Soc.* 129 (2007) 12847-12856.
257. T. Nagaoka, S. Oekzaew, T. Fujinaga, *J. Electroanal. Chem.* 133 (1982) 89-99.
258. C.O. Rangel-Yagui, A. Pessoa -Jr., L.C. Tavares, *J. Pharm. Pharm. Sci.* 8 (2005) 147–165.
259. S. Ramotowska, D. Zarzeczańska, I. Dąbkowska, A. Wcisło, P. Niedziałkowski, E. Czaczyk, B. Grobelna, T. Ossowski, *Spectrochim. Acta A Mol. Biomol.* 222 (5) (2019) 117226.
260. Cyrille Costentin, *Chem. Rev.* 108 (7) (2008) 2145–2179.
261. A. A. Isse, A. M. Abdurahman, E Vianello, *J. Chem. Soc. Perkin Trans. 2* (1996) 597-600.
262. M. Aguilar-Martínez, N. A. Macías-Ruvalcaba¹, J. A. Bautista-Martínez¹, M. Gómez, F. J. González, I. González, *Curr. Org. Chem.* 8 (2004) 1721-1738.
263. M. Gómez, F. J. González, I. González, *J. Electroanal. Chem.* 578 (2005) 193-202.
264. J. Gendell, W. R. Miller, Jr., G. K. Fraenkel, *J. Am. Chem. Soc.* 91(16) (1969) 4369–4380.
265. F. Valentini, F. Sabuzi, V. Conte, V. N. Nemykin, P. Galloni, *J. Org. Chem.* 86 (8) (2021) 5680–5689.

266. I. C. Monge-Romero, M. F. Suárez-Herrera, *Synth. Met.* 175 (2013) 36–41.
267. J. Glover, J.F. Pennock, G.A.J. Pitt, T. W. Goodwin, Richard Alan Morton, R.A. Morton, Ed., *Biochemistry of Quinones*, Academic Press New York, NY, USA, pp. 409-442, 1965.
268. A. Capon, R. Parsons, *Electroanal. Chem. Interfacial Electrochem.* 46 (1973) 215–222.
269. R. D. Rieke, T. Saji, N. Kujundzic, *J. Electroanal. Chem.* 102 (1979) 397–405.
270. K. J. A. Davies, J. H. Doroshov, *J. Biol. Chem.* 261 (1986) 3060-3067.
271. J. Tarasiuk, A. Garnier-Suillerot, E. Borowski, *Biochem.Pharmacol.* 38 (14) (1989) 2285-2289.
272. D. Jeziorek, D. Dyl, A. Liwo, W. Woźnicki, A. Tempczy, E. Borowski, *Anticancer Drug. Des.* 8 (3) (1993) 223-235.
273. D. Jeziorek, D. Dyl, A. Liwo, W. Woźnicki, A. Tempczy, E. Borowski, *Anticancer Drug. Des.* 9 (5) (1994) 435-448.
274. M. J. S. Dewar, E. G. Zoebish, E. F. Healey, J. J. P. Stewart. *J. Am. Chem. Soc.* 107 (13) (1985) 3902-3909.
275. A. R. Leach, *Molecular Modeling*, Longman, Essex, 1997.
276. C. Tosi, R. Fusco, G. Ranghino, *J. Mol. Struct. (Theochem)*, 134 (1986) 341-350.
277. R. Barthwal, P. Agrawal, A.N. Tripathi, U. Sharma, N. R. Jagannathan, G. Govil, *Arch. Biochem. Biophys.* 474 (2008) 48–64.
278. T. van Mourik, M. Bühl, M.P. Gaigeot, *Phil. Trans. R. Soc. A* 372 (2011) (2014).
279. M. B. Martins-Teixeira, I. Carvalho, *ChemMedChem.* 15 (11) (2020) 933-948.
280. M. Binaschi, M. Bigioni, A. Cipollone, C. Rossi, C. Goso, C. A. Maggi, G. Capranico, F. Animati, *Curr. Med. Chem. – Anti-Cancer Agents*, 1(2) (2001) (113-130).
281. J. Marinello, M. Delcuratolo, G. Capranico, *Int. J. Mol. Sci.* 19 (11) (2018) 3480.
282. F. Arcamone, G. Cassinelli, F. D. Matteo, S. Forenza, M. C. Ripamonti, G. Rivola, A. Vigevani, J. Clardy, T. Mc Cabe, *J. Am. Chem. Soc.* 102 (4) (1980) 1462-1463.

283. S. K. J. Arora, *Biomol. Struct. Dyn.* 3 (1985) 377-385.
284. P. S. Guin, P. C. Mandal, S. Das, *ChemPlusChem.* 77 (2012) 361–369.
285. S. Rossi, C. Tabolacci, A. Lentini, B. Provenzano, F. Carlomosti, S. Frezzotti, S. Beninati, *Anticancer Res.* 30 (2010) 445–449.
286. P. Das, C. K. Jain, S. K. Dey, R. Saha, A. D. Chowdhury, S. Roychoudhury, S. Kumar, H. K. Majumder, S. Das, *RSC Advances* 3 (2014) 59344–59357.
287. P. Das, D. Bhattacharya, P. Karmakar, S. Das, *RSC Adv.* 5 (2015) 73099–73111.
288. B. Mandal, H. K. Mondal, S. Das, *Biochem. Biophys. Res. Commun.* 515 (2019) 505–509.
289. S. Das, A. Saha, P. C. Mandal, *J. Radioanal. Nucl. Chem.* 196 (1996) 57–63.
290. H. Wang, E. Hua, P. Yang, *Talanta* 42 (1995) 1519–1524.
291. P. Yang, H. Wang, F. Gao, B. Yang, *J. Inorg. Biochem.* 62 (1996) 137–145.
292. T. Italia, D. I. Liegro, A. Cestelli, B. F. Matzanke, E. Bill, A. X. Trautwein, *BioMetals* 9 (1996) 121–130.
293. M. Kadarkaraisamy, D. Mukjerjee, C. C. Soh, A. G. Sykes, *Polyhedron* 26 (2007) 4085–4092.
294. M. Di Vaira, P. Orioli, F. Piccioli, B. Bruni, L. Messori, *Inorg. Chem.* 42 (2003) 3157–3159.
295. A. Jabłońska-Trypuć, G. Świdorski, R. K. Krętowski, W. Lewandowski, *Molecules* 22 (7) (2017) 1106.
296. T. A. Romyantseva, A. A. Alekseeva, M. A. Tkachenko, *Rus. J. Gen. Chem.* 90 (2020) 1660–1663.
297. S. Du, J. Feng, X. Lu, G. Wang, *Dalton Trans.* 42 (2013) 9699–9705.
298. H. Yuan, B. Cheng, J. Lei, L. Jiang, Z. Han, *Nat. Commun.* 12 (2021) 1835.
299. S. Roy, P. S. Sengupta, P. S. Guin, *Chem. Phys. Lett.* 694 (2018) 7–13.

300. J. B. Foresman, A. Frish, Exploring Chemistry with Electronic Structure Methods, Gaussian, Inc., Pittsburgh, PA, USA (2000), p.64.
301. O. Čudina, J. Brborić; I. Janković; K. Karljiković-Rajić; S. Vladimirov, Colloids Surf. B: Biointerfaces 65 (2008) 80–84.
302. S. Schreier, S. V.P. Malheiros, E. de Paula, Biochim. Biophys. Acta 1508 (2000) 210-234.
303. W. Caetano, M. Tabak, Spectrochim.Acta, Part A 55 (1999) 2513–2528.
304. N. Erdinc, S. Göktürk, M. Tunçay, J Pharm Sci, 93 (2004) 1566–1575.
305. H. Chakraborty, M. Sarkar, Biophys. Chem. 117 (2005) 79–85.
306. O. Čudina, K. Karljikovic-Raji, I. Ruvarac-Bugarci, I. Jankovic, Colloids and Surfaces A: Physicochem. Eng. Aspects 256 (2005) 225–232.
307. F. Akhtar, Md. A. Hoque, Md. A. Khan, J. Chem. Thermodyn. 40 (2008) 1082–1086.
308. J.B.F.N. Engberts, D. Hoekstra, Biochim.Biophys. Acta 1241 (1995) 323–340.
309. J. Xi, R. Guo, J. Pharm. Biomed. Anal. 43 (1) (2007) 111–118.
310. W. Sun, C. K. Larive, M. Z. Southard, J. Pharm. Sci. 92 (2) (2003) 424–435.
311. E. Santa, Z. S. Santa, Pharmazie 53 (1998) 109–112.
312. M. N. Jones, D. Chapman, Micelles, monolayers and biomembranes. Wiley-Liss, New York, 1995.
313. M. J. Rosen, Surfactants and interfacial phenomena, 2ed., John Wiley & Sons, New York, 1989.
314. J. N. Israelachvili, Intermolecular and Surface Forces, Academic Press, London, 1986.
315. J. H. Fendler, Membrane Mimetic Chemistry, Wiley-Inter- Science, New York, 1982.
316. C. Tanford, The Hydrophobic Effect, John Wiley and Sons, New York, 1980.
317. P. Mukerjee, J. Pharm. Sci. 63 (1974) 972- 981.
318. R. Nagarajan, E. Ruckenstein, Langmuir 7 (1991) 2934-2969.
319. J. R. Ernandes, H. Chaimovich, S. Schreier, Chem. Phys. Lipids 18 (1977) 304-315.

-
320. S. Schreier, J. R. Ernandes, I. M. Cuccovia, H. Chaimovich, J. Magn. Reson. 30 (1978) 283-298.
321. D. Nieciecka, A. Krolikowska, P. Krynski, Electrochim. Acta 165 (2015) 430–442.
322. W. Caetano, M. Tabak, J. Colloid Interface Sci. 225 (2000) 69–81.
323. V. P. Torchilin, J. Control. Release 73 (2001) 137–172.
324. A. T. Florence, N. Hussain, Adv. Drug Deliv. Rev. 50 (2001) S69–S89.
325. H. Cabral, K. Kataoka, J. Controlled Release 190(2014) 465-476.
326. X. Li, Y. Yu, Q. Ji, L. Qiu, Nanomedicine 11 (1) (2015) 175-184.
327. R. Basak, R. Bandyopadhyay, Langmuir 29 (2013) 4350-4356.
328. C. Saha, A. Kaushik, A. Das, S. Pal, D. Majumder, Cancer Treatment. PLOS ONE, 11 (5) (2016) e0155710.
329. K. Kurzatowska, M. A. Pazos, J. I. Herschkowitz, M. Hepel, Int. J. Mol. Sci. 22 (2021) 1362.
330. G. P. Van Balen, C. M. Martinet, G. Caron, G. Bouchard, M. Reist, P. A. Carrupt, R. Fruttero, A. Gasco, B. Testa, Med. Res. Rev. 24 (2004) 299-324.
331. R. Pignatello, T. Musumeci, L. Basile, C. Carbone, G. Puglisi, J. Pharm. Bio Allied Sci. 3 (1) (2011) 4-14.
332. A. M. Seddon, D. Casey, R.V. Law, A. Gee, R.H. Templer, O. Ces, Chem. Soc. Rev. 38 (9) (2009) 2509-2519.
333. I. D. Pogozeva, S. Tristram-Nagle, H. I. Mosberg, A. L. Lomize, Biochim. Biophys. Acta 1828 (11) (2013) 2592-2608.
334. B. Alberts, A. Johnson, J. Lewis, et al., Molecular Biology of the Cell, fourth ed., Garland Science, New York, 2002.
335. M. E. Dalmora, S.L. Dalmora, A.G. Oliveira, Int. J. Pharm. 222 (2001) 45-55.
336. C.O. Rangel-Yagui, H.W. L. Hsu, A. I. Pessoa Jr, L. C. Tavares, Braz. J. Pharm. Sci. 41 (2005) 237-246.

337. A. Datta, S. Roy, P. Mondal, P. S. Guin, *Journal of Molecular Liquids* 219 (2016) 1058–1064.
338. J. D. Dignam, X. Qu, J. Ren, J. B. Chaires, *J. Phys. Chem. B* 111 (39) (2007) 11576–11584.
339. M. Enache, I. Anghelache, E. Volanschi, *Int. J. Pharm.* 390 (2010) 100–106.
340. A. M. Toader, P. Oancea, M. Enache, *Acta Chim. Slov.* 67 (2020) 629–637.
341. M. Enache, A. M. Toader, M. I. Enache, *Molecules* 21 (10) (2016) 1356.
342. M. Enache, A. M. Toader, *J. Surfact. Deterg.* 21 (2018) 31–41.
343. M. Enache, E. Volanschi, *J. Pharm. Sci.* 100 (2) (2011) 558–565.

CHAPTER 3

Genesis and Scope of the Research

Anthracycline antibiotics adriamycin (doxorubicin), daunorubicin (daunomycin), aclacinomycin, carminomycin, nogalamycin, actinomycin-D, mitoxantrone, etc. are used in clinics in the treatment of various forms of human cancers since 1970s. However, the principal drawback of using anthracyclines as anticancer agents includes their cardiotoxic nature and high cost. For quite some time now, various efforts are on to identify cheap and efficient analogues as substitutes [1-8]. Earlier studies showed that the hydroxy-9,10-anthraquinone moiety present in anthracyclines is the seat of all biochemical and biophysical interactions and that in many studies, anthraquinone analogues or their derivatives were used as models for anthracyclines [8-15]. The drugs produce superoxide radical anion through several enzymatic reduction processes that are responsible for toxic side effects [16-18]. Earlier studies established the fact that sugar moiety present in the drugs assist in recognition of cancer cells [3, 19-22]. However, presence of the sugar moiety on the aliphatic side chain, connected to the hydroxy-9,10-anthraquinone unit in the drug makes them very costly and it becomes extremely difficult for many to continue treatment with these drugs. The problem is aggravated for people of economically marginalized families, particularly if they are from developing nations. Though there are wide applications of anthracyclines in cancer chemotherapy the two aspects mentioned above are really unfortunate and require serious consideration. This is discussed in *Chapter 2, Section 2.1*.

Though many hydroxy and amino hydroxy anthraquinones imitate a lot of the biochemical and biophysical actions of established anthracyclines, still there is a lot to be done. The focus of the present work was to evaluate whether amino hydroxy-9,10-anthraquinones taken in the form of sodium 3-amino-2-hydroxy-9,10-anthraquinone-1-sulphonate and its metal complexes and 1-amino-4-hydroxy-9,10-anthraquinone along with its Co^{III} complex, that are less expensive, could provide feasible alternatives to anthracycline anticancer drugs.

Complex formation of anthracyclines with metal ions modifies the anthraquinone moiety and resists formation of superoxide radical anion which might then definitely reduce toxicity imparted by the molecules. Many metal complexes of anthracyclines were tried in the treatment of different cancers and their increasing use has stimulated a growing interest on the role of different metal ions in such compounds [12, 16-18, 22-26]. In such metal complexes, one of the two quinone oxygen atoms is engaged in binding the metal ion while the other quinone oxygen is free. During the course of a chemical transformation, a quinone is converted to semiquinone. The electron at the semiquinone site is then quickly transferred to the metal centre, governed by electrode potential of $M^{n+}/M^{(n-1)+}$ and the stability of the lower oxidation state of the metal ion. These two factors decrease the possibility of superoxide radical anion formation appreciably that has an impact on decreasing cardiotoxicity considerably. As metal ions are good binding agents for cellular target DNA, complex formation results in better DNA targeting, apart from forming less cardiotoxic molecules [16-18]. This is discussed in *Chapter 2, Section 2.2*.

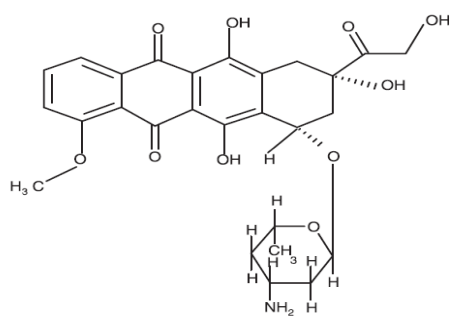
Redox properties of molecules determine their toxicity as well as chemotherapeutic efficiency [27-32]. In aqueous buffer, anthracycline drugs undergo a single step two-electron reduction [33, 34] while in non-aqueous media they undergo two steps of one-electron reduction, at first forming semiquinone and then quinone dianion [35-37]. Ionic strength, pH, polarity of the medium, presence of cations and anions from supporting electrolytes seriously influence reduction processes. This is discussed in *Chapter 2, Section 2.3*.

These days, studies on structure–activity relationships are gaining importance, more so in case of drug molecules, that leads to introduction of new medicines for various diseases. Hence various attempts have been made through several forms of studies [7, 15, 38] to build a proper understanding of structure–selectivity relationship that might have an impact in pharmaceutical-

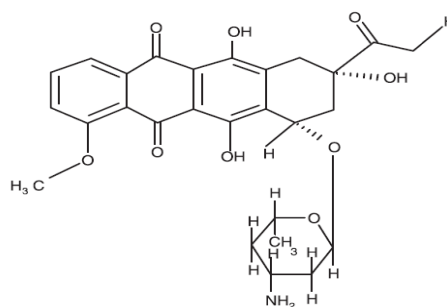
clinical domain. This may lead to the generation of a novel chemotherapeutic agent for treatment of cancer. Different computational and spectroscopic measurements were made to understand the electronic state of molecules [16-19]. These are discussed in *Chapter 2, Section 2.4*.

For the anthracyclines, among different mechanisms suggested for drug action intercalation into the DNA backbone was found to be the principal mode of drug action [43–45]. The mechanism of drug action is also related to interaction of the drug molecule with biological tissues through interaction with membranes at the molecular level [46–48]. Micellar systems have the ability to solubilize hydrophobic drugs [49-51] thereby increasing bio-availability. Hence, studies in micellar medium were performed as model systems to mimic bio-membranes and drug carriers in numerous drug delivery and drug targeting systems [52–54]. Interaction of drugs with surfactant micelles may then be treated as “model systems” for interaction of drugs with biological membranes. This is discussed in *Chapter 2, Section 2.1*.

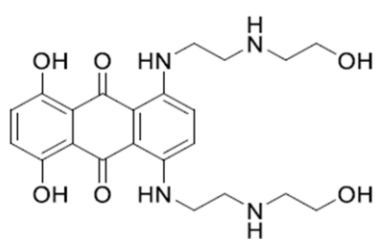
Keeping all these facts in mind, sodium 3-amino-2-hydroxy-9,10-anthraquinone-1-sulphonate, its Cu^{II} and Ni^{II} complexes and a Co^{III} complex of 1-amino-4-hydroxy-9,10-anthraquinone were tried in investigations related to biochemical and biophysical modes of action to see whether chosen compounds for this study mimic anthracycline anticancer agents. If it really does then it would be beneficial in developing cheaper, simpler alternatives in comparison to the costly anthracyclines. As already mentioned, experimental molecules closely resemble anthracyclines like adriamycin, daunorubicin and mitoxantrone. Further sodium 3-amino-2-hydroxy-9,10-anthraquinone-1-sulphonate is soluble in water and may find use under physiological conditions.



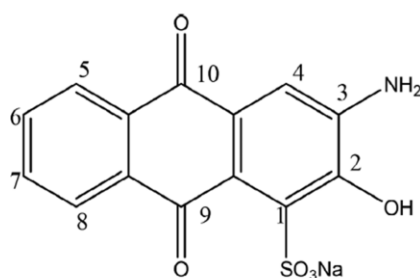
Adriamycin



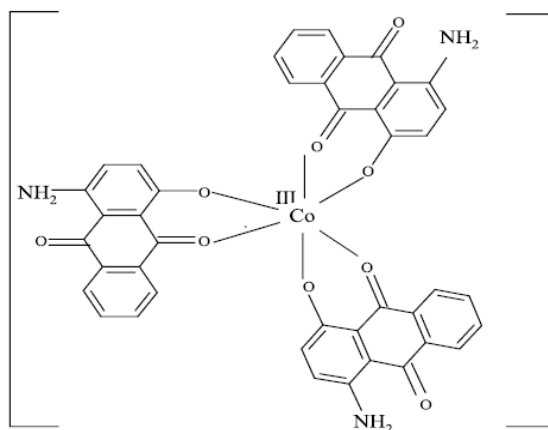
Daunorubicin



mitoxantrone



Sodium 3-amino-2-hydroxy-9,10-anthraquinone-1-sulphonate



Co^{III} complex of 1-amino-4-hydroxy-9,10-anthraquinone

Scheme 1: Some anthracycline anticancer drugs (adriamycin, daunorubicin, mitoxantrone), sodium 3-amino-2-hydroxy-9,10-anthraquinone-1-sulphonate and the Co^{III} complex of 1-amino-4-hydroxy-9,10-anthraquinone.

Studies on electrochemical behavior of sodium 3-amino-2-hydroxy-9,10-anthraquinone-1-sulphonate, its Cu^{II} and Ni^{II} complexes and the Co^{III} complex of 1-amino-4-hydroxy-9,10-anthraquinone would enable us to see any difference in activity between anthracyclines and their metal complexes. This may serve as a valuable tool in searching for a justification for lower cardiotoxicity due to complexes from an electrochemical point of view. Theoretical studies on experimental molecules may be fruitful in finding a structure – activity relationship.

Studies on interaction of sodium 3-amino-2-hydroxy-9,10-anthraquinone-1-sulphonate, its Cu^{II} and Ni^{II} complexes and a Co^{III} complex of 1-amino-4-hydroxy-9,10-anthraquinone with surfactant micelles may be useful in establishing permeation of molecules in different cancer cells. The mode of interaction of molecules with surfactant micelles, i.e. hydrophobic and hydrophilic mode of interaction might be fruitful in understanding interactions of such molecules with biological membrane. Finally, molecules were treated to various cancer cells to determine IC_{50} values and to see whether cell killing is by apoptosis or necrosis. The change in cellular morphology due to apoptosis was characterized by AO/EB staining method.

Therefore, theoretical and physicochemical studies on sodium 3-amino-2-hydroxy-9,10-anthraquinone-1-sulphonate, its Cu^{II} and Ni^{II} complexes and the Co^{III} complex of 1-amino-4-hydroxy-9,10-anthraquinone, their electrochemical behavior, interaction with surfactant micelles and different cancer cells could establish if such molecules, simpler analogues of anthracycline anticancer drugs would be cheaper but efficient alternatives to the costly anthracyclines.

References

1. D. Platel, P. Pouna, S. Bonoron-Adele, J. Robert, *Anticancer Drugs* 10 (7) (1999) 671-676.
2. J. Blasiak, E. Gloc, M. Warszawski ; *Acta Biochim. Pol.* 49 (1) (2002) 145-155.

3. L. Zhu, X. Cao, W. Chen, G. Zhang, D. Sun, P. G. Wang, *Bioorg. Med. Chem.* 13 (23) (2005) 6381-6387.
4. M. N. Preobrazhenskaya, A. N. Tevyashova, E. N. Olsufyeva, K.-F. Huang, H.-S. Huang, *J. Med. Sci.* 26(4) (2006) 119-128.
5. M. Grandi, G. Pezzoni, D. Ballinari, L. Capolongo, A. Suarato, A. Bargiotti, D. Faiardi, F. Spreafco, *Cancer Treat. Rev.* 17 (190) 133-138.
6. J. W. Lown, *Pharmac. Ther.* 60 (1993) 185-214.
7. M. B. Martins-Teixeira, I. Carvalho, *ChemMedChem.* 15 (11) (2020) 933-948.
8. B. M. Hoey, J. Butler, J. S. Lea, T. Sarna, *Free Rad. Res. Comms.* 5 (3) (1988) 169-176.
9. S. Das, A. Saha, P. C. Mandal, *Talanta* 43 (1) (1996) 95-102
10. S. Das, A. Saha, P. C. Mandal, *J. Radioanal. Nucl.Chem.* 196 (1) (1995) 57-63.
E. M. Malik, C. E. Mulle, *Med. Res. Rev.* 36(4) (2016) 705-748
12. S. Mukherjee Chatterjee, C. K. Jain, S. Singha, P. Das, S. Roychoudhury, H. K. Majumder, S. Das, *ACS Omega* 3 (2018) 10255–10266.
13. G. Pratesi, M. De Cesare, C. Caserini, P. Perego, L. Dal Bo, D. Polizzi, R. Supino, M. Bigioni, S. Manzini, E. lafrate, C. Salvatore, A. Casazza, F. Arcamone, F. Zunino, *Clin. Cancer Res.* 4 (11) (1998) 2833–2839.
14. V. Bonfante, L. Ferrari C. Brambilla, A. Rossi, F. Villani, F. Crippa, P. Valagussa, G. Bonadonna, *Eur. J. Cancer Clin. Oncol.* 22(11) (1986) 1379-1385.
15. M. Binaschi, M. Bigioni, A. Cipollone, C. Rossi, C. Goso, C. A. Maggi, G. Capranico, F. Animati, *Curr. Med. Chem. Anti-Cancer Agents*, 1(2) (2001) 113-130.
16. H. Beraldo, A. Gurnier-Suillerot, L. Tosi, F. Lavelle, *Biochemistry* 24 (2) (1985) 284-289.
17. M. M. L. Fiallo, A. Gurnier-Suillerot, *Biochemistry* 25 (4) (1986) 924-930.
18. M.M.L. Fiallo, A. Gurnier-Suillerot, *Biochim. Biophys. Acta* 840 (1) (1985) 91-98.
19. G. Capranico, M. Palumbo, S. Tinelli, M. Mabilia, A. Pozzan, F. Zunino, *J. Mol. Biol.* 235 (1994) 1218-1230.

20. G. Capranico, E. Butelli, F. Zunino, *Cancer Res.* 55 (2) (1995) 312-317.
21. W. Priebe, *Molecules* 5 (3) (2000) 299-301.
22. H. Beraldo, A. Garnier-Suillerot, L. Tosi, *Inorg. Chem.* 22 (26) (1983) 4117-4124.
23. S. Roy, G. Loganathan, D. Dharumadurai, Md. A. Akbarsha, P. S. Guin, *J. Coord. Chem.* 70 (12) (2017) 2128-2147.
24. P. S. Guin, S. Das, P. C. Mandal, *J. Inorg. Biochem.* 103 (12) (2009) 1702–1710.
25. P. Das, C. K. Jain, S. Roychoudhury, H. K. Majumder, S. Das, *Chemistry Select* 1 (2016) 6623 – 6631.
26. P. Das, C. K. Jain, S. K. Dey, R. Saha, A. D. Chowdhury, S. Roychoudhury, S. Kumar, H. K. Majumder, S. Das, *RSC Advances* 4 (2014) 59344–59357.
27. Y. Kawakami, A. J. Hopfinger, *Chem. Res. Toxicol.* 3 (1990) 244- 247
28. F. C. de Abreu, P. A. de Ferraz, M. O. F. Goulart, *J. Brazilian Chem. Soc.* 13 (1) (2002) 19-35.
29. J. Lown, H. Chen, J. A. Plambeck, *Biochem. Pharmacol.* 31(4) (1982) 575-581.
30. R. L. Blankespoor, E. L. Kusters, A. J. Post, D. P. VanMeurs, *J. Org. Chem.* 56 (4) (1991) 1609-1614.
31. A. Kumbhar, S. Padhye, D. Ross, *Biometals*, 9 (3) (1996) 235-240.
32. A. Bartoszek, *ActaBiochim. Polonica*, 49(2) (2002) 323-331.
33. D. O. Wipf, K. R. Wehmeyer, R. M. Wightman, *J. Org. Chem.*, 51(25) (1986) 4760-4764.
34. S. I. Bailey, I. M. Ritchie, *Electrochim. Acta* 30 (1) (1985) 3-12.
35. R. D. Reike, T. Saji, N. Kujundzic, *J. Electroanal. Chem.* 102 (3) (1979) 397-405.
36. M. D. Stallings, M. M. Morrison, D. T. Sawyer, *Inorg. Chem.* 20 (8) (1981) 2655-2660.
37. C. Rüssel, W. Jaenicke, *J. Electroanal. Chem.* 199 (1) (1986) 139-151.
38. J. Marinello, M. Delcuratolo, G. Capranico, *Int. J. Mol. Sci.* 19 (11) (2018) 3480.

39. P. Mondal, S. Roy, G. Loganathan , B. Mandal , D. Dharumadurai, Md. A. Akbarsha, P. S. Sengupta, S. Chattopadhyay, P. S. Guin, *Biochem. Biophys. Rep.*4 (2015) 312–323.
40. A. Das, S. Roy, P. Mondal, A. Datta, K. Mahali, G. Loganathan, D. Dharumadurai, P. S. Sengupta, Md.A. Akbarsha, P. S. Guin, *RSC Adv.*6 (2016) 28200–28212.
41. S. Roy, P. Mondal, P. S. Sengupta , D. Dhak, R. C. Santra, S. Das, P. S. Guin, *Dalton Trans.* 44 (2015) 5428-5440.
42. S. Roy, P. S. Sengupta, P. S. Guin, *Chem. Phys. Lett.* 694 (2018) 7–13
43. J. Nadas, D. Sun, *Exp. Opin. Drug Discov.*1 (6) (2006) 549-568.
44. M. Binaschi, M. Bigioni, A. Cipollone, C. Rossi, C. Goso, C.A. Maggi, G. Capranico, F. Animati, *Curr. Med. Chem.* 1 (2001) 113.
45. G. Minotti, P. Menna, E. Salvatorelli, G. Cario, L. Giani, *Pharmacol. Rev.* 56 (2) (2004) 185-229.
46. G. P. Van Balen, C. M. Martinet, G. Caron, G. Bouchard, M. Reist, P.A. Carrupt, R. Fruttero, A. Gasco, B. Testa, *Med. Res. Rev.* 24 (2004) 299-324.
47. R. Pignatello, T. Musumeci, L. Basile, C. Carbone, G. Puglisi, *J. Pharm. Bio Allied Sci.* 3 (1) (2011) 4-14.
48. A. M. Seddon, D. Casey, R.V. Law, A. Gee, R.H. Templer, O. Ces, *Chem. Soc. Rev.* 38 (9) (2009) 2509-2519.
49. J. Xi, R. Guo, *J. Pharm. Biomed. Anal.* 43 (1) (2007) 111-118.
50. N. Erdinc, S. Gokturk, M. Tuncay, *J. Pharm. Sci.* 93 (6) (2004) 1566-1576.
51. W. Sun, C. K. Larive, M. Z. Southard, *J. Pharm. Sci.* 92 (2) (2003) 424-435.
52. M. E. Dalmora, S. L. Dalmora, A. G. Oliveira, *Int. J. Pharm.* 222 (1) (2001) 45-55.
53. M. C. Jones, J. C. Leroux, *Eur. J. Pharm. Biopharm.* 48 (2) (1999) 101-111.
54. C. O. Rangel-Yagui, H. W. L. Hsu, A. I. Pessoa Jr, L. C. Tavares, *Braz. J. Pharm. Sci.* 41 (2005) 237-246.

CHAPTER 4

Experimental

4.1. Introduction

In the present study, complexes of sodium 3-amino-2-hydroxy-9,10-anthraquinone-1-sulphonate (AQSH) were prepared using Cu^{II} and Ni^{II} as metal ions. The complexes were characterized using different experimental and theoretical techniques. A Co^{III} complex of 1-amino-4-hydroxy-9,10-anthraquinone (QH) was also prepared and characterized. Spectroscopic and electrochemical behavior of all molecules used in the study was analyzed and different parameters that were required were evaluated. Interaction of the compounds used as a part of the study with micelles of sodium dodecyl sulphate (SDS), an anionic surfactant was carried out using UV-Vis spectroscopy. This was done as a model study to see whether the molecules used in the study have the potential or ability to permeate biological membranes. The molecules were also subjected to interaction with different cancer cells to estimate whether they are able to bring about apoptosis during the killing of such cells. Different assays like the cell viability assay, the acridine orange and ethidium bromide staining, Hoechst 33528 staining and JC-1 staining were used to characterize the mode of apoptosis and morphology of dead cells. This chapter mentions chemicals and apparatus that was required and used as a part of the study. It introduces and discusses various experimental techniques that were used.

4.2. Materials

2-Amino-3-hydroxy-9,10-anthraquinone (AQ) (95%) was bought from TCI, Japan while 1-amino-4-hydroxy-9,10-anthraquinone(QH) (>96%) was bought from Alfa Aesar, Germany. Both compounds were recrystallized using an equimolar mixture of ethanol and methanol before characterization and use. Experimental solutions of the compounds were stored in the dark owing to the high photo-responsive properties of the quinone moiety present in them. If the compounds are kept in the presence of light, unexpected decomposition of their experimental solution occurs that could lead to erroneous results in actual experiments. Analytical grade Sodium Sulphite (Na_2SO_3) and cupric oxide (CuO) were purchased from Merck, India that were used during the sulphonation of 2-amino-3-hydroxy-9,10-anthraquinone to produce sodium 3-amino-2-hydroxy-9,10-anthraquinone-1-sulphonate. $\text{CuCl}_2 \cdot 2\text{H}_2\text{O}$ (AR grade), $\text{NiCl}_2 \cdot 6\text{H}_2\text{O}$ (AR Grade) were purchased from Merck, India and BDH, London respectively. These were used to synthesize Cu^{II} and Ni^{II} complexes of sodium 3-amino-2-hydroxy-9,10-anthraquinone-1-sulphonate. Analytical grade $\text{CoCl}_2 \cdot 6\text{H}_2\text{O}$ was bought from Merck, India to prepare a Co^{III} complex of 1-amino-4-hydroxy-9,10-anthraquinone. pH of experimental solutions were adjusted using phosphate buffer prepared by using AR grade K_2HPO_4 and KH_2PO_4 (E-Merck, India). Analytical grade Sodium chloride (E-Merck, Germany) was used to maintain the ionic strength of the desired solution. Analytical grade KCl and tetrabutyl ammonium bromide [TBAB] from Spectrochem, India were used as supporting electrolytes in aqueous and non-aqueous media respectively during various electrochemical experiments. Dimethyl sulfoxide (DMSO) (99.0%, Spectrochem, India), N,N-Dimethyl formamide (DMF) (99.5%, Spectrochem, India) and acetonitrile (>99%, Spectrochem, India) were made anhydrous for use during electrochemical experiments. DMSO was dried using fused CaCl_2 for a minimum of 3-4 days and then distilled under reduced pressure [1]. In case of

DMF, such operation [2] was performed by initial distillation of DMF under reduced pressure providing an inert atmosphere through N₂ followed by re-distillation using dry K₂CO₃ (Merck) for at least one week. It was then further dried with dry P₂O₅ (Riedel) to get it in anhydrous form. Acetonitrile was purified [1, 3] by refluxing with KOH (Merck) for several hours followed by fractional distillation. Then it was refluxed with CaH₂ (Merck) for several hours followed by fractional distillation. The middle fraction was collected from each such distillation, ensuring removal of ammonia evolved during alkali treatment. Triple-distilled water was used during execution of each operation related to aqueous environment. Drug-surfactant interaction was studied by using SDS (AR grade) which was purchased from E-Merck, India.

4.3. Methods

4.3.1. Instruments

Using a Perkin-Elmer 2400 II elemental analyzer carbon, hydrogen and nitrogen analyses were done. FTIR analysis was performed on a Perkin Elmer RX-I spectrophotometer. Spectra were obtained using KBr pellets in the range 4000 cm⁻¹ – 400 cm⁻¹. Mass spectrum was recorded on Micromass Q-Tofmicro (Waters Corporation). Metal complexes were dissolved in anhydrous acetonitrile (solvent) and MS data was recorded using ESI positive mode. ¹H NMR of both ligands and their metal complexes were recorded on a Bruker Avance 300 NMR spectrometer using tetramethylsilane (TMS) as internal standard in DMSO-d₆ as solvent. PXRD data was collected on Bruker AXS D8 powder diffractometer using Cu-K α radiation ($\lambda = 1.548 \text{ \AA}$) generated at 40 kV and 40 mA. UV-visible spectroscopy was done on a spectrophotometer (Model: MECASYS OPTIZEN POP). Fluorescence spectra were recorded on FluoroMax-P (Horiba JobinYvon) fluorescence spectrophotometer. Experiments related to cyclic voltammetry

were performed using the conventional three-electrode system. Temperature was maintained at 25°C with the help of a circulating water bath. The working electrode, glassy carbon had a surface area of 0.07065 cm², the counter electrode was a platinum wire and reference electrode was Ag/AgCl, in satd. KCl. Using a potentiostat (Model DY2312, Digi-Ivy) all electrochemical studies were performed. The range of concentrations of different solutions were 5×10^{-5} moldm⁻³ to 1.5×10^{-3} moldm⁻³. Before a solution was subjected to cyclic voltammetry, it was degassed for nearly 30 minutes using highly pure Ar.

Experimental records coincided satisfactorily with corresponding equations and different parameters were predicted theoretically by using Grafit 3.0 and Origin 8.

4.3.2. Preparation and characterization of sodium 3-amino-2-hydroxy-9,10-anthraquinone-1-sulphonate (AQSH)

2-Amino-3-hydroxy-9,10-anthraquinone (AQ) was recrystallized from a methanol–ethanol mixture. 3.76 mmol of 2-amino-3-hydroxy-9,10-anthraquinone was taken in a round bottom flask containing 125 ml 4:1 ethanol–water mixture under nitrogen atmosphere at room temperature and stirred continuously until the compound dissolved completely. To it solid anhydrous Na₂SO₃ (2.8 mmol) was added and stirred for 10 min. 1.88 mmol CuO was introduced to the reaction mixture under refluxing conditions (Temperature of ~ 85°C and nitrogen atmosphere of approximately 30 hours). The deep pink coloured solution obtained was filtered. CuO and unreacted material got collected as residue. The filtrate was evaporated in air till volume of the experimental solution was 5 ml. It was again filtered to separate the product and subsequently dried in air. The product (AQSH) thus obtained was recrystallized from ethanol and dried in air. Elemental analysis, ESMS and NMR were done. Elemental analysis showed C, H and N contents to be 49.27%, 2.30 % and 4.13 % respectively (calculated values were C:

49.23%, H: 2.34%, N: 4.10%). Since quinone containing molecules are easily photo-bleached they were stored carefully. All solutions were prepared just before experiment. A standard solution of 1 mM AQSH in dimethylsulphoxide (DMSO) was made by weighing an exact amount of AQSH and subsequently diluted to desired strengths. 10% DMSO was used for studying AQSH–surfactant interaction. SDS (AR grade) was procured from E-Merck, India. Compounds were used in experiments without further purification.

4.3.3. Synthesis of Cu^{II} complex of sodium 3-amino-2-hydroxy-9,10-anthraquinone-1-sulphonate [Cu(AQS)₂]

The solid Cu^{II} complex of AQSH was prepared by mixing AQSH (0.58mmol) and CuCl₂.2H₂O (0.29mmol) in a molar ratio 2:1 in a mixed solvent system of ethanol and acetonitrile (1:1) in a nitrogen atmosphere and refluxing the reaction mixture for 25 hrs. After the reaction was over, the reaction mixture was cooled solvent was evaporated slowly in air to obtain a blackish violet mass. Finally, the product that was obtained was recrystallized from ethanol and dried in air. Results of elemental analysis showed the Cu^{II} complex has the formula [Cu(AQS)₂]. Found: C, 45.21 %; H, 1.88%; N, 3.79 %. Calculated: C, 45.18%; H, 1.90%; N= 3.76%.

4.3.4. Synthesis of Ni^{II} complex of sodium 3-amino-2-hydroxy-9,10-anthraquinone-1-sulphonate [Ni(AQS)Cl₂(H₂O)₂]

The solid Ni^{II} complex of AQSH was prepared by treating AQSH (0.58mmol) with NiCl₂.6H₂O(0.29mmol) in 2:1 proportion using equimolar mixture (1:1) of ethanol and acetonitrile and refluxing for 25 hours under nitrogen atmosphere to bring about an inert condition. After the completion of the reaction, the crude reaction mass was allowed to cool to room temperature. The solvent was evaporated gently in normal atmosphere. A blackish violet

mass was obtained. The complex was recrystallized from ethanol and dried carefully in air to collect the product. Results of elemental analysis showed the nickel (II) complex has the formula $[\text{Ni}(\text{AQS})\text{Cl}_2(\text{H}_2\text{O})_2]$. Found: C, 44.75 %; H, 2.96 %; N, 3.51 %. Calculated: C, 33.22%; H= 2.175%; N= 2.768%.

4.3.5. Synthesis of Co^{III} complex of 1-amino-4-hydroxy-9,10-anthraquinone (CoQ_3)

An aqueous solution of 0.5 mmol $\text{CoCl}_2 \cdot 6\text{H}_2\text{O}$ and a solution of 1.5 mmol QH in acetonitrile were mixed and stirred for about 6 hours using a magnetic stirrer. Co^{II} was oxidized to Co^{III} by purging air into the reaction media. The solution was kept for 7 days in air to allow it to evaporate till it was 5 mL. A violet coloured complex was separated by filtration followed by washing with acetonitrile. The complex was recrystallized from a methanol-acetonitrile mixture and dried in air. Results of elemental analysis showed it has the formula CoQ_3 . Found: C, 65.09%; H, 3.08%; N, 5.51%. Calculated: C, 65.13%; H, 3.10%; N, 5.43%. In 25% aqueous ethanol solution, 0.1 mM CoQ_3 showed a conductance less than 5 $\mu\text{S}/\text{cm}$ at 298.15 K indicating that it is a neutral species.

4.3.6: Preparation of solutions of complexes of $\text{Cu}(\text{AQS})_2$, $\text{Ni}(\text{AQS})\text{Cl}_2(\text{H}_2\text{O})_2$, CoQ_3 and surfactants

Since AQSH exhibits poor solubility in aqueous media, standard solutions of AQSH in ethanol and DMSO having strength of 1mM were prepared by dissolving an appropriate weighed amount of AQSH. These were further diluted as required in 0.1M phosphate buffer to produce 50 μM i.e. 50×10^{-6} M concentration of AQSH for various titrations and analysis. Similarly weighed amounts of Cu^{II} and Ni^{II} complexes of AQSH were dissolved in ethanol and DMSO to prepare

stock solutions having strength 1mM. These stock solutions were diluted to 0.1M. Phosphate buffer to produce 50 μM i.e. 50×10^{-6} M concentration for different titrations and analysis. Standard solutions of AQSH, its Cu^{II} and Ni^{II} complexes in anhydrous acetonitrile, DMF and DMSO media in 0.1M tetrabutyl ammonium bromide (TBAB) were also prepared having strength 1 mM which were further diluted in electrochemical analysis.

In case of CoQ_3 , 1mM standard solution was prepared which was further diluted to a concentration range of $5 \times 10^{-5} \text{mol dm}^{-3}$ to $1.5 \times 10^{-3} \text{mol dm}^{-3}$. UV-Visible spectra were recorded with the help of a spectrophotometer using 30% aqueous ethanolic solution of CoQ_3 . Electrochemical reduction was carried out with 1mM solution of CoQ_3 in anhydrous DMSO and DMF media using with 0.1M TBAB as supporting electrolyte.

Determination of pK_a of AQSH in the absence and presence of Cu^{II} and Ni^{II} was carried out with 50 μM aqueous-ethanolic solution of AQSH by pH metric titration using 0.01 M HCl and 0.01 M NaOH solution respectively. The same was monitored spectrophotometrically.

In studying the interaction of experimental molecules with surfactant, a 10mM stock solution of anionic surfactant SDS was prepared. The interaction was studied by spectrophotometric method with 50 μM AQSH solution in 100 mM phosphate buffer.

In the same way, surfactant interaction of $\text{Cu}(\text{AQS})_2$ and $\text{Ni}(\text{AQS})\text{Cl}_2(\text{H}_2\text{O})_2$ complexes were performed with 50 μM solution of each metal complexes with 10 mM solution of anionic surfactant SDS. The pK_a values of both metal complexes were evaluated with 50 μM aqueous solution of each metal complexes and 0.01 M HCl and 0.01 M NaOH respectively. Cyclic voltammetry was performed with 1mM solution of $\text{Cu}(\text{AQS})_2$ and $\text{Ni}(\text{AQS})\text{Cl}_2(\text{H}_2\text{O})_2$ complexes in anhydrous acetonitrile media in the presence of 0.1M tetrabutyl ammonium bromide (TBAB) as the supporting electrolyte.

4.3.7: Computational studies

Density functional theory was employed to estimate geometrical parameters and energy of AQSH. DFT level (Gradient corrected) used three-parameter fit exchange–correlation function of Becke (B3LYP), that comprised of the correlation function of Lee, Yang and Parr [4,5]. Minimization of energy and optimization of full unconstrained geometry of AQSH were done using Berny optimization algorithm under tight convergence. To compute the potential energy distribution (PED) Vibrational Energy Distribution Analysis (VEDA) 4.0 was introduced [6]. Vibrational modes of AQSH were assigned by using PED values and visual check using Gauss View 5.0.

The structure of CoQ₃ was optimized using DFT with Ahlrich SV basis [7, 8] and B3LYP functional [9-11], using Orca program suite [12] Electronic transitions were calculated by time-dependent DFT (TDDFT) method with the same basis set and functional using Orca. Pictures of molecular orbitals (MOs) were generated with the same basis set and functional using Gaussian 09W [13] and MaSK software [14].

4.3.8: Spectroscopic studies

In this section, we attempted a series of useful spectroscopic measurements for our investigating molecules. Absorption studies were performed by a standard spectrophotometer (model: OPTIZEN POP, MECASYS, South Korea) that contained a pair of quartz cuvette (10×10 mm). Fluorescence spectroscopy plays a significant role for investigating cell morphology and this was used with a standard fluorescent microscope (model: Carl Zeiss, Axioscope2plus) that contained an UV filter (450–490 nm) and a pair of 10×10 mm fluorescence cuvette. pH-metric titration was carried out using a standard pHmeter (model number of

microprocessor pH/ION Meter, pMX 3000) that was helpful for determining the pKa values of AQSH and its corresponding metal complexes. A sensitive thermo electronic peltier was used for controlling temperature of experimental solutions taken in a cuvette during spectrophotometric and fluorometric experiments.

4.3.9: Electrochemical studies

Using cyclic voltammetry we have studied electrochemical behavior of AQSH, its metal complexes and CoQ_3 in purely aqueous and different anhydrous organic media like acetonitrile, DMSO and DMF in the presence of either 0.1M NaCl or 0.1M TBAB as supporting electrolyte, respectively. An inert atmosphere was maintained by purging high purity argon gas for at least 30 minutes just before performing cyclic voltammetry experiments. All experimental solutions were prepared in the range of $5 \times 10^{-5} \text{ mol dm}^{-3}$ to $1.5 \times 10^{-3} \text{ mol dm}^{-3}$. Reduction potential values in solvents of different polarity were compared to find out the role of polarity of solvents in stabilizing reduced species formed. By comparing different electrochemical parameters and the cyclic voltammograms of free ligands and their metal complexes, effect of metalation of ligands during electrochemical behavior could be explained. By finding a linear relationship between reduction peak current and square root of scan rate, it was concluded that reduction was diffusion controlled and that there is no scope for adsorption on the electrode surface. Reversibility of the reaction was determined from ratio of cathodic peak current to anodic peak current. Different electrochemical parameters were evaluated using different equations and techniques. Electrochemical experiments were repeated four times and an average of electrochemical parameters were reported.

4.3.10: Studies on the interaction of compounds with surfactant micelles

UV–Vis spectroscopy was used to investigate surfactant interaction with AQSH and its metal complexes at physiological pH with anionic surfactant SDS as standard using 100 mM phosphate buffer in pre-micellar and micellar concentration ranges. Standard solution of AQSH and its metal complexes with a fixed concentration (50 μM) of each was titrated by gradual addition of SDS solution separately. Each solution was incubated with SDS for a minimum of 1-2 minutes. Changes in absorbance at a particular wavelength in the UV–Vis spectra of AQSH and its metal complexes were monitored. Critical micelle concentration (CMC) of each experimental solution was determined individually that helped further calculations of other binding parameters. CMC values of SDS in pure aqueous system and in 100 mM phosphate buffer were compared with previous results of similar kinds of experiments. Influences of different ions and molecules on CMC were also analyzed. Binding constant (K), partition coefficient (K_x), Gibbs free energy of binding (ΔG^0) and standard free energy change (ΔG_x^0) for transfer of AQSH and its metal complexes from aqueous to micellar phase for interaction of AQSH and its metal complexes with surfactants were also determined.

4.3.11. Determination of critical micelle concentration

Change of slope or discontinuity of physicochemical property–concentration dependence provides the CMC value. A series of mixtures of a certain concentration of AQSH and different concentrations of SDS were prepared. Absorbance of these solutions were measured at 320 nm for AQSH and plotted against concentration of SDS. Change of slope of absorbance – concentration dependence provides the CMC value.

4.3.12. Cell Culture

Human A549 lung cancer cells and MCF-7 human breast cancer cells were acquired from NCCS, Pune, India. In a CO₂ incubator (Thermo Scientific, USA), with humidified atmosphere containing 5% CO₂, cells were cultured at 37°C in DMEM high glucose medium (Sigma-Aldrich, USA), accompanied by 10% fetal bovine serum (HiMedia), and penicillin/streptomycin as antibiotics (HiMedia) in 96 well culture plates. Studies were done using cells from passage 15 or less.

4.3.13. Cell Viability Assay

Solid AQSH, its metal complexes and CoQ₃ were dissolved individually in dimethyl sulfoxide to prepare a stock solution that was diluted separately with media to obtain different concentrations of AQSH, its metal complexes and CoQ₃. 200 µL solution was then mixed with 5×10³ A549 cells per well. After an incubation of 24 hours, 20 µl of MTT [3-(4,5-dimethylthiazol-2-yl)-2,5-diphenyl-2H-tetrazolium bromide] solution (5mg/mL in PBS) was added to each well and the plate enfolded by Al foil. It was again incubated for 4 hours at 37°C [15]. The formazan product, purple in colour was liquefied by adding 100 µL dimethylsulfoxide in every well. With a 96-well plate reader (Bio-Rad, iMark, USA), the optical density was supervised at 570 nm for the measurement and 630 nm for reference. Experimental data were collected for three replicates each and used to determine the respective mean. Percentage inhibition was evaluated using the formula:

$$\text{Percentage inhibition} = \frac{[\text{Average OD of untreated cells (control)} - \text{Average OD of treated cells (treated)}] \times 100}{\text{Average absorbance of untreated cells (control)}}$$

By plotting % inhibition against concentration of AQSH, its metal complexes and CoQ₃, a standard curve was obtained. Concentration of AQSH that reduced viability to 50% (IC₅₀) was determined.

4.3.14. Acridine orange and ethidium bromide (AO/EB) staining

Following the technique illustrated by Spector and coworkers [16] apoptosis was studied by using AO/EB double staining technique with certain modifications. After incubating cells with an IC₅₀ concentration of AQSH, its metal complexes and CoQ₃ for 24 hours they were harvested and washed by using cold PBS. By using PBS again, cell pellets were re-suspended and diluted to 5×10^5 cells/mL. It was mixed with 25 μ L of PBS containing 3.8 μ M of AO and 2.5 μ M of EB on a clean slide and viewed through a microscope. Without wasting time, it was studied under a fluorescent microscope (Carl Zeiss, Axioscope2plus) having UV filter (450 – 490 nm). With staining the structure of the nucleus and membrane integrity, 300 cells for every sample were scored as necrotic, apoptotic or viable. The % of necrotic and apoptotic cells were calculated accordingly.

4.3.15. Hoechst 33258 staining

A549 and MCF-7 cells were cultured separately in separate 6-well plates and incubated with IC₅₀ concentration of AQSH, its metal complexes and CoQ₃ for 24 hours. Treated and control cells were harvested and stained with Hoechst 33258 stain (1 mg/mL, aqueous) for 5 min at room temperature [17]. A drop of cell suspension was introduced on a glass slide, and a coverslip was laid over into reduce light diffraction. In a fluorescent microscope, arbitrary 300 cells in triplicate were introduced and percentage cells undergoing pathological changes were

measured. Data were collected for three replicates each to calculate the mean and standard deviation.

4.3.16. Mitochondrial membrane potential assessment by JC1 staining

Mitochondrial membrane potential was measured by using the fluorescent probe JC-1. In this method orange-red fluorescence was observed when gathered in healthy cell mitochondria but when extracted out in cytosol it fluoresces green owing to loss of membrane potential leading to a negative internal potential [18]. A549 cells were grown in glass coverslips (22 × 22 mm) placed in wells of 6-well plates and treated with IC₅₀ of AQSH and its metal complexes separately. DMSO was employed as solvent control. After an exposure 12 hours, cells were stained with the dye. Depolarization patterns of mitochondria were found in fluorescent microscope and pathological changes in the cells were found and recorded.

References

1. P. B. Undre, P. W. Khirade, V. S. Rajenimbalkar, S. N. Helambe, S. C. Mehrotra, J. Korean Chem. Soc. 56 (2012) 416-423.
2. K. Bose, K. Kundu, Can. J. Chem. 57 (18) (1978) 2476-2481.
3. K. Mahali, S. Roy, B. K. Dolui, J. Soln. Chem. 42 (2013) 1096-1110.
4. A. D. Becke, J. Chem. Phys. 98 (1993) 5648-5652.
5. C. Lee, W. Yang, R. G. Parr, Phys. Rev. B: Condens. Matter 37 (1998) 785-789.
6. M. H. Jamroz, Vibrational Energy Distribution Analysis VEDA 4, Warsaw, Poland, 2004-2010.
7. A. Schäfer, H. Horn, R. Ahlrichs, Fully Optimized Contracted Gaussian Basis Sets for Atoms Li to Kr. J. Chem. Phys. 97 (1992) 2571-2577.

8. A. Schäfer, C. Huber, R. Ahlrichs, Fully optimized contracted Gaussian basis sets of triple zeta valence quality for atoms Li to Kr. *J. Chem. Phys.* 100 (1994) 5829–5835.
9. K. Raghavachari, Perspective on Density functional thermochemistry. III. The role of exact exchange. *Theor. Chem. Acc.* 103 (2000) 361-363.
9. A. D. Becke, Perspective on Density functional thermochemistry. III. The role of exact exchange. *J. Chem. Phys.* 98 (1993) 5648– 5652.
10. A. D. Becke, Density-functional exchange-energy approximation with correct asymptotic behavior. *Phys. Rev. A* 38 (1988) 3098– 3100.
11. C. Lee, W. Yang, R. G. Parr, Development of the Colle- Salvetti correlation-energy formula into a functional of the electron density. *Phys.Rev. B* 37 (1988) 785–789.
12. F. Neese , F. Wennmohs, U. Becker, C. Riplinger, *J. Chem. Phys.* 152 (22) (2020) 224108.
13. Gaussian 09, Revision A.02, M. J. Frisch et al., Gaussian, Inc., Wallingford, CT, 2009.
14. Y. Podolyan, J. Leszczynski, MaSK: A visualization tool for teaching and research in computational chemistry. *Int. J. Quantum Chem.* 109 (2009) 8–16.
15. T. Mosmann, *J. Immunol. Methods* 65 (1983) 55-63.
16. D. L. Spector, R. D. Goldman, L. A. Leinwand, *Cell: A Laboratory Manual, Culture and Biochemical Analysis of Cells*, Cold Spring Harbor Laboratory Press: Cold Spring Harbor, pp. 341–349, CSHL Press: New York, 1998.
17. G. P. A. H. Kasibhatla, D. Finucane, T. Brunner, E. B. Wetzel, D. R. Green, Protocol: Staining of suspension cells with Hoechst 33258 to detect apoptosis. in *Cell: A Laboratory Manual Culture and Biochemical Analysis of Cells*, Vol. 1, CSHL Press, Cold Spring Harbor, NY 1998, p. 155.
18. M. Reers, T. W. Smith, L. B. Chen, *Biochemistry* 30 (1991) 4480-4486.

Chapter 5

Solubilization of sodium 3-amino-2-hydroxy-9,10-anthraquinone-1-sulphonate in SDS micelles explains its permeation in A549 human lung cancer cell

5.1. INTRODUCTION

There is a constant effort by various researcher groups to find comparatively inexpensive alternatives to the anthracycline class of anticancer agents that could simultaneously reduce cardiomyopathy but such effort till date have met with limited success [1-9]. Previous studies have established the fact that the hydroxy-9,10-anthraquinone moiety present at the core of anthracyclines control biological action. For this reason, we selected a simple analogue, i.e. sodium 3-amino-2-hydroxy-9,10-anthraquinone-1-sulphate (AQSH) for this work. The efficacy of such molecules in penetrating biological cell membranes could be established by carrying out studies on molecule – surfactant interactions [10, 11].

Along with some of the above mentioned facts, molecular and electronic structures of drugs are also important since they enable formation of different types of hydrogen bonding and other forms of interactions with bio-membranes. This helps to find a structure–activity relationship for a molecule and may provide information in identifying new drugs for different diseases. In this study, computational measurements were performed to depict the electronic structure of AQSH. The objective of the present study was to see whether AQSH has the potential to permeate biological membranes, identified with model studies using an anionic surfactant micelle. AQSH was chosen in this study since it is inexpensive and has a planar hydroxy-9,10-anthraquinone unit. Interaction of AQSH with micelles of the anionic surfactant sodium dodecyl sulphate (SDS) was monitored by UV-Vis spectroscopy to estimate binding parameters for AQSH–surfactant interaction. In order to justify whether the results are important for the chosen molecule to permeate biological membrane, AQSH was treated with A549 human lung cancer cells and studied to see if interaction induces apoptosis.

5.2. RESULTS AND DISCUSSION

5.2.1. Structure of AQSH

In order to establish a structure–activity relationship for the current molecule, its molecular and electronic structures were characterized by theoretical and experimental studies.

5.2.2. Energy optimized structure from computation

Structure of AQSH was optimized with the help of B3LYP/6-31+g(d,p) (Figure 1). The optimum energy for the structure was found to be -1604.94a.u. Estimated bond lengths and bond angles for the molecule is mentioned in Table-1a and 1b respectively having been evaluated by HF/6-31+g(d,p), B3LYP/6-31+g(d,p) and PBEPBE/6-31+g(d,p).

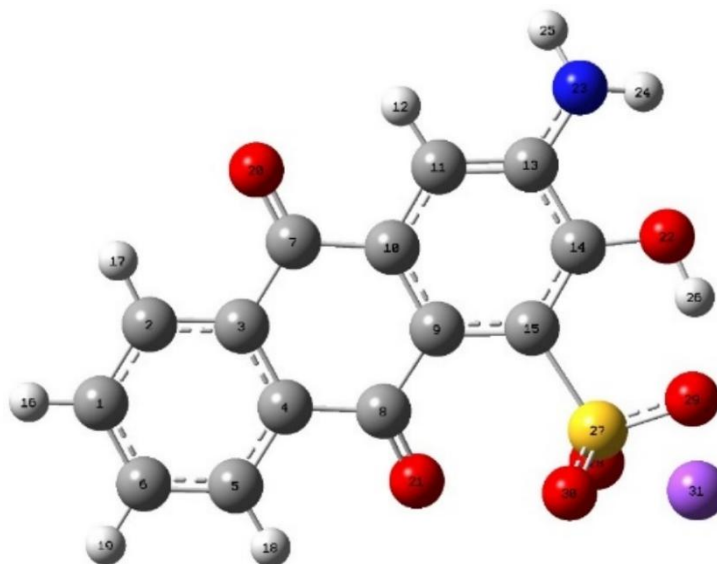


Figure 1: Optimized molecular structure of free AQSH using B3LYP/6-31+g(d,p) protocol.

For a molecule, the frontier molecular orbitals (FMO) are built by HOMO (highest occupied molecular orbital) and LUMO (lowest unoccupied molecular orbital). Examination of energy and population in these orbitals is important in determining donor-acceptor behavior of

the molecule when it interacts with any biologically important molecule [12]. Energy separation between HOMO and LUMO in FMO is related to chemical reactivity as HOMO functions as electron donor and LUMO as electron acceptor. In the present study, energy separation between HOMO and LUMO in AQSH was found to be 0.11904 a.u. The iso-density plot of FMO (Figure 2) clearly shows that HOMO and LUMO have different extents of delocalization.

Table 1a: Optimized bond lengths (Å) of AQSH.

Bond length	HF/6-31+g(d,p)	B3LYP/6-31+g(d,p)	PBEPBE/6-31+g(d,p)
C13-N23	1.359 (1.354)	1.377 (1.380)	1.390(1.395)
N23-H24	1.001 (1.005)	1.009 (1.015)	1.088 (1.055)
N23-H25	1.002 (1.001)	1.008 (1.009)	1.016 (1.019)
C14-O22	1.335 (1.330)	1.345 (1.355)	1.361 (1.368)
O22-H26	0.998(0.993)	1.001 (1.005)	1.017(1.201)
S27-O28	1.438 (1.444)	1.459 (1.444)	1.470 (1.478)
S27-O29	1.534 (1.539)	1.554 (1.555)	1.564 (1.569)
S27-O30	1.486 (1.490)	1.504 (1.511)	1.517 (1.514)
C8-O21	1.204 (1.210)	1.224 (1.220)	1.244 (1.249)
C4-C8	1.501 (1.503)	1.497 (1.501)	1.509 (1.515)
C9-C8	1.477 (1.480)	1.487(1.488)	1.501 (1.497)
C7-O20	1.216 (1.220)	1.228 (1.224)	1.239 (1.241)
C7-C3	1.468 (1.460)	1.484 (1.480)	1.499 (1.493)
C7-C10	1.502 (1.509)	1.491 (1.487)	1.505 (1.516)
C15-S27	1.816(1.820)	1.830 (1.828)	1.842 (1.848)
C11-C13	1.368(1.370)	1.385(1.379)	1.401 (1.411)
C13-C14	1.430(1.429)	1.428 (1.420)	1.440(1.445)

The data in the parenthesis are calculated in the solution.

Table 1b: Optimized bond angles (in degree) of AQSH

Bond angle	HF/6-31+g(d,p)	B3LYP/6-31+g(d,p)	PBEPBE/6-31+g(d,p)
H25-N23-H24	117.78 (117.70)	115.59 (116.15)	114.45 (114.44)
C13-N23-H25	117.65 (117.48)	116.86(117.39)	116.05 (1116.41)
C13-N23-H24	116.70 (116.76)	115.37(116.13)	114.40 (114.40)
C14-C13-N23	115.64 (115.44)	117.67(116.05)	119.96 (119.76)
C11-C13-N23	121.87 (121.42)	123.15 (123.06)	124.10 (124.92)
C14-O22-H26	108.72 (108.45)	107.39 (107.14)	105.62 (105.67)
C13-C14-O22	111.18 (111.07)	113.61 (113.10)	115.37 (115.88)
C15-C14-O22	125.51(125.59)	126.08 (126.85)	128.14 (128.76)
O28-S27-O29	114.54 (114.11)	111.75(111.30)	111.50 (111.43)
O30-S27-O28	119.49 (119.67)	118.51(117.99)	117.84 (117.65)
O30-S27-O29	106.68 (106.41)	104.11 (105.42)	103.45 (103.46)
C9-C15-S27	120.22(120.56)	122.42(122.04)	123.44(123.89)
C14-C15-S27	115.23(115.87)	117.56(117.89)	118.09(118.65)
C9-C8-O21	121.54(121.12)	122.35(122.98)	123.33(123.67)
C4-C8-O21	117.88(117.44)	119.39(119.10)	121.51(121.04)
C3-C7-O20	120.66(120.98)	121.09(121.66)	123.06(123.66)
C10-C7-O20	119.87(119.34)	121.03(121.44)	122.22(122.68)

The data in the parenthesis are calculated in solution

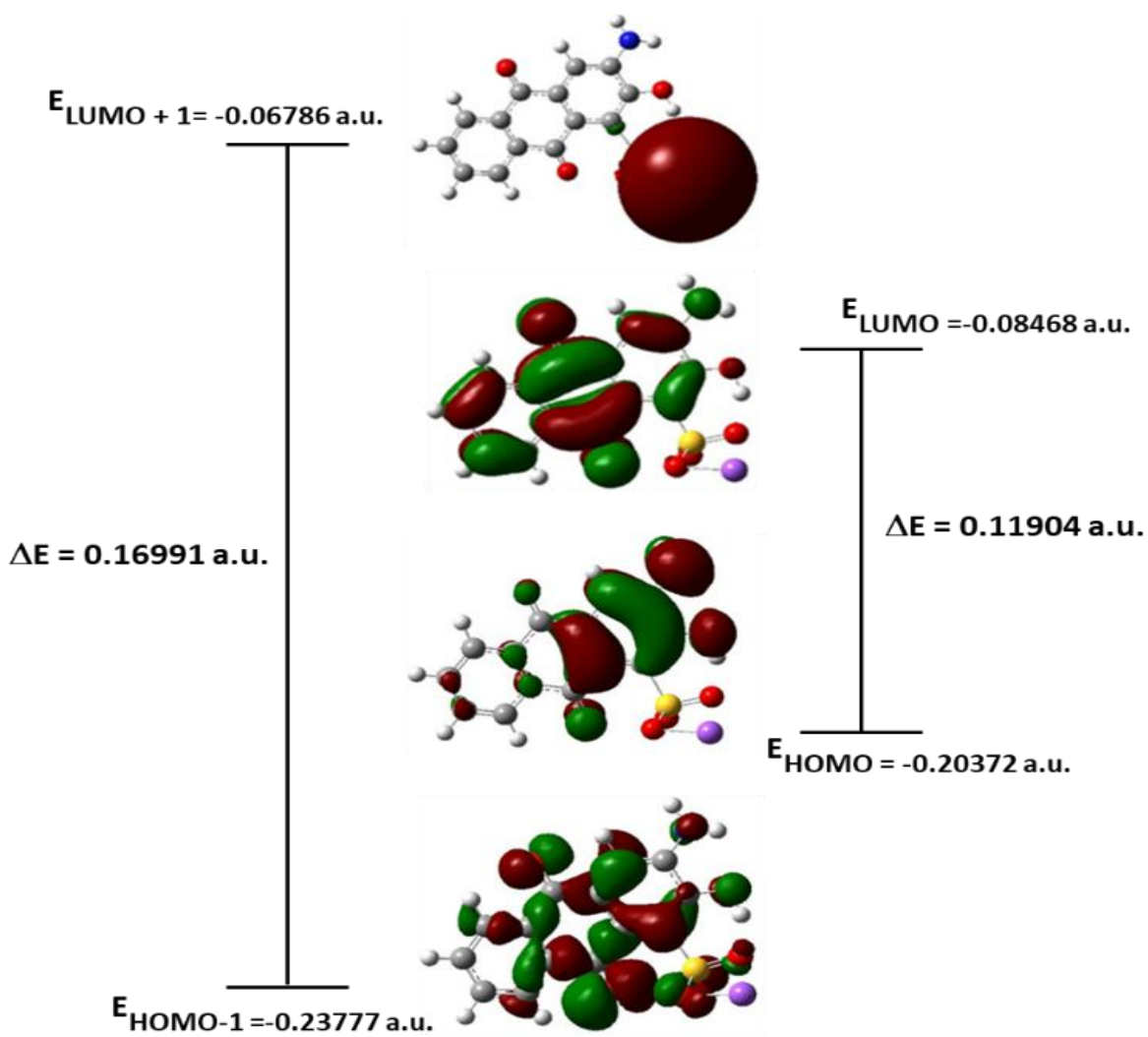


Figure 2: The iso-density plot of HOMO, LUMO, HOMO-1 and LUMO+1 for free AQSH.

5.2.3. NMR:

^1H NMR (300 MHz, CDCl_3): δ (ppm): 10.64 (s, 1H, Ar-OH), 7.93 (d, 2H, Ar-C₅, C₈), 7.36 (d, 2H, Ar-C₆, C₇), 6.05 (s, 1H, Ar-C₄), 3.31 (s, 2H, Ar-NH₂) (Figure 3).

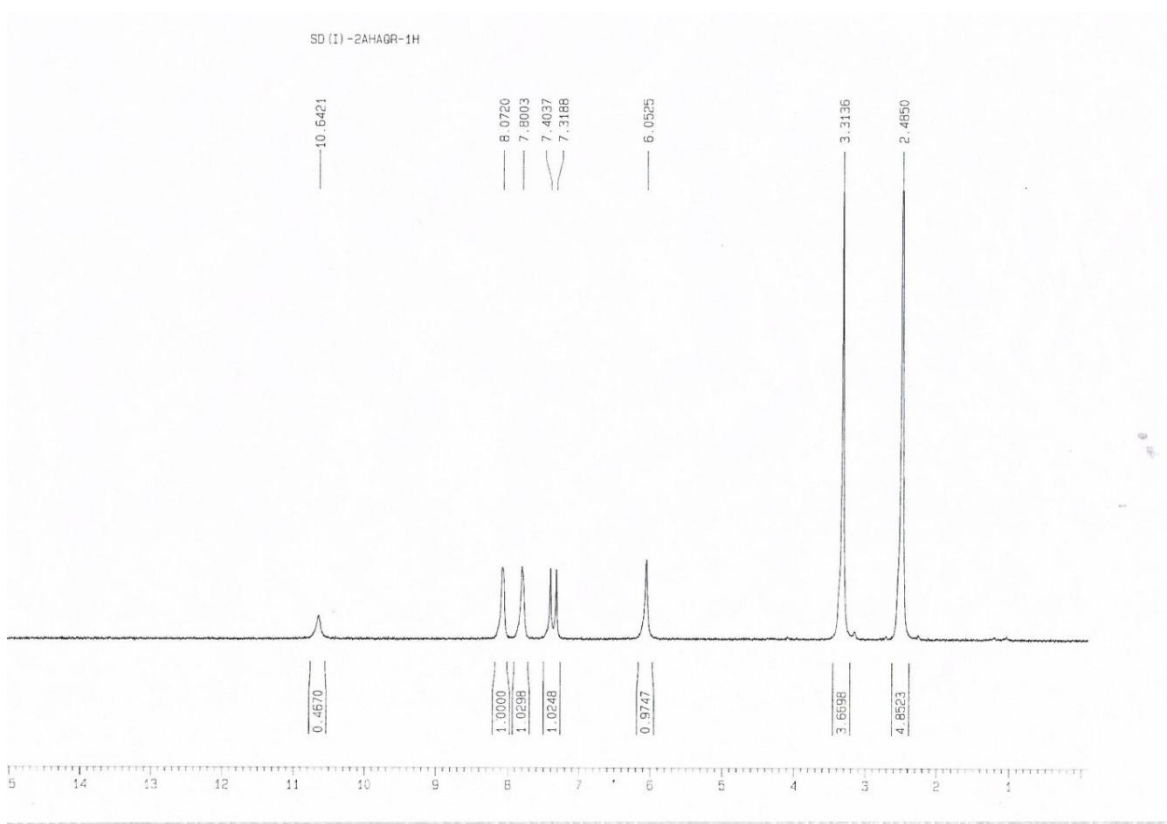


Figure 3: ^1H NMR of AQSH in DMSO-D₆.

In 2-amino-3-hydroxy-9,10-anthraquinone the OH and NH_2 protons appeared at δ 10.0 and δ 3.30 respectively [13]. However, due to incorporation of electron withdrawing sulphonate at *ortho*- position to $\text{C}_2\text{-OH}$, the peak for the $\text{C}_2\text{-OH}$ proton shifted to higher δ value and appeared at δ 10.64 as a singlet. However, no change was observed for -NH_2 protons and those appeared as singlet at δ 3.31. Since AQSH was prepared in presence of Na_2SO_3 suggesting that the medium was basic, sulphonation was more favored at *ortho* to $\text{C}_2\text{-OH}$ but not *ortho* to NH_2 (4- position). In sodium 3-amino-2-hydroxy-9,10-anthraquinone-1-sulphonate (AQSH) aromatic protons ($\text{C}_5\text{-H}$ and $\text{C}_8\text{-H}$) close to the electron withdrawing carbonyl group appeared at δ 7.93 as a doublet because of *ortho* coupling with adjacent protons. The other aromatic protons in the sulphonate product like $\text{C}_6\text{-H}$, $\text{C}_7\text{-H}$ and $\text{C}_4\text{-H}$ appeared at δ 7.36 as doublet and at δ 6.05 as

singlet respectively. Lower δ value of C₄-H protons arise due to electron releasing effect of adjacent -NH₂ group.

5.2.4. Mass spectroscopy

In the ESIMS of AQSH (Figure 4) the molecular ion peak (NaC₁₄H₈NSO₆) was detected at $m/z = 341.27$; the protonated molecular ion peak expected at $m/z = 342.27$ was not observed. However, an intense peak at $m/z = 338.30$ indicates that a species was obtained following deprotonation of three hydrogen atoms from AQSH. The peak at $m/z = 254.1088$ is probably the protonated fragment formed by loss of sodium, -NH₂, -OH and two oxygen atoms from AQSH. A very sharp signal at $m/z=240.03$ corresponds to the protonated fragment generated due to loss of -SO₃Na from AQSH. A less intense band at $m/z = 124.06$ is due to loss of -SO₃Na, -OH, -NH₂ and two quinone oxygen atoms, four carbon atoms and one hydrogen atom from AQSH.

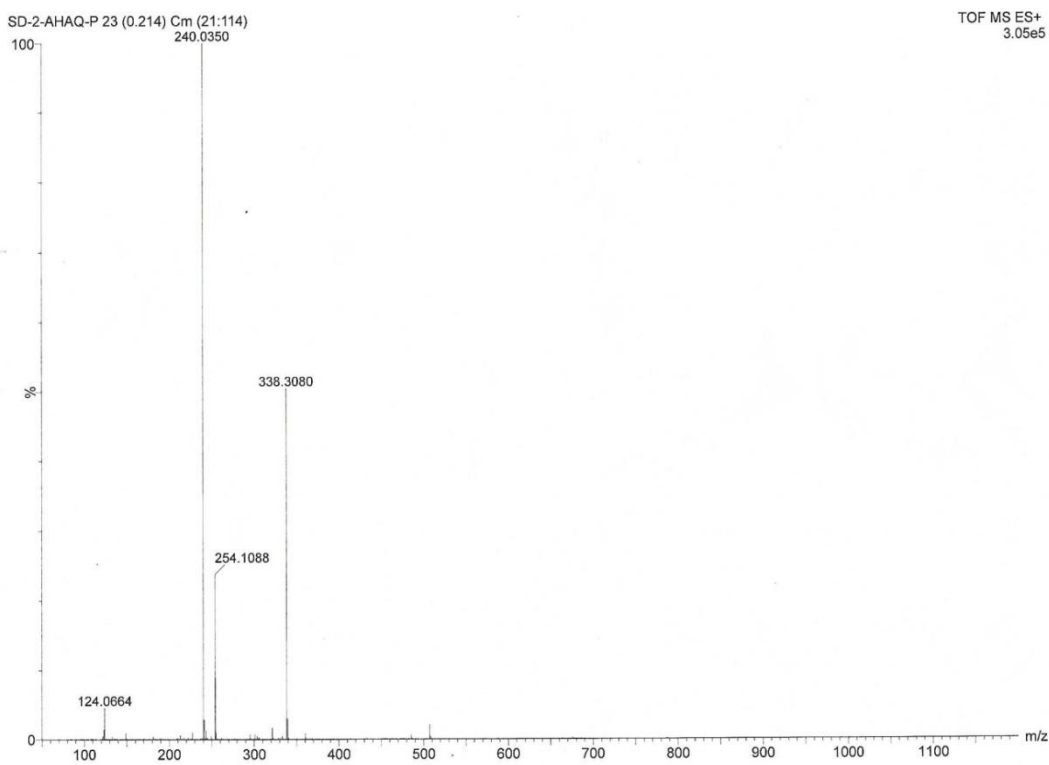


Figure 4: ESIMS of AQSH.

5.2.5. Theoretical and experimental vibrational spectra of AQSH

Using “Vibrational Energy Distribution Analysis” (VEDA) and PED (Potential Energy Distribution) analysis, the theoretical IR spectrum of AQSH was created. According to VEDA some normal modes are extended over the whole molecule. PED used at certain levels account for the contribution to movement of groups of atoms in a normal mode quantitatively. AQSH consists of 30 atoms and exhibits 84 IR active fundamental vibrations of which 29 are stretching, 28 bending and 27 torsional. Computed vibrational frequencies were overestimated and scaled by 0.9613 for B3LYP/6-31+ G (d,p) level of calculation [14, 15]. IR frequency and intensity, PED and modes of vibration for AQSH are shown in Table- 2. Comparing theoretical and experimental bands (Table- 2) and the spectra (Figures 5a and 5b) it could be said that both spectra do not match very well in the region of 3000 cm^{-1} to 1600 cm^{-1} . However, they matched better above 3000 cm^{-1} and below 1600 cm^{-1} . Deviation of results between theoretical and experimental spectra may be due to the effect of crystal field [16] or due to the fact that experimental and theoretical results were studied in different states like solid state in case of experiment and gaseous state in case of theoretical studies.

Table: 2. Comparison of theoretical and experimental IR stretching frequency of free AQSH.

$\nu_{\text{cal}}(\text{cm}^{-1})$	$\nu_{\text{scaled}}(\text{cm}^{-1})$	Intensity	PED (%)	Interpretation	$\nu_{\text{expt}}(\text{cm}^{-1})$
3714	3570	31	S ₂	$\nu_{\text{sym}}(\text{N}_{23}\text{-H}_{24}), \nu_{\text{asym}}(\text{N}_{23}\text{-H}_{25})$	3689
3592	3452	78	S ₃ (100)	$\nu_{\text{sym}}(\text{N}_{23}\text{-H}_{24}), \nu_{\text{asym}}(\text{N}_{23}\text{-H}_{25})$	3353
3119	2998	820	S ₁ (98)	$\nu_{\text{sym}}(\text{O}_{22}\text{-H}_{26})$	-
1752	1684	186	S ₉ (69) S ₁₀ (11)	$\nu_{\text{sym}}(\text{O}_{21}\text{-C}_8), \nu_{\text{sym}}(\text{O}_{20}\text{-C}_7)$	-

$\nu_{\text{cal}}(\text{cm}^{-1})$	$\nu_{\text{scaled}}(\text{cm}^{-1})$	Intensity	PED (%)	Interpretation	$\nu_{\text{expt}}(\text{cm}^{-1})$
1660	1595	42	S ₂₅ (-10)S ₃₇ (41)	$\nu_{\text{sym}}(\text{C}_3\text{-C}_7)$, $\nu_{\text{sym}}(\text{C}_5\text{-C}_6)$, $\nu_{\text{sym}}(\text{C}_7\text{-C}_{10})$, $\nu_{\text{sym}}(\text{C}_9\text{-C}_{15})$, $\nu_{\text{sym}}(\text{C}_{10}\text{-C}_{11})$, $\beta(\text{H}_{25}\text{-N}_{23}\text{-H}_{24})$	1655
1647	1583	68	S ₁₅ (54) S ₃₈ (16)	$\nu_{\text{sym}}(\text{C}_2\text{-C}_1)$, $\nu_{\text{sym}}(\text{C}_3\text{-C}_2)$, $\nu_{\text{sym}}(\text{C}_4\text{-C}_5)$, $\nu_{\text{sym}}(\text{C}_{13}\text{-C}_{11})$, $\beta(\text{H}_{17}\text{-C}_2\text{-C}_1)$, $\beta(\text{H}_{18}\text{-C}_5\text{-C}_6)$	1610
1636	1572	26	S ₁₁ (50) S ₃₁ (15)	$\nu_{\text{sym}}(\text{C}_1\text{-C}_6)$, $\nu_{\text{sym}}(\text{C}_2\text{-C}_3)$, $\nu_{\text{sym}}(\text{C}_9\text{-C}_{10})$, $\beta(\text{C}_2\text{-C}_1\text{-C}_6)$, $\beta(\text{C}_3\text{-C}_2\text{-C}_1)$, $\beta(\text{C}_4\text{-C}_5\text{-C}_6)$, $\beta(\text{C}_{13}\text{-C}_{11}\text{-C}_{10})$,	1526
1523	1464	161	S ₁₄ (-13)S ₃₅ (46)	$\nu_{\text{sym}}(\text{C}_1\text{-C}_6)$, $\nu_{\text{sym}}(\text{C}_6\text{-C}_5)$, $\nu_{\text{sym}}(\text{C}_9\text{-C}_{10})$, $\nu_{\text{sym}}(\text{C}_{11}\text{-C}_{10})$, $\beta(\text{H}_{26}\text{-O}_{22}\text{-C}_{14})$	1347
1437	1381	126	S ₁₉ (-12)S ₂₀ (16)S ₂₄ (-13)S ₂₅ (14)	$\nu_{\text{sym}}(\text{C}_9\text{-C}_{15})$, $\nu_{\text{sym}}(\text{C}_{14}\text{-C}_{15})$, $\nu_{\text{sym}}(\text{N}_{23}\text{-C}_{13})$, $\nu_{\text{sym}}(\text{O}_{22}\text{-C}_{14})$, $\nu_{\text{sym}}(\text{C}_3\text{-C}_7)$, $\nu_{\text{sym}}(\text{C}_9\text{-C}_{15})$, $\nu_{\text{sym}}(\text{C}_8\text{-C}_9)$,	1267
1282	1232	83	S ₂₆ (66)S ₂₇ (-10)	$\nu_{\text{sym}}(\text{S}_{27}\text{-O}_{28})$, $\nu_{\text{sym}}(\text{S}_{27}\text{-O}_{30})$,	1195
994	955	38	S ₆₄ (86)	$\tau(\text{H}_{16}\text{-C}_1\text{-C}_2\text{-C}_3)$, $\tau(\text{H}_{19}\text{-C}_6\text{-C}_1\text{-C}_2)$, $\tau(\text{H}_{16}\text{-C}_5\text{-C}_6\text{-C}_1)$, $\tau(\text{H}_{17}\text{-C}_2\text{-C}_1\text{-C}_6)$	967
897	862	38	S ₅₅ (-10)S ₆₀ (-12)	$\beta(\text{C}_8\text{-C}_9\text{-C}_{15})$, $\beta(\text{C}_{10}\text{-C}_7\text{-O}_{20})$, $\tau(\text{H}_{26}\text{-O}_{22}\text{-C}_{14}\text{-C}_{13})$,	891
837	804	63	S ₂₈ (-18) S ₆₀ (57)	$\nu_{\text{sym}}(\text{S}_{27}\text{-O}_{29})$, $\tau(\text{H}_{26}\text{-O}_{22}\text{-C}_{14}\text{-C}_{13})$	793
809	777	7	S ₆₃ (-54) S ₈₀ (13)	$\tau(\text{H}_{16}\text{-C}_1\text{-C}_2\text{-C}_3)$, $\tau(\text{H}_{19}\text{-C}_6\text{-C}_1\text{-C}_2)$, $\tau(\text{H}_{17}\text{-C}_2\text{-C}_1\text{-C}_6)$, $\tau(\text{N}_{23}\text{-C}_{11}\text{-C}_{14}\text{-C}_{13})$, $\tau(\text{O}_{20}\text{-C}_3\text{-C}_{10}\text{-C}_7)$, $\tau(\text{O}_{21}\text{-C}_4\text{-C}_9\text{-C}_8)$, $\tau(\text{O}_{22}\text{-C}_{13}\text{-C}_{15}\text{-C}_{14})$	712
623	598	65	S ₅₈ (-18)	$\beta(\text{O}_{29}\text{-S}_{27}\text{-O}_{30})$	612

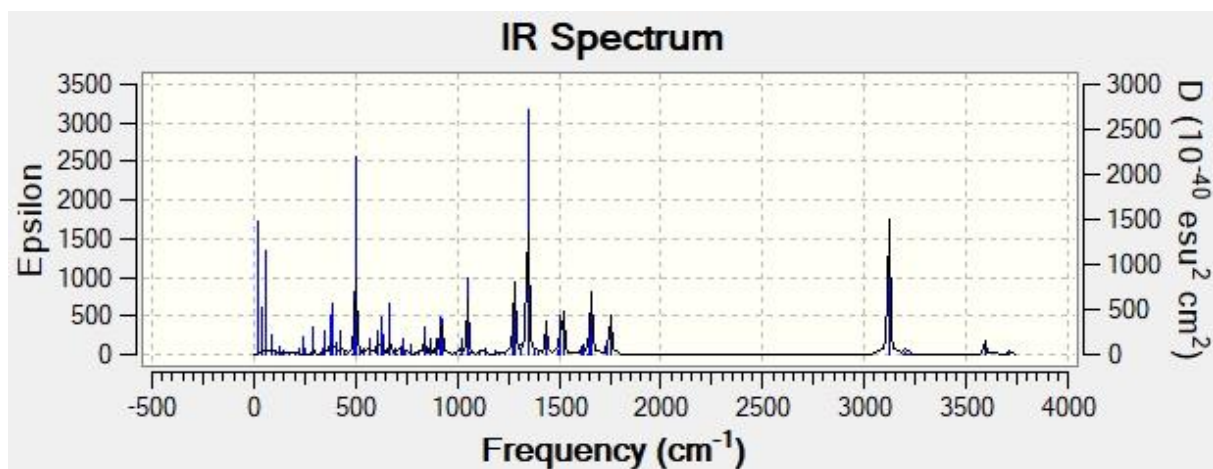


Figure 5a: Theoretical IR spectrum of AQSH using B3LYP/6-31+g(d,p)

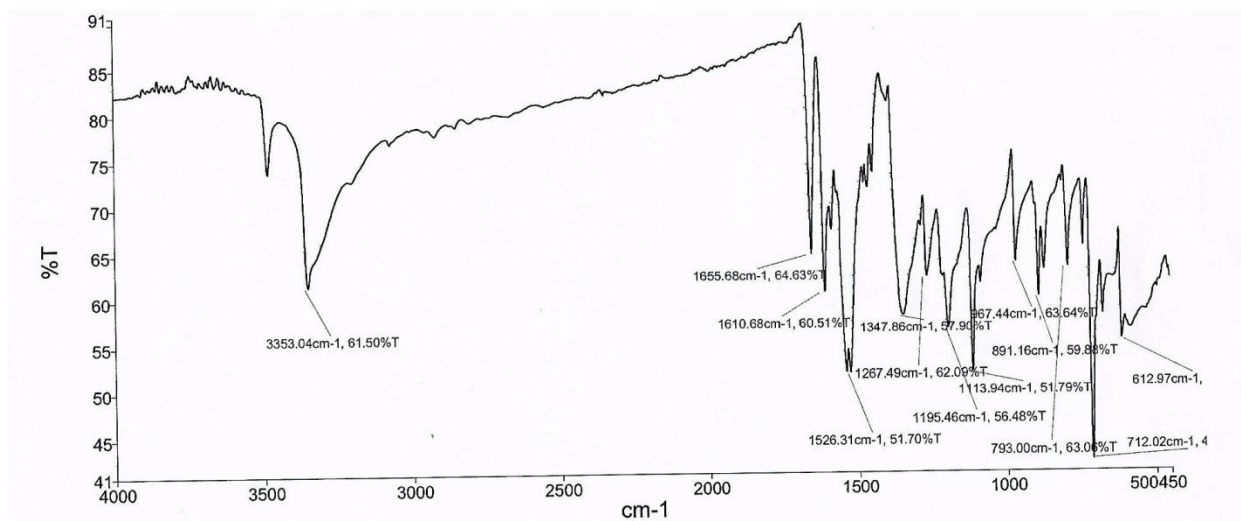


Figure 5b: Experimental IR spectrum of AQSH.

5.2.6. Determination of pK_a of AQSH

During interaction of the current molecule with surfactant micelles or biological cells, ionization of the phenolic $-OH$ group may play an important role [13]. This is why it is imperative to measure the pK_a of AQSH. This was done with the help of a spectrophotometric titration of AQSH with NaOH. Initially, 50 μM aqueous AQSH was acidified with 0.01 M HCl

to pH 2.23. It was then titrated with 0.01 M NaOH keeping concentration of AQSH constant. UV-Vis spectra of the experimental mixture were recorded (Figure 6) at different pH and a plot of absorbance at 560 nm against pH was fitted to equation 1 (Figure 7). A change in absorbance at 560 nm indicates dissociation of phenolic –OH in the pH range 7.30–9.10. pK_a was obtained as 8.10 ± 0.05 [reduced Chi squared = 0.00444].

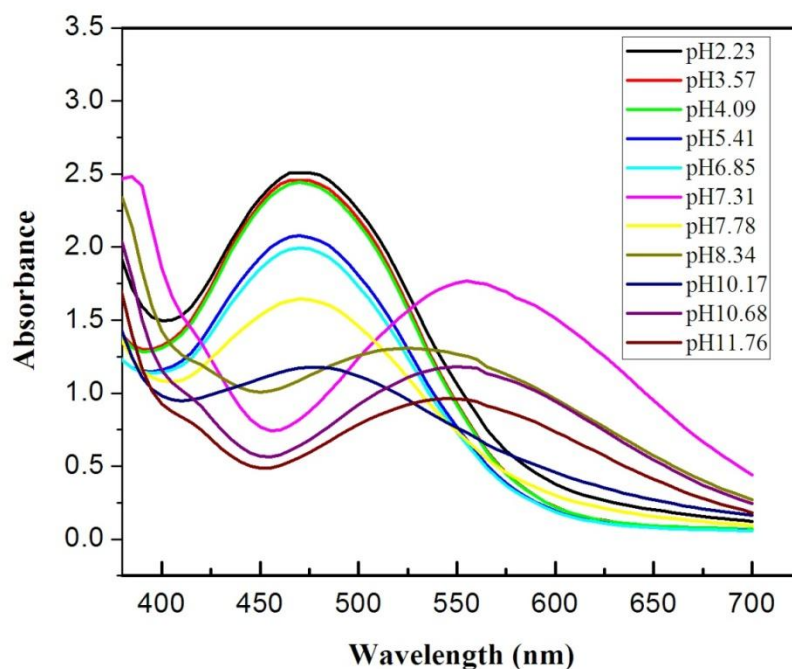


Figure 6: UV-Vis spectra of AQSH in aqueous media at different pH. [AQSH] = 50 μ M, [NaCl] = 0.01 M, T = 298.15 K.

Absorbance at 560 nm is fitted to equation 1

$$A_{560} = \frac{A_1}{1 + 10^{(pH-pK)}} + \frac{A_2}{1 + 10^{(pK-pH)}} \quad [1]$$

A_{560} is the overall absorbance of the solution at 560 nm at different pH; A_1 and A_2 are absorbance respectively of AQSH and the phenoxide ion(AQS⁻). pK_a for phenolic-OH of AQSH was higher than that of 2-amino-3-hydroxy anthraquinone (7.90 ± 0.06) [13], suggesting that the phenolic-

OH proton in AQSH is strongly held (probably through hydrogen bonding) by neighboring sulphonate.

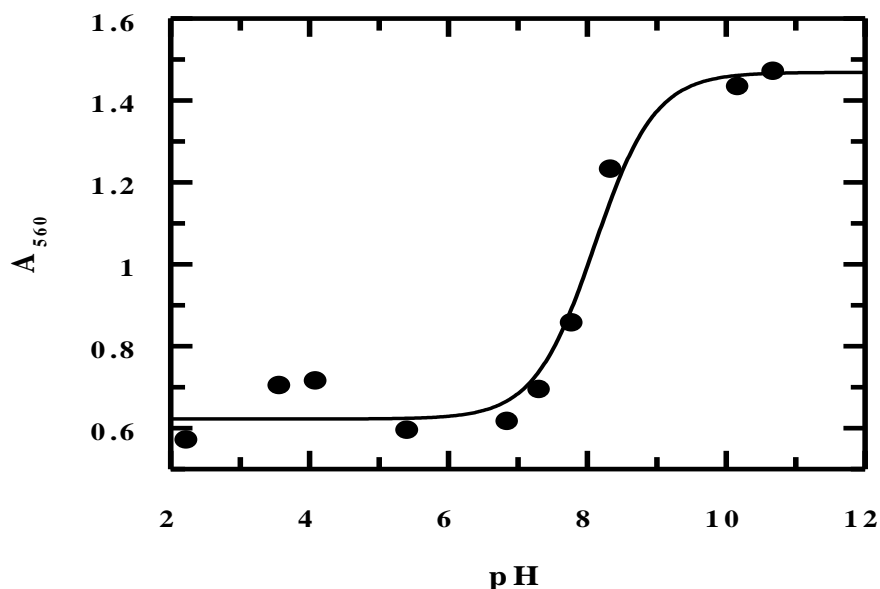


Figure 7: Variation of absorbance of AQSH at 560 nm with pH. [AQSH] = 50 μ M, [NaCl] = 0.01 M, T = 298.15 K.

5.2.7. Interaction of AQSH with sodium dodecyl sulfate (SDS)

A study on the interaction of AQSH with SDS was carried out using UV–Vis spectroscopy at pH 7.4 maintained with 100 mM phosphate buffer in pre-micellar and micellar concentration range. A series of mixtures containing a specific concentration of AQSH and variable concentration of SDS were prepared and the absorption at 320 nm was monitored to evaluate different parameters for the interaction of AQSH with SDS micelle. Absorbance of solutions was measured with the help of a spectrophotometer following incubation of SDS with AQSH for 1 - 2 minutes. Change in absorption of AQSH upon adding different concentrations of SDS is shown in Figure 8a. By monitoring changes in UV-Vis spectra (Figure 8a) of AQSH, the critical micelle concentration (CMC) of SDS in the presence of AQSH was evaluated and found to be 234 μ M. This value of

CMC was used in the entire calculation in evaluating binding parameters. CMC values of SDS in pure water and in 50 mM phosphate buffer were evaluated in an earlier study and found to be 8080 μM and 1990 μM respectively [17]. Lowering in CMC value of SDS in comparison to that obtained earlier may be explained as the influence of various ions and molecules present in the mixture [18]. The change in absorbance of AQSH at 510 nm with various surfactant concentrations is depicted in Figure 8b which shows that absorbance decreases with increasing SDS concentration until it reaches a saturation level for a particular concentration of SDS. This can be elucidated by assuming incorporation of AQSH into SDS micelles. Assuming 1:1 interaction between AQSH and SDS and considering Equation 2 the binding isotherm was examined (Figure 8b).

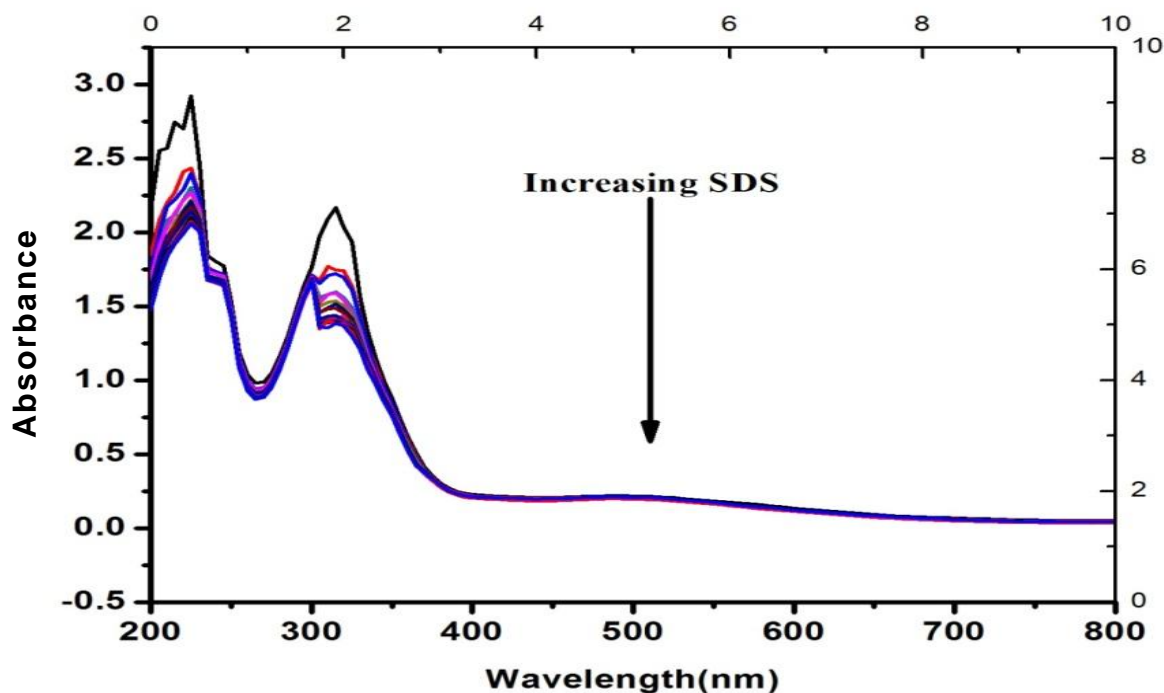


Figure 8(a): Absorption spectra of AQSH (50 μM) in the absence and presence of increasing concentrations of SDS. [Phosphate buffer] = 100 mM, pH 7.4, T = 298.15 K.

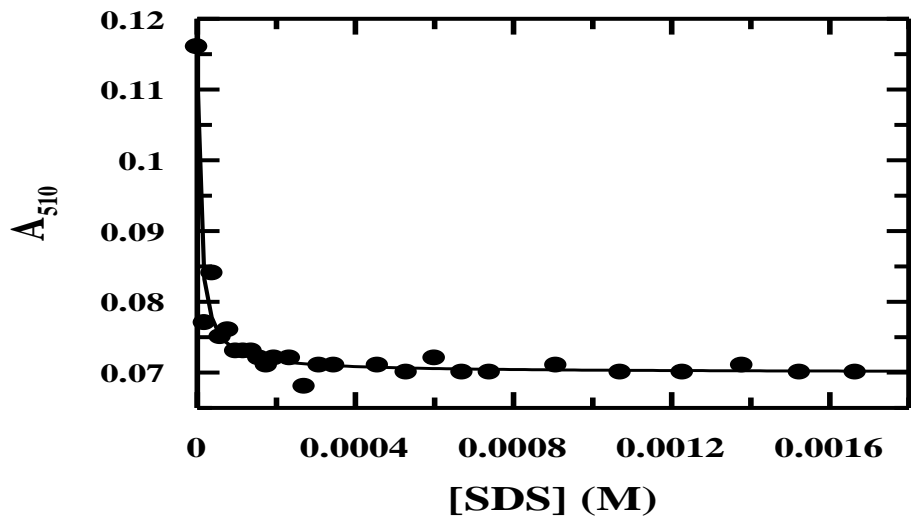


Figure 8(b): A non-linear fitting of the absorbance of AQSH at 320 nm using equation 2 considering 1:1 interaction between AQSH and SDS.

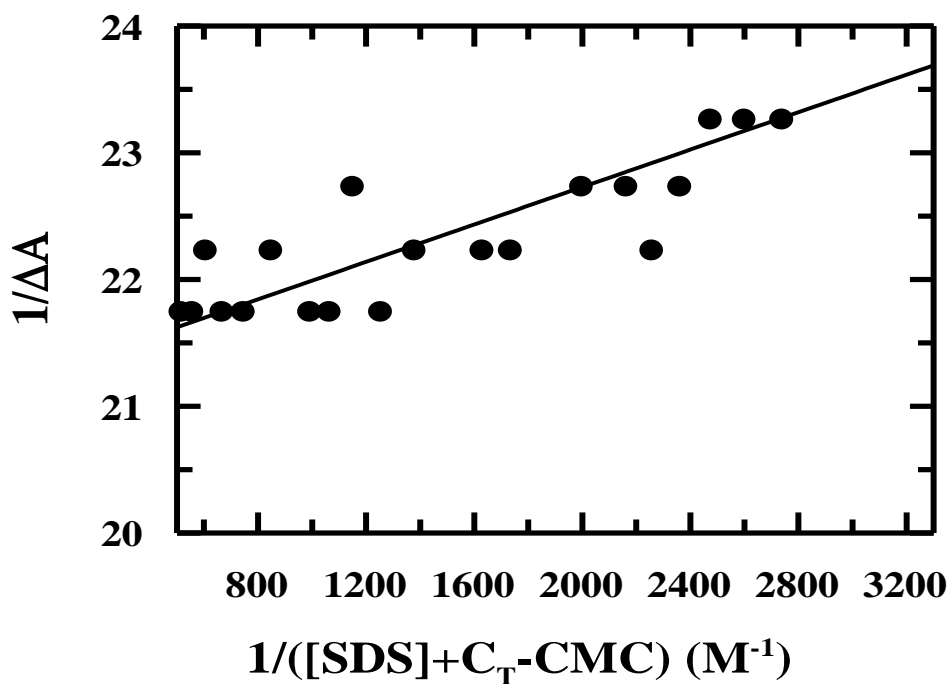


Figure 8(c): Plot of $1/|\Delta A|$ vs. $1/([SDS] + C_T - CMC)$ [Eq. 4] for AQSH (50 μ M) in SDS micelles at pH 7.4.

Binding constant was evaluated and found to be $(1.21 \pm 0.06) \times 10^5 \text{M}^{-1}$ (Table 3) [15, 16] (reduced Chi squared = 4.37×10^{-6}).

$$A = \frac{A_0 + A_\infty K[L]}{1 + K[L]} \quad [2]$$

L represents the surfactant used (here SDS); A and A_0 are absorbance of AQSH at 510 nm in the absence and presence of SDS whereas A_∞ corresponds to absorbance of AQSH bound to SDS. Gibbs free energy for interaction of AQSH to SDS micelles was calculated with the help of equation 3 and found to be -29.02 kJ/mol (Table 3) [19, 20].

$$\Delta G^0 = -RT \ln K \quad [3]$$

Where R is the molar gas constant and T = 298.15 K.

In a recent study [13], we observed that binding constant for 1:1 interaction of neutral 2-amino-3-hydroxyanthraquinone with anionic SDS was 652.81 where hydrophobic mode of interaction was established to be more important than the electrostatic mode. AQSH is an anionic molecule. It has a binding constant value of $(1.21 \pm 0.06) \times 10^5 \text{M}^{-1}$ which is greater than that of 2-amino-3-hydroxy-9,10-anthraquinone with SDS micelles under similar experimental conditions [13]. This indicates hydrophobic interactions are far stronger in the present study in comparison to that obtained earlier [13]. Binding constant for a 1:1 interaction of mitoxantrone, a cationic anthracycline drug with anionic surfactant SDS, as shown in a previous study [19] was $(1.14 \pm 0.05) \times 10^3 \text{M}^{-1}$. In that study it was shown, a cationic drug like mitoxantrone having one unit residual positive charge interacts with anionic SDS micelles through electrostatic and hydrophobic modes [19]. It is interesting to note here that binding constant for mitoxantrone–SDS micelles is less than that of AQSH–SDS micelles which means that hydrophobic interactions are more important. Using the pK_a value of phenolic-OH of AQSH as 8.10,

percentage of phenoxide ion (AQS⁻) in the experimental solution at pH 7.40 was found to be 19.95%. During interaction of AQSH with SDS micelles there is competition between AQS⁻ and AQSH to penetrate the micelle. Due to greater negative charge and lower concentration, AQS⁻ has lower probability of interaction compared to AQSH with anionic SDS.

Measurement of partition coefficient (K_X) is another important aspect for characterizing drug–membrane interactions since it depicts the affinity of a molecule to fuse into a micellar phase from an aqueous solution. K_X helps in illuminating the mechanism of solubilization of a drug molecule, helping us to understand biological phenomenon like interaction of drugs with biological membranes. By considering the pseudo-phase model [19, 21, 22] K_X was evaluated using equation 4:

$$\frac{1}{\Delta A} = \frac{1}{\Delta A_\infty} + \frac{n_w}{K_X A_\infty ([L] + C_T - \text{CMC})} \quad [4]$$

where, $\Delta A = A - A_0$, $\Delta A_\infty = A_b - A_0$, $[L] = [\text{SDS}]$ and $n_w = 55.51 \text{ M}$ is the molarity of water. Value of K_X was calculated from the slope of the plot of $1/\Delta A$ vs. $1/([\text{SDS}] + C_T - \text{CMC})$ (Figure 8c) and found to be $(1.59 \pm 0.04) \times 10^6$ (Table 3) [Reduced Chi squared = 0.14]. It is necessary to note that in a large region of the surfactant concentration, the above mentioned linear relation clutches fine, below which the curve tends to bend upwards with decreasing surfactant concentration. A departure from linearity was owing to estimation made in the evaluation of equation 4 [22].

The standard free energy change for the transfer of AQSH from the bulk aqueous phase to micellar phase was obtained as -35.40 kJ/mol (Table 3) by putting the value of K_X in Eq. 5 [20] (mentioned in Table 1).

$$\Delta G_x^0 = -RT \ln K_X \quad [5]$$

The partition coefficient corresponding to distribution of positively charged mitoxantrone in SDS micelle was studied by Enache et al. [19] in different concentrations of mitoxantrone and K_x values were found to be smaller than AQSH (a negatively charged molecule) in similar micelles as in the present study. In that study [19] mitoxantrone was established to be interacting with anionic surfactant both through electrostatic and hydrophobic modes. Under similar experimental conditions, K_x of 2-amino-3-hydroxyanthraquinone was 5.22×10^4 [13] which is smaller than that in the present work. Since in that study [13] hydrophobic interaction was suggested, comparing those results with the current report, it may be said hydrophobic interaction is more important in the distribution of AQSH in anionic SDS micelles.

Table 3: Binding constant (K), partition coefficient (K_x), Gibbs free energy of binding (ΔG^0) and the standard free energy change (ΔG^0_x) for the transfer of AQSH from aqueous to micellar phase for the interaction of AQSH with surfactants

Binding parameters	SDS
K, M^{-1}	$(1.21 \pm 0.06) \times 10^5$
$\Delta G^0, kJ mol^{-1}$	-29.02
K_x	$(1.59 \pm 0.04) \times 10^6$
$\Delta G^0_x, kJ mol^{-1}$	-35.40

5.2.8. Biological Study

To see whether information obtained from the analysis of the electronic and molecular structure of AQSH and its efficiency in penetrating a micellar phase is really useful in infusing a

biological membrane and induce apoptosis, it was allowed to interact with A549 human lung cancer cells which was studied by different assays.

5.2.9. Cell viability Assay

Cytotoxic activity of AQSH was investigated against A549 human lung cancer cells using MTT assay [23]. Cytotoxic activity was estimated according to dose values of the exposure of the experimental molecule required to reduce survival to 50% (IC_{50}) in comparison to untreated cells. The IC_{50} value was found to be $83.5 \pm 0.05 \mu M$ after incubation for 24 h. Results of MTT assay hint at the fact that AQSH exhibits dose dependent toxic effect on A549 cells (Figure 9).

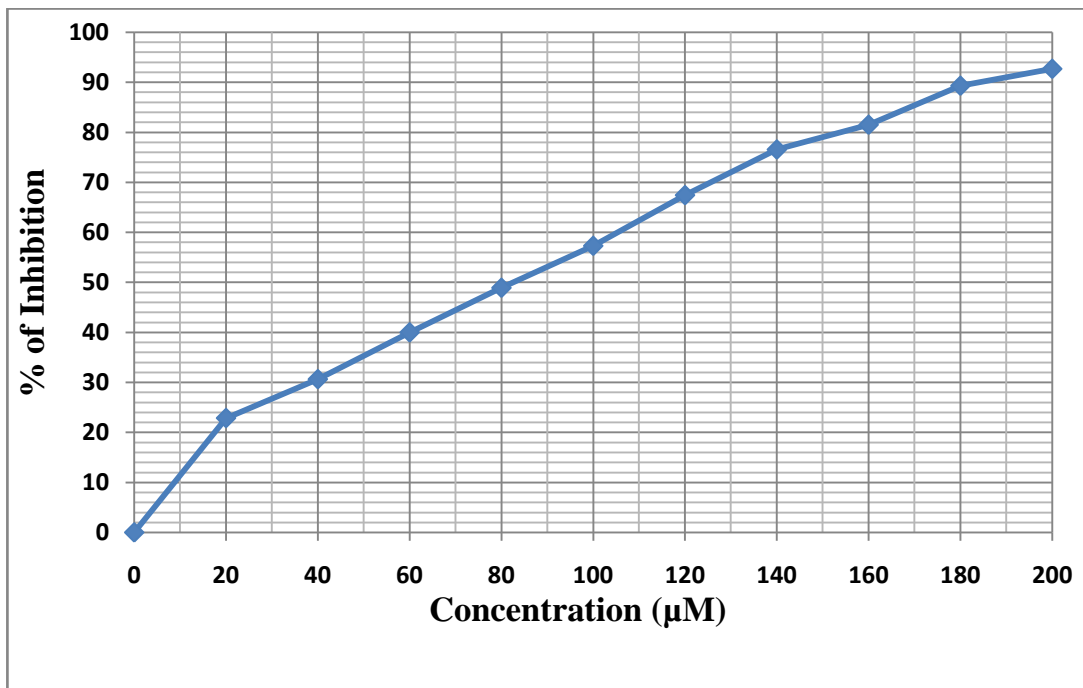


Figure- 9: Cytotoxic effect of AQSH on A549 cells after exposure for 24 h.

5.2.10. AO/EB staining

Morphological changes in apoptosis induced by AQSH were determined by AO/EB staining. Figure 10 shows AO/EB double-stained A549 human lung cancer cells which was treated with AQSH and incubated for 24 hours. Control or viable cells reveal green fluorescence and normal cells feature of uniform chromatin with an intact cell membrane, whereas late and early apoptotic cells showed yellowish green and orange-red color, respectively. The AO/EB results clearly indicate that AQSH leads most of the cell death by apoptosis mode and very few in the necrosis pathway after incubating for 24 hours (Figure 10).

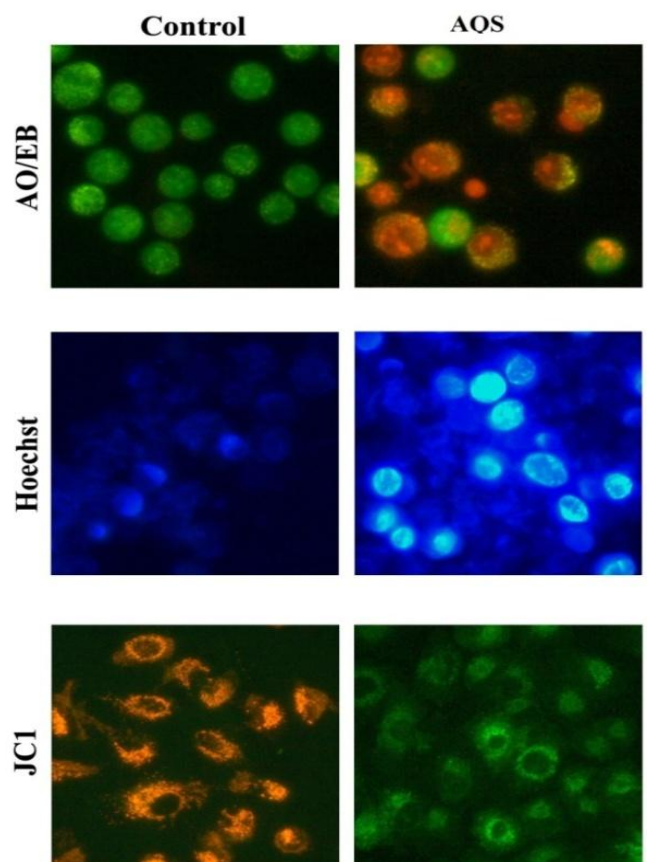


Figure 10: AO/EB staining, Hoechst, and JC-1 Staining. Control, DAU II, DNI-8, Ag-Nano and DAU+Ag+Bpy treated cells.

5.2.11. Hoechst 33528 staining

Hoechst staining was introduced to estimate apoptosis at a basic level. Results of Hoechst expressed the changes in morphology of the cells, with special reference to cytoplasm and nucleus. The observations expressed that early apoptotic features like chromatin condensation and fragmentation were mostly seen in AQSH treated cells; small numbers of necrotic cells were also observed (Figure 10 and 11).

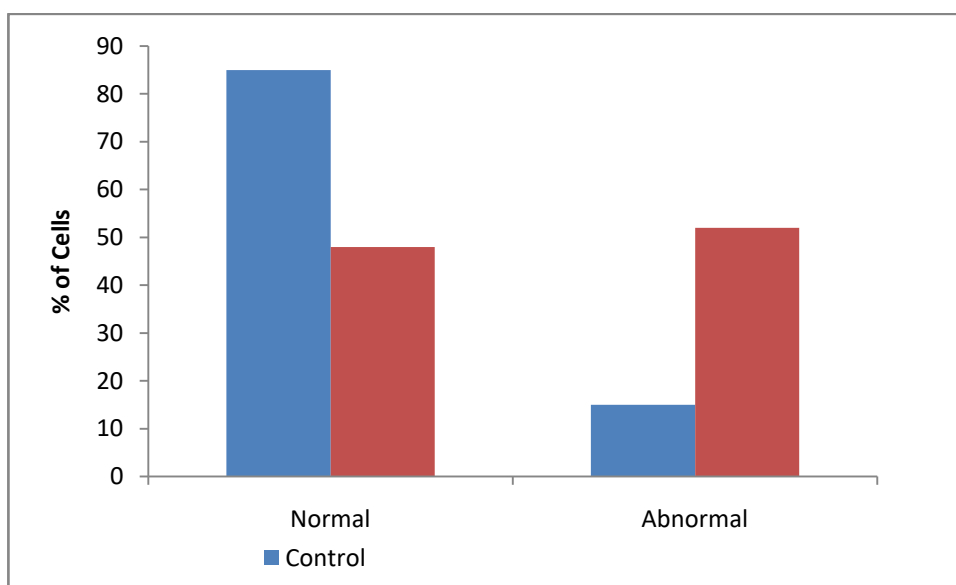


Figure 11: Hoechst 33258 staining study of control and AQSH treated cells. Graph is shown manual count of apoptotic cells in percentage.

5.2.12. Assessment of mitochondrial membrane potential (JC1 staining)

AQSH induced mitochondrial membrane potential depolarization was assessed with the JC-1 assay. The fluorescent cationic dye JC-1 accumulates in the mitochondria of control or healthy cells and emits red fluorescence. Conversely, cells undergoing apoptosis, fluoresce green due to mitochondrial membrane depolarization. Results of JC-1 staining of lung cancer cells

treated with AQSH at 12 hours incubation confirms loss of mitochondrial membrane potential while control cells were seen to have healthy mitochondria (Figure 10).

5.3. Conclusion

AQSH was prepared and characterized by different experimental and theoretical techniques. Binding constant for the interaction of AQSH with SDS was $(1.21 \pm 0.06) \times 10^5 \text{ M}^{-1}$ and the corresponding Gibbs free energy was $-29.02 \text{ kJmol}^{-1}$. Hydrophobic interactions were identified to be important in AQSH–SDS micellar interaction. In order to see whether these results are really important for AQSH to infuse a biological membrane and induce apoptosis it was allowed to interact with A549 human lung cancer cells. The studies showed that AQSH induced apoptosis in A549 human lung cancer cells with IC_{50} value found as $83.5 \pm 0.05 \text{ }\mu\text{M}$ for a 24 hour incubation.

References

1. S. Rossi, C. Tabolacci, A. Lentini, B. Provenzano, F. Carlomosti, S. Frezzotti, S. Beninati, *Anticancer Res.* 30 (2010) 445-450.
2. P. Das, C. K. Jain, S. K. Dey, R. Saha, A. D. Chowdhury, S. Roychoudhury, S. Kumar, H. K. Majumder, S. Das. *RSC Adv.* 4 (2014) 59344-59357.
3. P. Das, D. Bhattacharya, P. Karmakar, S. Das, *RSC Adv.* 5 (2015) 73099-73111.
4. P. Mondal, S. Roy, G. Loganathan, B. Mandal, D. Dharumadurai, M. A. Akbarsha, P. S. Sengupta, S. Chattopadhyay, P. S. Guin, *Biochem. Biophys. Rep.* 4 (2015) 312–323.
5. P. Das, P. S. Guin, P. C. Mandal, M. Paul, S. Paul, S. Das, *J. Phys. Org. Chem.* 24 (2011) 774-785.
6. S. Roy, P.S. Guin, *J. Electrochem. Soc.* 162 (2015) H124–H131.

7. S. Roy, P. Mondal, P. S. Sengupta, D. Dhak, R.C. Santra, S. Das, P. S. Guin, Dalton Trans. 44 (2015) 5428–5440.
8. P. S. Guin, S. Das, P. C. Mandal, J. Inorg. Biochem. 103 (12) (2009) 1702-1710.
9. P. S. Guin, P. C. Mandal, S. Das, ChemPlusChem, 77 (5) (2012) 361-369.
10. B. Alberts, A. Johnson, J. Lewis, et al. Molecular Biology of the Cell. 4th edition. New York: Garland Science (2002).
11. I. D. Pogozheva, S. Tristram-Nagle, H. I. Mosberg, A. L. Lomize, Biochim.etBiophys.Acta (BBA) – Biomembranes, Volume 1828, Issue 11 (November 2013) 2592–2608.
12. S. C. Oyaga, J. C. Valdés, S. B. Paez, K.H. Marquez, J. Theor. Chem. 2013, Article ID 526569, 8 pp.
13. A. Das, S. Roy, P. Mondal, A. Datta, K. Mahali, G. Loganathan, D. Dharumadurai, P. S. Sengupta, M. A. Akbarsha, P. S. Guin, RSC Adv., 6 (2016) 28200-28212.
14. M. H. Jamroz, Vibrational Energy Distribution Analysis VEDA 4, Warsaw, 2004-2010.
15. J. B. Foresman and A. Frish, Exploring Chemistry with electronic structure methods, Gaussian, Inc., Pittsburgh, PA, USA (2000) p. 64.
16. A.V. Iogansen, Spectrochim. Acta. Part A 55 (1999) 1585–1612.
17. E. Fuguet, C. Rafols, M. Roses, E. Bosch, Anal.Chim.Acta 548 (2005) 95–100.
18. M. Sarkar, S. Poddar, J. Colloid Interface Sci. 221 (2002) 181–185.
19. M. Enache, I. Anghelache, E. Volanschi, Int. J. Pharmaceutics 390 (2010) 100–106.
20. M. Enache, E. Volanschi, J. Pharma. Sci. 100 (2011) 558 – 565.
21. R. Sabate, M. Gallardo, J. Estelrich, J. Colloid Interface Sci. 233 (2001) 205–210.
22. R. Sabate, M. Gallardo, A. de la Maza, J. Estelrich, Langmuir 17 (2001) 6433–6437.
23. T. Mosmann, J. Immunol. Methods, 65 (1983) 55–63

Chapter: 6

Formation and characterization of a Cu^{II} complex of sodium 2-amino-3-hydroxy-9,10-anthraquinone-1-sulphonate and studies on its electrochemical behavior, interaction with SDS micelles and nucleation in A549 human lung cancer cells

6. 1. Introduction

Metal complex formation of anthracycline reduces the aspects of toxic side effects [1-3]. The presence of metal ion in such metal complexes stabilizes the semiquinone formed by the electrochemical reduction and hence reduces the toxicity [4, 5]. Therefore, for this study, we decided to prepare a Cu^{II} complex of sodium 2-amino-3-hydroxy-9,10-anthraquinone-1-sulphonate (AQSH) and look at its electrochemical behavior in different solvents having varying polarity, to see whether it mimics the action of anthracycline drugs.

The most important aspect of a molecule during the course of its biological action is its ability to pass through the cell membrane [6, 7]. Earlier studies have established that the mechanism of drug action is related to its binding to the membrane at the molecular level [8-11]. Drug – surfactant interactions have been studied by several workers using various techniques due to the wide spread application of surfactants in pharmaceutical field [12]. Micellar systems possess the ability to solubilize hydrophobic drugs [13–15] thereby increasing their bioavailability and can be used as a model system for bio-membrane, as well as drug carriers in numerous drug delivery and drug targeting systems [16–18]. The physicochemical interactions of drugs with surfactant micelles can be envisaged as an approximation for their interactions with biological membranes. This provides an insight into more complex biological processes like passage of drugs through cell membranes. Thus to see whether the prepared Cu^{II} complex is able to penetrate biological membranes, a model study on its interaction with SDS micelles was performed. The complex was also tried on A549 human lung cancer cells to find out if it is able to induce apoptosis, thereby, raising hopes that it might be used as an anticancer agent in the near future.

6.2. Results and Discussions

6.2.1. Stoichiometry of complex formation due to Cu^{II} and AQSH at neutral pH

Absorption spectra of sodium 2-amino-3-hydroxy-9,10-anthraquinone-1-sulphonate (AQSH) at neutral pH both in the absence and the presence of different amounts of Cu^{II} were recorded. To determine stoichiometry of the copper complex formed in solution, a mole-ratio study was performed. Keeping AQSH concentration fixed metal concentration was varied from a ratio of 0.10 to 6.40 and absorbance was measured at 520 nm. In the mole ratio plot, two straight lines were obtained, the intersection of which determines stoichiometry of complex formation in aqueous solution. Figure 1 suggests stoichiometry of the Cu^{II} complex in the solution has a metal to AQSH ratio of 1:2, at neutral pH.

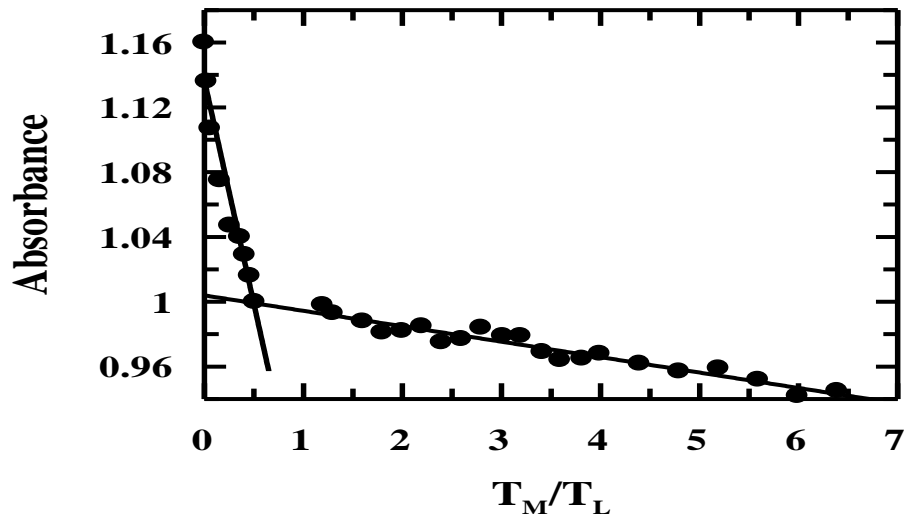


Figure 1: Mole-ratio plot of the absorbance of AQSH at 520 nm at varying $[\text{Cu}^{2+}]/[\text{AQSH}]$ for a fixed AQSH concentration, at neutral pH; $[\text{AQSH}] = 50 \mu\text{M}$, $[\text{NaCl}] = 10 \text{ mM}$, 25°C .

6.2.2. Determination of formation constant of Cu(AQS)₂ complex in aqueous solution

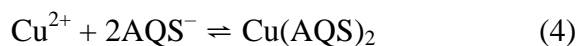
pK of AQSH in aqueous solution was determined by a spectrophotometric titration as described in Chapter 5 (Section 5.2.6). The value was found to be 8.10 ± 0.05 . To determine the binding constant of Cu(AQS)₂, Cu^{II} and AQSH were taken in the mole ratio 1:2 and a spectrophotometric titration was carried out. At first Cu^{II} and AQSH were taken in the ratio 1:2 and the mixture was acidified to pH 2.23. It was slowly titrated with 0.01 M NaOH solution keeping Cu^{II} and AQSH concentrations fixed. Absorption spectra at various pH were recorded (Figure 2). It was found that intensity of the peak at 520 nm gradually increased with an increase in pH. The change in absorbance at 520 nm was monitored against pH (Figure 3). A_{obs} for AQSH at 520 nm in the presence of Cu^{II} was fitted according to equation (1).

$$A_{520} = \frac{A_1}{1 + 10^{(pH-pK)}} + \frac{A_2}{1 + 10^{(pK-pH)}} \quad [1]$$

A_{520} denotes the overall absorbance of the solution at 520 nm at different pH while A_1 and A_2 are absorbances of AQSH and AQS⁻ respectively in presence of Cu^{II}. Fitting the experimental data according to equation 1, pK was found to be 6.03 ± 0.04 . During complex formation, the phenolic-OH proton of AQSH would be released. This value of pK (6.03 ± 0.04) was used to determine the binding constant of the complex. Formation constants β^* and β for the 1:2 complex can then be described as follows:



$$\beta^* = \frac{[\text{Cu}(\text{AQS})_2][\text{H}^+]^2}{[\text{Cu}^{2+}][\text{AQSH}]^2} \quad (3)$$



$$\beta = \frac{[\text{Cu}(\text{AQS})_2]}{[\text{Cu}^{2+}][\text{AQS}^-]^2} \quad (5)$$

From equations (3) and (5) β can be deduced as

$$\beta = \beta^* / K^2 \quad (6)$$

where K is the equilibrium constant for the dissociation of phenolic-OH of AQSH. Hence, formation constant β^* and β of the Cu^{II} complex were determined. β was found to be 5.52×10^{12} and $\log \beta$ was 12.74.

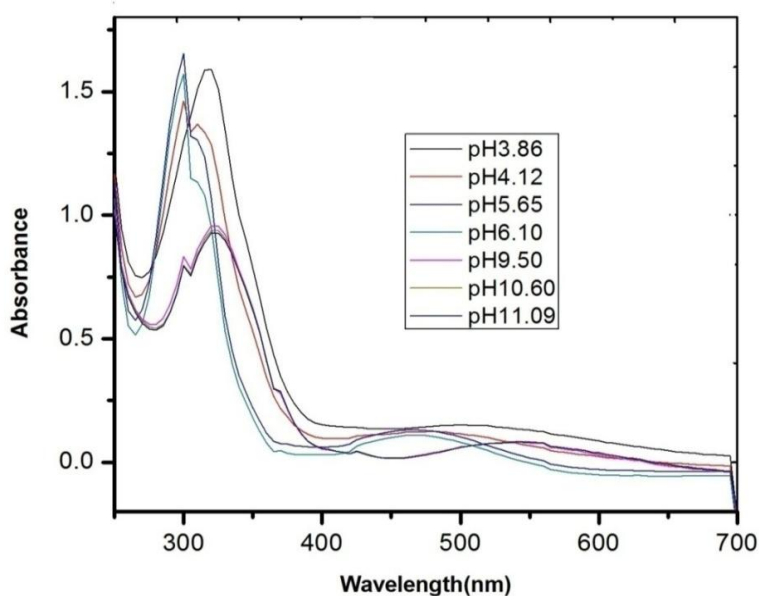


Figure 2: UV-Vis spectra of a 1:2 mixture of Cu^{II} and AQSH in aqueous media at different pH. $[\text{Cu}^{\text{II}}] = 25 \mu\text{M}$, $[\text{AQSH}] = 50 \mu\text{M}$, $[\text{NaCl}] = 0.01 \text{ M}$, $T = 298.15 \text{ K}$.

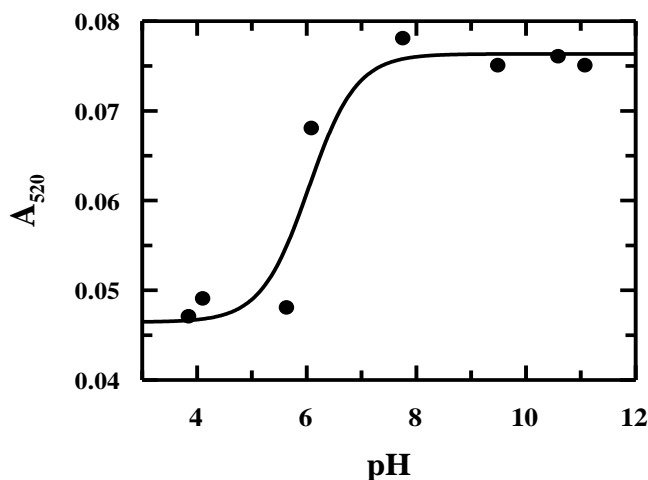


Figure 3: Spectrophotometric titration of AQSH in presence of Cu^{2+} , shown by a variation in absorbance at 520 nm; $[\text{AQSH}] = 50 \mu\text{M}$, $[\text{Cu}^{2+}] = 25 \mu\text{M}$, $[\text{NaCl}] = 10 \text{ mM}$, 25°C .

6.2.3. Analysis of thermo-gravimetric response due to the copper complex

The thermo-gravimetric analysis was performed based on the fact that Cu^{II} forms an octahedral complex with two quinone ligands having a molecular weight of 743.66. At 134°C there is a slight decrease corresponding to a molecular mass of 691.66. Hence, loss in weight of 52.00 might correspond to the loss of one butadiene unit. The next characteristic decrease was observed at 170°C and corresponds to a mass of 636.59. Hence, the decrease in mass of 107.06 is due to the loss of two butadiene units, one from each ligand. The next decrease was noticed at 232.56°C having a mass at this stage of 568.30. Hence the breakaway portion could be due to loss of two butadiene units, one from each ligand and four quinone oxygens.

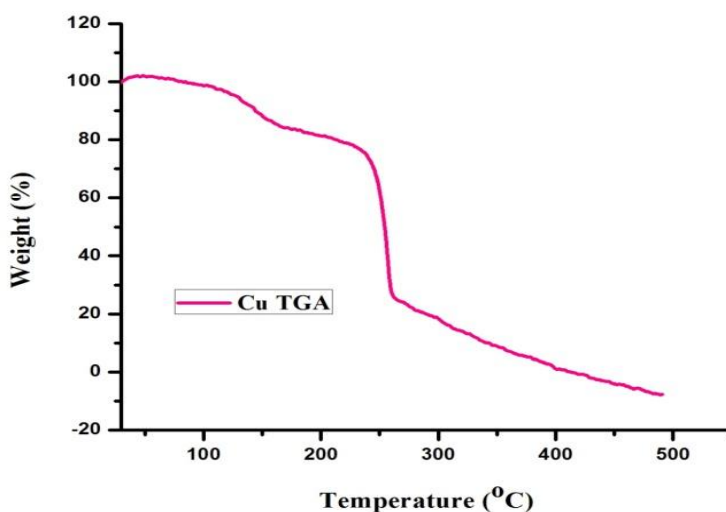


Figure 4: TG analysis of the copper complex.

6.2.4. Analysis of the IR spectrum of the copper complex

In the IR spectrum of AQSH (Figure 5b, Chapter 5, Sec. 5.2.5) O–H and N–H stretching frequencies were found at 3500 and 3353.04 cm^{-1} respectively. In case of the complex (Figure 5),

important changes were seen in the range 3300 – 3500 cm^{-1} . The O–H peak at 3500 cm^{-1} is not seen due to formation of a covalent bond between the phenoxide unit and Cu^{2+} ion. In Figure 5 the N-H stretching frequency shifts slightly at 3349 cm^{-1} [19] suggesting nitrogen of $-\text{NH}_2$ coordinates with Cu^{II} . Other characteristic peaks of the free ligand did not change in case of the complex. This clearly indicates that phenolic $-\text{OH}$ and $-\text{NH}_2$ are involved in complex formation with Cu^{II} (Scheme- 1).

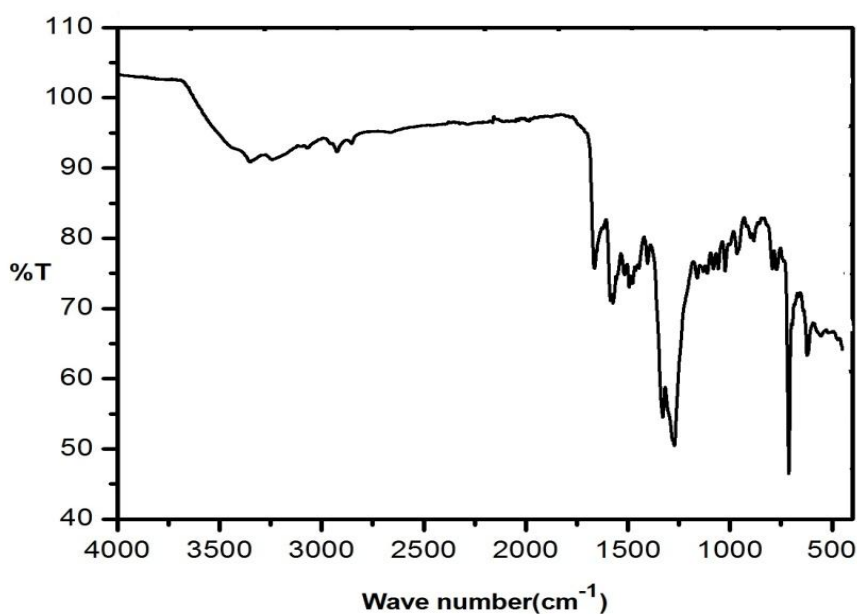
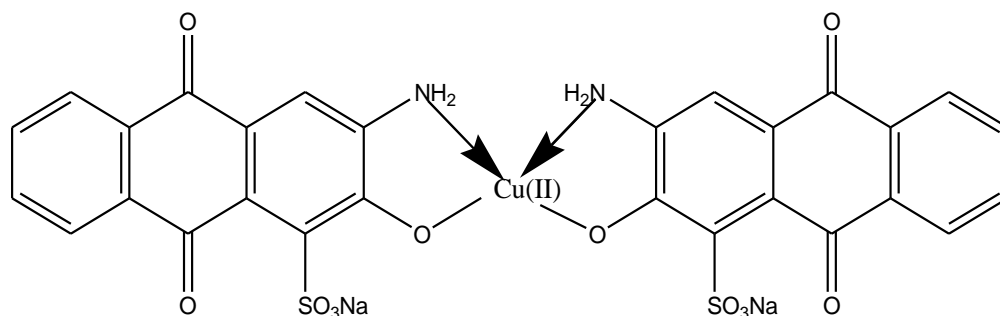


Figure 5: IR spectra of $\text{Cu}(\text{AQS})_2$.



Scheme 1: Structure of the Cu^{II} complex of AQS.

6.2.5. Analysis of the EPR spectra of the copper complex

ESR spectrum of the copper complex (Figure 6) in the solid state provides information about the environment around metal ion in the complex. Room-temperature ESR spectrum of crystalline $\text{Cu}(\text{AQS})_2$ exhibits only one large signal without hyperfine splitting, with a g value of 2.06 ($\Delta H_{\text{pp}} = 3.7$ mT) which is greater than the g value of a free electron, 2.0023. This clearly indicates that there is increase in covalent nature of bonding between metal ion and AQS [20].

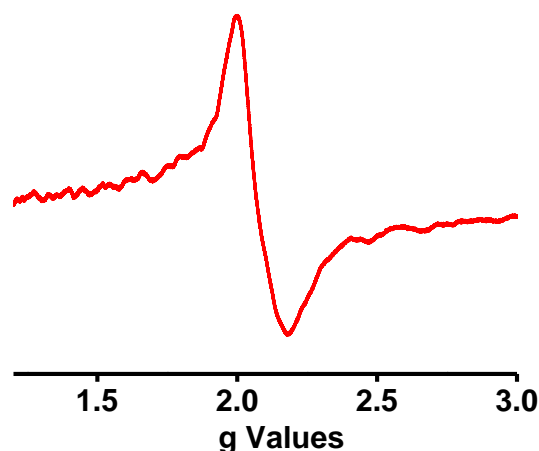


Figure 6: The ESR spectrum of $\text{Cu}(\text{AQS})_2$.

6.2.6. Electrochemical behavior of AQS and its Cu^{II} complex in anhydrous non-aqueous media

As observed earlier for similar quinone systems [21,22], in anhydrous acetonitrile (ACN) and dimethyl formamide (DMF) in the presence of 0.1 M tetrabutyl ammonium bromide (TBAB), AQS also undergoes successive two one-electron reduction to give semiquinone -935 and -940 mV in ACN and DMF respectively and quinone dianion at -1270 and -1340 mV in ACN and DMF respectively. The two reduction peaks are well separated by 335 and 400 mV in ACN and DMF respectively (Figure 7 and 8). From the cyclic voltammograms (Figure 7 and Figure 8) it is clear that both the reductions are irreversible in both solvents at different scan

rates. Irreversibility in reductions is probably due to the presence of an electron withdrawing sulphonate group having – R effect at C1-position of AQSH. The first reduction potentials are almost same while the second reduction potentials are significantly different in both solvents. The more negative second reduction potential of AQSH in anhydrous DMF in comparison to that in anhydrous ACN is due to greater polarity of DMF than ACN. The quinone dianion formed by AQSH in two successive reduction steps is more stabilized in DMF than in ACN as the former has greater polarity. Both first reductions were seen to be diffusion controlled as cathodic reduction peak current (I_{pc}) varies linearly with square root of scan rate ($v^{1/2}$). The diffusion coefficient (D_0) was calculated by using Equation 7 and by plotting cathodic peak current (I_{pc}) versus square root of scan rate ($v^{1/2}$) (Figure 9) it was estimated to be 1.344×10^{-5} and 7.84×10^{-6} cm^2s^{-1} in anhydrous ACN and DMF respectively.

$$I_{pc} = (2.687 \times 10^5) n^{3/2} D_0^{1/2} A C v^{1/2} \quad (7)$$

I_{pc} = Cathodic peak current in amperes, n = number of electrons involved in the reduction, A = Area of the electrode (cm^2); C = Concentration (moles/ cm^3), v = Scan rate (V/s).

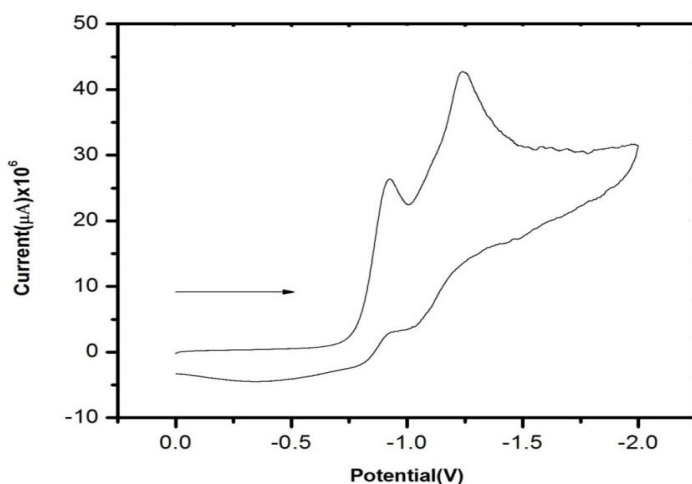


Figure 7: Cyclic voltammogram of AQSH in anhydrous ACN. Scan rate: 0.10 V s^{-1} . $[\text{AQS}] = 1 \times 10^{-3} \text{ M}$, $[\text{TBAB}] = 0.1 \text{ M}$, $T = 298.15 \text{ K}$.

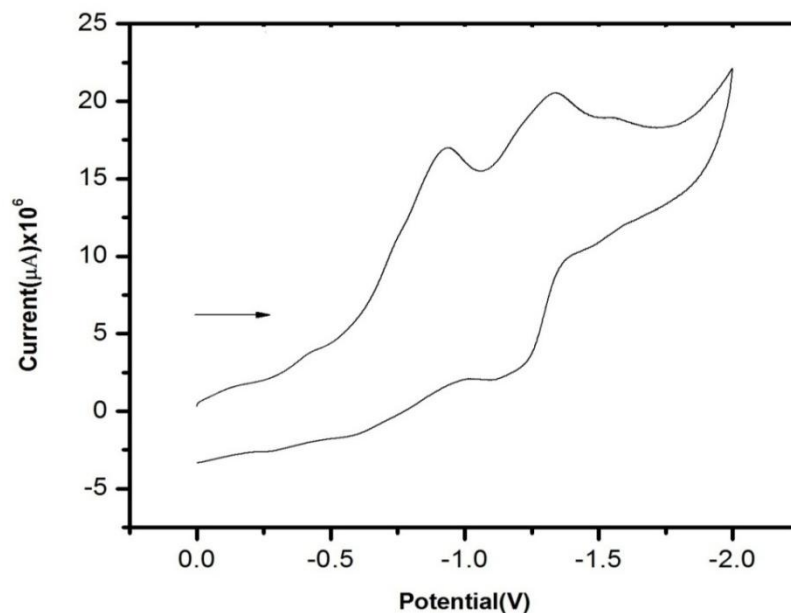


Figure 8: Cyclic voltammogram of AQSH in anhydrous DMF. Scan rate: 0.10 V s^{-1} . [AQSH] = $1 \times 10^{-3} \text{ M}$, [TBAB] = 0.1 M , $T = 298.15 \text{ K}$.

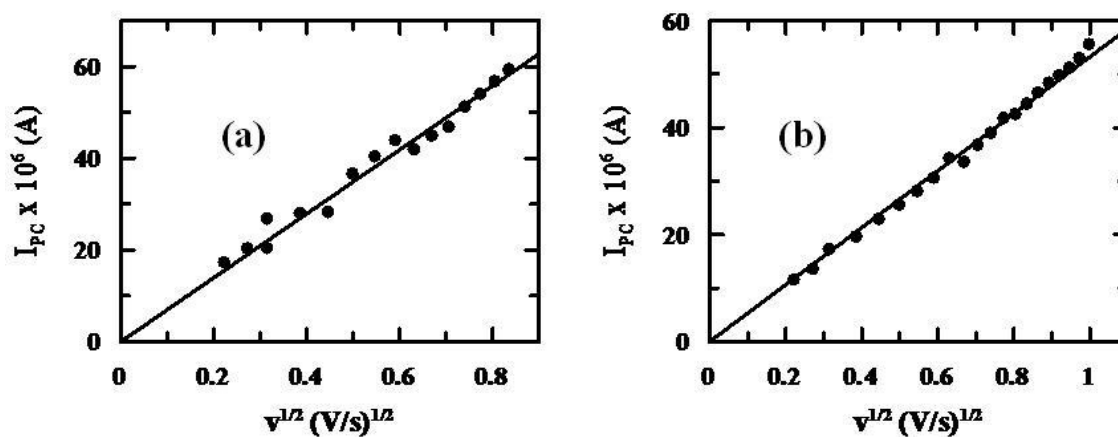


Figure 9: Plot of I_{pc} vs. square root of scan rate ($v^{1/2}$) of AQSH in (a) anhydrous ACN media and in (b) anhydrous DMF media.

Cyclic voltammograms of $\text{Cu}(\text{AQS})_2$ in anhydrous ACN and DMF in the presence of 0.1 M tetrabutyl ammonium bromide (TBAB) are shown in Figure 10 and 11 respectively. In anhydrous ACN, $\text{Cu}(\text{AQS})_2$ undergoes successive three one-electron reduction with reduction

potentials of -775 , -920 and -1260 mV respectively. Comparing the cyclic voltammogram of $\text{Cu}(\text{AQS})_2$ in ACN (Figure 10) with that of free AQSH in ACN (Figure 7), it can be said that the second and third reduction potentials of $\text{Cu}(\text{AQS})_2$ are comparable to those of AQSH though such potential values are increased to some extent in the metal complex. Such increase in the second and third reduction potentials in $\text{Cu}(\text{AQS})_2$ is probably due to stabilization of the formed semiquinone and quinone dianion by Cu^{2+} . However, the first weak reduction peak at -775 mV is probably due to the reduction of a third quinone moiety in AQSH present in the complex since there is a total of four quinone moieties present in $\text{Cu}(\text{AQS})_2$. An oxidation peak at -400 mV is most probably due to oxidation of Cu^{I} formed by electron transfer from the formed semiquinone and quinone dianion to Cu^{2+} . The second and third reduction potentials are slightly greater than that of free AQSH which is probably due to stabilization of the semiquinone and quinone dianion by Cu^{II} .

In anhydrous DMF, there are three reduction peaks of $\text{Cu}(\text{AQS})_2$ at -925 -1220 and -1330 mV (Figure 11). As found in ACN, an oxidation peak at -400 mV is also seen in DMF. Such reduction and oxidation of the experimental molecule in DMF can be explained as discussed above for ACN. The diffusion coefficient (D_0) for reduction of $\text{Cu}(\text{AQS})_2$ was calculated by plotting the cathodic peak current (I_{pc}) versus square root of scan rate ($v^{1/2}$) using Equation 7 (Figure 12). D_0 was estimated to be 9.69×10^{-3} and $8.05 \times 10^{-3} \text{ cm}^2 \text{ s}^{-1}$ in anhydrous ACN and DMF respectively. Comparing electrochemical behaviour of $\text{Cu}(\text{AQS})_2$ with AQSH it can be said that this behaviour of AQSH is significantly modified when bonded to Cu^{II} in $\text{Cu}(\text{AQS})_2$.

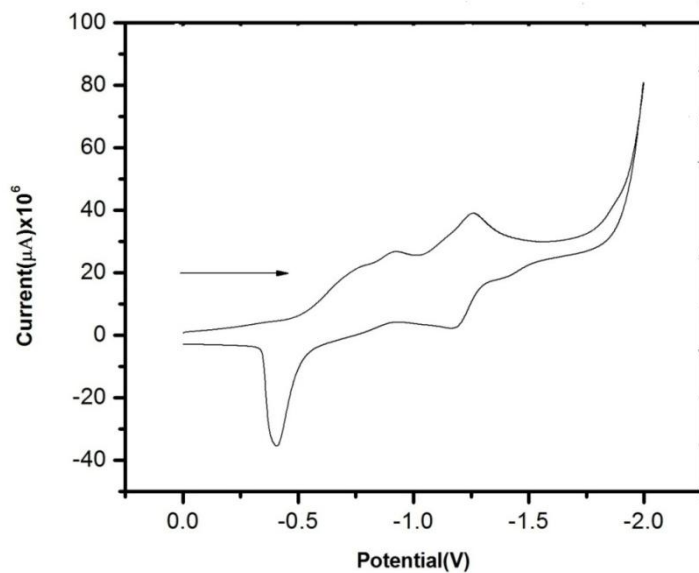


Figure 10: Cyclic voltammogram of $\text{Cu}(\text{AQS})_2$ in anhydrous ACN. Scan rate: 0.10 Vs^{-1} . $[\text{Cu}(\text{AQS})_2] = 50 \times 10^{-6} \text{ M}$, $[\text{TBAB}] = 0.1 \text{ M}$, $T = 298.15 \text{ K}$.

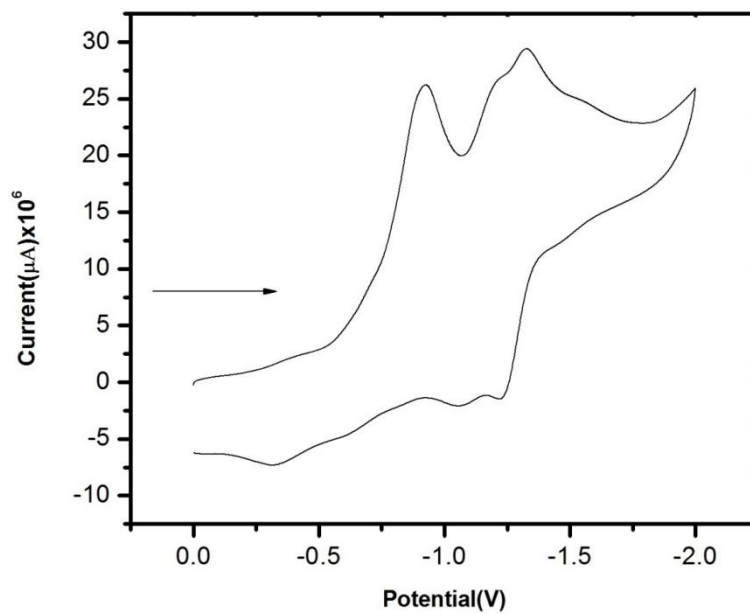


Figure 11: Cyclic voltammogram of $\text{Cu}(\text{AQS})_2$ in anhydrous DMF media. Scan rate: 0.10 Vs^{-1} . $[\text{Cu}(\text{AQS})_2] = 50 \times 10^{-6} \text{ M}$, $[\text{TBAB}] = 0.1 \text{ M}$, $T = 298.15 \text{ K}$.

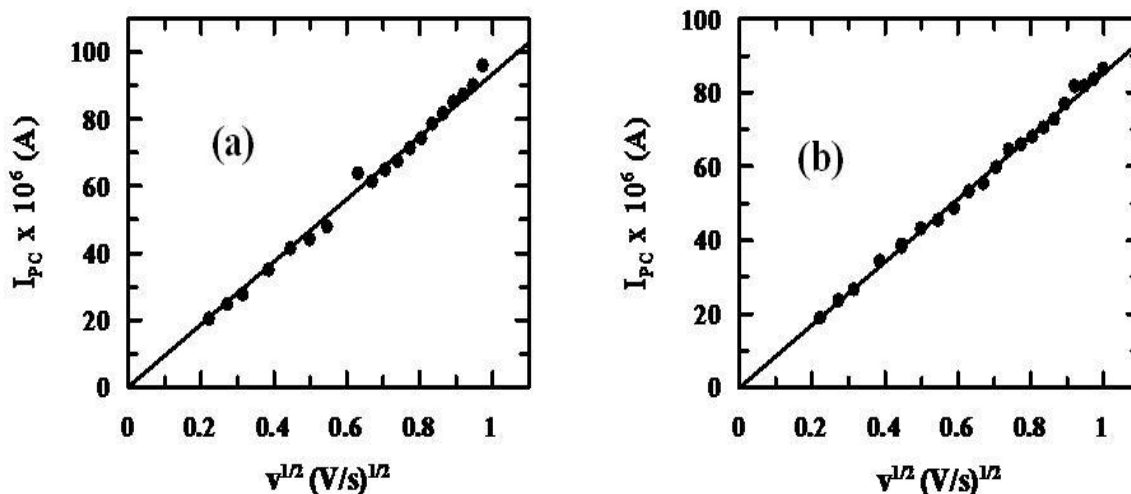


Figure 12: Plot of I_{pc} vs. square root of scan rate ($v^{1/2}$) for $\text{Cu}(\text{AQS})_2$ in (a) anhydrous ACN (b) and in anhydrous DMF.

6.2.7. Interaction of $\text{Cu}(\text{AQS})_2$ with SDS micelles

Surfactant interaction of $\text{Cu}(\text{AQS})_2$ was performed at physiological pH with SDS micelles. This was followed with the help of UV–Vis spectroscopy in pre-micellar and micellar concentration span under the influence of phosphate buffer having a concentration of 100 mM. Spectrophotometric titration was carried out at a wavelength of 510 nm by keeping concentration of $\text{Cu}(\text{AQS})_2$ fixed with changing concentrations of SDS that was already prepared. Thus the corresponding parameters of such $\text{Cu}(\text{AQS})_2$ –SDS interaction was determined. Each reaction mixture was incubated for 1–2 min. Gradual addition of SDS micelle to the experimental solution of $\text{Cu}(\text{AQS})_2$ leads to a variation of absorbance of $\text{Cu}(\text{AQS})_2$ depicted by Figure 13. The change in absorbance is significant for calculating the CMC of SDS during interaction with $\text{Cu}(\text{AQS})_2$ and it was evaluated to be 157 μM , This value of CMC was used for the entire calculation to evaluate binding parameters. CMC of SDS in pure water and in 50 mM phosphate buffer were evaluated as in an earlier study and found to be 8080 μM and 1990 μM respectively

[23]. Lowering of CMC value of SDS in comparison to that obtained earlier may be explained as an influence of various ions and molecules present in the mixture [24]. It was observed that increasing SDS concentration, the absorbance of Cu(AQS)₂ gradually decreased (wavelength 510 nm) which implies that enhanced surfactant concentration induced insertion of Cu(AQS)₂ at the interior of micelles till all binding sites inside the surfactant were occupied i.e. saturated. This results to a decrease in absorbance of Cu(AQS)₂ at a particular concentration of surfactant and thus CMC was achieved. A number of such studies have reported [23-30] the binding mode between metal-drug complex and surfactant through non-linear analysis by incorporating 1:1 interaction between them. Nature of binding isotherm was determined by using equation 8. Considering 1:1 interaction between Cu(AQS)₂ and SDS (Figure 14) the corresponding binding constant was evaluated as $(2.83 \pm 0.04) \times 10^4 \text{ M}^{-1}$ (Table 1) [25,26] (reduced Chi squared = 1.50×10^{-6}).

$$A = \frac{A_0 + A_\infty K [L]}{1 + K[L]} \quad (8)$$

L represents the surfactant (here SDS); A and A₀ are absorbance of Cu(AQS)₂ at 510 nm in the absence and presence of SDS. A_∞ corresponds to absorbance of Cu(AQS)₂ bound to SDS. Gibbs free energy for interaction of Cu(AQS)₂ to SDS micelles was calculated with the help of equation 9 and found to be -25.41 kJ/mol (Table 1) [27, 28].

$$\Delta G^0 = - RT \ln K \quad (9)$$

where R is the molar gas constant at 298.15 K.

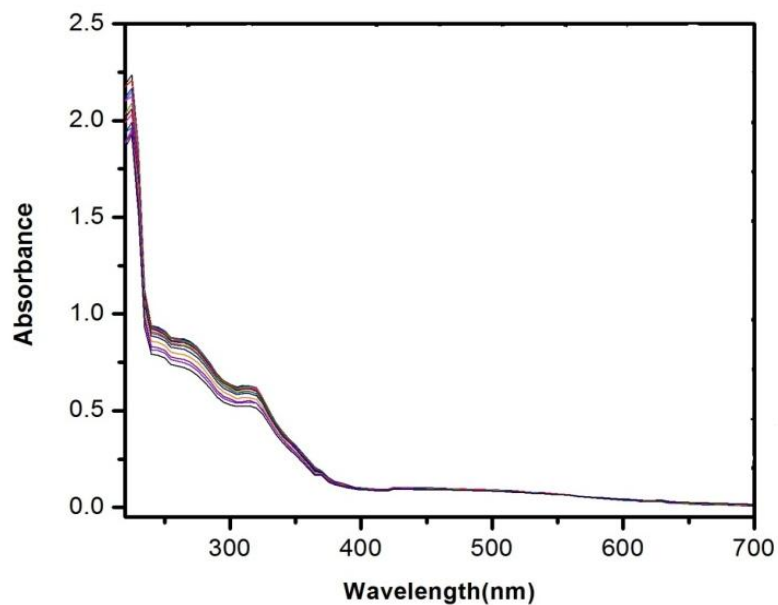


Figure 13: Absorption spectra of Cu(AQS)_2 ($50 \mu\text{M}$) in the absence and presence of increasing concentrations of SDS. [Phosphate buffer] = 100 mM, pH 7.4, T = 298.15 K.

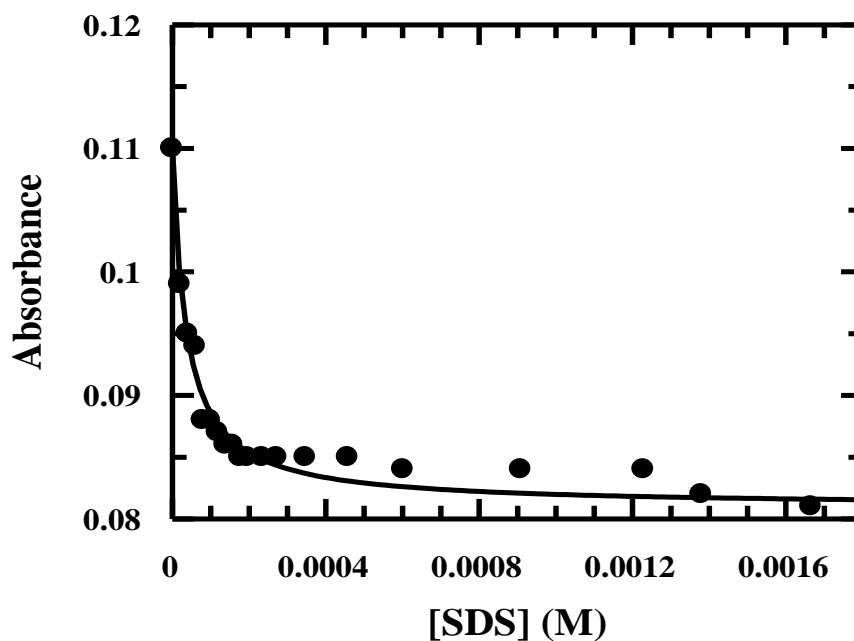


Figure 14: A non-linear fitting of the absorbance of Cu(AQS)_2 at 510 nm using equation- 9 considering 1:1 interaction between Cu(AQS)_2 and SDS.

Role of hydrophobic interaction in the binding of an analogous molecule with SDS micelles is more superior over the electrostatic interaction established by investigating a 1:1 interaction [31] of neutral 2-amino-3-hydroxyanthraquinone with SDS. In such a study the binding constant for the interaction was found as 652.81. In the present study, binding constant for the interaction of $\text{Cu}(\text{AQS})_2$ with SDS micelles was evaluated to be $(2.83 \pm 0.04) \times 10^4 \text{ M}^{-1}$. The present value is far greater than the earlier value [31] which means that in case of the present study hydrophobic interactions predominate over hydrophilic interaction. Under similar experimental conditions, the binding constant for 1:1 AQSH–SDS micelle interaction was found to be $(1.21 \pm 0.06) \times 10^5 \text{ M}^{-1}$ (Chapter 5, Section 5.2.7). This is indicative of the fact that $\text{Cu}(\text{AQS})_2$ is less efficient in penetrating SDS micelles and hence in penetrating a biomembrane in comparison to AQSH. The partition coefficient (K_X) for the transfer of $\text{Cu}(\text{AQS})_2$ from aqueous to micellar phase provides valuable information related to solubility of hydrophobic drugs. The value of partition coefficient (K_X) was determined by using a pseudo-phase model [27,29, 30] according to equation 10 as shown below.

$$\frac{1}{\Delta A} = \frac{1}{A_\infty} + \frac{n_w}{K_X A_\infty ([\text{SDS}] + C_T - \text{CMC})} \quad (10)$$

where, $\Delta A = A - A_0$, $\Delta A_\infty = A_b - A_0$, $[\text{L}] = [\text{SDS}]$ and $n_w = 55.55 \text{ M}$ is the molarity of water. The nature of the curve is linear upto a large concentration of surfactant but linearity falls sharply with decreasing surfactant concentration which can be measured by equation 10 [30]. The value of K_X was calculated from the slope of the plot of $1/\Delta A$ versus $1/([\text{SDS}] + C_T - \text{CMC})$ (Figure 15) and found to be $(4.48 \pm 0.05) \times 10^5$ [reduced Chi squared = 1.812].

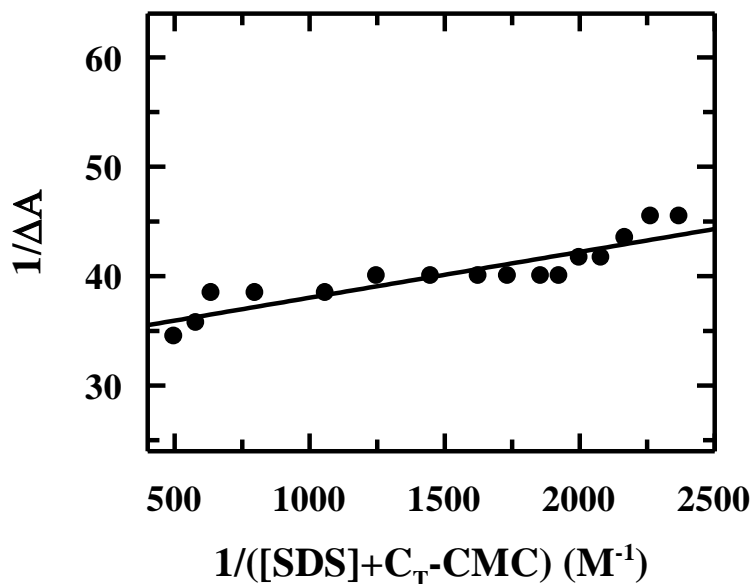


Figure 15: Plot of $1/|\Delta A|$ vs. $1/([SDS] + C_T - CMC)$ [equation-11] for $Cu(AQS)_2$ ($50 \mu M$) in SDS micelles at pH 7.4.

The value of partition coefficient thus obtained was compared with The standard free energy change for the transfer of $Cu(AQS)_2$ from aqueous to micellar phase was measured as -32.26 kJ/mol and may be calculated using equation 11 [28] (mentioned in Table- 1). As the standard free energy change is highly negative, movement of $Cu(AQS)_2$ molecule into the micellar phase from the hydrophilic location is thermodynamically feasible.

$$\Delta G^0_{x=} = - RT \ln K_x \quad (11)$$

Comparison with previous studies and it has been suggested that hydrophobic interactions play a fundamental role in the distribution of $Cu(AQS)_2$ in anionic SDS micelles.

Table 1: Binding constant (K), partition coefficient (K_x), standard Gibbs free energy of binding (ΔG^0) and the standard free energy change (ΔG^0_x) for the transfer of $\text{Cu}(\text{AQS})_2$ from aqueous to micellar phase for the interaction of $\text{Cu}(\text{AQS})_2$ with surfactants.

Binding parameters	SDS
K, M^{-1}	$(2.83 \pm 0.04) \times 10^4$
$\Delta G^0, \text{kJ mol}^{-1}$	-25.41
K_x	$(4.48 \pm 0.05) \times 10^5$
$\Delta G^0_x, \text{kJ mol}^{-1}$	-32.26

6.2.8. Cell Viability Assay

Cytotoxic activities of AQSH and $\text{Cu}(\text{AQS})_2$ were investigated against A549 human lung cancer cells by the MTT assay [19]. The cytotoxic activity was determined according to the dose used for exposure of the complex required to reduce survival to 50% (IC_{50}), compared to untreated cells. The IC_{50} values of AQSH and $\text{Cu}(\text{AQS})_2$ were found to be $(83.5 \pm 0.05) \mu\text{M}$ and $(125 \pm 0.05) \mu\text{M}$ respectively. Results of the MTT assay indicate that compounds exhibit dose dependent toxic effects against the treatment with A549 cells (Figure 17).

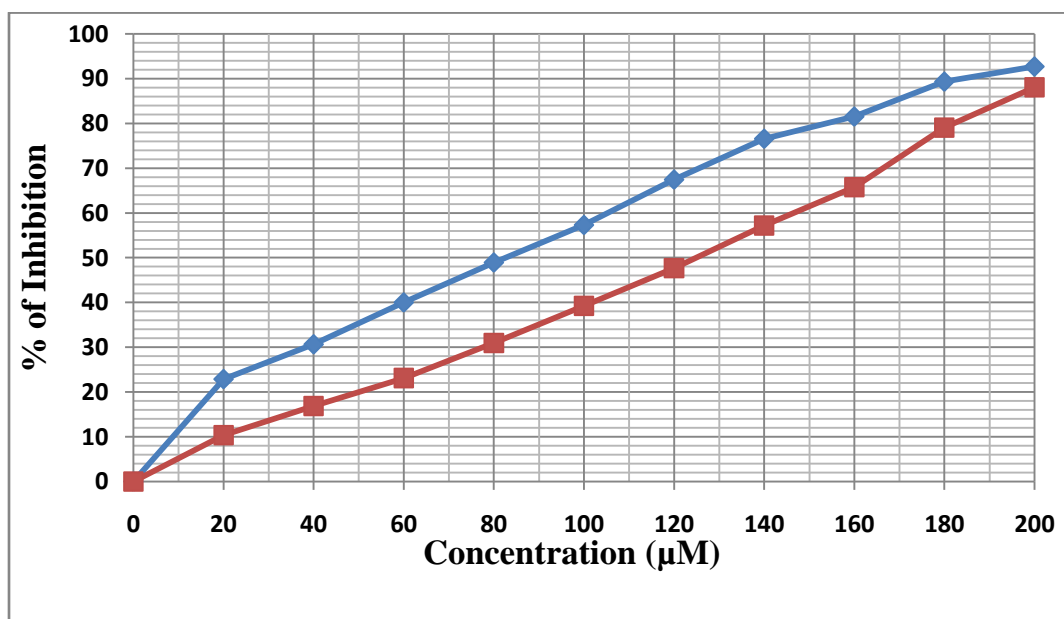


Figure 16: Cytotoxic effect of AQSH (Blue Curve) and $\text{Cu}(\text{AQS})_2$ (Red Curve) on A549 cells after exposure for 24 h

6.2.9. Acridine orange (AO) and ethidium bromide (EB) staining

Morphological changes in apoptosis induced by AQSH and $\text{Cu}(\text{AQS})_2$ were determined by AO/EB staining. Figure 17 represents that AO/EB double-stained A549 human lung cancer cells treated with the experimental molecules for incubation of 24 h. This shows that such cells underwent cell death through apoptosis mode. Control or viable cells show green fluorescence. The normal cell features of uniform chromatin with an intact cell membrane. In contrast, early apoptotic and late apoptotic cells show yellowish green and orange-red color, respectively. The AO/EB results demonstrate that the compounds induce the majority of cell death through apoptosis mode and very fewer by necrosis for 24 h incubation (Figure 18).

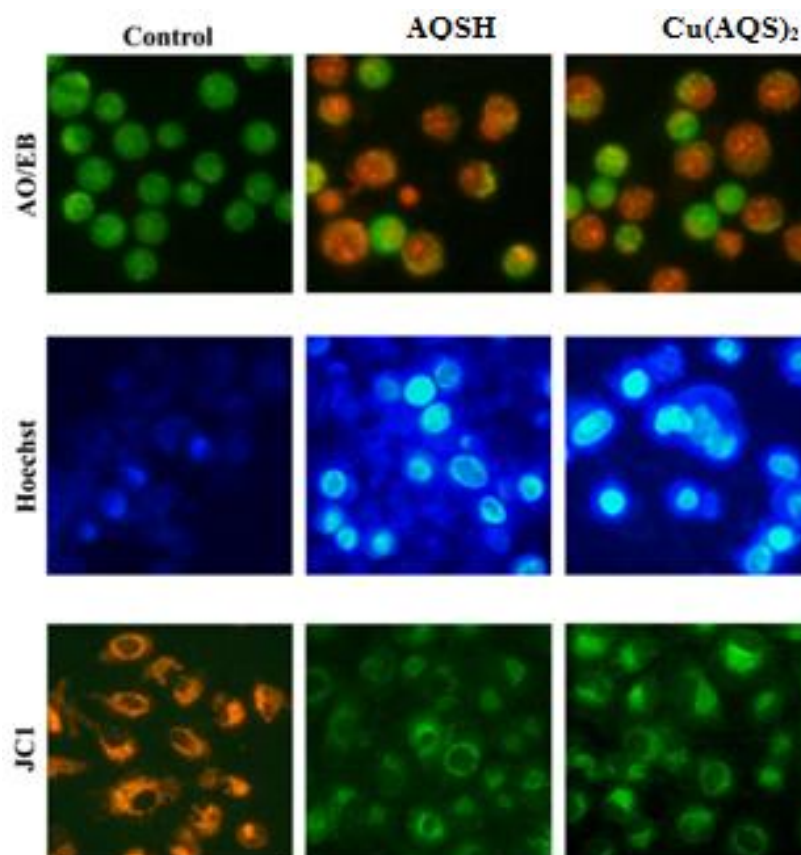


Figure 17: AO/EB staining, Hoechst, and JC-1 Staining. Control, DAU II, DNI-8, Ag-Nano and DAU+Ag+Bpy treated cells

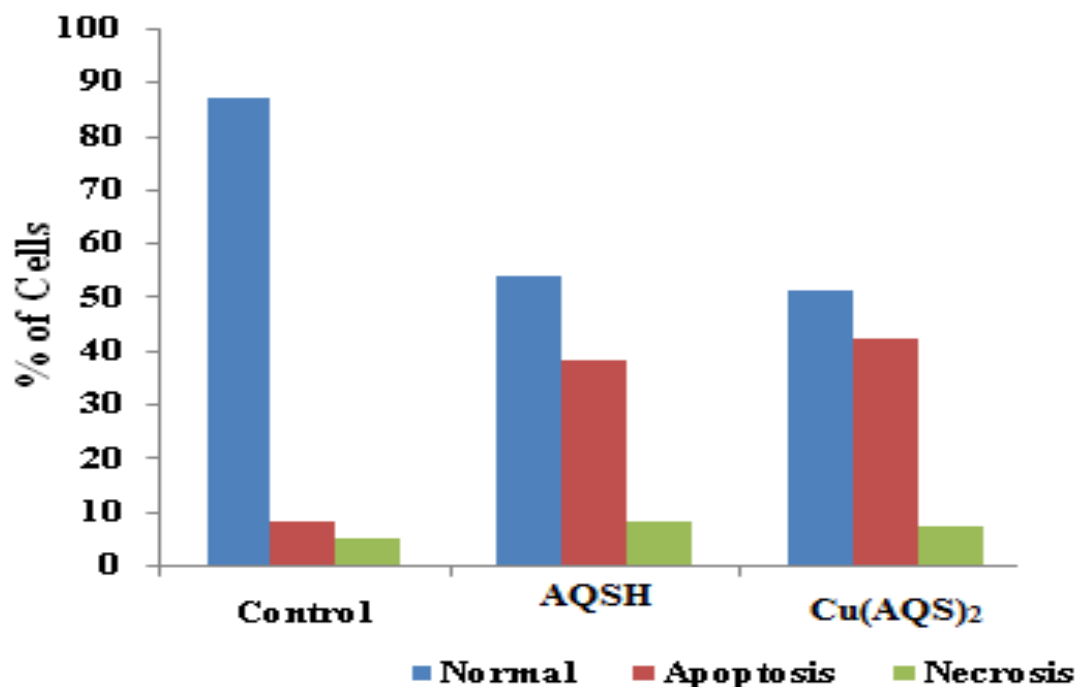


Figure 18: AO/EB fluorescent study of control and experimental molecule induced apoptosis of cells. Graph is shown manual count of apoptotic cells in percentage

6.2.10. Hoechst 33528 staining

Hoechst staining was adopted to determine apoptosis at a basic level. Results of Hoechst staining revealed the changes in morphology of cells with special reference to cytoplasm and the nucleus. Observations reveal that early apoptotic features such as chromatin condensation, and fragmentation were seen mostly in complex treated cells. Small numbers of necrotic cells were also observed (Figure 17 and 19).

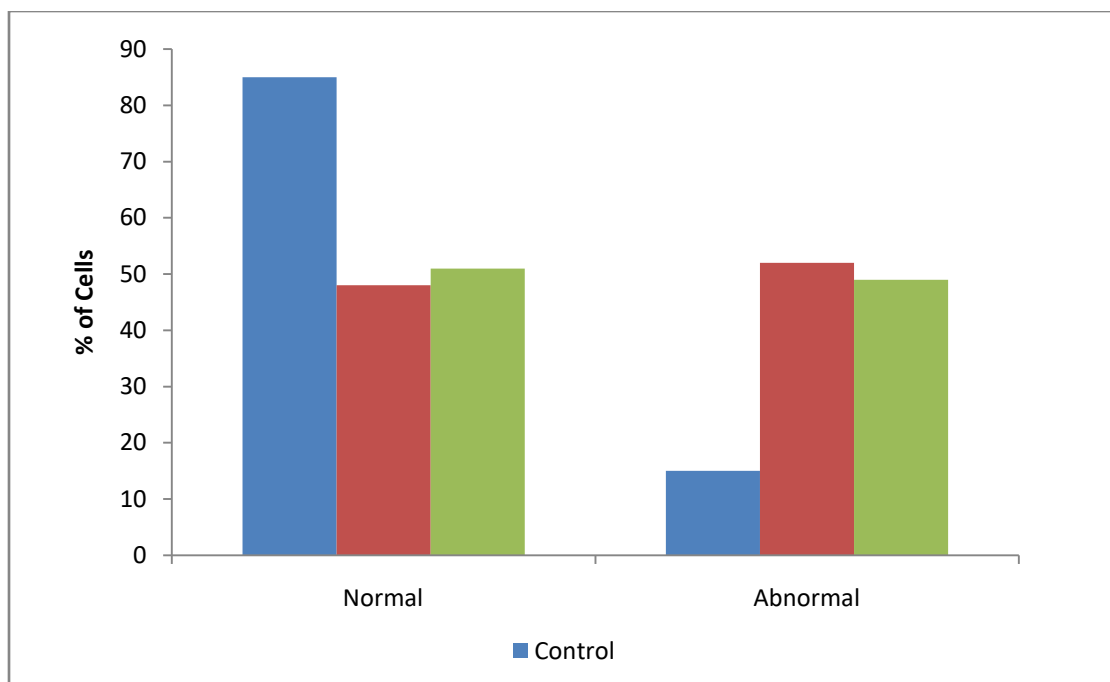


Figure 19: Hoechst 33258 staining study of control [blue] and AQSH [red] and Cu(AQS)₂ [green] treated cells. Graph is shown manual count of apoptotic cells in percentage.

6.2.11. Assessment of mitochondrial membrane potential (JC1 staining)

Mitochondrial membrane potential depolarization induced by AQSH and Cu(AQS)₂ was characterized by JC-1 assay. The fluorescent cationic dye JC-1 accumulation in the mitochondria of control or healthy cells emits red fluorescence. Consequently, cells undergoing apoptosis fluoresce green due to mitochondrial membrane depolarization. Results of JC-1 staining of lung cancer cells treated with compounds at 12 h of incubation confirms the loss of mitochondrial membrane potential; control cells were observed with healthy mitochondria (Figure 17).

6.3. Conclusion

The 1:2 Cu(II) complex of sodium 2-amino-3-hydroxy-9,10-anthraquinone-1-sulphonate (AQSH) having the molecular formula Cu(AQS)₂ was synthesized and characterized by different

techniques. The stability constant was evaluated as 5.52×10^{12} . The study showed that the electrochemical behaviour of AQS is significantly modified when it is bonded to Cu(II). The binding constant and Gibbs free energy for the interaction of Cu(AQS)₂ with SDS micelles were calculated as $(2.83 \pm 0.04) \times 10^4 \text{ M}^{-1}$ and -25.41 kJ/mol , respectively. Various assays established that Cu(AQS)₂ induced apoptosis in A549 human lung cancer cells. The IC₅₀ value of Cu(AQS)₂ was found as $125 \pm 0.05 \text{ }\mu\text{M}$ for a 24 hour incubation.

References

1. M. M. L. Fiallo, A. Garnier-Suillerot, *Inorg. Chim. Acta.* 137 (1987) 119-121.
2. S. Mukherjee Chatterjee, C. K. Jain, S. Singha, P. Das, S. Roychoudhury, H. K. Majumder, S. Das, *ACS Omega* 3 (2018) 10255–10266.
3. P. Das, C. K. Jain, S. K. Dey, R. Saha, A. D. Chowdhury, S. Roychoudhury, S. Kumar, H. K. Majumder, S. Das, *RSC Advances* 4 (2014) 59344–59357.
4. P. S. Guin, S. Das, P.C. Mandal, *J. Inorg. Biochem.* 103 (2009) 1702–1710.
5. P. S. Guin, S. Das, *Russ. J. Phys. Chem. A* 90 (2016) 876–881.
6. R. Pignatello, T. Musumeci, L. Basile, C. Carbone, G. Puglisi, *J. Pharm. Bio Allied Sci.* 3 (2011) 4-14.
7. G. P. Van Balen, C. M. Martinet, G. Caron, G. Bouchard, M. Reist, P. A. Carrupt, R. Fruttero, A. Gasco, B. Testa, *Med. Res. Rev.* 24 (2004) 299-324.
8. A. M. Seddon, D. Casey, R.V. Law, A. Gee, R. H. Templer, O. Ces, *Chem. Soc. Rev.* 38 (2009) 2509-2519.
9. J. K. Seydel, E. A. Coats, H. P. Cordes, M. Wiese, *Arch. Pharm.* 327 (1994) 601–610.
10. S. Schreiera, S. V. P. Malheiros, E. de Paula, *Biochim. Biophys. Acta* 1508 (2000) 210–234;
11. M. Lúcio, J. L. Lima, S. Reis, *Curr. Med. Chem.* 17 (2010) 1795–1809.

12. L. Laurier, L. Schramm, E. N. Stasiuk, D. G. Marangon, *Annu. Rep. Prog. Chem., Sect. C: Phys. Chem.* 99 (2003) 3–48.
13. W. Sun, C. K. Larive, M. Z. Southard, *J. Pharm. Sci.* 92 (2003) 424–435.
14. N. Erdinc, S. Gokturk, M. Tuncay, *J. Pharm. Sci.* 93 (2004) 1566–1576.
15. J. Xi, R. Guo, *J. Pharm. Biomed. Anal.* 43 (2007) 111–118.
16. M. C. Jones, J. C. Leroux, *Eur. J. Pharm. Biopharm.* 48 (1999) 101–111.
17. M. E. Dalmora, S. L. Dalmora, A. G. Oliveira, *Int. J. Pharm.* 222 (2001) 45–55.
18. C. O. Rangel-Yagui, H. W. L. Hsu, A. I. Pessoa Jr, L. C. Tavares, *Braz. J. Pharm. Sci.* 41 (2005) 237–246.
- 19.** 19. J. T. Burke, *J. Chem. Educ. Easton* 74 (10) (1997) 1213.
20. N. Raman, S. J. Raja, J. Joseph, J. D. Raja, *J. Chil. Chem. Soc.* 52 (2007) 1138–1141.
21. P. S. Guin, S. Das, P.C. Mandal, *Inter. J. Electrochem.* 2011 (2011) 1-22.
22. M. Tariq, I. Ullah, *SN Appl. Sci.* 2 (2020) 868.
23. E. Fuguet, C. Rafols, M. Roses, E. Bosch, *Anal. Chim. Acta.* 548 (2005) 95–100.
24. M. Sarkar, S. Poddar, *J. Colloid Interface Sci.* 221 (2002) 181–185.
25. J. B. Foresman, A. Frish, *Exploring Chemistry with Electronic Structure Methods*, Gaussian, Inc., Pittsburgh, PA 2000, p. 64.
26. A. V. Iogansen, *Spectrochim. Acta. Part A* 55 (1999) 1585.
27. M. Enache, I. Anghelache, E. Volanschi, *Int. J. Pharm.* 390 (2010) 100.
28. M. Enache, E. Volanschi, *J. Pharma. Sci.* 100 (2011) 558.
29. R. Sabate, M. Gallardo, J. Estelrich, *J. Colloid Interface Sci.* 233 (2001) 205.
30. R. Sabate, M. Gallardo, A. de la Maza, J. Estelrich, *Langmuir* 17 (2001) 6433.
31. A. Das, S. Roy, P. Mondal, A. Datta, K. Mahali, G. Loganathan, D. Dharumadurai, P. S. Sengupta, M. A. Akbarsha, P. S. Guin, *RSC Adv.* 6 (2016) 28200-.
32. T. Mosmann, *J. Immunol. Methods.* 65 (1–2) (1983) 55-63.

Chapter: 7

Studies on synthesis and characterization of a Ni^{II} complex of sodium 2-amino-3-hydroxy-9,10-anthraquinone-1-sulphonate, its electrochemical behavior and interaction with SDS micelles and A549 human lung cancer cells

7. 1. Introduction

The presence of metal ions in complexes formed by anthracyclines were found to reduce the toxicity of anthracycline drugs [1-3] through modification of their electrochemical behavior and stability of the radical intermediates [4-6]. Several studies [7-10] explored that the mechanism of action of a biologically active molecule is related to its interaction with biological tissues through binding to membranes at the molecular level. Several biological processes have been observed to occur at the ionizable surface of bio-membranes or along their hydrophobic area, leading to a comparative study on interaction of such molecules with cationic, zwitterionic, anionic and neutral surfactants [7-10]. This provides helpful information on nature of drug–membrane interactions. This is why studies on drug–surfactant interactions were carried out by several researchers using various models and techniques owing to extensive application of surfactants in the field of pharmaceutical research.

In the present study, a Ni^{II} complex of sodium 2-amino-3-hydroxy-9,10-anthraquinone-1-sulphonate (AQSH) was synthesized and characterized. Its electrochemical behavior was studied in different solvents to see whether that is modified with regard to sodium 2-amino-3-hydroxy-9,10-anthraquinone-1-sulphonate. Interaction of the molecule with SDS micelle was studied to see if it is able to nucleate a biological membrane. Finally, the molecule was tried on A549 human lung cancer cells to see if it induces apoptosis.

7.2. Results and discussions

7.2.1. Stoichiometry of Ni^{II} interacting with AQSH at neutral pH in solution

The absorption spectra of sodium 2-amino-3-hydroxy-9,10-anthraquinone-1-sulphonate (AQSH) at neutral pH in the absence and presence of different amounts of Ni^{II} were measured. To find the stoichiometry of the Ni^{II} complex in solution, a mole-ratio study was performed. In this case, concentration of AQSH was constant (50 μM) and the metal concentration was varied from a ratio of 0.10 to 4.20. Absorbance was measured at 520 nm. In the mole ratio plot two lines were obtained, the intersection of which determines the stoichiometry of the complex formed in aqueous solution. Figure 1 shows that stoichiometry of the Ni^{II} complex in solution for metal to ligand (AQSH) is 1:1 at neutral pH.

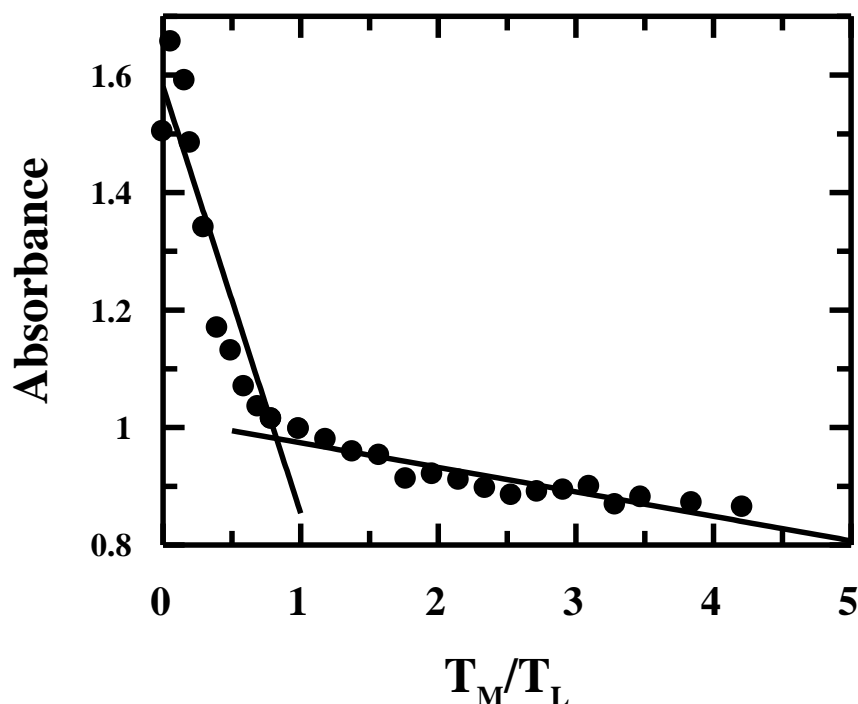
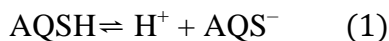


Figure 1: Mole-ratio plot of absorbance of [Ni²⁺]/[AQSH] at a fixed ligand (AQSH) concentration at neutral pH; [AQSH] = 50 μM, [NaCl] = 10 mM, 25⁰C.

7.2.2. Determination of formation constant of a 1:1 Ni^{II}-AQSH complex

AQSH exists in aqueous solution in two distinct forms (AQSH and AQS⁻) depending on the pH of the medium. The dissociation of the molecule may be described as follows:



$$K = \frac{[\text{H}^+][\text{AQS}^-]}{[\text{AQSH}]} \quad (2)$$

Proton dissociation constant K was calculated from the change in absorbance of the compound at 520 nm in the pH range 3.53 – 12.02. The observed absorbance at 520 nm would be given by

$$A_{520} = \frac{A_1}{1 + 10^{(pH-pK)}} + \frac{A_2}{1 + 10^{(pK-pH)}} \quad [3]$$

A_{520} is the overall absorbance of the solution at 520 nm at different pH; A_1 and A_2 are the absorbance of AQSH and the phenoxide ion, AQS⁻, respectively. pK value of AQSH was determined by spectrometric titration as described in Chapter 5, Section 5.2.6. The pK found as $pK = (8.10 \pm 0.05)$.

To determine the binding constant of Ni^{II}-AQSH complex, Ni^{II} and AQSH were taken in molar ratio 1:1 and a spectrophotometric titration was carried out. At first the 1:1 Ni^{II}-AQSH mixture was acidified to pH 3.53 and it was slowly titrated with 0.01M NaOH solution keeping Ni^{II} and AQSH concentrations fixed. Absorption spectra at various pH values were collected (Figure 2). It was found that the intensity of the peak at 520 nm gradually increases with an increase in pH. Change in the absorbance at 520 nm was monitored against pH (Figure 3). The absorbance A_{obs} at 520 nm of AQSH in the presence of Ni^{II} was fitted according to equation (3). In this case A_1 and A_2 are the absorbances of AQSH and AQS⁻ respectively, in the presence of Ni^{II}. Fitting the experimental data according to equation (3), pK was found as (7.73 ± 0.05) .

During complex formation the phenolic proton of AQSH is released and so $pK (=7.73 \pm 0.05)$ was used to determine the binding constant of the complex. The formation constants β^* and β for the 1:1 complex can be described as follows:



$$\beta^* = \frac{[\text{Ni}(\text{AQS})][\text{H}^+]}{[\text{Ni}^{2+}][\text{AQSH}]} \quad (5)$$



$$\beta = \frac{[\text{Ni}(\text{AQS})]}{[\text{Ni}^{2+}][\text{AQS}^-]} \quad (7)$$

From equations (1), (5) and (7) β can be deduced as

$$\beta = \beta^* / K \quad (8)$$

where, K is the equilibrium constant for dissociation of the first proton of AQSH as shown in equation 1. Formation constant β^* was determined from the above spectrophotometric titration. Formation constant β of the 1:1 complex was calculated using expression 7 and found to be 4.69×10^4 .

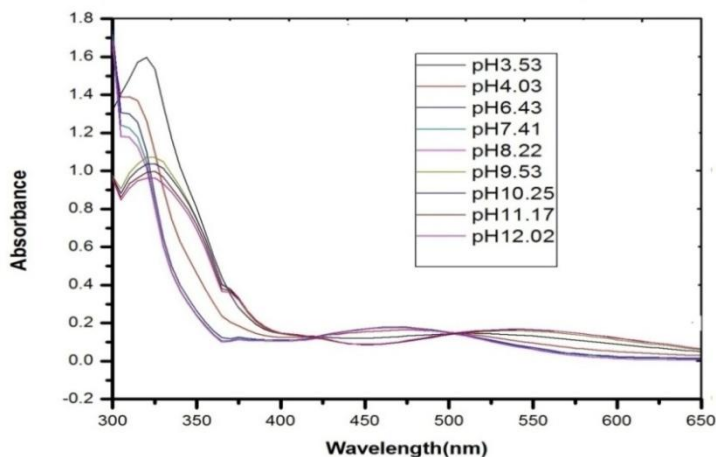


Figure 2: UV-Vis spectra of a 1:1 mixture of Ni^{II} and AQSH in aqueous media at different pH.

$[\text{Ni}^{\text{II}}] = 25\mu\text{M}$, $[\text{AQSH}] = 50\mu\text{M}$, $[\text{NaCl}] = 0.01 \text{ M}$, $T = 298.15 \text{ K}$.

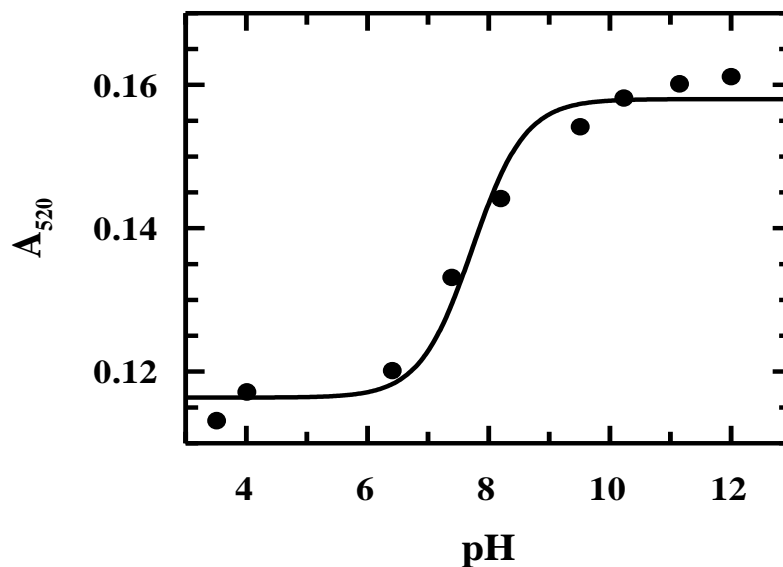


Figure 3: Spectrophotometric titration of AQSH in presence of Ni^{2+} as shown by a variation of absorbance at 520 nm; $[\text{AQSH}] = 50 \mu\text{M}$, $[\text{Ni}^{2+}] = 50 \mu\text{M}$, $[\text{NaCl}] = 10 \text{ mM}$, 25°C .

7.2.3. Analysis of the mass spectra of the Ni^{II} complex of AQSH

Considering the complex to be $\text{Ni}(\text{AQS})\text{Cl}_2(\text{H}_2\text{O})_2$, the obtained mass spectrum (Figure 4) was analyzed. Molecular ion peaks expected at $m/z = 506.0$ or 508.0 or 510.0 based on isotope distribution of Cl (^{35}Cl and ^{37}Cl) were actually obtained at $m/z = 507.19$ and 508.19 respectively (minor deviations may be attributed to loss of one or more protons). A relatively less intense peak at $m/z = 413.20$ may be assigned to a species formed due to loss of Na^+ and two Cl atoms from the molecular ion peak. The peak at $m/z = 360.264$ corresponds to a species obtained due to a further removal of two coordinated water molecules and an $-\text{NH}_2$ from the ligand (AQSH).

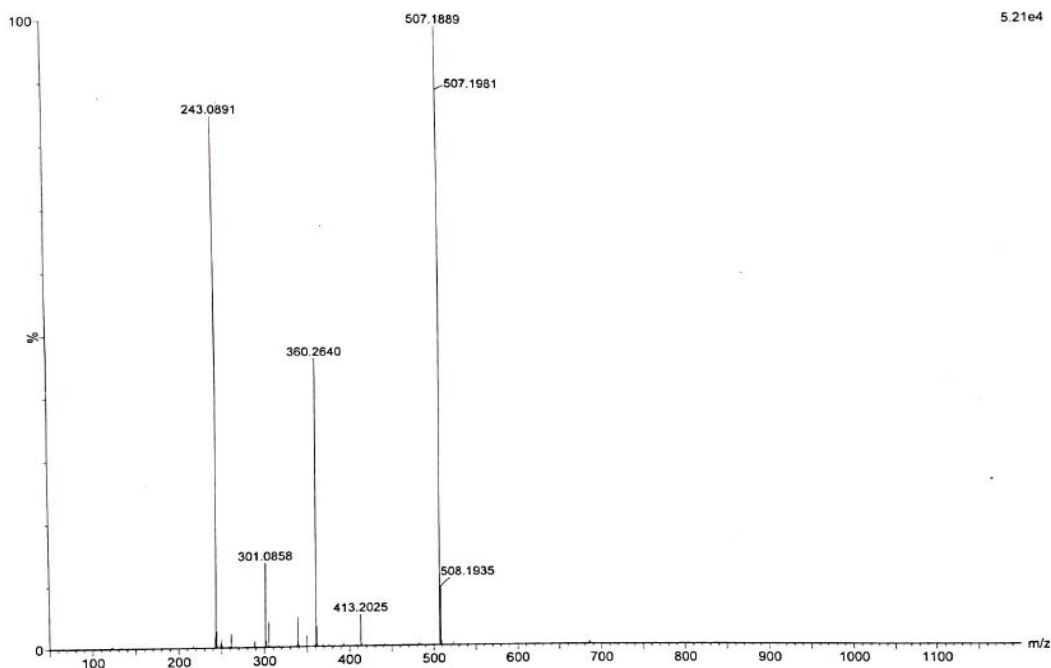


Figure 4: Mass spectrum of the Ni^{II} complex.

7.2.4. TGA of the Ni^{II} complex

Thermo-gravimetric analysis was performed on the basis that Ni^{II} forms an octahedral complex with AQS, two Cl⁻ and two water molecules having a molecular weight 506.0. The first sharp decrease at 101^oC corresponds to a molecular mass of 343.42. Hence, loss in weight of 162.58 might correspond to the loss of the -SO₃ unit, two quinone oxygens, a molecule of water and a Cl atom. The next characteristic decrease was observed at 247.57^oC and corresponds to a mass of 306.86. Hence, the decrease attests to the loss of the -SO₃ unit, two quinone oxygens, a molecule of water and two Cl atoms. The next decrease was noticed at 377.1^oC. The sample remaining corresponds to a mass of 257.92. Hence the breakaway portion could be due to the loss of the -SO₃ unit, the butadiene unit, two quinone oxygens from the ligand, along with a coordinated water molecule and two Cl⁻. Hence, at this stage of the TG analysis it may be said

that in the complex Ni^{II} is bound to a naphthaquinone moiety. The point of ligation to the metal centre via $-\text{NH}_2$ and O^- remains and therefore can be termed to be pretty stable. Hence, a logical fragmentation as mentioned above suggests Ni^{II} forms an octahedral complex with AQS^- , two molecules of water and two Cl^- .

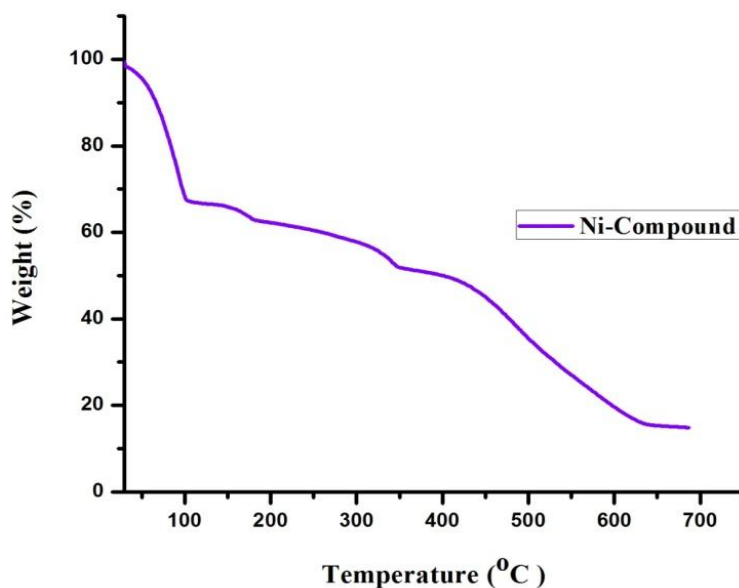


Figure 5: TG analysis of the Ni^{II} complex.

7.2.5. Analysis of IR spectrum of $\text{Ni}(\text{AQS})\text{Cl}_2(\text{H}_2\text{O})_2$

In AQSH, O–H and N–H stretching frequencies show up at 3500 cm^{-1} and 3353.04 cm^{-1} respectively (*Fig. 5b, Chapter 5, Section 5.2.5*). In the IR spectrum of the Ni^{II} complex (Figure 6) disappearance of $-\text{OH}$ peak at 3500 cm^{-1} is attributed to coordination to Ni^{II} by the phenolate oxygen. That there is a change in $-\text{NH}$ stretching frequency suggests coordination of Ni^{II} via $-\text{NH}_2$ group of AQSH. Thus coordination of $\text{Ni}(\text{II})$ occurs via phenolic $-\text{OH}$ and $-\text{NH}_2$ groups of AQSH (Scheme- 1).

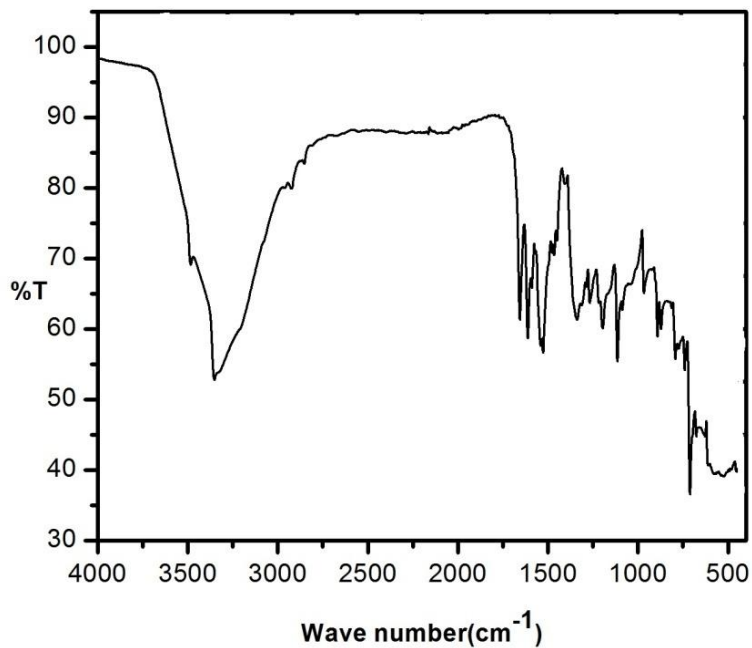
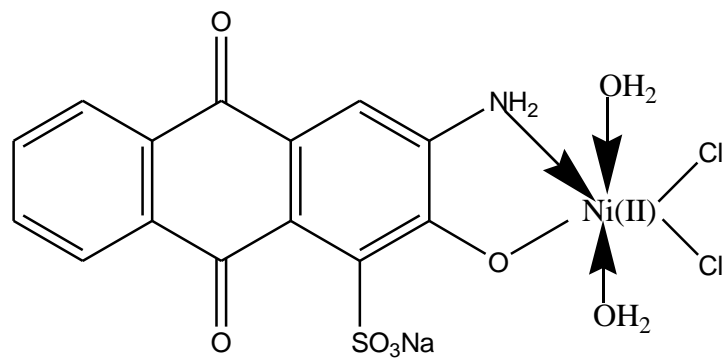


Figure-6: IR spectra of Ni(AQS)Cl₂(H₂O)₂.



Scheme 1: Proposed structure of Ni(AQS)Cl₂(H₂O)₂.

7.2.6. Electrochemical behavior of the Ni^{II} complex in anhydrous acetonitrile, dimethylformamide and dimethylsulphoxide.

Cyclic voltammograms of Ni(AQS)Cl₂(H₂O)₂ in anhydrous acetonitrile in presence of 0.1 M tetrabutyl ammonium bromide (TBAB) is shown in Figure 7. In anhydrous acetonitrile, Ni(AQS)Cl₂(H₂O)₂ undergoes two successive one-electron reductions with reduction potentials of -990 mV and -1310 mV respectively. Under similar experimental conditions AQSH shows two reduction peaks at -935 mV and -1270 mV in anhydrous acetonitrile (*Chapter 6, Section 6.2.6*). This indicates electrochemical behaviour of AQSH is altered significantly when it is bound to Ni^{II}. In anhydrous DMF, Ni(AQS)Cl₂(H₂O)₂ undergoes successive two one-electron reductions with reduction potentials of -970 mV, and -1390 mV, respectively (Figure 8). Two oxidation peaks were observed at -1050 mV and -1260 mV (Figure 8). Hence, reduction at -1235 mV and -1390 mV are quasi reversible. Comparing the cyclic voltammograms of the present complex with that of AQSH (*Chapter 6, Section 6.2.6*), it may be said that the electrochemical behaviour of Ni(AQS)Cl₂(H₂O)₂ is significantly different from that of AQSH. The diffusion coefficient (D₀) for the reduction of Ni(AQS)Cl₂(H₂O)₂ was calculated by plotting cathodic peak current (I_{pc}) versus square root of scan rate (v^{1/2}) (Figure 9) using equation 9. D₀ were 3.88 × 10⁻² and 5.52 × 10⁻³ cm² s⁻¹ in anhydrous ACN and DMF respectively.

$$I_{pc} = (2.687 \times 10^5) n^{3/2} D_0^{1/2} A C v^{1/2} \quad (9)$$

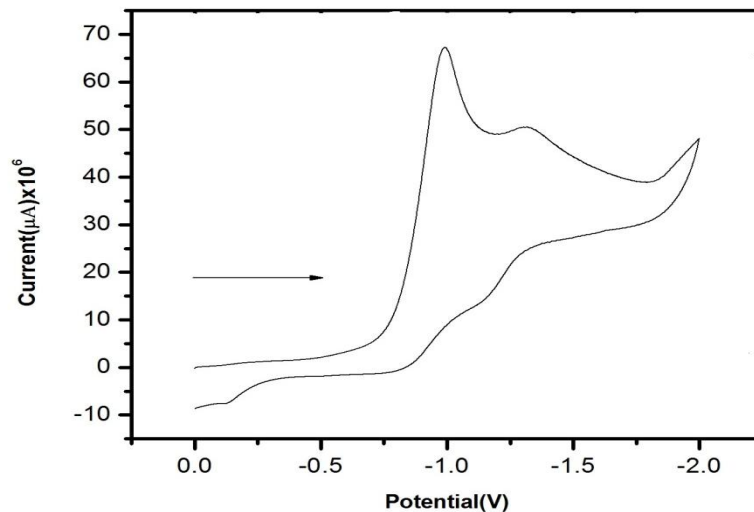


Figure 7: Cyclic voltammogram of $\text{Ni}(\text{AQS})\text{Cl}_2(\text{H}_2\text{O})_2$ in anhydrous acetonitrile media. Scan rate: 0.10 Vs^{-1} . $[\text{Ni}(\text{AQS})\text{Cl}_2(\text{H}_2\text{O})_2] = 50 \times 10^{-6} \text{ M}$, $[\text{TBAB}] = 0.1 \text{ M}$, $T = 298.15 \text{ K}$.

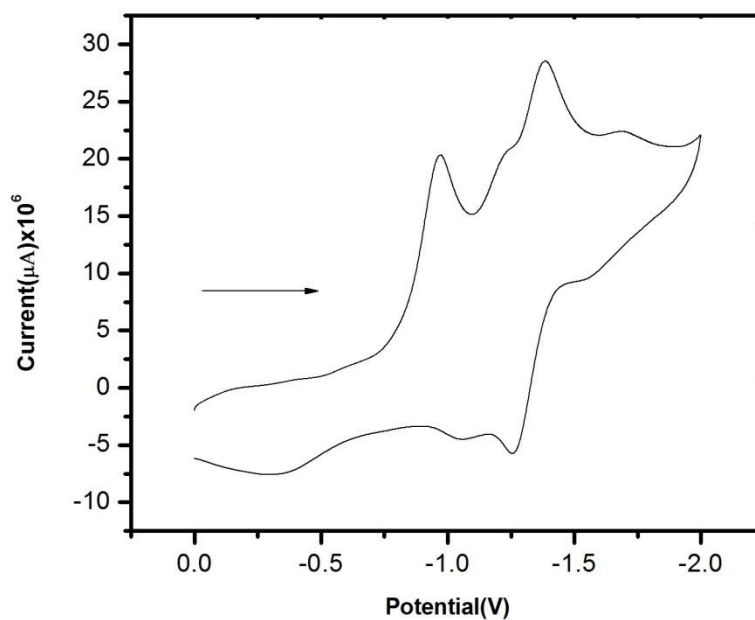


Figure 8: Cyclic voltammogram of $\text{Ni}(\text{AQS})\text{Cl}_2(\text{H}_2\text{O})_2$ in anhydrous dimethyl formamide media. Scan rate: 0.10 Vs^{-1} . $[\text{Ni}(\text{AQS})\text{Cl}_2(\text{H}_2\text{O})_2] = 50 \times 10^{-6} \text{ M}$, $[\text{TBAB}] = 0.1 \text{ M}$, $T = 298.15 \text{ K}$.

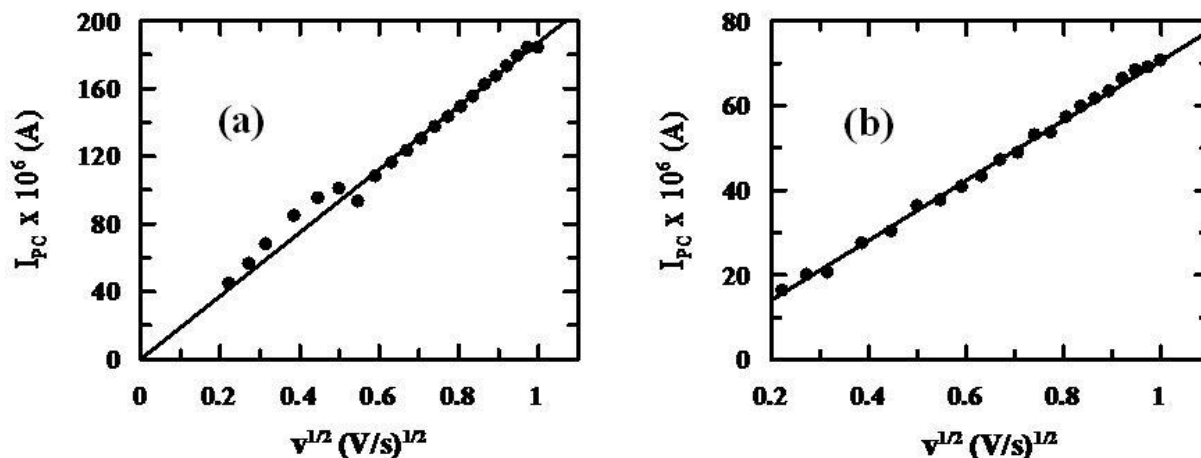


Figure 9: Plot of I_{pc} vs. square root of scan rate ($v^{1/2}$) of $\text{Ni}(\text{AQS})\text{Cl}_2(\text{H}_2\text{O})_2$ in (a) anhydrous ACN and (b) anhydrous DMF.

7.2.7. Interaction of $\text{Ni}(\text{AQS})\text{Cl}_2(\text{H}_2\text{O})_2$ with SDS micelles

Interaction of anionic surfactant (SDS) micelles with $\text{Ni}(\text{AQS})\text{Cl}_2(\text{H}_2\text{O})_2$ was studied at physiological pH using UV–Vis spectroscopy in pre-micellar and micellar concentration range in aqueous phosphate buffer (Figure 10). A spectrophotometric titration was performed by maintaining a constant concentration of $\text{Ni}(\text{AQS})\text{Cl}_2(\text{H}_2\text{O})_2$ and varying concentrations of SDS (Figure 10). The reaction mixture was incubated for 1–2 minutes and absorbance at 320 nm was measured. The change in absorbance at 320 nm of $\text{Ni}(\text{AQS})\text{Cl}_2(\text{H}_2\text{O})_2$ by adding increasing amounts of SDS is shown in Figure 11 which was used to calculate the CMC of SDS during the course of interaction with $\text{Ni}(\text{AQS})\text{Cl}_2(\text{H}_2\text{O})_2$. The critical micelle concentration (CMC) evaluated was $160\mu\text{M}$. This value of CMC was used in all calculations to estimate binding parameters. In an earlier study, the CMC values of SDS in pure water and in 50 mM phosphate buffer were evaluated and found to be $8080\mu\text{M}$ and $1990\mu\text{M}$ respectively [11]. Lowering in CMC value of SDS in the present study in comparison to that obtained earlier may be due to an influence that various ions and molecules present in the mixture might have [12]. It was observed

that as SDS concentration increases absorbance of Ni(AQS)Cl₂(H₂O)₂ steadily decreases at 320 nm which indicates enhanced surfactant concentration induced insertion of the experimental molecule at the interior of the micelles till all binding sites inside the surfactant got saturated. This leads to a decrease in absorbance of Ni(AQS)Cl₂(H₂O)₂ at a particular concentration of surfactant i.e. CMC. The nonlinear analysis by incorporating 1:1 interaction between an experimental molecule with a surfactant micelle has been shown as the most accepted model. Thus the present binding isotherm was analyzed by using equation 10. By considering 1:1 interaction between Ni(AQS)Cl₂(H₂O)₂ and SDS (Figure 11) the corresponding binding constant was evaluated as $(1.40 \pm 0.06) \times 10^5 \text{ M}^{-1}$ (Table 1) [13,14] (reduced Chi squared = 2.67×10^{-5}).

$$A = \frac{A_0 + A_\infty K [L]}{1 + K[L]} \quad (10)$$

Where L represents the surfactant used (here SDS); A and A₀ are absorbance of Ni(AQS)Cl₂(H₂O)₂ at 320 nm in the absence and presence of SDS. A_∞ corresponds to absorbance of Ni(AQS)Cl₂(H₂O)₂ bound to SDS. Gibbs free energy for the interaction of Ni(AQS)Cl₂(H₂O)₂ to SDS micelles was calculated with the help of equation 11 and found to be -29.38 kJ/mol (Table 1) [15,16].

$$\Delta G^0 = - RT \ln K \quad (11)$$

Where R is the molar gas constant and T = 298.15 K.

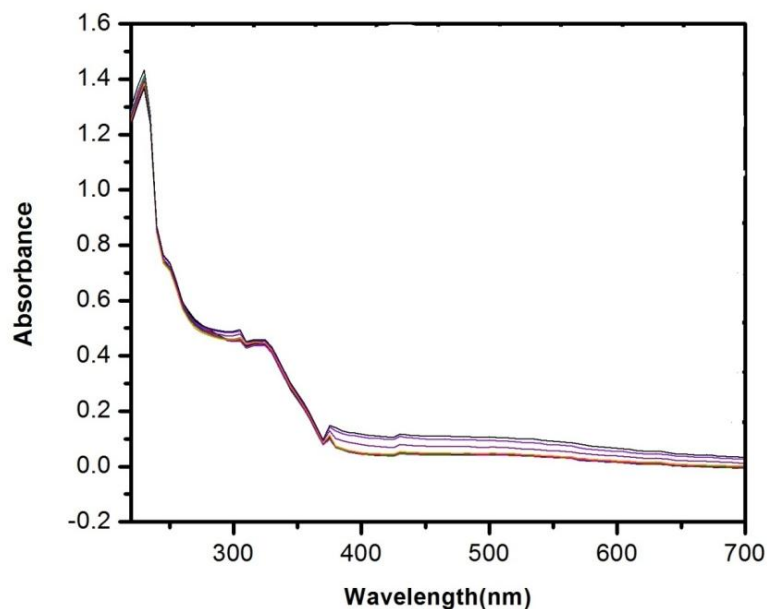


Figure 10: Absorption spectra of Ni(AQS)Cl₂(H₂O)₂ (50 μM) in the absence and presence of increasing concentrations of SDS. [Phosphate buffer] = 100 mM, pH 7.4, T = 298.15 K.

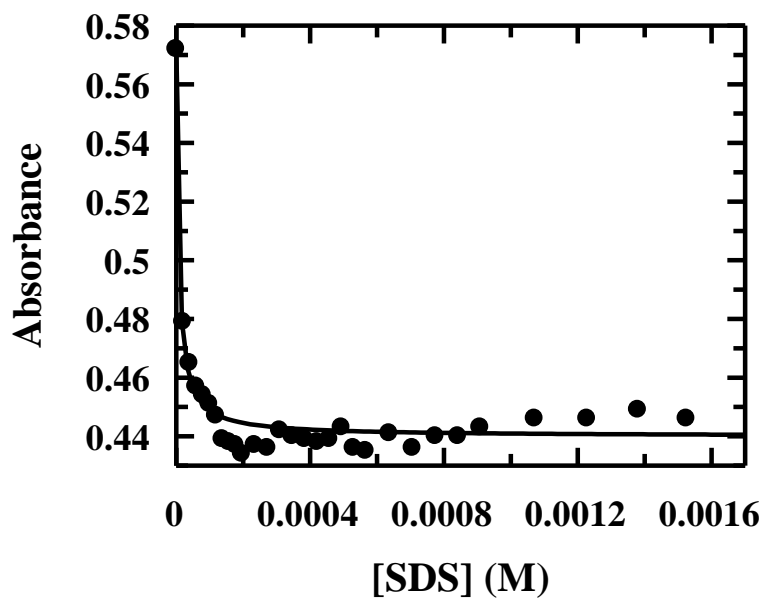


Figure 11: A non-linear fit of absorbance of Ni(AQS)Cl₂(H₂O)₂ at 320 nm using equation 10 considering 1:1 interaction between Ni(AQS)Cl₂(H₂O)₂ and SDS.

In an earlier study on interaction of neutral 2-amino-3-hydroxyanthraquinone with anionic SDS micelles binding constant was evaluated and found to be 652.81 under similar experimental condition [17]. In such study binding of 2-amino-3-hydroxyanthraquinone with anionic SDS micelles was justified by using hydrophobic mode as the dominating mode of interaction. In the present study, binding constant for interaction of Ni(AQS)Cl₂(H₂O)₂ with SDS micelles was $(1.40 \pm 0.06) \times 10^5 \text{M}^{-1}$ which is far greater than the previous value of the analogous molecule [17]. Further both SDS and Ni(AQS)Cl₂(H₂O)₂ are anionic in aqueous solution which means hydrophilic interaction between them is unimportant. Thus in the present study, hydrophobic interaction plays a superior role over hydrophilic interaction. Under similar conditions the binding constant for 1:1 interaction of Cu(AQS)₂ with SDS micelles was calculated and found to be $(2.83 \pm 0.04) \times 10^4 \text{M}^{-1}$ (Chapter 6, Section- 6.2.7) while it was $(1.21 \pm 0.06) \times 10^5 \text{M}^{-1}$ for 1:1 AQSH–SDS micelle interaction (Chapter 5, Section: 5.2.7). This clearly shows that binding constant of Ni(AQS)Cl₂(H₂O)₂ is greater than free AQSH ligand and Cu(AQS)₂. Thus Ni(AQS)Cl₂(H₂O)₂ is an efficient agent in penetrating SDS micelles and hence a bio-membrane. The value of partition coefficient (K_x) was determined using the pseudo-phase model [15,18, 19] according to equation 12.

$$\frac{1}{\Delta A} = \frac{1}{A_{\infty}} + \frac{n_w}{K_x A_{\infty} ([\text{SDS}] + C_T - \text{CMC})} \quad (12)$$

Where, $\Delta A = A - A_0$, $\Delta A_{\infty} = A_b - A_0$, $[L] = [\text{SDS}]$ and $n_w = 55.55 \text{M}$ is the molarity of water. The nature of the curve is linear upto a large concentration of surfactant but linearity falls sharply with decreasing surfactant concentration that can be measured using equation 12 [19]. The value

of K_x was calculated from the slope of the plot of $1/\Delta A$ versus $1/([SDS] + C_T - CMC)$ (Figure 12) and found to be $(6.32 \pm 0.05) \times 10^5$ [reduced Chi squared = 0.16].

The standard free energy change for the transfer of $Ni(AQS)Cl_2(H_2O)_2$ from the aqueous phase to the micellar phase was measured and found to be -33.11 kJ/mol that can be calculated using equation 13 [16] (mentioned in Table 1). This justifies that the movement of $Ni(AQS)Cl_2(H_2O)_2$ into the micellar phase from its hydrophilic location is thermodynamically feasible which can be confirmed by the standard free energy change.

$$\Delta G^0_{x} = -RT \ln K_x \quad (13)$$

The value of partition coefficient thus obtained was compared with previous studies [17] and from such comparison it was suggested that hydrophobic interaction plays a fundamental role in the distribution of $Ni(AQS)Cl_2(H_2O)_2$ in anionic SDS micelles.

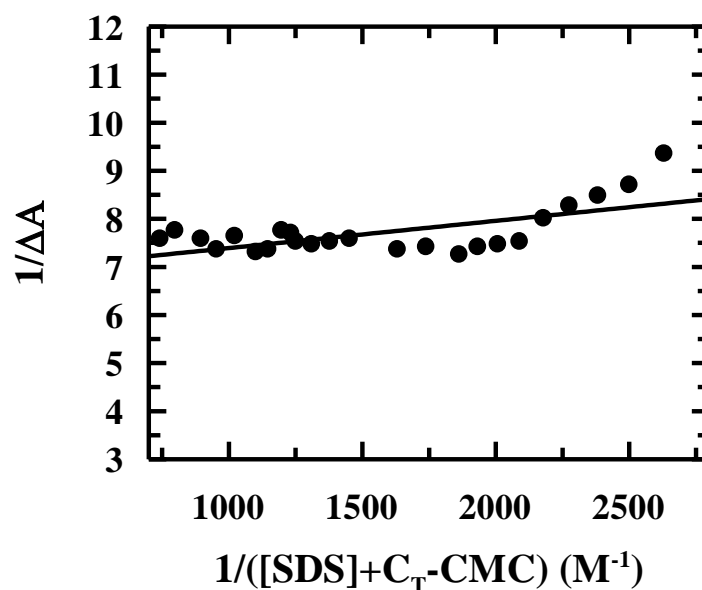


Figure 12: Plot of $1/|\Delta A|$ vs. $1/([SDS] + C_T - CMC)$ [equation12] for $Ni(AQS)Cl_2(H_2O)_2$ (50 μM) in SDS micelles at pH 7.4.

Table 1: Binding constant (K), partition coefficient (K_x), standard Gibbs free energy of binding (ΔG^0) and the standard free energy change (ΔG^0_x) for the transfer of $Ni(AQS)Cl_2(H_2O)_2$ from aqueous to micellar phase for the interaction of $Ni(AQS)Cl_2(H_2O)_2$ with surfactants.

K, M^{-1}	$(1.40 \pm 0.06) \times 10^5$
$\Delta G^0, kJ mol^{-1}$	-29.38
K_x	$(6.32 \pm 0.05) \times 10^5$
$\Delta G^0_x, kJ mol^{-1}$	-33.11

7.2.8. Cell Viability Assay

The cytotoxic activity of $Ni(AQS)Cl_2(H_2O)_2$ was investigated against A549 human lung cancer cells using the MTT assay [20]. The cytotoxic activity was determined according to dose of exposure of the complex required to reduce survival to 50% (IC_{50}) compared to untreated cells. IC_{50} value of $Ni(AQS)Cl_2(H_2O)_2$ treated cells was $68.5 \pm 0.05 \mu M$. IC_{50} of AQSH and $Cu(AQS)_2$ treated cells were evaluated and found to be $83.5 \pm 0.05 \mu M$ and $125 \pm 0.05 \mu M$ respectively [Chapter 5, Section: 5.2.9 and Chapter 6, Section: 6.2.8]. This indicates that the $Ni(AQS)Cl_2(H_2O)_2$ is more efficient in killing cancer cells than AQSH and $Cu(AQS)_2$. The results of the MTT assay indicate $Ni(AQS)Cl_2(H_2O)_2$ exhibits dose dependent toxic effects against A549 cells (Figure 13). Results of AQSH and $Cu(AQS)_2$ are also shown in Figure 13 to draw a comparative account of their efficacy (Table- 2).

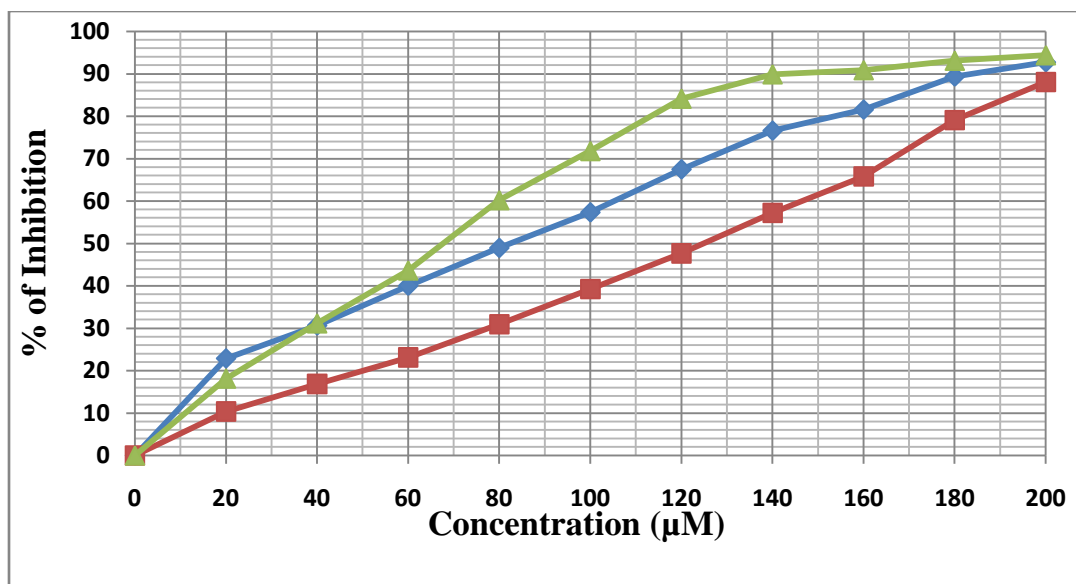


Figure13: Cytotoxic effect of AQSH (blue curve), Cu(AQS)₂(red curve), and Ni(AQS)Cl₂(H₂O)₂ (green curve) on A549 cells following an exposure of 24 hours.

Table 2. *In vitro* cytotoxicity assays for AQSH, Cu(AQS)₂ and Ni(AQS)Cl₂(H₂O)₂ against human A 549 lung cancer cells.

Compound	IC ₅₀ values (24 h incubation)
AQSH	83.5 ± 0.05 µM
Cu(AQS) ₂	125.0 ± 0.05 µM
Ni(AQS)Cl ₂ (H ₂ O) ₂	68.5 ± 0.05 µM

7.2.9. Acridine orange (AO) and ethidium bromide (EB) staining

Morphological changes of cells in apoptosis induced by Ni(AQS)Cl₂(H₂O)₂ were determined by AO/EB staining. Figure 14 represents AO/EB double-stained A549 human lung cancer cells treated with Ni(AQS)Cl₂(H₂O)₂ after incubation for 24 hours that underwent the apoptosis mode of cell death. Results of Ni(AQS)Cl₂(H₂O)₂ were compared with AQSH and Cu(AQS)₂ (Figures 14 and 15). Control or viable cells show green fluorescence while normal

cell features of uniform chromatin with an intact cell membrane. In contrast, early apoptotic and late apoptotic cells show yellowish green and orange-red color respectively. The AO/EB results demonstrate that compounds induce cell death, largely by apoptosis, and few by the necrosis pathway during the 24 hour incubation period (Figure 15).

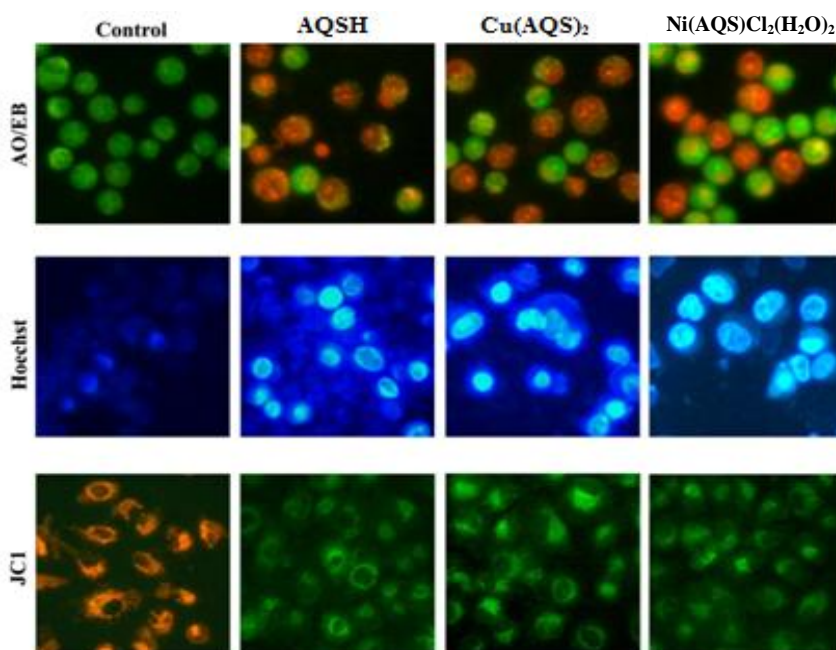


Figure 14: AO/EB staining, Hoechst, and JC-1 Staining. Control, DAU II, DNI-8, Ag-Nano and DAU + Ag + Bpy treated cells.

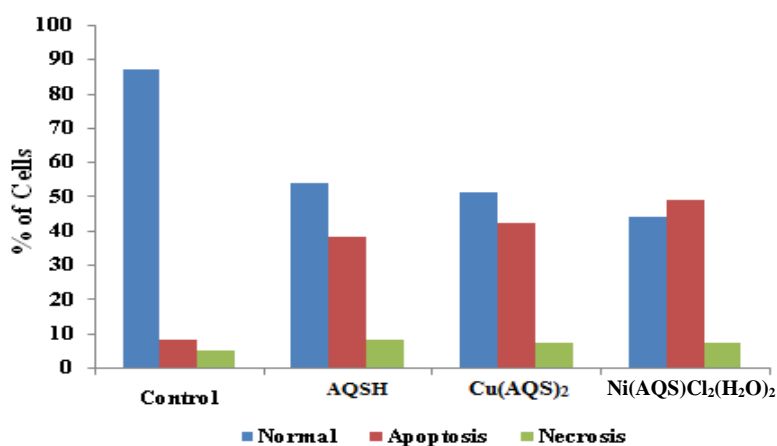


Figure 15: AO/EB fluorescent study of control and experimental molecule induced apoptosis of cells. Graph is shown manual count of apoptotic cells in percentage.

7.2.10. Hoechst 33528 staining

Hoechst staining was adopted to determine apoptosis. The results of Hoechst staining revealed changes in morphology of cells, with particular reference to the cytoplasm and the nucleus. Observations revealed early apoptotic features like chromatin condensation and fragmentation in Ni(AQS)Cl₂(H₂O)₂ treated cells. Small number of necrotic cells were also observed (Figure 14 and 16). Results obtained with Ni(AQS)Cl₂(H₂O)₂ was compared with those of AQS and Cu(AQS)₂.

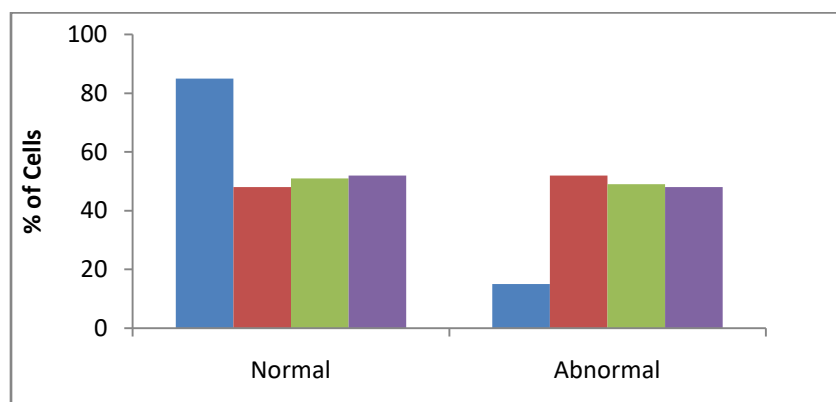


Figure 16: Hoechst 33258 staining study of control [blue], AQS [red], Cu(AQS)₂ [green] and Ni(AQS)Cl₂(H₂O)₂ [violet] treated cells. Graph shows a manual count of apoptotic cells in percentage.

7.2.11. Assessment of mitochondrial membrane potential (JC1 staining)

Mitochondrial membrane potential depolarization induced by Ni(AQS)Cl₂(H₂O)₂ was determined by JC-1 assay. Accumulation of the fluorescent cationic dye (JC-1) in the mitochondria of control or healthy cells emitted fluorescence. Consequently, cells undergoing apoptosis fluoresce green due to mitochondrial membrane depolarization. Results of JC-1 staining of lung cancer cells treated with compounds at 12 hour incubation confirms loss of

mitochondrial membrane potential; control cells were observed with healthy mitochondria (Figure 14).

7.3. Conclusion

The 1:1 Ni^{II} complex of sodium 2-amino-3-hydroxy-9,10-anthraquinone-1-sulphonate (AQSH) with the molecular formula Ni(AQS)Cl₂(H₂O)₂ was prepared and characterized by different techniques. The electrochemical behaviour of Ni(AQS)Cl₂(H₂O)₂ was studied in anhydrous organic solvents and it was compared with that of the free ligand (AQSH). The binding constant and Gibbs free energy for the interaction of Ni(AQS)Cl₂(H₂O)₂ with SDS micelles were calculated as $(1.40 \pm 0.06) \times 10^5 \text{ M}^{-1}$ and -29.38 kJ/mol , respectively. The study showed that the experimental molecule penetrates the SDS micelle through hydrophobic mode of interaction. Ni(AQS)Cl₂(H₂O)₂ induces apoptosis in A549 human lung cancer cells. The IC₅₀ value was found as $68.5 \pm 0.05 \text{ }\mu\text{M}$ for 24 hour incubation.

References

1. B. H. Trachtenberg, D. C. Landy, V. I. Franco, J. M. Henkel, E. J. Pearson, T. L. Miller, S. E. Lipshultz, *Pediatr. Cardiol.* 32 (2011) 342–353.
2. Y. Shi, M. Moon, S. Dawood, B. McManus, P. P. Liu, *Herz.* 36 (2011) 296–305.
3. D. Outomuro, D. R. Grana, F. Azzato, J. Milei, *Int. J. Cardiol.* 117 (2007) 6–15.
4. P. S. Guin, S. Das, P.C. Mandal, *J. Inorg. Biochem.* 103 (2009) 1702–1710.
5. P. S. Guin, S. Das, *Russ. J. Phys. Chem. A* 90 (2016) 876-881.
6. M. Saha, S. Das, *Heliyon* 7(8) (2021) e07746.
7. A. Datta, S. Roy, P. Mondal, P. S. Guin, *J. Mol. Liq.* 219 (2016) 1058–1064.

8. O. Cudina, J. Brboric, I. Jankovic, K. Karljickovic-Rajic, S. Vladimirov, *Colloids Surf. B: Biointerfaces* 65 (2008) 80–84.
9. W. Caetano, M. Tabak, *Spectrochim. Acta A* 55 (1999) 2513–2528.
10. W. Caetano, M. Tabak, *J. Colloid Interface Sci.* 225 (2000) 69–81.
11. E. Fuguet, C. Rafols, M. Roses, E. Bosch, *Anal.Chim.Acta.* 548 (2005) 95–100.
12. M. Sarkar, S. Poddar, *J. Colloid Interface Sci.* 221 (2002) 181–185.
13. J. B. Foresman, A. Frish, *Exploring Chemistry with Electronic Structure Methods*, Gaussian, Inc., Pittsburgh, PA 2000, p. 64.
14. A. V. Iogansen, *Spectrochim. Acta.Part A* 55 (1999) 1585-1612.
15. M. Enache, I. Anghelache, E. Volanschi, *Int. J. Pharm.* 390 (2010) 100-106.
16. M. Enache, E. Volanschi, *J. Pharma. Sci.* 100 (2) (2011) 558-565.
17. A. Das, S. Roy, P. Mondal, A. Datta, K. Mahali, G. Loganathan, D. Dharumadurai, P. S. Sengupta, M. A. Akbarsha, P. S. Guin, *RSC Adv.* 6 (2016) 28200-28212.
18. R. Sabate, M. Gallardo, J. Estelrich, *J. Colloid Interface Sci.* 233(2) (2001) 205-210.
19. R. Sabate, M. Gallardo, A. de la Maza, J. Estelrich, *Langmuir* 17 (2001) 6433-6437.
20. T. Mosmann, *J. Immunol. Methods.* 65 (1–2) (1983) 55-63.

Chapter: 8

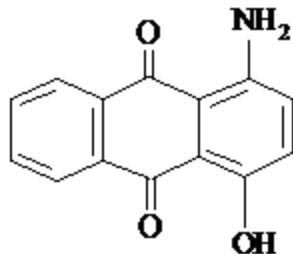
A Co^{III} Complex of 1-Amino-4-hydroxy-9,10-anthraquinone Exhibits Apoptotic Action against MCF-7 Human Breast Cancer Cells

8.1. Introduction

Anthracycline drugs are used to treat different forms of human carcinoma [1-4]. They are often questioned for their associated cardiotoxicity and high cost involved. Hence, there is an effort worldwide [5-19] to find alternative, less costly analogues that are less cardiotoxic [5-10]. Earlier studies have shown that 1-amino-4-hydroxy-9,10-anthraquinone (QH) [Scheme- 1] behaves as potential alternatives to anthracyclines [6-9].

Participating in reactions of the respiratory chain, they produce semiquinone radical anion and related intermediates by one-electron reduction of the quinone that are responsible for chemotherapeutic efficacy as well as for cardiotoxicity [20-24]. Previous research on the subject suggests complex formation of these drugs with different metal ions lead to decreased toxicity. Metal complexes stabilize the semiquinone radical-anion formed. Hence, superoxide formation due to a reaction between a semiquinone radical-anion and molecular oxygen is either inhibited or decreased drastically. In this chapter, we have studied the formation of a Co^{III} complex of 1-amino-4-hydroxy-9,10-anthraquinone to see whether it has any improvement in biochemical properties than QH and it mimics the action of anthracycline drugs.

As single crystals for CoQ_3 was not obtained, we made an effort to characterize CoQ_3 theoretically using density functional theory (DFT) based on experimental data. The complex was tested on MCF-7 human breast cancer cells to see whether it initiates apoptosis and thus could be considered as less costly alternative to anthracyclines that are in use.



Scheme 1: 1-Amino-4-hydroxy-9,10-anthraquinone (QH)

8.2. Results and Discussion:

8.2.1. Analysis of the mass spectra of CoQ₃

Assuming that the formula of the complex is CoQ₃ (Scheme 2), analysis of its mass spectrum (Figure 1) was attempted. The molecular ion or protonated molecular ion peak expected at a region around $m/z = 773.62$ was not found. However, a clear signal at $m/z = 689.46$ corresponding to a fragment remaining of the complex following the loss of an-NH₂ group from each ligand (i. e. loss of 28 mass units from each ligand; 78 mass units from the complex) to result in a peak theoretically expected at $m/z = 689.62$, was obtained. From this peak, the loss of two quinone oxygens would result in a peak theoretically expected at $m/z = 661.62$. Hence, an experimental peak at 661.45 could be this species. Loss of four quinone oxygens from the first fragment results in a peak theoretically expected at $m/z = 633.62$; this was experimentally found at $m/z = 633.42$. Similarly, loss of six quinone oxygens of three ligands, from the first fragment should result in a peak at $m/z = 605.62$. This was experimentally observed at $m/z = 605.39$ indicating close agreement.

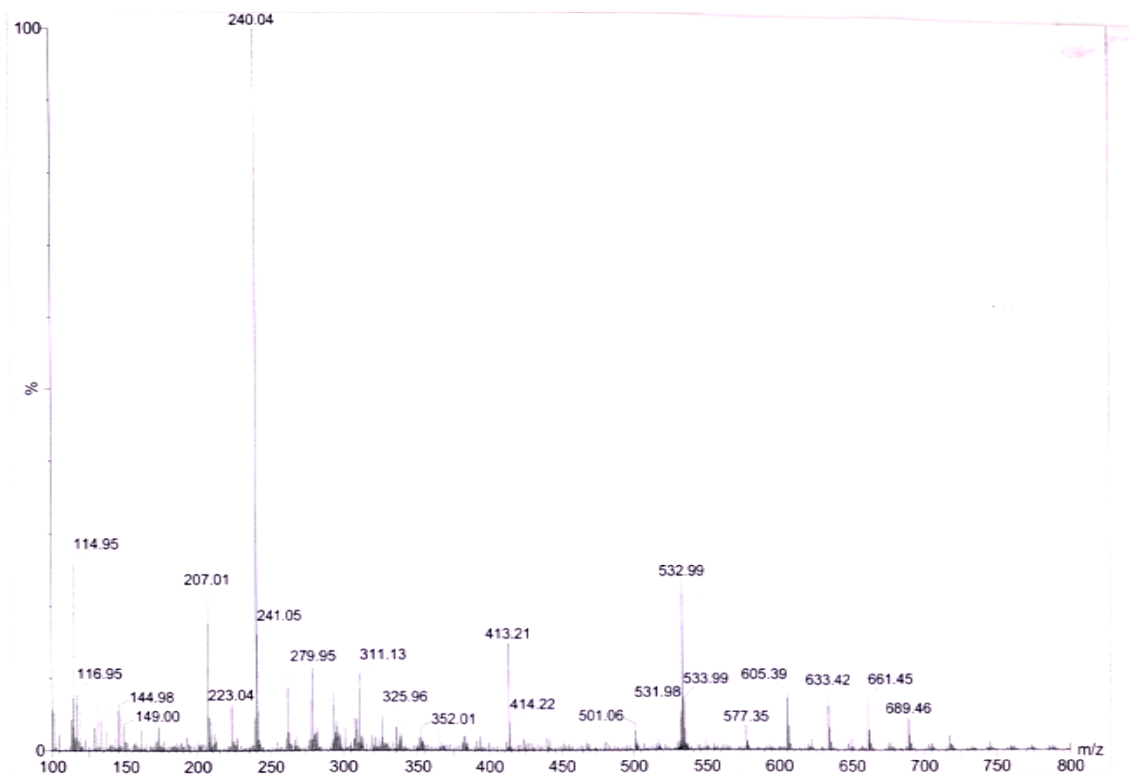


Figure 1: ESIMS of CoQ₃.

At this stage of fragment formation in mass analysis the metal centre is bound to three ligands via three phenolic –OH on each of them. The peaks identified above categorically indicate formation of a 1:3 complex. Subsequent to fragmentations mentioned above, further loss of 2 carbon atoms and a few hydrogens at a time explains peaks at $m/z = 577.35$ and also the cluster of peaks at m/z values of 533.99, 532.99 and 531.98, respectively. Peaks at lower m/z values correspond to smaller fragments. Therefore, from the analysis of the mass spectrum of the cobalt complex it may be concluded that the complex has a formula CoQ₃ as shown in Scheme 3.

8.2.2. Analysis of IR spectrum of CoQ₃

The FTIR spectrum for QH (Figure 2) shows a peak at 3431 cm⁻¹ which is due to N-H bond stretching while that at 3300 cm⁻¹ is due to the stretching of O-H bond[6]. The O-H stretching is modified significantly in the complex (Figure 3) indicating involvement of the -OH group during complex formation. Since there is deprotonation of -OH during complex formation, the molecule ceases to show intra-molecular hydrogen bonding which is identified. Peaks in this region do not disappear completely in the complex if compared with QH indicating the presence of free -NH₂ on each ligand (just as that observed in the IR spectrum of QH). In the IR spectrum of CoQ₃ (Figure 3), peaks at 1625 cm⁻¹, 1586 cm⁻¹ and 1537 cm⁻¹ are attributed to stretching due to free carbonyl and C=C respectively, or a combination of both. In an earlier study[6], we showed peaks obtained in the region 1464 cm⁻¹ to 1031 cm⁻¹ in the IR spectrum of the ligand (QH) may be attributed to combinations of O-H, N-H and C-H bending modes. Nature of peaks in this region is somewhat different in the complex. More specifically, the peak at 1121 cm⁻¹ is reduced significantly, probably due to binding of oxygen of the -OH group to Co^{III}, following its deprotonation.

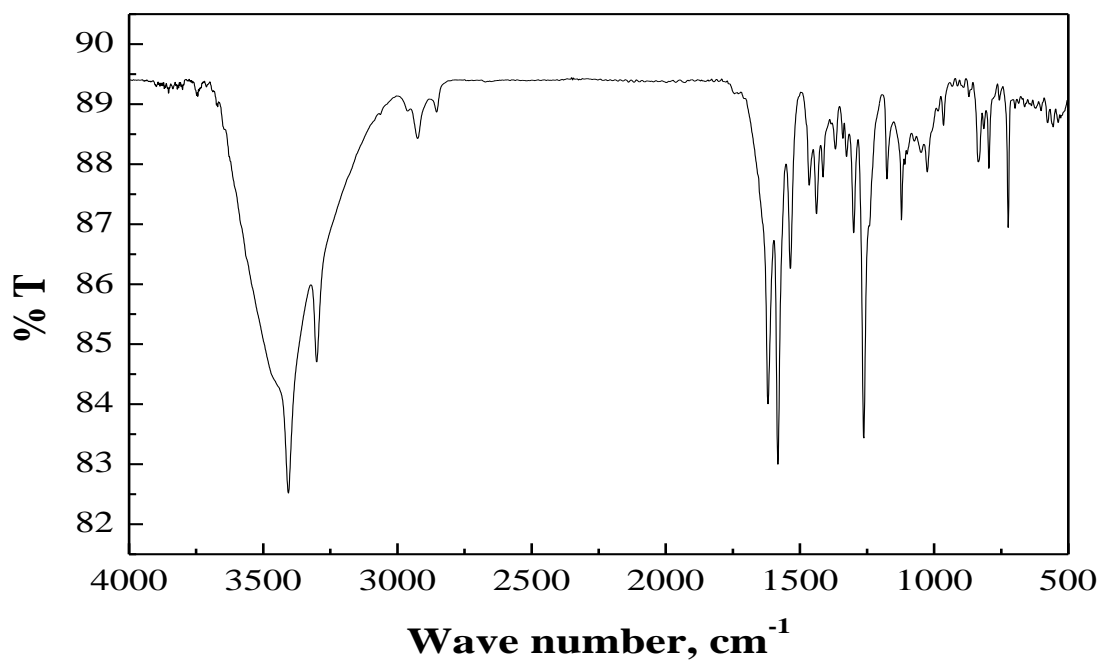
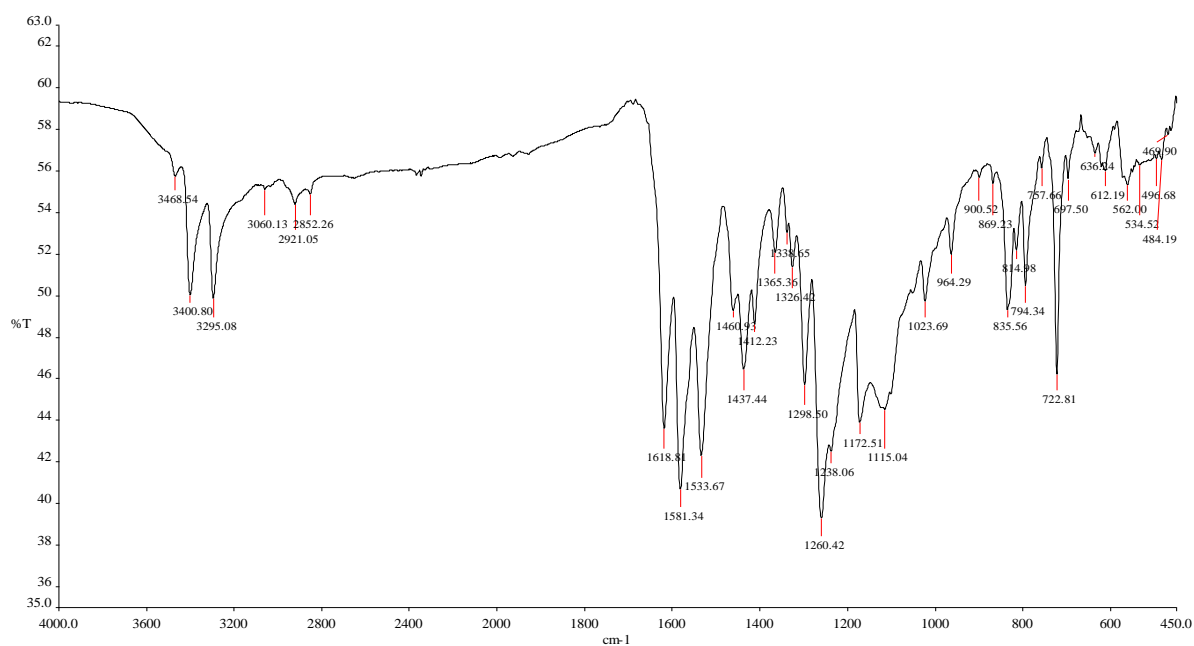


Figure 2: IR Spectrum of QH.

Figure 3: IR spectrum of CoQ₃.

8.2.3. Powder X-ray Diffraction of CoQ₃

Powder X-ray diffraction (PXRD) pattern of CoQ₃ is shown in Figure 4. All peaks can be indexed with a space group R32(155), CuK α = 1.5406Å using the WINPLOTR program. Refined cell parameters were found to be a = 7.45 Å, b = 6.52 Å, c = 27.8 Å. The unit cell volume was 1352 Å³; α = 33.43°, β = 90°, γ = 90°. Thus PXRD analysis provides information about the dimension of the unit cell of crystalline CoQ₃.

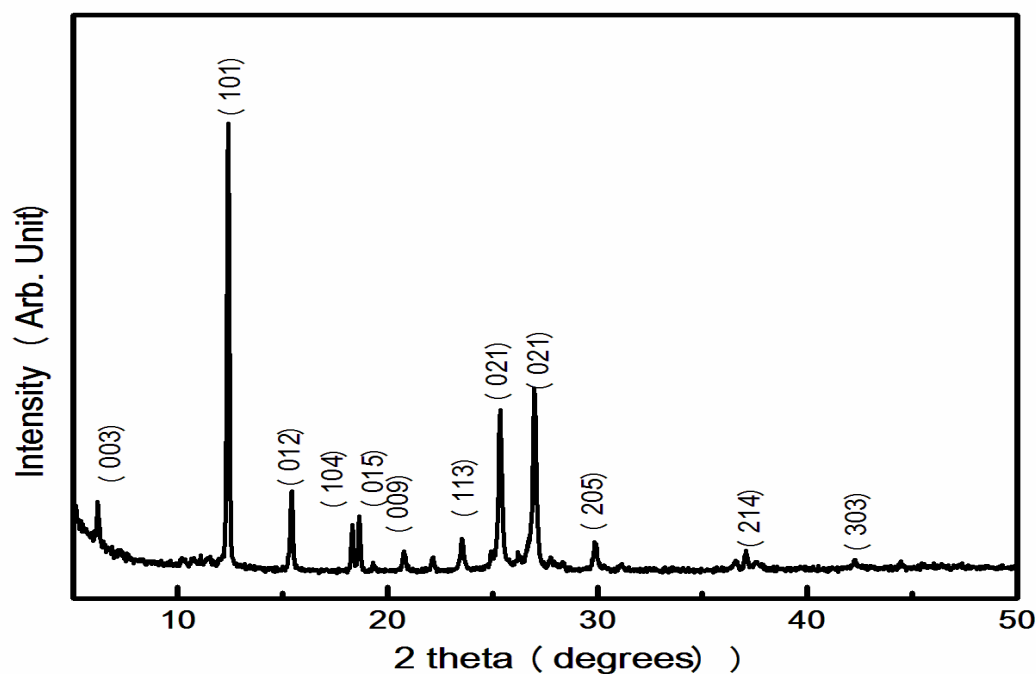


Figure 4: Powder X-ray diffraction patterns of CoQ₃.

8.2.4. Structure of CoQ₃ from density functional theory

Energy optimized molecular structure of CoQ₃ is shown in Figure 5 and structural parameters are summarized in Table-1. Figure 5 shows three QH molecules coordinated to Co^{III} through phenolic- O⁻ and quinone oxygen forming CoQ₃.

The energy level diagrams of QH and CoQ_3 are shown in Figure 6. HOMO (H) and LUMO (L) are indicated in each case (Figure 7). Red lines indicate the π orbitals, black lines indicate σ and blue lines represent mixed metal-ligand (M-L) orbitals. Some M-L type MOs may have mixed σ and π character. The three ligands are arranged in such a manner that σ of one may mix with π of another. Metal orbitals are mainly $d\pi$, with some $p\pi$ mixed. Co^{III} orbitals are much lower in energy to be shown in the above diagram. It should also be noted that HOMO and LUMO are M-L type orbitals.

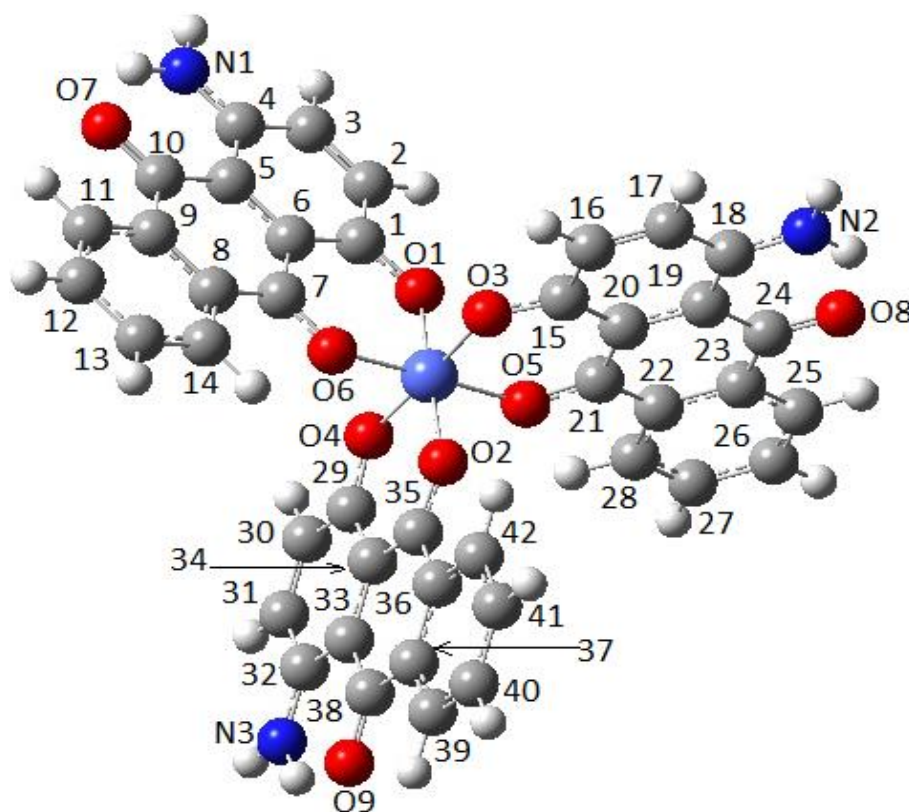


Figure 5: Energy optimized structure of CoQ_3 .

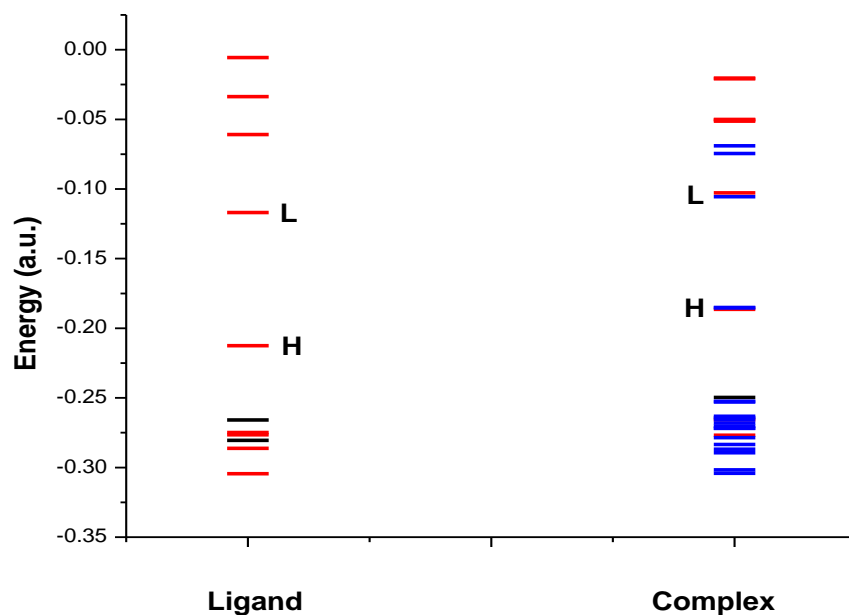
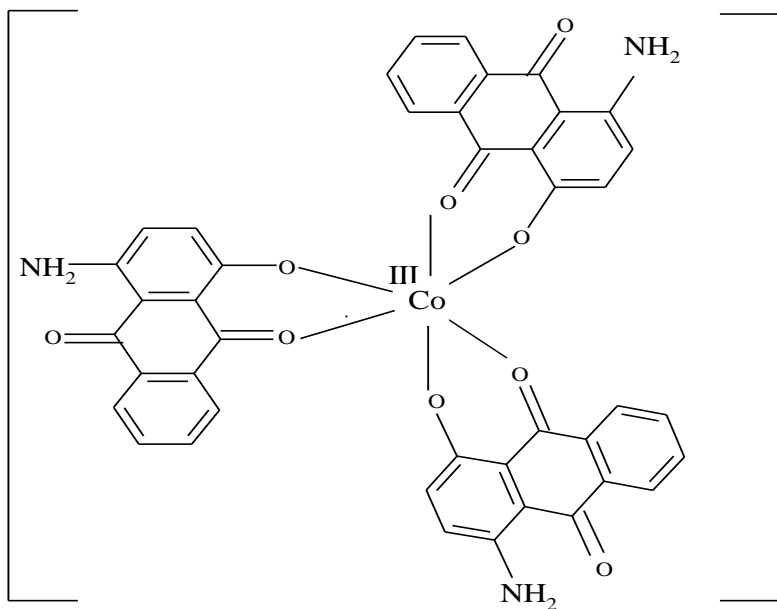


Figure 6: Energy level diagram of QH and CoQ₃.



Scheme 2: Structure of CoQ₃.

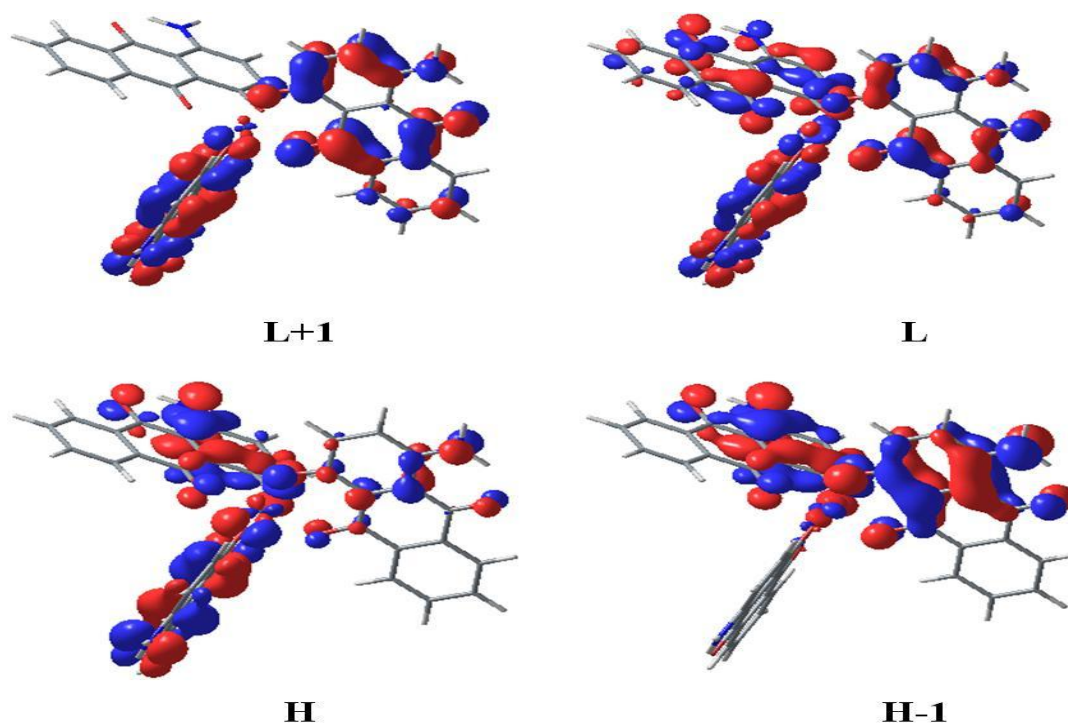


Figure 7: Different HOMOs (H) and LUMOs (L) of CoQ₃.

Table 1: Structural parameters of CoQ₃.

Bond distances (in Å)

Co – O1	1.87915	Co – O2	1.89840	Co – O3	1.88397
Co – O4	1.88654	Co – O5	1.89389	Co – O6	1.89270
O1 – 1	1.30411	1 – 2	1.44976	2 – 3	1.36438
3 – 4	1.44799	4 – 5	1.45335	5 – 6	1.41605
6 – 1	1.44955	6 – 7	1.46966	7 – 8	1.45978
8 – 9	1.42373	9 – 10	1.47250	10 – 5	1.49120
4 – N1	1.33954	10 – O7	1.26097	9 – 11	1.40485
11 – 12	1.40744	12 – 13	1.40809	13 – 14	1.40290
14 – 8	1.41394	O3 – 15	1.30378	15 – 16	1.44995
16 – 17	1.36419	17 – 18	1.44802	18 – 19	1.45337
19 – 20	1.41579	20 – 15	1.44991	20 – 21	1.46986
O5 – 21	1.29163	O6 – 7	1.29166	21 – 22	1.45961
22 – 23	1.42351	23 – 24	1.47244	18 – N2	1.33967
24 – O8	1.26087	24 – 19	1.49122	23 – 25	1.40483
25 – 26	1.40743	26 – 27	1.40801	27 – 28	1.40274

A Co^{III} complexhuman breast cancer cells

28 – 22	1.41400	O4 – 29	1.30386	29 – 30	1.44993
30 – 31	1.36436	31 – 32	1.44804	32 – 33	1.45350
32 – N3	1.33971	33 – 34	1.41591	34 – 29	1.45013
34 – 35	1.47016	35 – O2	1.29061	35 – 36	1.46024
36 – 37	1.42352	37 – 38	1.47256	38 – 33	1.49147
37 – 39	1.40504	39 – 40	1.40728	40 – 41	1.40814
41 – 42	1.40305	42 – 36	1.41392	38 – O9	1.26089

Bond angles (in degrees)

O1 – Co – O3	89.002	O1 – Co – O5	89.225	O1 – Co – O2	178.303
O1 – Co – O4	89.773	O1 – Co – O6	91.684	O3 – Co – O5	91.435
O3 – Co – O2	90.106	O3 – Co – O4	178.089	O3 – Co – O6	89.562
O5 – Co – O2	89.354	O5 – Co – O4	90.014	O5 – Co – O6	178.663
O2 – Co – O4	91.155	O2 – Co – O6	89.753	O4 – Co – O6	89.008
Co – O1 – 1	129.056	O1 – 1 – 2	115.897	1 – 2 – 3	121.341
2 – 3 – 4	120.858	3 – 4 – 5	119.072	4 – 5 – 6	119.956
3 – 4 – N1	119.505	N1 – 4 – 5	121.423	5 – 6 – 1	119.751
5 – 6 – 7	120.017	6 – 7 – 8	120.235	7 – 8 – 9	120.064
8 – 9 – 10	120.614	9 – 10 – 5	118.647	10 – 5 – 4	119.687
10 – 5 – 6	120.356	9 – 10 – O7	120.837	O7 – 10 – 5	120.514
7 – 6 – 1	120.230	Co – O6 – 7	131.401	O6 – 7 – 6	122.322
O6 – 7 – 8	117.443	7 – 8 – 14	120.526	8 – 14 – 13	120.202
14 – 13 – 12	120.172	13 – 12 – 11	120.150	12 – 11 – 9	120.086
11 – 9 – 8	119.980	11 – 9 – 10	119.406	Co – O3 – 15	129.201
O3 – 15 – 16	115.925	15 – 16 – 17	121.346	16 – 17 – 18	120.848
17 – 18 – 19	119.093	17 – 18 – N2	119.461	N2 – 18 – 19	121.445
18 – 19 – 20	119.949	19 – 20 – 15	119.755	20 – 15 – 16	119.005
20 – 15 – O3	125.070	18 – 19 – 24	119.673	19 – 24 – O8	120.523
O8 – 24 – 23	120.840	24 – 23 – 22	120.616	23 – 22 – 21	120.102
22 – 21 – O5	117.481	Co – O5 – 21	131.423	O5 – 21 – 20	122.301
21 – 20 – 15	120.217	21 – 20 – 19	120.023	O1 – 1 – 6	125.084
22 – 23 – 25	119.975	23 – 25 – 26	120.097	25 – 26 – 27	120.150
26 – 27 – 28	120.152	27 – 28 – 22	120.229	28 – 22 – 21	120.501
28 – 22 – 23	119.396	Co – O4 – 29	129.392	O4 – 29 – 30	115.970
O4 – 29 – 34	125.084	29 – 30 – 31	121.381	30 – 31 – 32	120.857
31 – 32 – 33	119.071	32 – 33 – 34	119.943	31 – 32 – N3	119.479
N3 – 32 – 33	121.450	33 – 34 – 29	119.798	34 – 29 – 30	118.945

29 – 34 – 35	120.169	34 – 35 – 36	120.201	35 – 36 – 37	120.107
36 – 37 – 38	120.600	37 – 38 – 09	120.837	09 – 38 – 33	120.496
38 – 33 – 34	120.360	38 – 33 – 32	119.696	38 – 37 – 39	119.433
36 – 37 – 39	119.967	37 – 39 – 40	120.077	39 – 40 – 41	120.176
40 – 41 – 42	120.149	41 – 42 – 36	120.196	42 – 36 – 37	119.433

Dihedral angles (degrees)

Co – O1 – 1 – 2	-175.665	O1 – 1 – 2 – 3	-179.630
Co – O1 – 1 – 6	4.962	O1 – 1 – 6 – 5	179.040
O1 – 1 – 7 – 6	-0.500	1 – 2 – 3 – 4	0.227
2 – 3 – 4 – 5	0.281	3 – 4 – 5 – 6	-0.807
4 – 5 – 6 – 1	0.818	5 – 6 – 1 – 2	-0.315
6 – 1 – 2 – 3	-0.217	2 – 3 – 4 – N1	-179.865
N1 – 4 – 5 – 6	179.342	N1 – 4 – 5 – 10	-0.879
4 – 5 – 6 – 7	-179.641	5 – 6 – 7 – 8	-2.579
6 – 7 – 8 – 9	2.464	7 – 8 – 9 – 10	-0.349
8 – 9 – 10 – 5	-1.610	9 – 10 – 5 – 6	1.490
10 – 5 – 6 – 7	0.581	10 – 5 – 6 – 1	-178.959
O6 – 7 – 6 – 5	177.175	O6 – 7 – 8 – 9	-177.302
8 – 9 – 10 – O7	178.826	O7 – 10 – 5 – 6	-178.945
O7 – 10 – 5 – 4	1.277	9 – 10 – 5 – 4	-178.288
5 – 10 – 9 – 11	178.360	10 – 9 – 11 – 12	-179.726
O7 – 10 – 9 – 11	-1.204	9 – 11 – 12 – 13	0.036
11 – 12 – 13 – 14	-0.212	12 – 13 – 14 – 8	0.104
13 – 14 – 8 – 9	0.175	14 – 8 – 9 – 11	-0.349
2 – 1 – 6 – 7	-179.854	1 – 6 – 7 – 8	176.959
6 – 7 – 8 – 14	-177.505	7 – 8 – 14 – 13	-179.855
Co – O6 – 7 – 6	2.650	Co – O6 – 7 – 8	-177.590
Co – O3 – 15 – 16	179.828	Co – O3 – 15 – 20	0.024
O3 – 15 – 16 – 17	-179.186	O3 – 15 – 20 – 21	-1.740
15 – 16 – 17 – 18	-0.127	16 – 17 – 18 – 19	-0.273
17 – 18 – 19 – 20	0.158	18 – 19 – 20 – 15	0.345
19 – 20 – 15 – 16	-0.733	20 – 15 – 16 – 17	0.631
16 – 17 – 18 – N2	179.871	N2 – 18 – 19 – 20	-179.988
N2 – 18 – 19 – 24	0.129	18 – 19 – 20 – 21	-178.851
19 – 20 – 21 – 22	-1.997	20 – 21 – 22 – 23	1.627
21 – 22 – 23 – 24	-0.301	22 – 23 – 24 – 19	-0.650
23 – 24 – 19 – 20	0.277	24 – 19 – 20 – 21	1.031

A Co^{III} complexhuman breast cancer cells

20 – 19 – 24 – 08	-179.874	08 – 24 – 23 – 22	179.502
Co – 05 – 21 – 20	7.031	Co – 05 – 21 – 22	-173.481
21 – 22 – 23 – 25	179.981	22 – 23 – 25 – 26	0.215
23 – 25 – 26 – 27	0.061	25 – 26 – 27 – 28	-0.187
26 – 27 – 28 – 22	0.034	27 – 28 – 22 – 23	0.241
28 – 22 – 23 – 24	-0.365	17 – 18 – 19 – 24	-179.724
18 – 19 – 24 – 23	-179.841	19 – 24 – 23 – 25	179.069
24 – 23 – 25 – 26	-179.505	16 – 15 – 20 – 21	178.461
15 – 20 – 21 – 22	178.811	20 – 21 – 22 – 28	-178.023
21 – 22 – 28 – 27	179.893	08 – 24 – 19 – 18	0.008
Co – 04 – 29 – 30	-177.001	Co – 04 – 29 – 34	3.270
04 – 29 – 30 – 31	-179.701	29 – 30 – 31 – 32	0.194
30 – 31 – 32 – 33	-0.008	31 – 32 – 33 – 34	-0.425
32 – 33 – 34 – 29	0.663	33 – 34 – 29 – 30	-0.477
34 – 29 – 30 – 31	0.045	30 – 31 – 32 – N3	-179.979
N3 – 32 – 33 – 34	179.545	32 – 33 – 34 – 35	-179.544
33 – 34 – 35 – 36	-1.956	34 – 35 – 36 – 37	1.892
35 – 36 – 37 – 38	-0.438	36 – 37 – 38 – 33	-0.928
37 – 38 – 33 – 34	0.861	38 – 33 – 34 – 35	0.567
34 – 33 – 38 – 09	-179.578	09 – 38 – 37 – 36	179.512
35 – 36 – 37 – 39	179.669	36 – 37 – 39 – 40	0.296
37 – 39 – 40 – 41	0.014	39 – 40 – 41 – 42	-0.232
40 – 41 – 42 – 36	0.136	41 – 42 – 36 – 37	0.172
42 – 36 – 37 – 39	-0.388	31 – 32 – 33 – 38	179.464
32 – 33 – 38 – 37	-179.028	33 – 38 – 37 – 39	178.965
38 – 37 – 39 – 40	-179.598	30 – 29 – 34 – 35	179.730
29 – 34 – 35 – 36	177.836	34 – 35 – 36 – 42	-178.050
35 – 36 – 42 – 41	-179.885	04 – 29 – 34 – 35	-0.549
29 – 34 – 35 – 02	-2.302	Co – 02 – 35 – 34	2.497
Co – 02 – 35 – 36	-177.638		

8.2.5. UV-Vis spectroscopy of CoQ₃

The absorption spectrum of QH (Figure 8a) in 30% ethanol[6,7] shows four absorption bands (at 250 nm, 290 nm, 530 nm and 565 nm) due to $\pi-\pi^*$ and $n-\pi^*$ transitions of its various tautomeric forms in rapid equilibrium in aqueous solution[6,7,25]. From the UV-Vis spectrum of CoQ₃ (Figure 8b) it is clear the absorption peaks at 250 nm, 290 nm, 530 nm and 565 nm remain almost unaltered, which indicate that electronic absorption spectrum of CoQ₃ depends weakly on the nature of Co^{III} and is primarily defined by the ligand (QH)[25]. However, appearance of a new peak at 600 nm is characteristic of the complex (CoQ₃). It is important to mention here that tautomeric structures found for free QH [25] in aqueous media are not possible for CoQ₃, since phenolic -OH in QH are deprotonated owing to coordination with Co^{III} by phenolic oxygens.

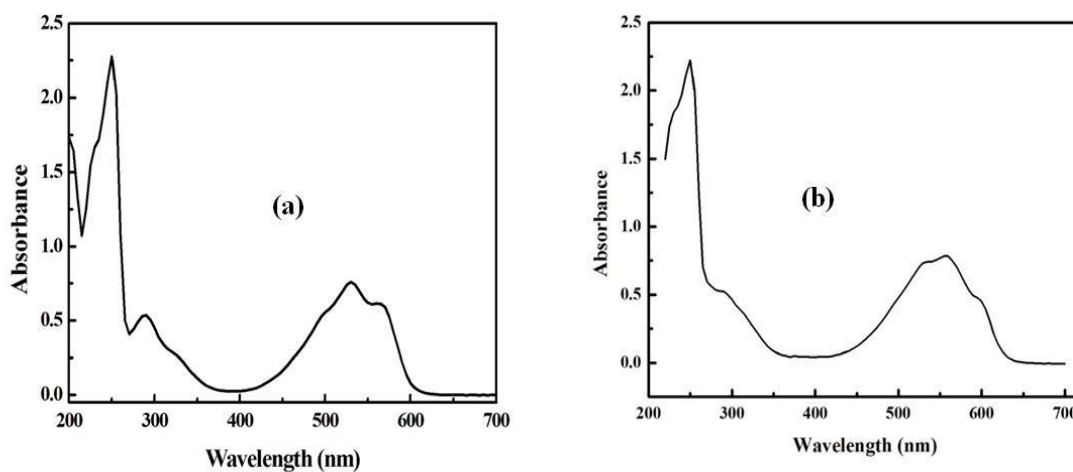


Figure 8: UV-Vis spectrum of (a) QH (b) CoQ₃ in aqueous ethanol.

8.2.6. Fluorescence spectroscopy of CoQ₃

Fluorescence spectra of QH and CoQ₃ are shown in Figure 9, recorded following excitation at 530 nm. Emission spectrum exhibits a maximum at 590 nm for QH and 594 nm for CoQ₃. The difference in emission peak of CoQ₃ compared to QH is due to the metal ligand bond.

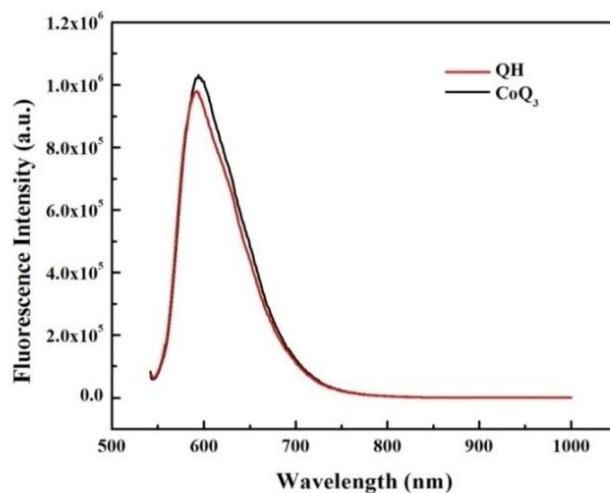


Figure 9: Fluorescence spectra of QH and CoQ₃ in aqueous ethanol.

8.2.7. Electrochemical reduction of CoQ₃ in organic polar solvents

Electrochemical behavior of CoQ₃ was studied in anhydrous DMSO and DMF in presence of TBAB as supporting electrolyte using cyclic voltammetry. In anhydrous DMSO, CoQ₃ undergoes successive three one-electron reductions having peak potentials (E_{pc}) at -0.795, -1.010 and -1.295V, respectively, vs. Ag/AgCl/saturated KCl (Figure 10, Table- 2). In this case, the first reduction is reversible, while the other two shows quasi-reversible at different scan rates. These three one-electron reduction steps are owing to reduction of the three free quinone centres of three Q⁻ bound to Co^{III} in CoQ₃ [Scheme 3]. For these reductions, the formal potentials (E) of the respective reduction steps were at -0.750, -0.987 and -1.255 V respectively. It is to be noted although there are three equivalent free quinone sites in CoQ₃ (Scheme 3), there is a difference in their formal potential values which is appreciable. Thus, after reduction at the first free quinone in CoQ₃, reduction of the second and third quinone sites are significantly delayed. In other words, the reduced species (semiquinone radical anion) formed due to the first or second reduction is stabilized in a metal ion environment due to delocalization of the negative charge.

This is important with regard to the compound's biochemical action, since a stabilized semiquinone would delay the reaction between semiquinone and molecular oxygen [24, 26–29] within cells where it would be employed. Further, three distinctly different reduction potentials could have a biological implication and serve as an important attribute of complex formation.

In anhydrous DMF, under similar experimental conditions, CoQ₃ undergoes three-one electron reductions having peak potentials (E_{pc}) at -1.025 V, -1.225 V and -1.475 V respectively; the corresponding formal potentials (E) being -0.950 V, -1.195 V and -1.405 V, respectively (Figure 11, Table- 2). Considering polarity of DMF is less than DMSO [30] and comparing three reduction potentials of CoQ₃ in the two solvents, it can be said that with increasing polarity of the medium reduction potentials move in a positive direction and that reductions become more feasible as polarity of the solvent increases. This implies stability of formed semiquinone increases with an increase in the polarity of the medium. Stabilization of the semiquinone is also reflected in the formal reduction potential data. This aspect is important with respect to chemotherapeutic efficiency [24, 26–29]. Owing to the stabilization of semiquinone radical anion, the probability for the reaction of semiquinone radical anion with molecular oxygen would be delayed and that might reduce cardiotoxicity, if the molecule were to be employed as an anticancer agent [24,26–29].

Under similar experimental conditions, cyclic voltammogram of QH shows two reversible waves at -0.816V and -1.355 V in anhydrous DMSO and at -0.832 V and -1.309 V in anhydrous DMF versus Ag/AgCl, saturated KCl, forming semiquinone radical anion and quinone dianion respectively [7,8]. Formal potentials for such reductions were evaluated as -0.770 and -1.308V in anhydrous DMSO and -0.785 and -1.258 V in anhydrous DMF[8]. Comparing electrochemical parameters and cyclic voltammograms (Figure 10 and Figure 11) of CoQ₃ with those of QH in anhydrous DMSO and anhydrous DMF [8], one can say electrochemical behavior of QH bound to Co^{III} in CoQ₃ as Q⁻ is significantly altered.

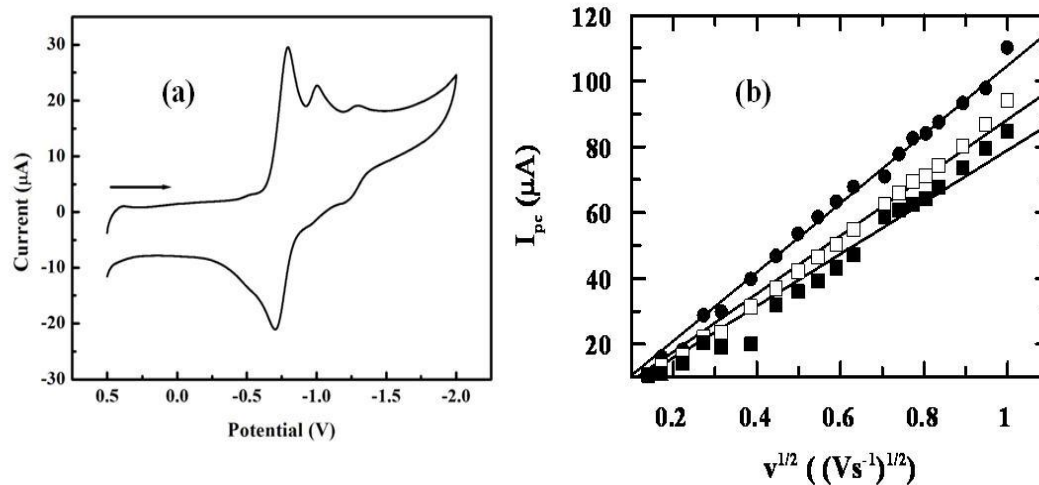


Figure 10(a): Cyclic voltammogram of CoQ_3 in anhydrous DMSO media. Scan rate: 0.10 Vs^{-1} . $[\text{CoQ}_3] = 1 \times 10^{-3} \text{ M}$, $[\text{TBAB}] = 0.1 \text{ M}$, $T = 298.15 \text{ K}$. **(b):** Plot of cathodic peak current vs. square root of scan rate for first (\bullet), second (\square) and third reduction (\blacksquare) of CoQ_3 in anhydrous DMSO.

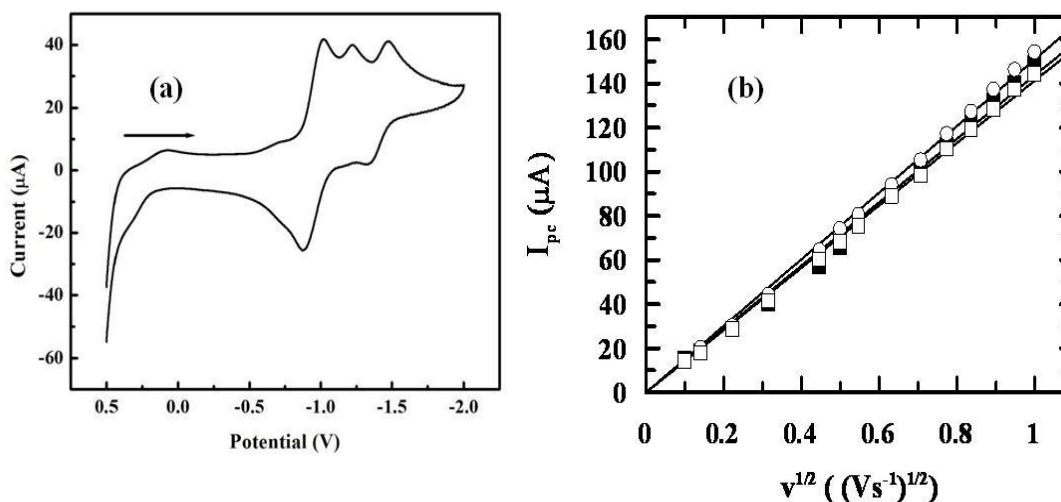


Figure 11(a): Cyclic voltammogram of CoQ_3 in anhydrous DMF media. Scan rate: 0.10 Vs^{-1} . $[\text{CoQ}_3] = 1 \times 10^{-3} \text{ M}$, $[\text{TBAB}] = 0.1 \text{ M}$, $T = 298.15 \text{ K}$. **(b):** Plot of cathodic peak current vs. square root of scan rate for first (\circ), second (\square) and third reduction (\blacksquare) of CoQ_3 in anhydrous DMF.

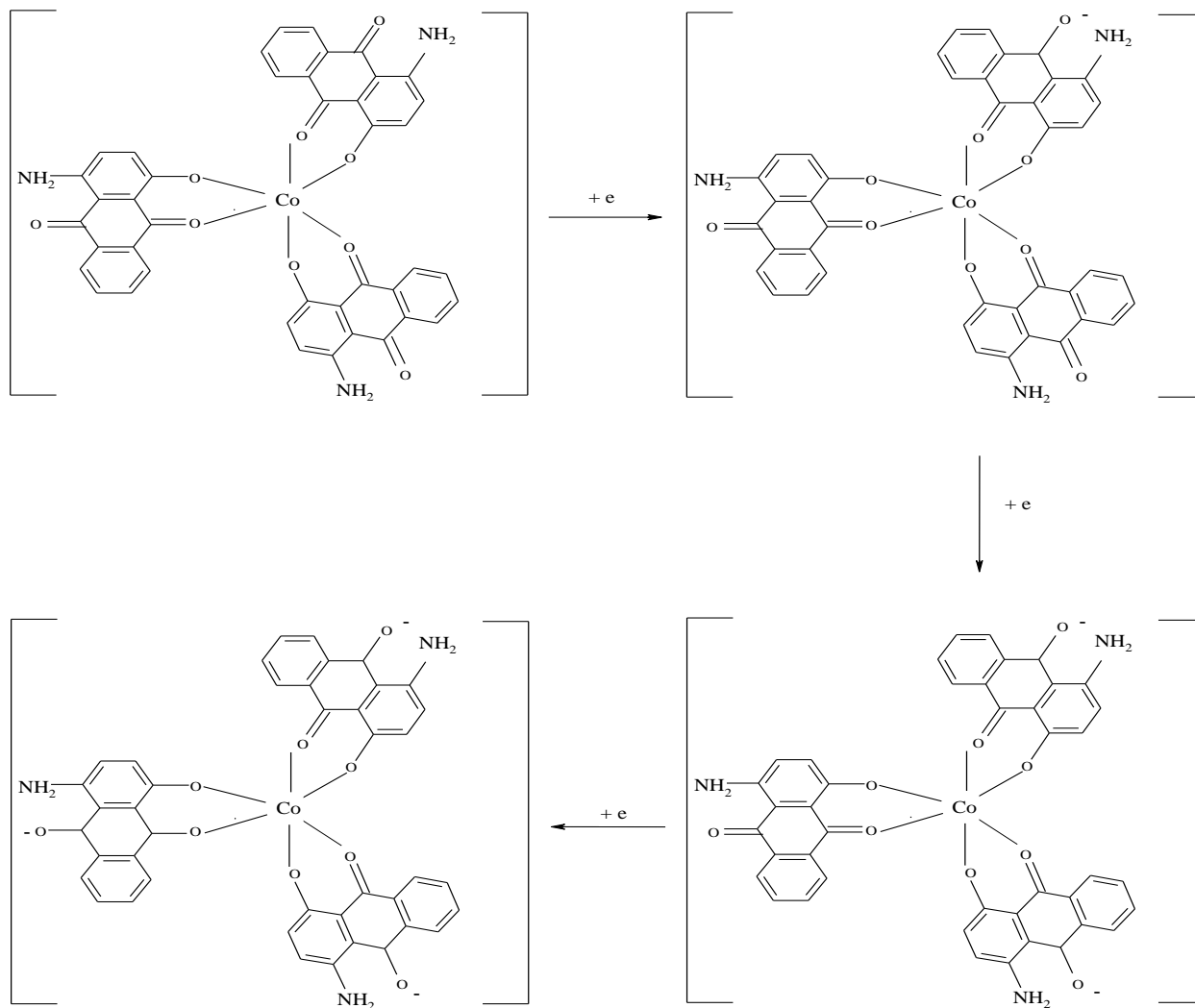
It is seen that reduction peak currents (I_{pc}) for three successive reductions of CoQ_3 in both DMSO and DMF have a linear relationship with square root of scan rate and that it passes

through the origin (Figure 10 and Figure 11). This suggests such reductions are fully diffusion controlled and that there is no adsorption on the electrode surface. The diffusion coefficient (D_O) of CoQ_3 was determined using the relation shown in equation 1[31] and found to be 3.04×10^{-5} and $6.31 \times 10^{-5} \text{ cm}^2 \text{ s}^{-1}$ in DMSO and DMF respectively (summarized in Table- 2).

$$I_{pc} = (2.69 \times 10^5) n^{3/2} D_O^{1/2} A C v^{1/2} \quad [1]$$

where I_{pc} = cathodic peak current in amperes, n = number of electron involved in the reduction, A = area of the electrode (cm^2), C = concentration ($\text{moles} \cdot \text{cm}^{-3}$) and v = scan rate ($\text{V} \cdot \text{s}^{-1}$).

From values of diffusion coefficients of CoQ_3 in two different solvents (Table- 2) it is evident D_O increases as the polarity of the solvent decreases, clearly indicating greater solvation of CoQ_3 in a more polar solvent that causes lower diffusion onto the surface of the electrode. Thus CoQ_3 is more solvated in DMSO due to hydrogen bonding and other electrostatic interactions [8]. Intermolecular hydrogen bonding between one of the two hydrogen of the amino group ($-NH_2$) of QH and negatively charged oxygen of the solvent (DMSO) is very strong [8]. This type of hydrogen bonding would be weak in DMF, since for this solvent oxygen has a less partial negative charge than that on oxygen in DMSO [8].



Scheme 3: The three step one-electron reductions of CoQ₃ in organic polar solvents like DMSO and DMF.

Table- 2: Electrochemical Parameters of CoQ₃

Media	Epc-1 (V)	Epc-2 (V)	Epc-3 (V)	E-1 (V)	E-2 (V)	E-3 (V)	D ₀ (Cm ² s ⁻¹)
DMSO	-0.795	-1.010	-1.295	-0.750	-0.987	-1.255	3.04×10 ⁻⁵
DMF	-1.025	-1.225	-1.475	-0.950	-1.195	-1.405	6.31×10 ⁻⁵

(Potentials were measured with respect to vs. Ag/AgCl/saturated KCl.)

8.2.8. Effect of CoQ₃ on viability of MCF-7 human breast cancer cells by the MTT assay

Using MTT assay, the cytotoxic activity of CoQ₃ was analyzed against MCF-7 human breast cancer cells (Figure 12). It was estimated according to dose values of exposure of CoQ₃ required to reduce the survival to 50% (IC₅₀) in comparison to that of untreated cells. The IC₅₀ value for 24 h was found to be (95±0.05) µg/mL. This indicates CoQ₃ is cytotoxic against MCF-7 breast cancer cells.

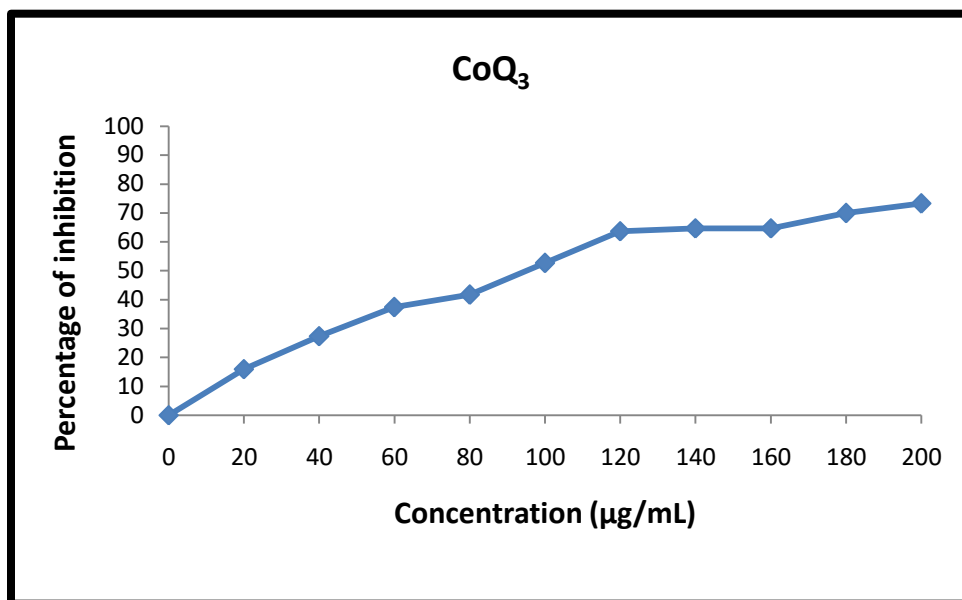


Figure 12: Cytotoxic effect of CoQ₃ on MCF-7 human breast cancer cells after exposure for 24 h.

8.2.9. AO/EB Staining

Apoptosis is the hallmark of cell death and can be characterized by cellular morphological changes observed during the process of cell death. The dual staining method of AO/EB detects such morphological changes. Figure 13 corresponds to AO/EB staining of control/non-treated and CoQ₃ treated MCF7 breast cancer cells. Based on fluorescence emission

and nuclei morphology, the cells were distinguished to have viable, apoptotic or necrotic characteristics. Viable cells were observed to have uniform green colored nuclei with typical cell morphology and intact membrane. On the other hand, apoptotic cells showed irregular cell morphologies with orange to red condensed chromatin and/or fragmented nuclei. Furthermore the large orange to red fluorescent swollen cells with no fragmented nuclei were differentiated as necrotic cells. The results from AO/EB staining reveal that the control group contains more viable cells and a few apoptotic and necrotic cells. In contrast, CoQ₃ treated MCF7 breast cancer cells induced majority of cell death through apoptosis mode and actually very few by necrosis. Furthermore, condensed and fragmented morphologies were mostly observed in CoQ₃ treatment group. The results of calculating the percentage of apoptotic cell death induced by CoQ₃ and analyzed by fluorescent images of AO/EB staining revealed that AQS-treated cells generated a higher percentage of apoptotic cells and a much lower percentage of necrotic cells than untreated cells (Figure 14). The graph depicts a percentage count of apoptotic normal and abnormal cells. The error bar represents the standard deviation across three replicates.

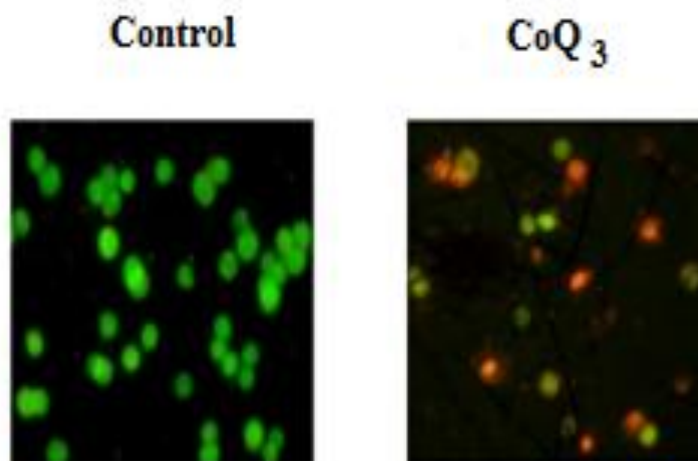


Figure 13: AO/EB Staining of control and CoQ₃ treated MCF-7 human breast cancer cells.

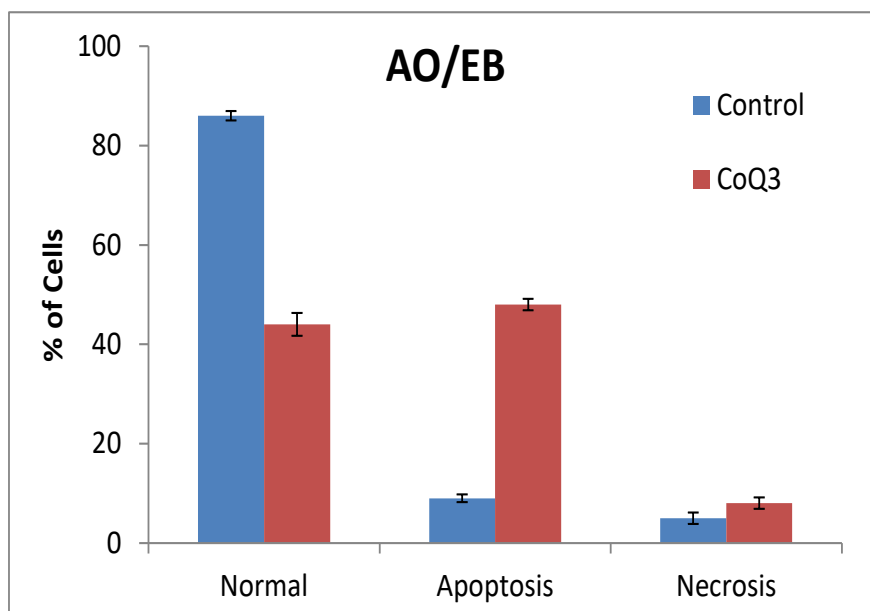


Figure 14: Comparison of percentage of cells in apoptotic death compared to healthy cells and necrotic death.

8.3. Conclusions:

A Co^{III} complex of 1-amino-4-hydroxy-9,10-anthraquinone having molecular formula CoQ₃ was synthesized and characterized by different methods. Optimized molecular structure of CoQ₃ was estimated using computational methods. HOMO and LUMO of CoQ₃ were characterized by this method. Electrochemical properties of CoQ₃ were studied in anhydrous DMSO and anhydrous DMF using cyclic voltammetry and the mechanism of reduction was established. It showed that different reduced anions of CoQ₃ are stabilized in a metal surrounding environment and that reductions would be delayed. Polarity of solvents affect stability of the reduced anion. A significant modification of electrochemical properties of QH was seen when it was bound to Co^{III} in CoQ₃. IC₅₀ of CoQ₃ for 24 hour incubation corresponding to cytotoxicity of CoQ₃ on MCF-7 human breast cancer cells was evaluated as 95±0.05 µg/mL. The study revealed that such cancer cells underwent both early and late apoptosis due to CoQ₃.

References

1. J. -G. Hardman, A.-G. Gilman, L.-E.Limbird, Goodman and Gilman's The Pharmacological Basis of Therapeutics, 9th ed.; McGraw-Hill Companies: New York, 1996.
2. K. H.Lim, H. S.Kim, Y. M.Yang, S. D.Lee, W. B. Kim, J.Yang, J.G. Park, Cancer Chemother. Pharmacol. 40 (1997) 23-30.
3. M. N. Preobrazhenskaya, A. N.Tevyashova, E. N. Olsufyeva, K.-F. Huang, H.-S.Huang, J. Med. Sci.26 (2006) 119-128.
4. F. Q. Hu, L. N. Liu, Y. Z. Du, H. Yuan, Biomaterials. 30 (2009) 6955-6963.
5. A. Das, S. Roy, P. Mondal, A. Datta, K. Mahali, G. Loganathan, D. Dharumadurai, P. S. Sengupta, Md A. Akbarsha, P. S. Guin, RSC Adv. 6 (2016) 28200-28212.
6. P. Mondal, S. Roy, G. Loganathan , B. Mandal , D. Dharumadurai , Md. A. Akbarsha, P. S.Sengupta, S. Chattopadhyay , P. S. Guin, Biochem. Biophys. Rep.4 (2015) 312–323.
7. S. Roy, P. Mondal, P. S. Sengupta, D. Dhak, R. C. Santra, S. Das, P. S. Guin, Dalton Trans. 44 (2015) 5428 –5440.
8. S. Roy, P. S. Guin, J. Electrochem. Soc. 162 (3) (2015) H124-H131.
9. S. Roy, P. S. Guin, J. Mol. Liq. 211 (2015) 846–853.
10. P.S. Guin, S. Das, P.C. Mandal, J. Inorg. Biochem. 103 (12) (2009) 1702–1710.
11. P. S. Guin, P. C.Mandal, S. Das, ChemPlusChem. 77 (2012) 361-369.
12. S. Rossi, C. Tabolacci, A. Lentini, B. Provenzano, F. Carlomosti, S. Frezzotti, S. Beninati, Anticancer Res. 30 (2010) 445-449.
13. P. Das, C. K. Jain, S. K. Dey, R. Saha, A. D. Chowdhury, S. Roychoudhury, S. Kumar, H. K. Majumder, S. Das, RSC Adv. 4 (2014) 59344-59357.
14. P. Das, D. Bhattacharya, P. Karmakar, S. Das, RSC Adv. 5 (2015) 73099-73111.
15. P. Das, P. S. Guin, P. C. Mandal, M. Paul, S. Paul, S. Das, J. Phys. Org. Chem. 24 (2011) 774-785.

16. B. Mandal, S. Singha, S. K. Dey, S. Mazumdar, T. K. Mondal, P. Karmakar, S. Kumar, S. Das, *RSC Adv.* 6 (2016) 51520-51532.
17. T. Nakayama, N. Okumura, B. Uno, *J. Phys. Chem. B.* 124 (2020) 848–860.
18. W. Tian, C. Wang, D. Li, H. Hou, *Future Med. Chem.* 12 (7) (2020) 627-644.
19. A. S. Tikhomirov, A. A. Shtil, A. E. Shchekotikhin, *A.E. Rec. Pat. Anti-Can. Drug Dis.* 13 (2) (2018) 159-183.
20. B. H. Trachtenberg, D. C. Landy, V. I. Franco, J. M. Henkel, E. J. Pearson, T. L. Miller, S. E. Lipshultz, *Pediatr. Cardiol.* 32 (2011) 342-353.
21. Y. Shi, M. Moon, S. Dawood, B. McManus, P. P. Liu, *Herz.* 36 (2011) 296–305.
22. D. Outomuro, D. R. Grana, F. Azzato, J. Milei, *Int. J. Cardiol.* 117 (2007) 6–15.
23. V. J. Ferrans, *Cancer Treat. Rep.* 62 (1978) 955-961.
24. D. Barasch, O. Zipori, I. Ringel, I. Ginsburg, A. Samuni, J. Katzhendler, *Eur. J. Med. Chem.* 34 (1999) 597-615.
25. V. Y. Fain, B. E. Zaitsev, M. A. Ryabov, *Russ. J. Coord. Chem.* 36 (2010) 396–400.
26. A. Kumbhar, S. Padhye, D. Ross, *Biometals.* 9 (1995) 235–240.
27. A. Bartoszek, *Acta Biochim. Pol.* 49 (2002) 323-331.
28. B. Mandal, H. K. Mondal, S. Das, *Biochem. Biophys. Res. Comm.* 515 (2019) 505-509.
29. S. Das, A. Saha, P. C. Mandal, *J. Radioanal. Nucl. Chem.* 196 (1996) 57–63.
30. P. B. Undre, P. W. Khirade, V. S. Rajenimbalkar, S. N. Helambe, S. C. Mehrotra, *J. Korean. Chem. Soc.* 56 (2012) 416 - 423.
31. A. J. Bard, L. R. Faulkner, *Electrochemical Methods: Fundamentals and Applications*, 2nd ed.; John Wiley & Sons: New York, 1980.

CHAPTER 9

Summary and Conclusion

2-amino-3-hydroxy-9,10-anthraquinone representing the core of anthracycline anticancer agents has a good amount of similarity on a number of aspects. Its 1-sulphonate derivative, sodium 3-amino-2-hydroxy-9,10-anthraquinone-1-sulphonate (AQSH) was prepared since it would increase the former's solubility in aqueous solution. As part of the work, AQSH was investigated with the help of several model studies and tried on cancer cell lines to determine biochemical and biophysical parameters.

Complex formation of anthracyclines with metal ions has been reported to decrease toxicity and metal ions play a significant role during various biochemical action. Metalation of sodium 3-amino-2-hydroxy-9,10-anthraquinone-1-sulphonate (AQSH) with Cu^{II} and Ni^{II} was investigated in aqueous solution and in solid state using different techniques (Chapters 6&7). Our study revealed Cu^{II} forms a 1:2 metal-ligand complex in aqueous solution while Ni^{II} forms a metal-ligand complex having 1:1 stoichiometry. Formation constants of the Cu^{II} and Ni^{II} complexes of AQSH were 5.52×10^{12} (Chapter 6) and 4.69×10^4 (Chapter 7) respectively. Solid AQSH, its Cu^{II} complex $[\text{Cu}(\text{AQS})_2]$ and Ni^{II} complex $[\text{Ni}(\text{AQS})\text{Cl}_2 \cdot 2\text{H}_2\text{O}]$ were synthesized and characterized by different techniques (Chapters 4, 5, 6 and 7 respectively). Nature of metal–ligand bond in $\text{Cu}(\text{AQS})_2$ was characterized by EPR spectroscopy and found to be mostly covalent in nature. A ternary (1:3) Co^{III} complex of 1-amino-4-hydroxy-9,10-anthraquinone (QH) having the molecular formula CoQ_3 was prepared and characterized by different techniques (Chapter 8). Although various metal complexes of 1-amino-4-hydroxy-9,10-anthraquinone have been studied earlier, a Co^{III} complex was not prepared. In the absence of a crystal structure, computational measurements were performed to depict the electronic structure of AQSH (Chapter 5) and CoQ_3 (Chapter 8).

Electrochemical behavior being an important aspect in understanding the mechanism of action of anthracyclines and its analogues, cyclic voltammetry of AQSH and its metal complexes (*Chapters 6 and 7*) formed an important part of the study. These were done in acetonitrile and dimethyl formamide as solvents. The study showed electrochemical behavior of AQSH is significantly modified when bound to Cu^{II} and Ni^{II} . Findings were compared with data available on anthracyclines.

Electrochemical properties of CoQ_3 were studied in different solvents using cyclic voltammetry and the mechanism of reduction was realized (*Chapter- 8*). Our investigation concludes that in anhydrous non-aqueous media, CoQ_3 undergoes three successive one-electron reduction attributed to reduction of three free quinone centres in the complex bound to Co^{III} . In this case, the first reduction is reversible, while the other two are quasi-reversible at different scan rates. Comparing three reduction potentials of CoQ_3 in different solvents, it was concluded that with increasing polarity of the medium, reduction potentials move in a positive direction and that reductions become more feasible as polarity of solvent increases. It was found that there is a significant modification of electrochemical properties of QH bound to Co^{III} in CoQ_3 .

A molecule is considered to be biologically competent when it penetrates biological membranes through different physicochemical or biophysical interactions with such membranes. Hence, surfactant interactions of AQSH and its corresponding metal complexes were performed to investigate efficacy through model studies using an anionic surfactant micelle, sodium dodecyl sulphate (SDS). This was studied in aqueous phosphate buffer at pH 7.4 using UV-Vis spectroscopy (*Chapter 5*). The outcome of the study was compared with similar molecules. Binding constant for the interaction of AQSH with SDS was $(1.21 \pm 0.06) \times 10^5 \text{ M}^{-1}$ and corresponding Gibbs free energy was $-29.02 \text{ kJmol}^{-1}$. Partition coefficient and Gibbs free energy

for distribution of AQSH between bulk aqueous and micellar phases were $(1.59 \pm 0.04) \times 10^6 \text{M}^{-1}$ and -35.40kJmol^{-1} respectively. Hydrophobic interactions were identified to be important in AQSH–SDS micellar interactions. These have a fundamental role in the distribution of AQSH between surfactant micelle–water phase. The study also established the fact that sulphonation of AQ producing AQSH brings about improvement in binding with SDS since binding constant and partition coefficient of AQSH–SDS interaction was greater than AQ–SDS interaction. This could lead to improvement in biological interactions of AQSH over that of AQ.

Under similar condition Cu^{II} and Ni^{II} complexes of AQSH were allowed to interact with SDS micelles to see whether these are able to penetrate biological membranes. Binding constants and Gibbs free energies were calculated and found to be $(2.83 \pm 0.04) \times 10^4 \text{M}^{-1}$ and -25.41kJ/mol for $\text{Cu}(\text{AQS})_2$ and $(1.40 \pm 0.06) \times 10^5 \text{M}^{-1}$ and -29.38kJ/mol for $\text{Ni}(\text{AQS})\text{Cl}_2(\text{H}_2\text{O})_2$. The study showed both compounds $\text{Cu}(\text{AQS})_2$ and $\text{Ni}(\text{AQS})\text{Cl}_2(\text{H}_2\text{O})_2$ penetrate SDS micelles by hydrophobic mode of interaction. The value of partition coefficient (K_x) and corresponding Gibbs free energy for the distribution of $\text{Cu}(\text{AQS})_2$ from the aqueous phase to the micellar phase was estimated to be $(4.48 \pm 0.05) \times 10^5$ and -32.26kJ/mol respectively while for $\text{Ni}(\text{AQS})\text{Cl}_2(\text{H}_2\text{O})_2$ these were found to be $(6.32 \pm 0.05) \times 10^5$ and -33.11kJ/mol respectively. Comparison of such binding parameters of metal complexes with AQSH under similar experimental conditions indicate that values for $\text{Cu}(\text{AQS})_2$ were less than that for AQSH while they were higher in case of $\text{Ni}(\text{AQS})\text{Cl}_2(\text{H}_2\text{O})_2$. Thus comparing binding constants and partition coefficients of metal complexes of AQSH with AQSH it can be inferred that $\text{Cu}(\text{AQS})_2$ is less efficient in penetrating biological membranes than AQSH while $\text{Ni}(\text{AQS})\text{Cl}_2(\text{H}_2\text{O})_2$ would exhibit a greater efficiency. Thus the nickel complex should be more efficient in penetrating biological membrane.

Studies were performed with AQSH and its metal complexes on A549 human lung cancer cell and that of CoQ₃ on MCF-7 human breast cancer cell using a series of assays viz. cell viability assay, AO/EB staining, Hoechst 33528 staining and JC-1 staining (*Chapters 5,6,7,8*). IC₅₀ values were (83.5±0.05) μM, (125±0.05) μM and (68.5±0.05) μM for AQSH, Cu(AQS)₂, Ni(AQS)Cl₂(H₂O)₂ after incubation for 24 hours. Data shows Ni(AQS)Cl₂(H₂O)₂ is the most efficient among the compounds in inducing apoptosis in A549 human lung cancer cells. The result corroborates well with binding constant and partition coefficient values for interaction of compounds with SDS micelles.

Similarly, IC₅₀ value of CoQ₃ for 24 hour incubation corresponding to cytotoxicity of CoQ₃ on human breast cancer cells MCF-7 was evaluated as (95±0.05) μg/mL. It was found that such cancer cells underwent both early and late apoptosis due to CoQ₃.

Thus after considering all aspects of biophysical and biochemical properties displayed with regard to AQSH, its Cu^{II} and Ni^{II} complexes and the Co^{III} complex of 1-amino-4-hydroxy-9,10-anthraquinone, facts indicate a close similarity between behavior of amino-hydroxy-9,10-anthraquinones, their metal complexes with anthracyclines as anticancer agents keeping open the possibility that the compounds that are much cheaper may be utilized in cancer chemotherapy.

APPENDIX-1

Publications

1. **Somenath Banerjee**, Sanjay Roy, Arup Datta, Palash Mondal, Monali Mishra, Balaji Perumalsamy, Ramasamy Thirumurugan, Dhanasekaran Dharumadurai, Saurabh Das, Partha Sarathi Guin, Solubilization of sodium 3-amino-2-hydroxyanthraquinone-1-sulphonate in sodium dodecyl sulfate micelles explains its permeation in A549 human lung cancer cell, *Journal of Chinese Chemical Society* (2020) 1-13.
2. **Somenath Banerjee**, Sanjay Roy, Dhanasekaran Dharumadurai, Balaji Perumalsamy, Ramasamy Thirumurugan, Saurabh Das, Asoke Prasun Chattopadhyay, Partha Sarathi Guin, A Co(III) complex of 1-amino-4-hydroxy-9,10-anthraquinone exhibits apoptotic action against MCF-7 human breast cancer cells, *ACS Omega* 7 (2022) 1428-1436.

Probable publications from the work reported in the thesis


1. **Somenath Banerjee**, Saurabh Das, Partha Sarathi Guin, Formation and characterization of a Cu(II) complex of sodium 2-amino-3-hydroxy-9,10-anthraquinone-1-sulphonate and studies on its electrochemical behavior, interaction with SDS micelles and nucleation in A549 human lung cancer cells.
2. **Somenath Banerjee**, Saurabh Das, Partha Sarathi Guin, Studies on synthesis and characterization of a Ni(II) complex of sodium 2-amino-3-hydroxy-9,10-anthraquinone-1-sulphonate, its electrochemical behavior and interaction with SDS micelles and A549 human lung cancer cells.

APPENDIX-2

Reprint of publications included in the thesis

ARTICLE

Solubilization of sodium 3-amino-2-hydroxyanthraquinone-1-sulphonate in sodium dodecyl sulfate micelles explains its permeation in A549 human lung cancer cell

Somenath Banerjee^{1,2} | Sanjay Roy³ | Arup Datta¹ | Palash Mondal⁴ |
Monali Mishra⁵ | Balaji Perumalsamy⁵ | Ramasamy Thirumurugan⁵ |
Dhanasekaran Dharumadurai^{5,6} | Saurabh Das² | Partha Sarathi Guin¹ 

¹Department of Chemistry, Shibpur Dinobundhoo Institution (College), Howrah, West Bengal, India

²Department of Chemistry, Jadavpur University, Kolkata, West Bengal, India

³Department of Chemistry, Netaji Subhas Open University, Regional Centre Kalyani, Nadia, West Bengal, India

⁴Department of Chemistry, Vivekananda Mahavidyalaya, Burdwan, West Bengal, India

⁵National Centre for Alternatives to Animal Experiments (NCAAE), Bharathidasan University, Tiruchirappalli, Tamil Nadu, India

⁶Department of Microbiology, School of Life Sciences, Bharathidasan University, Tiruchirappalli, Tamil Nadu, India

Correspondence

Saurabh Das, Department of Chemistry, Jadavpur University, Raja S. C. Mullick Road, Kolkata 700032, West Bengal, India.
Email: sdas@chemistry.jdvu.ac.in

Partha Sarathi Guin, Department of Chemistry, Shibpur Dinobundhoo Institution (College), 412/1 G. T. Road (South), Howrah 711102, West Bengal, India.
Email: parthasg@gmail.com

Abstract

Sodium 3-amino-2-hydroxyanthraquinone-1-sulphonate (AQS) is an analogue of the anthracycline based chemotherapeutic drugs that was prepared as a part of the reported study. As the surfactant micelles mimics the biological membrane the present study comprises the interaction of AQS with an anionic surfactant, sodium dodecyl sulfate (SDS) in aqueous media at pH 7.4 which was monitored by using UV-Visible spectroscopy. The aim of the study is to see whether the present molecule penetrates a biological membrane. Different binding parameters like binding constant, partition coefficient, and corresponding Gibbs free energies of the interaction of AQS and its distribution between aqueous media and SDS micelles were measured. The study revealed that hydrophobic interactions play the most important role in binding of AQS to SDS micelles. To see whether AQS really permeates a biological membrane and induces apoptosis, it was allowed to interact with A549 human lung cancer cells. This study established the fact that AQS results apoptosis by means of nucleation into this cell.

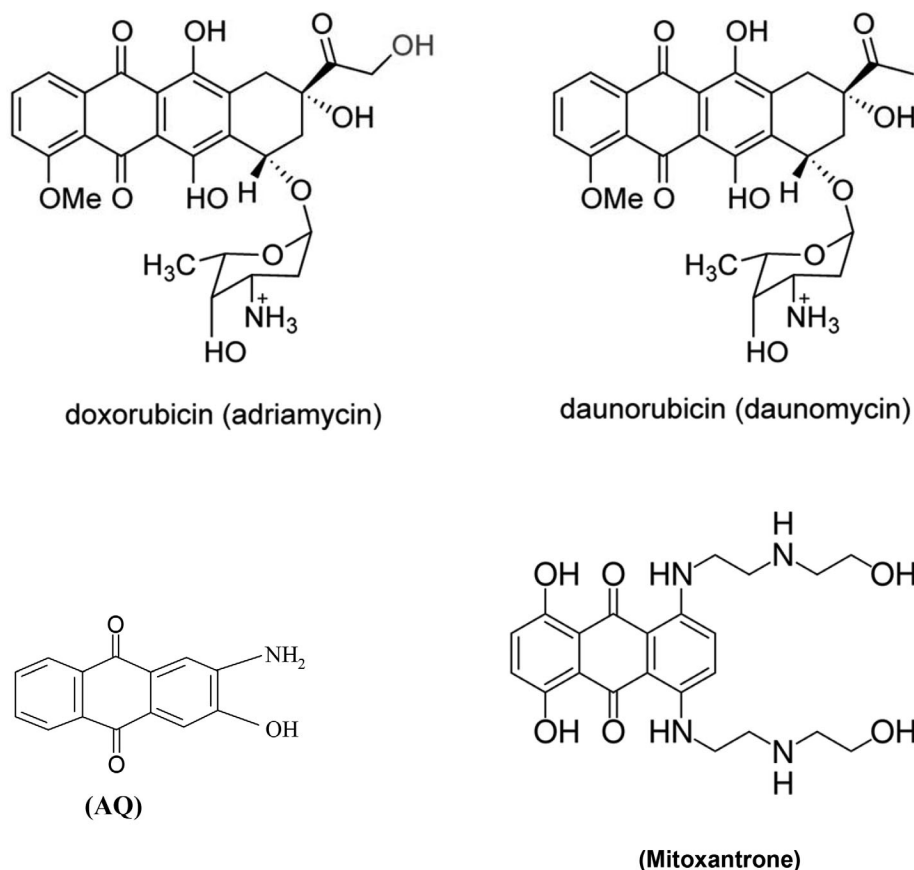
KEYWORDS

A549 human lung cancer cell, apoptosis, AQS, density functional theory, hydrophobic interactions, SDS micelles

Abbreviations: AQS, sodium 3-amino-2-hydroxyanthraquinone-1-sulphonate; AQ, 2-amino-3-hydroxyanthraquinone; SDS, sodium dodecyl sulfate.

1 | INTRODUCTION

Anthracycline based anticancer drugs with the hydroxy-9, 10-anthraquinone moiety at its core like in doxorubicin hydrochloride, daunorubicin, carminomycin, mitoxantrone (Scheme 1), are common chemotherapeutic agents used in the treatment of different forms of human cancers.^[1-4] The



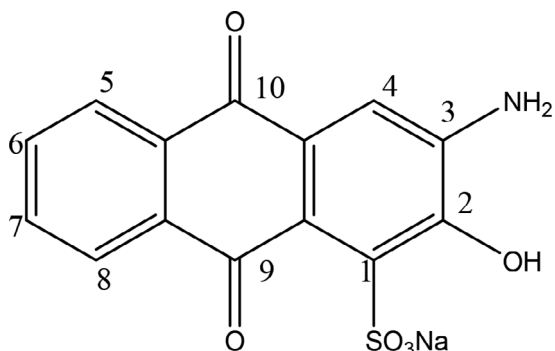
SCHEME 1 Chemical structures of different anthracyclines and their analogues

drugs are very expensive and their use is limited due to adverse drug reactions and cardiotoxicity.^[5-7] Efforts by different groups to find comparatively inexpensive alternatives that could simultaneously reduce cardiomyopathy have met with limited success.^[8-16] Previous studies established the fact that hydroxy-9,10-anthraquinones, present at the core of the anthracyclines control biological action. For this reason, different hydroxy-9, 10-anthraquinones, henceforth referred to as simpler analogues, were studied both from a chemical point of view as well as a biological point of view to check whether they could be promoted as inexpensive alternatives to some of the anthracycline drugs already in use.^[8-16]

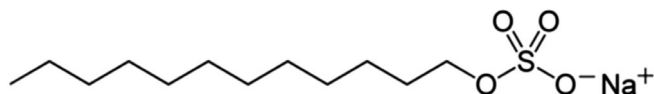
Any molecule is screened as biologically efficient only if it shows effectiveness in penetrating biological membranes^[17,18] through different physicochemical or biophysical interactions with the bio-membranes.^[19-22] Both hydrophobic and hydrophilic parts of a membrane were identified that helped in characterizing such interactions taking place with a foreign body, that is, the target molecule.^[17-22] Efficacy of molecules could be established by carrying out studies on molecule-surfactant interactions^[23,24] that serve as models for drug-membrane interactions.^[23,24] Various methods have been introduced by different workers in monitoring drug-surfactant interactions since this has enormous potential in pharmaceutical

research.^[25] Further, a micellar system has the potential to solubilize a hydrophobic drug^[26-28] which introduces it as a replica for bio-membrane plus drug carrier in various drug delivery and drug targeting systems.^[29-31]

Along with some of the above mentioned facts, molecular and electronic structures of drugs are also important that enable the formation of different types of hydrogen bonding and other interactions with bio-membranes. This helps to find a structure-activity relationship for a molecule that may provide information in identifying new drugs for different diseases. In this study, computational measurements were also performed to depict the electronic structure of sodium 3-amino-2-hydroxyanthraquinone-1-sulfonate (AQS) (Scheme 2), a simple analogue of anthracyclines. Objective of the present study was to see whether AQS has the potential to permeate biological membranes, identified with the help of model studies using an anionic surfactant micelle. AQS was chosen in this study since it is inexpensive, has a planar hydroxy-9, 10-anthraquinone that serves as a representative to the core moiety of many established anthracyclines, and playing a crucial role in biological functions for the molecule. Interaction of AQS with micelles of the anionic surfactant sodium dodecyl sulfate (SDS) (Scheme 3) was monitored by UV-Vis spectroscopy to estimate binding parameters for the AQS-surfactant interaction. In order to



SCHEME 2 Sodium 3-amino-2-hydroxyanthraquinone-1-sulphonate (AQS)



SCHEME 3 Chemical structure of SDS

justify whether the results are important for the chosen molecule to permeate biological membrane, AQS was treated with A549 human lung cancer cells and studied to see if interaction induces apoptosis.

2 | EXPERIMENTAL

2.1 | Materials and methods

2-Amino-3-hydroxyanthraquinone (>95%) was acquired from TCI, Japan and recrystallized from a methanol-ethanol mixture. Methyl alcohol (HPLC grade, E-Merck, India), absolute ethyl alcohol (AR grade), and dimethylsulfoxide (AR grade, Spectrochem India) were used in experiments. 3.76 mmol of 2-amino-3-hydroxyanthraquinone (AQ) was taken in a round bottomed flask containing 125 ml 4:1 ethanol-water mixture under nitrogen atmosphere at room temperature and stirred continuously until the compound dissolved completely. To it, solid anhydrous Na_2CO_3 (2.8 mmol) was added and stirred for 10 min. 1.88 mmol CuO was introduced to the reaction mixture under refluxing conditions (Temperature $\sim 85^\circ\text{C}$) and nitrogen atmosphere for approximately 30 hr. The deep pink colored solution that was obtained was filtered. CuO and unreacted material got collected as residue. The filtrate was evaporated in air till the volume of the experimental solution was about 5 ml. It was again filtered to separate the product that was subsequently dried in air. The product thus obtained was recrystallized from ethanol and dried in air. Elemental analysis, ESMS, and nuclear magnetic resonance (NMR) were done. Elemental analysis was carried out on a 2,400 Series II CHN Analyzer, Perkin Elmer, which found C, H,

and N contents to be 49.27, 2.30, and 4.13%, respectively (calculated values being C: 49.23%, H: 2.34%, N: 4.10%). Since quinone containing molecules are easily photo-bleached they were stored carefully; solutions prepared just before an experiment. A standard solution of 1 mM AQS in dimethylsulphoxide (DMSO) was made by weighing an exact amount of AQS and subsequently diluted to desired strengths. Ten percentage DMSO solution was used for studying AQS-surfactant interaction. SDS (AR grade) was procured from E-Merck, India. Compounds were used in the experiments without further purification. pH (~ 7.4) of all experimental solutions were maintained with the help of phosphate buffer. All aqueous solutions were made using triple distilled water. UV-Vis spectra were recorded on a spectrophotometer (OPTIZEN POP, MECASYS, South Korea).

2.2 | Computational methods

Density functional theory was employed to estimate the geometrical parameters and energy of AQS. Discrete Fourier transform level (Gradient corrected) used three-parameter fit exchange-correlation function of Becke (B3LYP), which comprised of the correlation function of Lee, Yang, and Parr.^[32,33] Minimization of energy and optimization of full unconstrained geometry of AQS were done using the Berny optimization algorithm under tight convergence. To compute the potential energy distribution (PED) Vibrational Energy Distribution Analysis (VEDA) 4.0 was introduced.^[34] Vibrational modes of AQS were assigned by using PED values and visual check using Gauss View 5.0.

2.3 | Determination of critical micelle concentration

Change of slope or discontinuity of property-concentration dependence gives the critical micelle concentration (CMC) value.

A series of mixtures of a certain concentration of AQS and different concentrations of SDS were prepared. Absorbance of these solutions were measured at 510 nm and plotted against concentrations of SDS. Change of the slope of absorbance-concentration dependence provides the CMC value.

2.4 | Cell culture

Human A549 lung cancer cells were acquired from NCCS, Pune, India. In a CO_2 incubator (Thermo

Scientific) with humidified atmosphere containing 5% CO₂ cells were cultured at 37°C in DMEM high glucose medium (Sigma-Aldrich) which was accompanied by 10% fetal bovine serum (HiMedia) and with penicillin/streptomycin as antibiotics (HiMedia) in 96 well culture plates. The studies were done using cells from passage 15 or less.

2.5 | Cell viability assay

Solid AQS was dissolved in DMSO to prepare a stock solution that was diluted separately with the media to obtain different concentrations of AQS. Two-hundred microliters solution was then mixed with 5×10^3 A549 cells per well. After an incubation for 24 hr, 20 μ l of MTT [3-(4,5-dimethylthiazol-2-yl)-2,5-diphenyl-2H-tetrazolium bromide] solution (5 mg/ml in PBS) was added to each well and the plate enfolded by Al foil. It was again incubated for 4 hr at 37°C.^[35] The formazan product which is purple in color was liquefied by adding 100 μ l DMSO in every well. With a 96-well plate reader (Bio-Rad, iMark) the optical density was supervised at 570 nm for the measurement and 630 nm for reference. Experimental data were collected for three replicates each and used to determine the respective mean. Percentage inhibition was evaluated using the formula:

By plotting % inhibition against concentration of AQS, a standard curve was obtained and the concentration of AQS that reduced the viability to 50% (IC₅₀) was determined.

$$\text{Percentage inhibition} = \frac{[\text{Average OD of untreated cells (control)} - \text{Average OD of treated cells (treated)}] \times 100}{\text{Average absorbance of untreated cells (control)}} \quad (1)$$

2.6 | Acridine orange and ethidium bromide staining

Following the technique illustrated by Spector and coworkers^[36] apoptosis was studied by using acridine orange and ethidium bromide (AO/EB) double staining technique with certain modifications. After incubating cells with an IC₅₀ concentration of AQS for 24 hr, they were harvested and washed by using cold PBS. By using PBS again, cell pellets were resuspended and diluted to 5×10^5 cells/ml. It was mixed with 25 μ l of PBS containing 3.8 μ M of AO and 2.5 μ M of EB on a clean slide and viewed through a microscope. Quickly it was studied under a fluorescent microscope (Carl Zeiss, Axioscope2plus) having a UV filter (450–490 nm). With staining the structure of

nucleus and membrane integrity, 300 cells for every sample were scored as necrotic, apoptotic or viable. The % of necrotic and apoptotic cells were calculated accordingly.

2.7 | Hoechst 33528 staining

A549 cells were cultured in separate 6-well plates and incubated with IC₅₀ concentration of AQS for 24 hr. Then treated and control cells were harvested and stained with Hoechst 33258 stain (1 mg/ml, aqueous) for 5 min at room temperature.^[37] A drop of cell suspension was introduced on a glass slide, and a coverslip was laid over it to reduce light diffraction. In fluorescent microscope, arbitrary 300 cells in triplicate were introduced and percentage cells undergoing pathological changes were measured. Data were collected for three replicates each to calculate mean and the SD.

2.8 | Mitochondrial membrane potential assessment by JC-1 staining

Mitochondrial membrane potential was measured by using the fluorescent probe JC-1. In this method, orange-red fluorescence is observed when gathered in healthy cell mitochondria but when extracted out in cytosol it fluoresces green owing to the loss of membrane potential leading to a negative internal potential.^[38] The A549 cells were grown in glass coverslips (22 \times 22 mm) placed in the wells

of 6-well plates and treated with IC₅₀ of AQS. DMSO was employed as solvent control. After 12 hr exposure cells were stained with the dye. Depolarization patterns of mitochondria were found in fluorescent microscope and pathological changes in the cells were found and recorded.

3 | RESULTS AND DISCUSSION

3.1 | Structure of AQS

In order to establish a structure–activity relationship for the current molecule, its molecular and electronic structures were characterized by different theoretical and experimental studies.

3.1.1 | Energy optimized structure from computational study

Structure of AQS was optimized with the help of B3LYP/6-31+g(d,p) (Figure 1). The optimum energy for the structure was found to be -1,604.94 a.u. Estimated bond lengths and bond angles for the molecule are mentioned in Tables 1 and 2 respectively having been evaluated by HF/6-31+g(d,p), B3LYP/6-31+g(d,p) and PBEPBE/6-31+g(d,p).

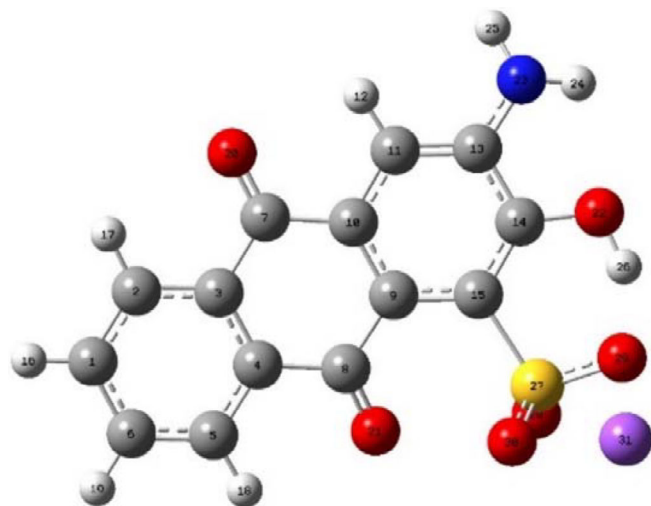


FIGURE 1 Optimized molecular structure of free AQS using B3LYP/6-31 + g(d,p) protocol

TABLE 1 Optimized bond lengths (Å) of AQS

Bond length	HF/6-31+g(d,p)	B3LYP/6-31+g(d,p)	PBEPBE/6-31+g(d,p)
C13–N23	1.359 (1.354)	1.377 (1.380)	1.390 (1.395)
N23–H24	1.001 (1.005)	1.009 (1.015)	1.088 (1.055)
N23–H25	1.002 (1.001)	1.008 (1.009)	1.016 (1.019)
C14–O22	1.335 (1.330)	1.345 (1.355)	1.361 (1.368)
O22–H26	0.998 (0.993)	1.001 (1.005)	1.017 (1.201)
S27–O28	1.438 (1.444)	1.459 (1.444)	1.470 (1.478)
S27–O29	1.534 (1.539)	1.554 (1.555)	1.564 (1.569)
S27–O30	1.486 (1.490)	1.504 (1.511)	1.517 (1.514)
C8–O21	1.204 (1.210)	1.224 (1.220)	1.244 (1.249)
C4–C8	1.501 (1.503)	1.497 (1.501)	1.509 (1.515)
C9–C8	1.477 (1.480)	1.487 (1.488)	1.501 (1.497)
C7–O20	1.216 (1.220)	1.228 (1.224)	1.239 (1.241)
C7–C3	1.468 (1.460)	1.484 (1.480)	1.499 (1.493)
C7–C10	1.502 (1.509)	1.491 (1.487)	1.505 (1.516)
C15–S27	1.816 (1.820)	1.830 (1.828)	1.842 (1.848)
C11–C13	1.368 (1.370)	1.385 (1.379)	1.401 (1.411)
C13–C14	1.430 (1.429)	1.428 (1.420)	1.440 (1.445)

Note: The data in the parenthesis are calculated in the solution.

For a molecule, the frontier molecular orbitals (FMO) are built by HOMO (highest occupied molecular orbital) and LUMO (lowest unoccupied molecular orbital). Examination of energy and population in these orbitals is important in determining donor-acceptor behavior of the molecule when it interacts with a biologically important molecule.^[39] Energy separation between HOMO and LUMO in FMO is related to chemical reactivity as the HOMO functions as electron donor and LUMO as electron acceptor. In the present study, energy separation between HOMO and LUMO in AQS was found to be 0.11904 a.u. The iso-density plot of FMO (Figure 2) clearly shows that HOMO and LUMO have different extents of delocalization.

3.1.2 | Nuclear magnetic resonance

¹H NMR (300 MHz, CDCl₃): δ(ppm): 10.64 (s,1H, Ar–OH), 7.93 (d,2H, Ar–C₅, C₈), 7.36 (d,2H, Ar–C₆,C₇), 6.05 (s,1H,Ar–C₄), 3.31 (s,2H,Ar–NH₂) (Figure S1).

In 2-amino-3-hydroxy-9,10-anthraquinone -OH and -NH₂ protons appeared at δ10.0 and δ3.30, respectively.^[40] However, due to incorporation of an electron withdrawing sulphonate at *ortho*-position to the C₂–OH, peak for the C₂–OH proton got shifted to higher δ value and appeared at δ10.64 as a singlet. However, no change was observed for –NH₂ protons and those appeared as singlet at δ3.31. Since AQS was prepared in the presence

Bond angle	HF/6-31+g(d,p)	B3LYP/6-31+g(d,p)	PBEPBE/6-31+g(d,p)
H25–N23–H24	117.78 (117.70)	115.59 (116.15)	114.45 (114.44)
C13–N23–H25	117.65 (117.48)	116.86 (117.39)	116.05 (1,116.41)
C13–N23–H24	116.70 (116.76)	115.37 (116.13)	114.40 (114.40)
C14–C13–N23	115.64 (115.44)	117.67 (116.05)	119.96 (119.76)
C11–C13–N23	121.87 (121.42)	123.15 (123.06)	124.10 (124.92)
C14–O22–H26	108.72 (108.45)	107.39 (107.14)	105.62 (105.67)
C13–C14–O22	111.18 (111.07)	113.61 (113.10)	115.37 (115.88)
C15–C14–O22	125.51 (125.59)	126.08 (126.85)	128.14 (128.76)
O28–S27–O29	114.54 (114.11)	111.75 (111.30)	111.50 (111.43)
O30–S27–O28	119.49 (119.67)	118.51 (117.99)	117.84 (117.65)
O30–S27–O29	106.68 (106.41)	104.11 (105.42)	103.45 (103.46)
C9–C15–S27	120.22 (120.56)	122.42 (122.04)	123.44 (123.89)
C14–C15–S27	115.23 (115.87)	117.56 (117.89)	118.09 (118.65)
C9–C8–O21	121.54 (121.12)	122.35 (122.98)	123.33 (123.67)
C4–C8–O21	117.88 (117.44)	119.39 (119.10)	121.51 (121.04)
C3–C7–O20	120.66 (120.98)	121.09 (121.66)	123.06 (123.66)
C10–C7–O20	119.87 (119.34)	121.03 (121.44)	122.22 (122.68)

TABLE 2 Optimized bond angles (in degree) of AQS

Note: The data in the parenthesis are calculated in solution.

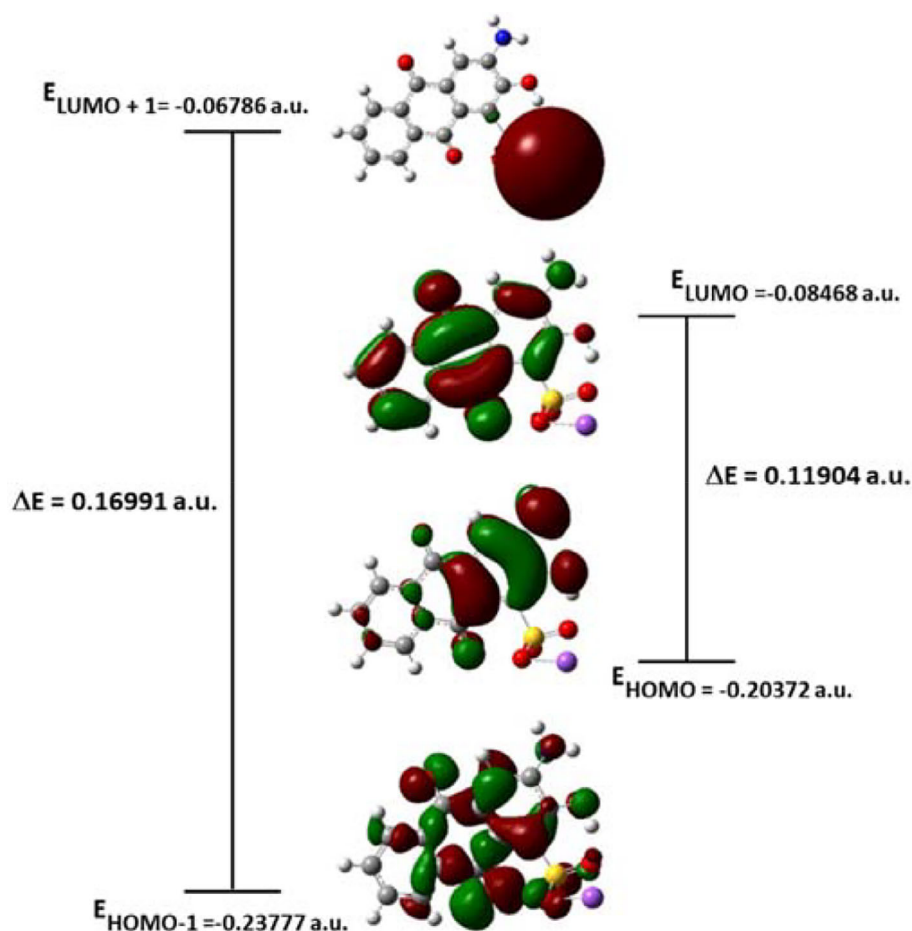


FIGURE 2 The iso-density plot of HOMO, LUMO, HOMO-1 and LUMO+1 for free AQS

of Na_2CO_3 suggesting that the medium was basic, the sulfonation reaction was more favored at *ortho* to $\text{C}_2\text{-OH}$ but not *ortho* to NH_2 (4-position). In AQS aromatic protons ($\text{C}_5\text{-H}$ and $\text{C}_8\text{-H}$) close to the electron withdrawing carbonyl group appeared at $\delta 7.93$ as doublet because of *ortho* coupling with adjacent protons. The other aromatic protons in the sulphonate product like $\text{C}_6\text{-H}$, $\text{C}_7\text{-H}$, and $\text{C}_4\text{-H}$ appeared at $\delta 7.36$ as doublet and at $\delta 6.05$ as singlet, respectively. Lower δ value of $\text{C}_4\text{-H}$ protons arise due to electron releasing effect of the adjacent -NH_2 group.

3.1.3 | Mass spectroscopy

In the ESIMS of AQS (Figure S2) small molecular ion peak ($\text{NaC}_{14}\text{H}_8\text{NSO}_6$) was detected at $m/z = 341.27$ but the protonated molecular ion peak at $m/z = 342.27$ was not observed. However, an intense peak at $m/z = 338.30$ indicates a species obtained by deprotonation of three hydrogen atoms from AQS. Peak at $m/z = 254.1088$ is probably the protonated fragment formed by the loss of sodium, -NH_2 , -OH , and two oxygen atoms from AQS. The sharp signal at $m/z = 240.03$ corresponds to the protonated fragment generated due to the loss of $\text{-SO}_3\text{Na}$ from AQS. A less intense band at $m/z = 124.06$ is due to loss of $\text{-SO}_3\text{Na}$, -OH , -NH_2 , and two quinone oxygen atoms, four carbon atoms, and one hydrogen atom from AQS.

3.1.4 | Theoretical and experimental vibrational spectra of AQS

Using VEDA and PED analysis, the theoretical IR spectrum of AQS could be created. According to VEDA, some normal modes are extended over the whole molecule. PED used at certain levels accounted for the contribution to movement of groups of atoms in a normal mode quantitatively. AQS consists of 30 atoms and exhibits 84 IR active fundamental vibrations of which 29 are stretching, 28 are bending and 27 are torsional. Computed vibrational frequencies were overestimated and scaled by 0.9613 for B3LYP/6-31+G (d,p) level of calculation.^[34,41] IR frequency and intensity, PED, and modes of vibration for AQS are shown in Table 3. Comparing theoretical and experimental bands (Table 3) and the spectra (Figure 3a,b) it could be said that both spectra do not match very well in the region of $3,000\text{-}1,600\text{ cm}^{-1}$. However, they matched better above $3,000\text{ cm}^{-1}$ and below $1,600\text{ cm}^{-1}$. Deviation of results between theoretical and experimental spectra may be due to the effect of crystal field^[42] or due to the fact that experimental and

theoretical results were studied in different states such as solid state in case of experiment and gaseous state in case of theoretical study.

3.1.5 | Determination of pK_a of AQS

During the interaction of the current molecule with surfactant micelles or biological cells the ionization of phenolic -OH group may play an important role.^[40] This is why it is imperative to measure its pK_a of AQS. This was done with the help of a spectrophotometric titration of AQS with NaOH. Initially, $50\text{ }\mu\text{M}$ aqueous AQS was acidified with 0.01 M HCl to a pH of 2.23. It was then titrated with a 0.01 M NaOH keeping concentration of AQS constant. UV-Vis spectra of the experimental mixture were recorded (Figure 4) at different pH and the plot of absorbance at 560 nm against pH was fitted to Equation (1) (Figure 5). A change in absorbance at 560 nm indicates the dissociation of phenolic -OH in the pH range $7.30\text{-}9.10$. pK_a was obtained as 8.10 ± 0.05 [reduced Chi squared = 0.00444].

$$A_{560} = \frac{A_1}{1 + 10^{(\text{pH} - \text{pK})}} + \frac{A_2}{1 + 10^{(\text{pK} - \text{pH})}} \quad (1)$$

A_{560} is the overall absorbance of the solution at 560 nm at different pH; A_1 and A_2 are the absorbance, respectively, of AQS and the phenoxide ion. The pK_a for phenolic-OH of our molecule (AQS) was higher than that of 2-amino-3-hydroxy anthraquinone (7.90 ± 0.06),^[40] suggesting that the phenolic-OH proton in AQS is strongly held (probably through hydrogen bonding) by the neighboring sulphonate.

3.2 | Interaction of AQS with SDS

A study on the interaction of AQS with SDS was carried out using UV-Vis spectroscopy at pH 7.4 maintained with 100 mM phosphate buffer in pre-micellar and micellar concentration range. A series of mixtures containing a specific concentration of AQS and variable concentrations of SDS were prepared and absorption at 510 nm was monitored to evaluate different parameters for the interaction of AQS with the SDS micelle. The compound AQS has only a visible peak at 510 nm which is why we have monitored this peak in the present study. Absorbance of the solutions were measured with the help of a spectrophotometer following incubation of SDS with AQS for 1–2 min. Change in absorption of AQS upon adding different concentrations of SDS is shown in Figure 6a. By monitoring changes in the UV-Vis spectra

TABLE 3 Comparison of theoretical and experimental IR stretching frequency of free AQS

ν_{cal} (cm^{-1})	ν_{scaled} (cm^{-1})	Intensity	PED (%)	Interpretation	ν_{expt} (cm^{-1})
3,714	3,570	31	S ₂	ν_{sym} (N ₂₃ –H ₂₄), ν_{asym} (N ₂₃ –H ₂₅)	3,689
3,592	3,452	78	S ₃ (100)	ν_{sym} (N ₂₃ –H ₂₄), ν_{asym} (N ₂₃ –H ₂₅)	3,353
3,119	2,998	820	S ₁ (98)	ν_{sym} (O ₂₂ –H ₂₆)	-
1,752	1,684	186	S ₉ (69) S ₁₀ (11)	ν_{sym} (O ₂₁ –C ₈), ν_{sym} (O ₂₀ –C ₇)	-
1,660	1,595	42	S ₂₅ (–10) S ₃₇ (41)	ν_{sym} (C ₃ –C ₇), ν_{sym} (C ₅ –C ₆), ν_{sym} (C ₇ –C ₁₀), ν_{sym} (C ₉ –C ₁₅), ν_{sym} (C ₁₀ –C ₁₁), β (H ₂₅ –N ₂₃ –H ₂₄)	1,655
1,647	1,583	68	S ₁₅ (54) S ₃₈ (16)	ν_{sym} (C ₂ –C ₁), ν_{sym} (C ₃ –C ₂), ν_{sym} (C ₄ –C ₅), ν_{sym} (C ₁₃ –C ₁₁), β (H ₁₇ –C ₂ –C ₁), β (H ₁₈ –C ₅ –C ₆)	1,610
1,636	1,572	26	S ₁₁ (50) S ₃₁ (15)	ν_{sym} (C ₁ –C ₆), ν_{sym} (C ₂ –C ₃), ν_{sym} (C ₉ –C ₁₀), β (C ₂ –C ₁ –C ₆), β (C ₃ –C ₂ –C ₁), β (C ₄ –C ₅ –C ₆), β (C ₁₃ –C ₁₁ –C ₁₀),	1,526
1,523	1,464	161	S ₁₄ (–13) S ₃₅ (46)	ν_{sym} (C ₁ –C ₆), ν_{sym} (C ₆ –C ₅), ν_{sym} (C ₉ –C ₁₀), ν_{sym} (C ₁₁ –C ₁₀), β (H ₂₆ –O ₂₂ –C ₁₄)	1,347
1,437	1,381	126	S ₁₉ (–12) S ₂₀ (16) S ₂₄ (–13) S ₂₅ (14)	ν_{sym} (C ₉ –C ₁₅), ν_{sym} (C ₁₄ –C ₁₅), ν_{sym} (N ₂₃ –C ₁₃), ν_{sym} (O ₂₂ –C ₁₄), ν_{sym} (C ₃ –C ₇), ν_{sym} (C ₉ –C ₁₅), ν_{sym} (C ₈ –C ₉),	1,267
1,282	1,232	83	S ₂₆ (66) S ₂₇ (–10)	ν_{sym} (S ₂₇ –O ₂₈), ν_{sym} (S ₂₇ –O ₃₀),	1,195
994	955	38	S ₆₄ (86)	τ (H ₁₆ –C ₁ –C ₂ –C ₃), τ (H ₁₉ –C ₆ –C ₁ –C ₂), τ (H ₁₆ –C ₅ –C ₆ –C ₁), τ (H ₁₇ –C ₂ –C ₁ –C ₆)	967
897	862	38	S ₅₅ (–10) S ₆₀ (–12)	β (C ₈ –C ₉ –C ₁₅), β (C ₁₀ –C ₇ –O ₂₀), τ (H ₂₆ –O ₂₂ –C ₁₄ –C ₁₃),	891
837	804	63	S ₂₈ (–18) S ₆₀ (57)	ν_{sym} (S ₂₇ –O ₂₉), τ (H ₂₆ –O ₂₂ –C ₁₄ –C ₁₃)	793
809	777	7	S ₆₃ (–54) S ₈₀ (13)	τ (H ₁₆ –C ₁ –C ₂ –C ₃), τ (H ₁₉ –C ₆ –C ₁ –C ₂), τ (H ₁₇ –C ₂ –C ₁ –C ₆), τ (N ₂₃ –C ₁₁ –C ₁₄ –C ₁₃), τ (O ₂₀ –C ₃ –C ₁₀ –C ₇), τ (O ₂₁ –C ₄ –C ₉ –C ₈), τ (O ₂₂ –C ₁₃ –C ₁₅ –C ₁₄)	712
623	598	65	S ₅₈ (–18)	β (O ₂₉ –S ₂₇ –O ₃₀)	612

(Figure 6a) of AQS, the CMC of SDS in the presence of AQS was evaluated and found to be 234 μM . This value of CMC was used in the entire calculation in evaluating binding parameters. CMC values of SDS in pure water and in 50 mM phosphate buffer were evaluated in an earlier study and found to be 8,080 and 1990 μM , respectively.^[43] Lowering in CMC value of SDS in comparison to that obtained earlier may be explained by means of the influence of various ions and molecules present in the mixture.^[44] The change in absorbance of AQS at 510 nm with various surfactant concentrations is depicted in Figure 6b which shows that absorbance decreases with increasing SDS concentration until it reaches a saturation level for a particular concentration of SDS. This can be elucidated by assuming incorporation of AQS into the SDS micelles. Usually in studying small molecule–surfactant interaction a nonlinear analysis has been introduced by several workers^[41–48] considering 1:1 interaction

between the molecule and surfactant to analyze the binding isotherm (Figure 6b). Thus assuming 1:1 interaction between AQS and SDS and considering Equation (2), the binding isotherm was examined (Figure 6b). The binding constant was evaluated and found to be $(1.21 \pm 0.06) \times 10^5 \text{ M}^{-1}$ (Table 4)^[41,42] (reduced Chi squared = 4.37×10^{-6}).

$$A = \frac{A_0 + A_\infty K[L]}{1 + K[L]} \quad (2)$$

L represents the surfactant used (here SDS); A and A_0 are absorbance of AQS at 510 nm in the absence and presence of SDS whereas A_∞ corresponds to the absorbance of AQS bound to SDS. Gibbs free energy for interaction of AQS to SDS micelles was calculated with the help of Equation (3) and found as -29.02 kJ/mol (Table 4).^[45,46]

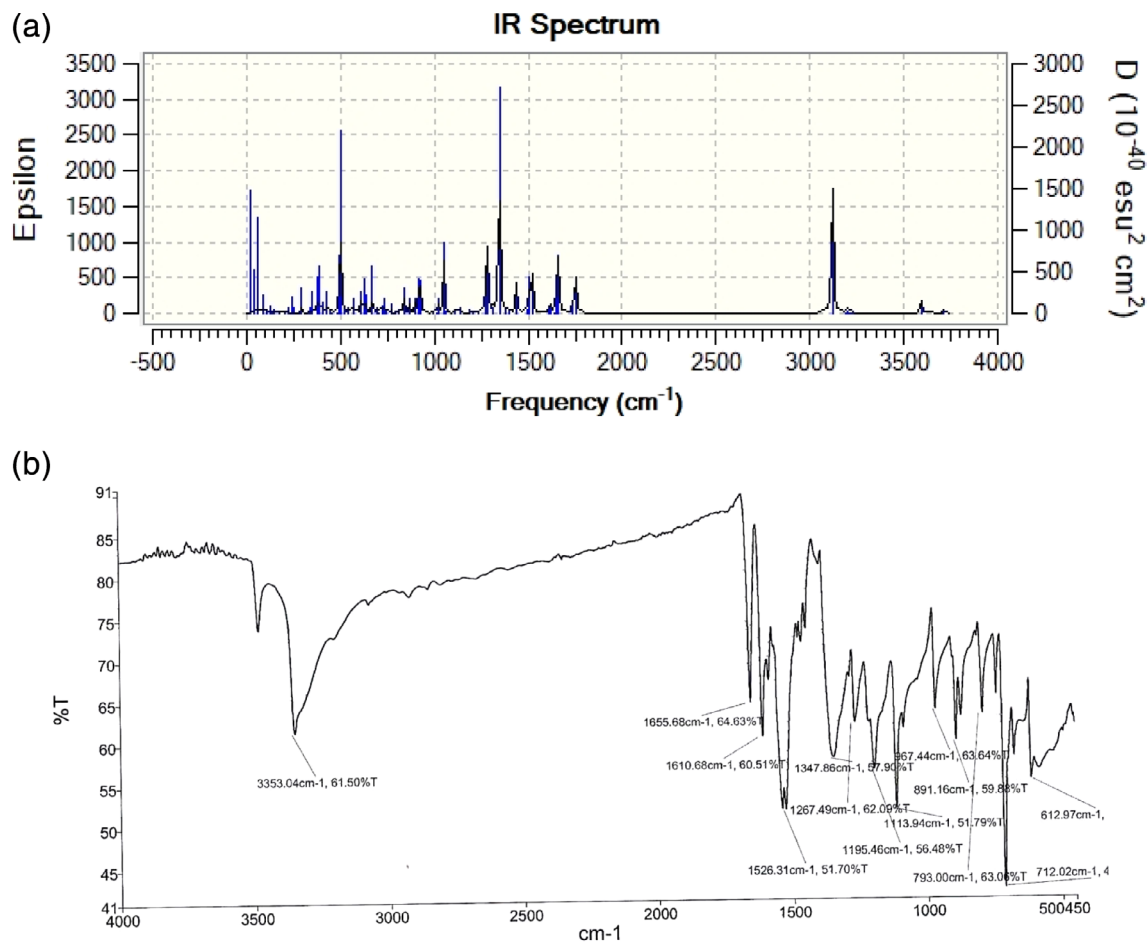


FIGURE 3 (a) Theoretical IR spectrum of AQS using B3LYP/6-31 + g(d,p). (b) Experimental IR spectrum of AQS

$$\Delta G^0 = -RT \ln K \quad (3)$$

where R is the molar gas constant while $T = 298.15$ K.

In a recent study,^[40] we observed that the binding constant for a 1:1 interaction of neutral 2-amino-3-hydroxyanthraquinone with anionic SDS was 652.81 where the hydrophobic mode of interaction was established to be more important than electrostatic mode. AQS is an anionic molecule. It has a binding constant value of $(1.21 \pm 0.06) \times 10^5 \text{ M}^{-1}$ which is greater than that of 2-amino-3-hydroxyanthraquinone with SDS micelles under similar experimental conditions.^[40] This indicates that hydrophobic interactions are far stronger in the present study in comparison to the earlier.^[40] Binding constant for a 1:1 interaction of mitoxantrone, a cationic anthracycline drug with anionic surfactant SDS, as shown in a previous study^[45] was $(1.14 \pm 0.05) \times 10^3 \text{ M}^{-1}$. In that study, it was shown that a cationic drug like mitoxantrone having one unit residual positive charge interacts with anionic SDS micelles through electrostatic and hydrophobic modes.^[45] It is interesting to note here that binding constant for mitoxantrone-SDS micelles is less than that of AQS-SDS

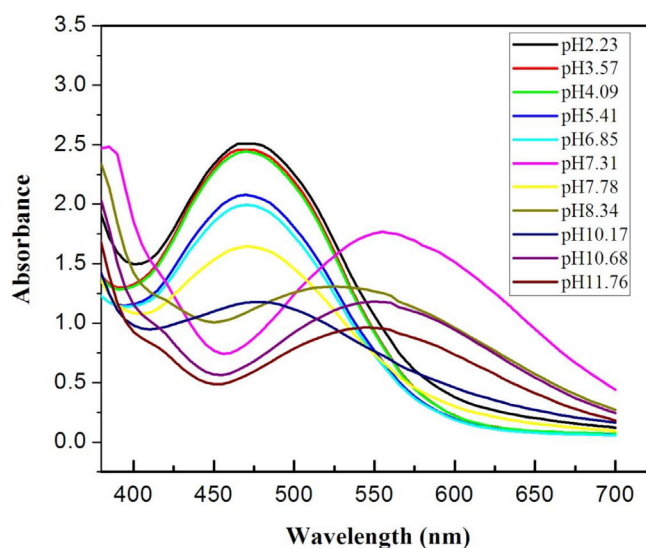


FIGURE 4 UV-Vis spectra of AQS in aqueous media at different pH. [AQS] = 50 μM , [NaCl] = 0.01 M, $T = 298.15$ K

micelles which means that hydrophobic interactions are more important. Using the pK_a value of phenolic-OH of AQS as 8.10, percentage of phenoxide ion (AQS⁻) in the

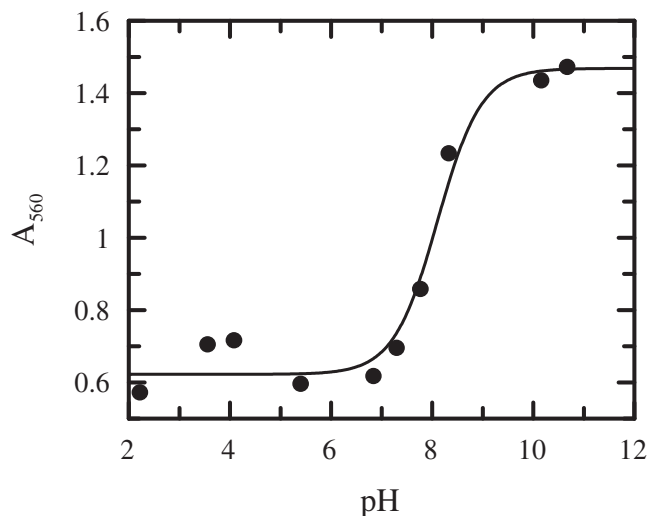


FIGURE 5 Variation of absorbance of AQS at 560 nm with pH. [AQS] = 50 μ M, [NaCl] = 0.01 M, $T = 298.15$ K

TABLE 4 Binding constant (K), partition coefficient (K_x), Gibbs free energy of binding (ΔG^0) and the standard free energy change (ΔG_x^0) for the transfer of AQS from aqueous to micellar phase for the interaction of AQS with surfactants

Binding parameters	SDS
K (M^{-1})	$(1.21 \pm 0.06) \times 10^5$
ΔG^0 (kJ/mol) ¹	-29.02
K_x	$(1.59 \pm 0.04) \times 10^6$
ΔG_x^0 (kJ/mol)	-35.40

experimental solution at pH 7.40 was found to be 19.95%. During interaction of AQS with SDS micelles there is competition between AQS and AQS to penetrate the micelle. Due to greater negative charge and lower concentration, AQS has lower probability of interaction compared to AQS with anionic SDS.

The measurement of partition coefficient (K_x) is another important aspect for characterizing drug-membrane interactions since it depicts the affinity of a molecule to fuse into a micellar phase from an aqueous solution. K_x helps in illuminating the mechanism of solubilization of a drug molecule, helping us to understand biological phenomenon like interaction of drugs with biological membranes. By considering the pseudo-phase model^[45,47,48] K_x was evaluated using Equation (4):

$$\frac{1}{\Delta A} = \frac{1}{\Delta A_\infty} + \frac{n_w}{K_x A_\infty ([L] + C_T - CMC)} \quad (4)$$

where, $\Delta A = A - A_0$, $\Delta A_\infty = A_b - A_0$, $[L] = [SDS]$ and $n_w = 55.51$ M is the molarity of water. The value of K_x

was calculated from the slope of the plot of $1/\Delta A$ versus $1/([SDS] + C_T - CMC)$ (Figure 6c) and found as $(1.59 \pm 0.04) \times 10^6$ [Reduced Chi squared = 0.14]. It is necessary to note that in a large region of the surfactant concentration the above mentioned linear relation clutches fine, below which the curve tends to bend upwards with decreasing surfactant concentration. A departure from linearity was owing to the estimation made in the evaluation of Equation (4).^[48]

The standard free energy change for the transfer of AQS from the bulk aqueous phase to the micellar phase was obtained as -35.40 kJ/mol by putting the value of K_x in Equation (5)^[46] (mentioned in Table 4).

$$\Delta G_x^0 = -RT \ln K_x \quad (5)$$

The partition coefficient corresponding to distribution of the positively charged mitoxantrone in SDS micelle has been studied by Enache et al.^[45] in different concentrations of mitoxantrone and the K_x values were found to be smaller than AQS (a negatively charged molecule) in similar micelles as in the present study. In that study^[45] mitoxantrone was established to be interacting with anionic surfactant both through electrostatic and hydrophobic modes. Under similar experimental conditions, K_x of 2-amino-3-hydroxyanthraquinone was 5.22×10^4 ^[40] which is smaller than that in the present work. Since in that study^[40] a hydrophobic interaction was suggested, comparing those results with the current report, it may be said that hydrophobic interaction is more important in the distribution of AQS in anionic SDS micelles.

3.3 | Biological study

In order to see whether information obtained from the analysis of the electronic and molecular structure of AQS and its efficiency in penetrating a micellar phase can really be useful in infusing a biological membrane and induce apoptosis, it was allowed to interact with A549 human lung cancer cells which was studied by different assays.

3.3.1 | Cell viability assay

Cytotoxic activity of AQS was investigated against A549 human lung cancer cells using the MTT assay.^[35] Cytotoxic activity was estimated according to dose values of the exposure of the experimental molecule required to reduce survival to 50% (IC_{50}) in comparison to untreated cells. The IC_{50} value was found to be 83.5 ± 0.05 μ M after incubation for 24 hr. Results of the MTT assay hint at the fact that AQS exhibits dose dependent toxic effect on

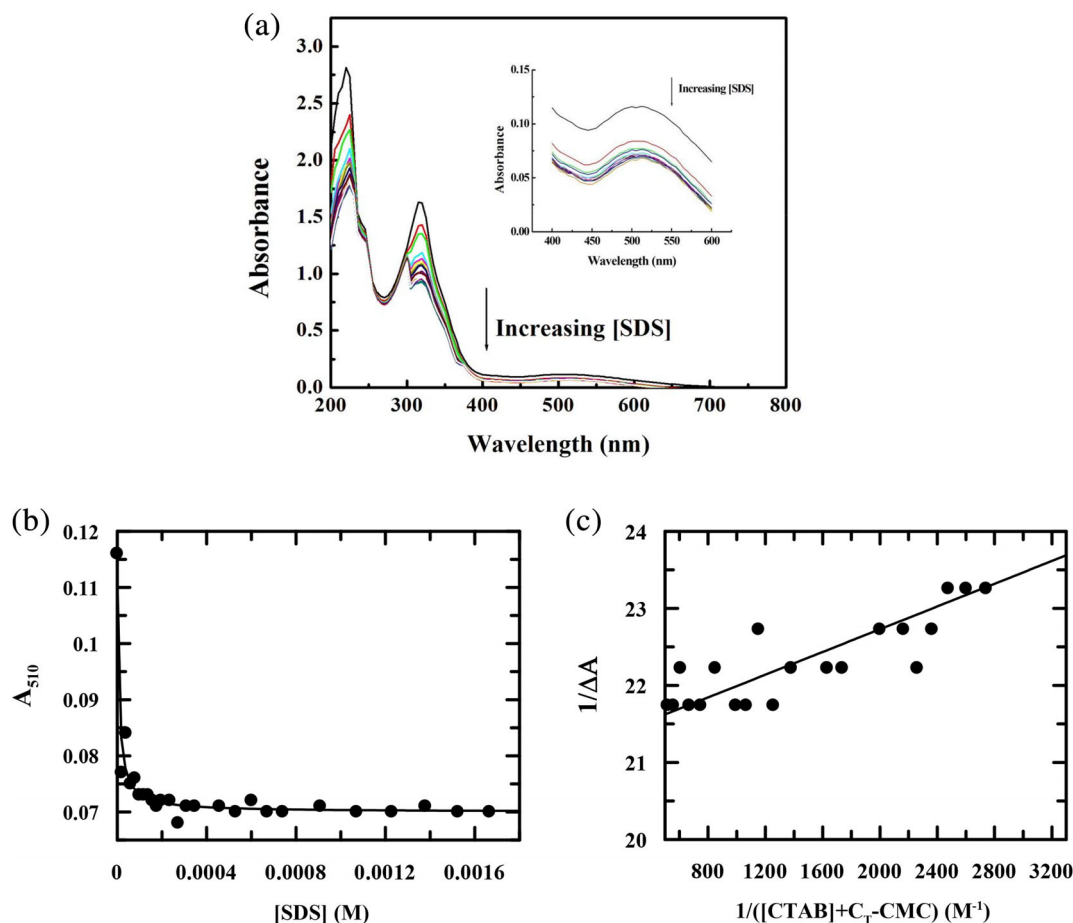


FIGURE 6 (a) Absorption spectra of AQS (50 μ M) in the absence and presence of increasing concentrations of SDS. [Phosphate buffer] = 100 mM, pH 7.4, $T = 298.15$ K. Inset: Change of the spectra in the wavelength range 400–600 nm with increasing SDS concentration. (b) A non-linear fitting of the absorbance of AQS at 320 nm using Equation (2) considering 1:1 interaction between AQS and SDS. (c) Plot of $1/|\Delta A|$ versus $1/([SDS] + C_T - CMC)$ (Equation 4) for AQS (50 μ M) in SDS micelles at pH 7.4

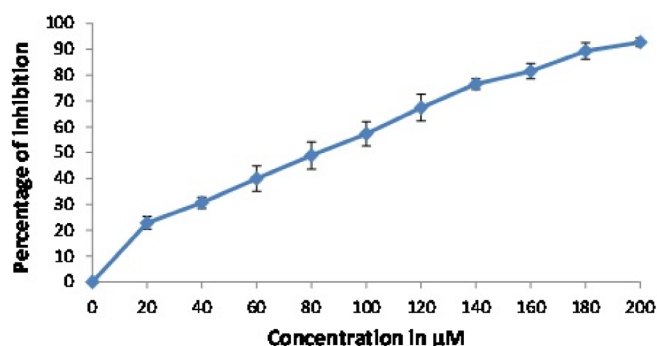


FIGURE 7 Cytotoxic effect of AQS on A549 cells after exposure for 24 hr. Error bar denotes SD of three replicates

A549 cells (Figure 7). The result of MTT assay detects that the AQS induced cell death is linear. Since the MTT assay tests cell viability according to a linear relationship between cell activity and absorption, increased concentrations are expected to produce a linear range of cell

deaths. Furthermore, the effect of drug on cells is mainly dependent on (a) effective concentrations of drug, (b) incubation time, and (c) the number of cell. Further research is, therefore, necessary to elucidate the mechanism behind this phenomenon.

3.3.2 | AO/EB staining

Morphological changes in apoptosis induced by AQS were determined by AO/EB staining. Figure 8 shows AO/EB double-stained A549 human lung cancer cells which was treated with AQS and incubated for 24 hr. The control or viable cells reveal green fluorescence and normal cells feature of uniform chromatin with an intact cell membrane, whereas late and early apoptotic cells showed yellowish green and orange-red color, respectively. The AO/EB results clearly indicate that AQS leads most of the cell death by apoptosis mode and very fewer in necrosis after incubating 24 hr (Figure 8).

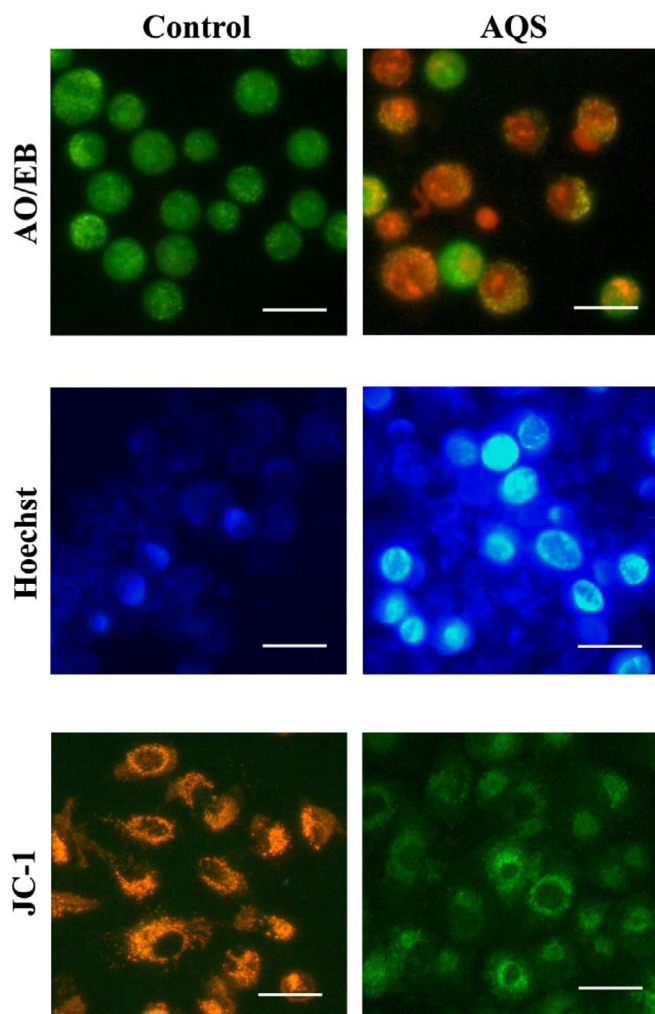


FIGURE 8 AO/EB staining, Hoechst, and JC-1 Staining of Control and AQS treated cells. Scale bar denotes 50 μm

3.3.3 | Hoechst 33528 staining

Hoechst staining was introduced to estimate the apoptosis at a basic level. The results of Hoechst expressed the changes in morphology of the cells, with special reference to cytoplasm and nucleus. The observations expressed that early apoptotic features like chromatin condensation and fragmentation were mostly seen in AQS treated cells and small numbers of necrotic cells were also observed (Figures 8 and 9).

3.3.4 | Assessment of mitochondrial membrane potential (JC1 staining)

AQS induced mitochondrial membrane potential depolarization was assessed with the help of the JC-1 assay. The fluorescent cationic dye JC-1 accumulation in the mitochondria of control or healthy cells emits red

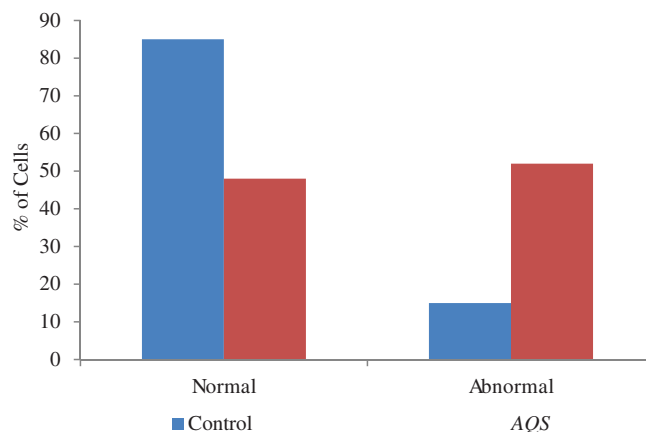


FIGURE 9 Hoechst 33258 staining study of control and AQS treated cells. Graph is shown manual count of normal and abnormal cells in percentage

fluorescence. Conversely, cells undergoing apoptosis, fluoresce green due to mitochondrial membrane depolarization. The results of the JC-1 staining of lung cancer cells treated with AQS at 12 hr incubation confirms the loss of mitochondrial membrane potential while control cells were seen to have healthy mitochondria (Figure 8).

4 | CONCLUSIONS

Interaction of AQS with anionic surfactant SDS was studied in aqueous phosphate buffer at pH 7.4 using UV-Vis spectroscopy. The outcome of the study was compared with similar molecules. Binding constant for the interaction of AQS with SDS was $(1.21 \pm 0.06) \times 10^5 \text{ M}^{-1}$ and the corresponding Gibbs free energy was -29.02 kJ/mol . Partition coefficient and Gibbs free energy for the distribution of AQS between the bulk aqueous and micellar phases were $(1.59 \pm 0.04) \times 10^6 \text{ M}^{-1}$ and -35.40 kJ/mol , respectively. Hydrophobic interactions were identified to be important in AQS-SDS micellar interactions. This interaction also has a fundamental role in the distribution of AQS between surfactant micelle-water phase. The study clearly established that sulphonation of 2-amino-3-hydroxyanthraquinone (AQ) producing AQS brings about an improvement in binding of the molecule with SDS because the binding constant and partition coefficient of AQS-SDS interaction is greater than those of 2-amino-3-hydroxyanthraquinone-SDS interaction. This may lead to an improvement in biological properties of AQS over that of 2-amino-3-hydroxyanthraquinone. In order to see whether these results are really important for AQS to infuse a biological membrane and induce apoptosis, it was allowed to interact with A549 human lung cancer cells that was studied by different assays. Such studies showed that AQS

induced apoptosis in A549 human lung cancer cell. The IC₅₀ value was found to be 83.5 ± 0.05 μM for a 24 hr incubation.

ORCID

Partha Sarathi Guin  <https://orcid.org/0000-0001-9258-9227>

REFERENCES

- [1] D. A. Gewirtz, *Biochem. Pharmacol.* **1999**, *57*, 727.
- [2] F. Arcamone, S. Penco, in *Anthracycline and Anthracenedione-Based Anticancer Agents* (Ed: J. W. Lown), Elsevier, Amsterdam **1988**.
- [3] N. Ashley, J. Poulton, *Biochem. Biophys. Res. Commun.* **2009**, *378*, 450.
- [4] G. Minotti, P. Menna, E. Salvatorelli, G. Cario, L. Giani, *Pharmacol. Rev.* **2004**, *56*, 185.
- [5] A. D. Hanna, A. Lam, S. Tham, A. F. Dulhunty, N. A. Beard, *Mol. Pharmacol.* **2014**, *86*, 438.
- [6] P. A. Henriksen, *Heart* **2018**, *104*, 971.
- [7] L. Roca-Alonso, L. Pellegrino, L. Castellano, J. Stebbing, *Cardiology* **2012**, *122*, 253.
- [8] S. Rossi, C. Tabolacci, A. Lentini, B. Provenzano, F. Carlomosti, S. Frezzotti, S. Beninati, *Anticancer Res.* **2010**, *30*, 445.
- [9] P. Das, C. K. Jain, S. K. Dey, R. Saha, A. D. Chowdhury, S. Roychoudhury, S. Kumar, H. K. Majumder, S. Das, *RSC Adv.* **2014**, *4*, 59344.
- [10] P. Das, D. Bhattacharya, P. Karmakar, S. Das, *RSC Adv.* **2015**, *5*, 73099.
- [11] P. Mondal, S. Roy, G. Loganathan, B. Mandal, D. Dharumadurai, M. A. Akbarsha, S. ParthaSarathiSengupta, P. S. G. Chattopadhyay, *Biochem. Biophys. Rep.* **2015**, *4*, 312.
- [12] P. Das, P. S. Guin, P. C. Mandal, M. Paul, S. Paul, S. Das, *J. Phys. Org. Chem.* **2011**, *24*, 774.
- [13] S. Roy, P. S. Guin, *J. Electrochem. Soc.* **2015**, *162*, H124.
- [14] S. Roy, P. Mondal, P. S. Sengupta, D. Dhak, R. C. Santra, S. Das, P. S. Guin, *Dalton Trans.* **2015**, *44*, 5428.
- [15] P. S. Guin, S. Das, P. C. Mandal, *J. Inorg. Biochem.* **2009**, *103*, 1702.
- [16] P. S. Guin, P. C. Mandal, S. Das, *ChemPlusChem* **2012**, *77*, 361.
- [17] R. Pignatello, T. Musumeci, L. Basile, C. Carbone, G. Puglisi, *J. Pharm. Bioallied Sci.* **2011**, *3*, 4.
- [18] G. P. Van Balen, C. M. Martinet, G. Caron, G. Bouchard, M. Reist, P. A. Carrupt, R. Fruttero, A. Gasco, B. Testa, *Med. Res. Rev.* **2004**, *24*, 299.
- [19] A. M. Seddon, D. Casey, R. V. Law, A. Gee, R. H. Templer, O. Ces, *Chem. Soc. Rev.* **2009**, *38*, 2509.
- [20] J. K. Seydel, E. A. Coats, H. P. Cordes, M. Wiese, *Archiv. der Pharmazie* **1994**, *327*, 601.
- [21] S. Schreiera, S. V. P. Malheiros, E. de Paula, *Biochim. Biophys. Acta Biomembr.* **2000**, *1508*, 210.
- [22] M. Lúcio, J. L. Lima, S. Reis, *Curr. Med. Chem.* **2010**, *17*, 1795.
- [23] B. Alberts, A. Johnson, J. Lewis, et al., *Molecular Biology of the Cell*, 4th ed., Garland Science, New York **2002**.
- [24] I. D. Pogozeva, S. Tristram-Nagle, H. I. Mosberg, A. L. Lomize, *Biochim. Biophys. Acta Biomembr.* **2013**, *1828*(11), 2592.
- [25] L. L. Schramm, E. N. Stasiuk, D. G. Marangon, *Annu. Rep. Prog. Chem. Sect. C* **2003**, *99*, 3.
- [26] W. Sun, C. K. Larive, M. Z. Southard, *J. Pharm. Sci.* **2003**, *92*, 424.
- [27] N. Erdinc, S. Gokturk, M. Tuncay, *J. Pharm. Sci.* **2004**, *93*, 1566.
- [28] J. Xi, R. Guo, *J. Pharm. Biomed. Anal.* **2007**, *43*, 111.
- [29] M. C. Jones, J. C. Leroux, *Eur. J. Pharm. Biopharm.* **1999**, *48*, 101.
- [30] M. E. Dalmora, S. L. Dalmora, A. G. Oliveira, *Int. J. Pharm.* **2001**, *222*, 45.
- [31] C. O. Rangel-Yagui, H. W. L. Hsu, A. I. Pessoa Jr., L. C. Tavares, *Braz. J. Pharm. Sci.* **2005**, *41*, 237.
- [32] A. D. Becke, *J. Chem. Phys.* **1993**, *98*, 5648.
- [33] C. Lee, W. Yang, R. G. Parr, *Phys. Rev. B: Condens. Matter* **1998**, *37*, 785.
- [34] M. H. Jamroz, *Vibrational Energy Distribution Analysis VEDA 4*, Warsaw, Poland, 2004–2010.
- [35] T. Mosmann, *J. Immunol. Methods* **1983**, *65*, 55.
- [36] D. L. Spector, R. D. Goldman, L. A. Leinwand, *Cell: A Laboratory Manual, Culture and Biochemical Analysis of Cells*, Cold Spring Harbor Laboratory Press, Cold Spring Harbor, NY **1998**, p. 341.
- [37] G. P. A. H. Kasibhatla, D. Finucane, T. Brunner, E. B. Wetzel, D. R. Green, Protocol: Staining of suspension cells with Hoechst 33258 to detect apoptosis. in *Cell: A Laboratory Manual Culture and Biochemical Analysis of Cells*, Vol. 1, CSHL Press, Cold Spring Harbor, NY **1998**, p. 15.5.
- [38] M. Reers, T. W. Smith, L. B. Chen, *Biochemistry* **1991**, *30*, 4480.
- [39] S. C. Oyaga, J. C. Valdés, S. B. Paez, K. H. Marquez, *J. Theor. Chem.* **2013**, *2013*, 8.
- [40] A. Das, S. Roy, P. Mondal, A. Datta, K. Mahali, G. Loganathan, D. Dharumadurai, P. S. Sengupta, M. A. Akbarsha, P. S. Guin, *RSC Adv.* **2016**, *6*, 28200.
- [41] J. B. Foresman, A. Frish, *Exploring Chemistry with Electronic Structure Methods*, Gaussian, Inc., Pittsburgh, PA **2000**, p. 64.
- [42] A. V. Iogansen, *Spectrochim. Acta. Part A* **1999**, *55*, 1585.
- [43] E. Fuguet, C. Rafols, M. Roses, E. Bosch, *Anal. Chim. Acta* **2005**, *548*, 95.
- [44] M. Sarkar, S. Poddar, *J. Colloid Interface Sci.* **2002**, *221*, 181.
- [45] M. Enache, I. Anghelache, E. Volanschi, *Int. J. Pharm.* **2010**, *390*, 100.
- [46] M. Enache, E. Volanschi, *J. Pharma. Sci.* **2011**, *100*, 558.
- [47] R. Sabate, M. Gallardo, J. Estelrich, *J. Colloid Interface Sci.* **2001**, *233*, 205.
- [48] R. Sabate, M. Gallardo, A. de la Maza, J. Estelrich, *Langmuir* **2001**, *17*, 6433.

SUPPORTING INFORMATION

Additional supporting information may be found online in the Supporting Information section at the end of this article.

How to cite this article: Banerjee S, Roy S, Datta A, et al. Solubilization of sodium 3-amino-2-hydroxyanthraquinone-1-sulphonate in sodium dodecyl sulfate micelles explains its permeation in A549 human lung cancer cell. *J Chin Chem Soc.* 2020;1–13. <https://doi.org/10.1002/jccs.202000328>

A Co(III) Complex of 1-Amino-4-hydroxy-9,10-anthraquinone Exhibits Apoptotic Action against MCF-7 Human Breast Cancer Cells

Somenath Banerjee, Sanjay Roy, Dhanasekaran Dharumadurai, Balaji Perumalsamy, Ramasamy Thirumurugan, Saurabh Das,* Asoke Prasun Chattopadhyay,* and Partha Sarathi Guin*



Cite This: *ACS Omega* 2022, 7, 1428–1436



Read Online

ACCESS |



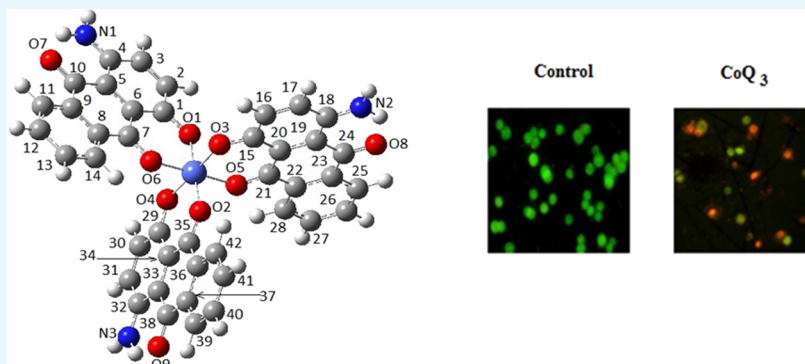
Metrics & More



Article Recommendations



Supporting Information



ABSTRACT: A Co(III) complex of 1-amino-4-hydroxy-9,10-anthraquinone (QH) (Scheme-1) having the molecular formula CoQ_3 (Scheme-2) was prepared and characterized by elemental analysis, FTIR spectroscopy, UV–vis spectroscopy, fluorescence spectroscopy, and mass spectrometry. In the absence of a single crystal, the energy-optimized molecular structure of CoQ_3 was determined by employing computational methods that was validated using spectroscopic evidences, elemental analysis, and mass spectrometry data. The electrochemical properties of the complex were analyzed using cyclic voltammetry and indicate a substantial modification of the electrochemical properties of the parent amino-hydroxy-9,10-anthraquinone. CoQ_3 was thereafter tested on MCF-7 human breast cancer cells. The IC_{50} value for a 24 h incubation was found to be $(95 \pm 0.05) \mu\text{g}/\text{mL}$. The study showed that such cancer cells underwent both early and late apoptosis following the interaction with CoQ_3 .

1. INTRODUCTION

Anthracycline drugs are anticancer agents used in treating different forms of human carcinoma.^{1–4} Although they enjoy wide acceptance in chemotherapy, their use is often questioned for the associated cardiotoxicity and high cost involved, particularly for people from economically weaker sections of the society. Hence, there is an effort worldwide^{5–19} to find alternative cheaper analogues that are less cardiotoxic.^{5–10} These are either derivatives of anthracyclines that are less costly or their simpler analogues.^{11–20}

The limitation due to acute and chronic toxicity,^{21–25} of which cardiotoxicity receives the maximum attention, is the most disturbing regarding the use of anthracyclines or their derivatives and analogues as anticancer agents.^{26–31} Participating in reactions of the respiratory chain, they produce semiquinone radical anions and related intermediates by one-electron reduction of the quinone. Although a pre-requisite for chemotherapeutic efficacy, such generation is also responsible for cardiotoxicity.^{26–30} Semiquinone upon reaction with O_2 generates superoxide radical anion ($\text{O}_2^{\bullet-}$) that in turn produce $\text{H}_2\text{O}_2/\text{OH}^{\bullet}$.^{20,30–33} These species participate in a wide range

of redox reactions as in oxidative phosphorylation, complex formation with phospholipid, and in lipid peroxidation.^{30–32}

Previous research on the subject suggests that complex formation of these drugs with different metal ions leads to decreased toxicity, the magnitude of which depends on the metal ion. Those metal ions having a stable lower oxidation state were found to cause maximum decrease in $\text{O}_2^{\bullet-}$ formation in an assay where NADH was the electron donor and cytochrome c was the electron acceptor. Hence, studies related to metal complexes gained a lot of importance regarding this matter.^{7,12,14,31,32} Metal complexes stabilize the semiquinone radical anion formed. Hence, superoxide formation due to a reaction between a semiquinone radical anion and molecular oxygen is either inhibited or decreased drastically. It is

Received: November 1, 2021

Accepted: December 22, 2021

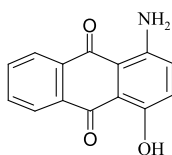
Published: December 29, 2021



therefore imperative to study such metal complexes, particularly with regard to their electrochemical behavior under different experimental conditions.

It is worth mentioning that although several metal complexes of adriamycin, daunorubicin, mitoxantrone, and their analogues with Fe(III), Al(III), Cu(II), Ni(II), Pd(II), and Tb(III) were prepared and characterized,^{7,10–14,33–46} comprehensive knowledge on structures of these metal complexes is lacking due to inherent difficulties in obtaining single crystals for X-ray diffraction studies. Single-crystal X-ray diffraction structures of only a few hydroxy-9,10-anthraquinone complexes are reported.^{44,47,48} In this study also, different methods were employed to obtain single crystals of CoQ₃ taking different compositions of solvents. However, all efforts in getting an appropriate single crystal for CoQ₃ failed. The planarity of the anthraquinone unit in these complexes could possibly be a hindrance in getting single crystals.⁷ For this reason, we made an effort to characterize CoQ₃ theoretically using density functional theory (DFT) based on experimental data we obtained such as elemental analysis, IR spectroscopy, mass spectrometry, powder X-ray diffraction, molecular spectroscopy, and electrochemistry. DFT is helpful in generating the energy optimized structure, and various essential parameters of the complex may also be obtained from this study. The thus prepared complex was tested on MCF-7 human breast cancer cells to see whether it initiates apoptosis and thus could be considered as a less costly alternative to anthracyclines already in use.

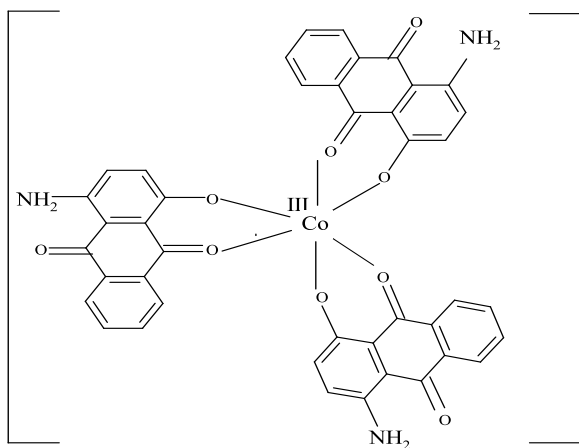
Scheme 1. 1-Amino-4-hydroxy-9,10-anthraquinone (QH)



2. RESULTS AND DISCUSSION

2.1. Analysis of the Mass Spectra of CoQ₃. Assuming that the formula of the complex is CoQ₃ (Scheme 2), an analysis of its mass spectrum (Figure S1, SI) was attempted. The molecular ion peak or that of the protonated molecular ion expected at $m/z = 773.62$ was not found. However, a clear

Scheme 2. Structure of CoQ₃



signal at $m/z = 689.46$ corresponds to a fragment remaining of the complex following loss of a carbon-bound $-NH_2$ group from each ligand (a loss of 28 mass units from each ligand, i.e., 78 mass units from the complex) to result in a peak theoretically expected at $m/z = 689.62$. From this peak, loss of two quinone oxygens would result in a peak theoretically expected at $m/z = 661.62$. The experimental value is 661.45, which tallies with the expected value. Loss of four quinone oxygens from the first fragment results in a peak theoretically expected at $m/z = 633.62$ and experimentally found at 633.42. Here also, the agreement is close. Similarly, loss of six quinone oxygens from all the three ligands of the first fragment should result in a theoretical peak at $m/z = 605.62$. This was experimentally observed at 605.39, again pointing to a close agreement. At this stage of fragment formation in mass analysis, the metal center is bound to three ligands via the three phenolic $-OH$ groups on each of them. The peaks identified above therefore categorically indicate the formation of a 1:3 complex. Subsequent to the fragmentations mentioned above, further loss of two carbon atoms and a few hydrogens at a time explains peaks at an m/z value of 577.35 and also the cluster of peaks at m/z values of 533.99, 532.99, and 531.98, respectively. Peaks at lower m/z values correspond to smaller fragments. Therefore, from an analysis of the mass spectrum of the cobalt complex, it may be concluded that the complex has the formula CoQ₃ as shown in Scheme 2.

2.2. Analysis of the IR Spectra of CoQ₃. The FTIR spectrum for QH (Figure S2, SI) shows a peak at 3431 cm^{-1} , which is due to N–H bond stretching, while that at 3300 cm^{-1} is due to stretching of O–H bonds.⁹ The O–H stretching is modified significantly in the complex (Figure S3, SI), indicating an involvement of the $-OH$ group during complex formation. Since there is deprotonation of $-OH$ during complex formation, the molecule ceases to show intramolecular hydrogen bonding identified in QH. Peaks in this region do not disappear completely in the complex when compared with QH, indicating the presence of free $-NH_2$ on each ligand (just as that observed or the IR spectrum of QH). In the IR spectrum of CoQ₃ (Figure S3, SI), peaks at 1625, 1586, and 1537 cm^{-1} are attributed to stretching due to free carbonyl and C=C or a combination of both, respectively. In an earlier study,⁶ we showed that peaks obtained in the region $1464\text{--}1031\text{ cm}^{-1}$ in the IR spectrum of the ligand (QH) may be attributed to combinations of O–H, N–H, and C–H bending modes. Natures of the peaks in this region are somewhat different in the complex. More specifically, the peak at 1121 cm^{-1} is reduced significantly, probably due to binding of oxygen of the $-OH$ group to Co(III) following its deprotonation.

2.3. Powder X-ray Diffraction of CoQ₃. The powder X-ray diffraction (PXRD) pattern of CoQ₃ is shown in Figure 1. All peaks can be indexed with the space group R32(155), and Cu $K\alpha = 1.5406\text{ \AA}$ using the WINPLOTR program. Refined cell parameters were found to be $a = 7.45\text{ \AA}$, $b = 6.52\text{ \AA}$, and $c = 27.8\text{ \AA}$. The unit cell volume was 1352 \AA^3 ; $\alpha = 33.43^\circ$, $\beta = 90^\circ$, and $\gamma = 90^\circ$. Thus, PXRD analysis provides information about the dimension of the unit cell of a crystalline CoQ₃.

2.4. Structure of CoQ₃ from Density Functional Theory Methods. The energy-optimized molecular structure of CoQ₃ is shown in Figure 2, and structural parameters are summarized in Table S1 (SI). Figure 2 shows three QH molecules coordinated to Co(III) through phenolic O[−] and quinone oxygen, forming CoQ₃.

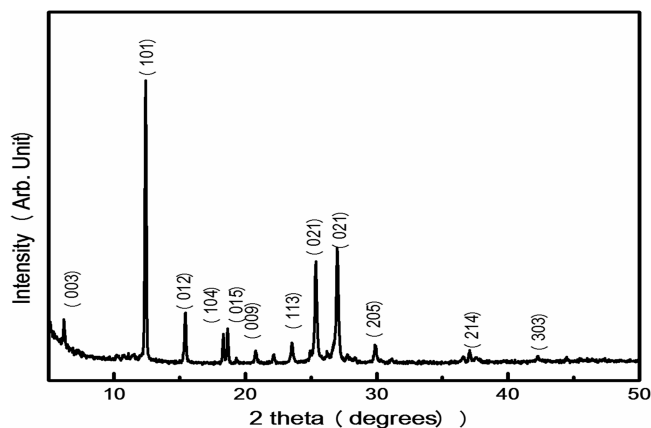


Figure 1. Powder X-ray diffraction patterns of CoQ₃.

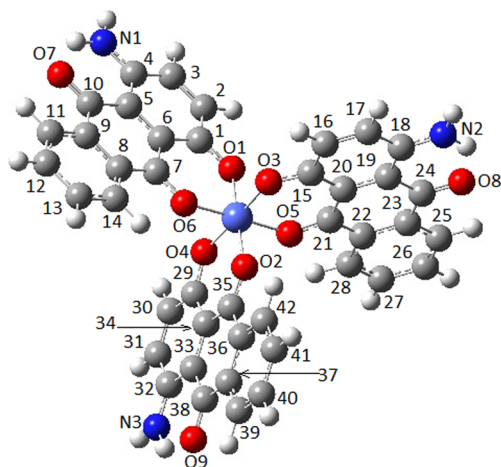


Figure 2. Energy optimized structure of CoQ₃.

The energy level diagrams of QH and CoQ₃ are shown in Figure S3 (SI). The HOMO (H) and LUMO (L) are indicated in each case (Figure 3). Red lines indicate the π

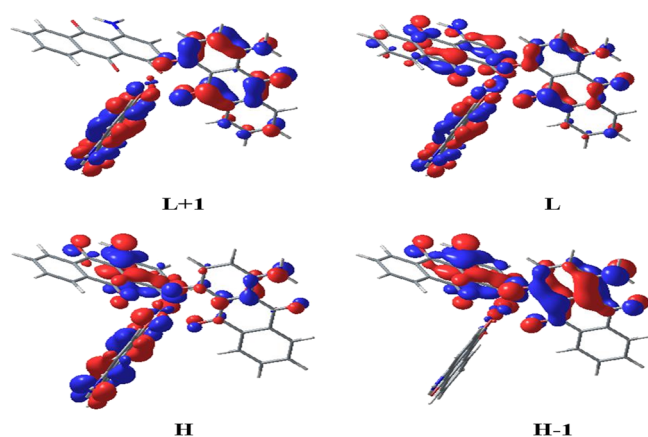


Figure 3. Different HOMOs (H) and LUMOs (L) of CoQ₃.

orbitals, black lines indicate σ , and blue lines represent mixed metal–ligand (M–L) orbitals. Some M–L type MOs may have mixed σ and π characters as the three ligands are arranged in such a manner that σ of one may mix with π of another. Metal orbitals are mainly $d\pi$, with some $p\pi$ mixed. Co(III) orbitals are much lower in energy to be shown in the above diagram. It

should also be noted that the HOMO and LUMO are M–L type orbitals.

2.5. UV–vis Spectroscopy of CoQ₃. The absorption spectrum of QH (Figure 4a) in 30% ethanol^{16,7} shows four absorption bands (at 250, 290, 530, and 565 nm) due to π – π^* and n – π^* transitions of its various tautomeric forms in rapid equilibrium in aqueous solution.^{6,7,49} From the UV–vis spectrum of CoQ₃ (Figure 4b), it is clear that the absorption peaks at 250, 290, 530, and 565 nm remain almost unaltered, which indicate that the electronic absorption spectrum of CoQ₃ depends weakly on the nature of the metal and is primarily defined by the ligand (QH).⁴⁹ However, the appearance of a new peak at 600 nm is characteristic of the complex (CoQ₃). It is important to mention here that tautomeric structures found for free QH⁴⁹ in aqueous media are not possible for CoQ₃ since phenolic –OH groups in the QH molecule are deprotonated owing to coordination of Co(III) by phenolic oxygens.

2.6. Fluorescence Spectroscopy of CoQ₃. Fluorescence spectra of QH and CoQ₃ are shown in Figure S4 (SI) recorded following an excitation at 530 nm. The emission spectrum exhibits a maximum at 590 nm for QH and 594 nm for CoQ₃. The difference in the emission peak of CoQ₃ compared to QH is due to the metal ligand bond.

2.7. Electrochemical Reduction of CoQ₃ in Organic Polar Solvents. Electrochemical behavior of CoQ₃ was studied in anhydrous DMSO and DMF in the presence of TBAB as the supporting electrolyte using cyclic voltammetry. In anhydrous DMSO, CoQ₃ undergoes successive three one-electron reductions having peak potentials (E_{pc}) at -0.795 , -1.010 , and -1.295 V, respectively, vs Ag/AgCl/saturated KCl (Figure 5 and Table 1). In this case, the first reduction is reversible, while the other two are quasi-reversible at different scan rates. These three one-electron reduction steps are due to the reduction of the three free quinone centers of the three Q[–] bound to Co(III) in CoQ₃ (Scheme 3). For these reductions, the formal potentials (E) of the respective reduction steps were found at -0.750 , -0.987 , and -1.255 V, respectively. It is noted that although there are three equivalent free quinone sites in CoQ₃ (Scheme 3), there exists a difference in their formal potential values, which is quite appreciable. Thus, after reduction at the first free quinone in CoQ₃, reduction of the second and third quinone sites is significantly delayed. In other words, the reduced species (semiquinone radical anion) that formed due to the first or second reduction is stabilized in the metal ion environment due to delocalization of the negative charge. This is important with regard to the compound's biochemical action since a stabilized semiquinone would delay the reaction between semiquinone and molecular oxygen^{30–34} within cells where it would be employed.

In anhydrous DMF, under similar experimental conditions, CoQ₃ undergoes three one electron reductions having peak potentials (E_{pc}) at -1.025 , -1.225 , and -1.475 V, respectively, with the corresponding formal potentials (E) being -0.950 , -1.195 , and -1.405 V, respectively (Figure 6 and Table 1). Considering the fact that the polarity of DMF is less than that of DMSO⁵¹ and comparing the three reduction potentials of CoQ₃ in the two solvents, it can be said that with the increasing polarity of the medium, reduction potentials move in a positive direction and that reductions become more feasible as the polarity of solvent increases. This means stability of the formed semiquinone species is increased with an increase in the polarity of the medium. Stabilization of the

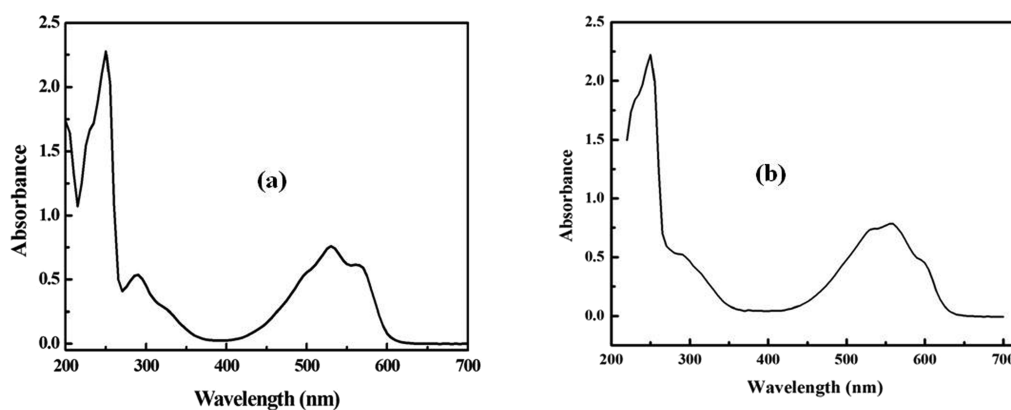


Figure 4. UV-vis spectrum of (a) QH and (b) CoQ₃ in aqueous ethanol.

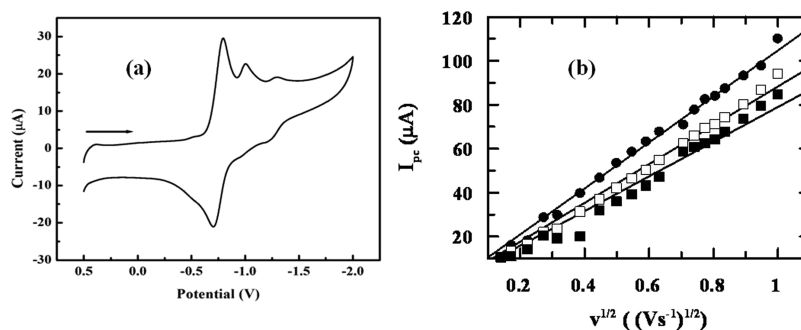


Figure 5. (a) Cyclic voltammogram of CoQ₃ in anhydrous DMSO media. Scan rate: 0.10 V s⁻¹. [CoQ₃] = 1 × 10⁻³ M, [TBAB] = 0.1 M, T = 298.15 K. (b) Plot of cathodic peak current vs square root of scan rate for first (solid circles), second (open squares), and third reduction (solid squares) of CoQ₃ in anhydrous DMSO.

Table 1. Electrochemical Parameters of CoQ₃^a

media	Epc-1 (V)	Epc-2 (V)	Epc-3 (V)	E-1 (V)	E-2 (V)	E-3 (V)	D ₀ (cm ² s ⁻¹)
DMSO	-0.795	-1.010	-1.295	-0.750	-0.987	-1.255	3.04 × 10 ⁻⁵
DMF	-1.025	-1.225	-1.475	-0.950	-1.195	-1.405	6.31 × 10 ⁻⁵

^aPotentials were measured with respect to vs Ag/AgCl/saturated KCl.

semiquinone is also reflected in the formal reduction potential data. This aspect is important with respect to its chemotherapeutic efficiency.^{30–34} Owing to stabilization of the semiquinone radical anion, the probability for reaction of a semiquinone radical anion with molecular oxygen would be delayed and that may reduce cardiotoxicity if the molecule were to be employed as an anticancer agent.^{30–34}

Under similar experimental conditions, a cyclic voltammogram of QH shows two reversible waves at -0.816 and -1.355 V in anhydrous DMSO and at -0.832 and -1.309 V in anhydrous DMF vs Ag/AgCl, with saturated KCl forming a semiquinone radical anion and quinone dianion, respectively.^{7,8} Formal potentials for such reductions were evaluated as -0.770 and -1.308 V in anhydrous DMSO and -0.785 and -1.258 V in anhydrous DMF.⁸ Comparing electrochemical parameters and cyclic voltammograms (Figures 5 and 6) of CoQ₃ with those of QH in anhydrous DMSO and anhydrous DMF,⁸ one can say that the electrochemical behavior of QH bound to a metal ion as Q⁻ (as in CoQ₃) is significantly altered.

It is seen that the reduction peak currents (*I*_{pc}) for three successive reductions of CoQ₃ in both DMSO and DMF have a linear relationship with the square root of the scan rate and that it passes through the origin (Figures 5 and 6). This suggests that such reductions are fully diffusion controlled and

that there is no adsorption on the electrode surface. The diffusion coefficient (*D*₀) of CoQ₃ was determined by the relation shown in eq 1⁵⁰ and found as 3.04 × 10⁻⁵ and 6.31 × 10⁻⁵ cm² s⁻¹ in DMSO and DMF, respectively (summarized in Table 1).

$$I_{pc} = (2.69 \times 10^5) n^{3/2} D_0^{1/2} A C \nu^{1/2} \quad (1)$$

where *I*_{pc} = cathodic peak current (A), *n* = number of electron involved in the reduction, *A* = area of the electrode (cm²), *C* = concentration (mol·cm⁻³), and *ν* = scan rate (V·s⁻¹).

From values of diffusion coefficients of CoQ₃ in two different solvents (Table 1), it is evident that *D*₀ increases as the polarity of the solvent decreases, clearly indicating greater solvation of CoQ₃ in a more polar solvent that causes lower diffusion onto the surface of the electrode. Thus, CoQ₃ is more solvated in DMSO due to hydrogen bonding and other electrostatic interactions.⁸ Intermolecular hydrogen bonding between one of the two hydrogen of aromatic amino group (-NH₂) of QH and negatively charged oxygen of the solvent (DMSO) is very strong.⁸ This type of hydrogen bonding would be weak in the case of DMF since for this solvent, oxygen has a less partial negative charge than that on oxygen in DMSO.⁸

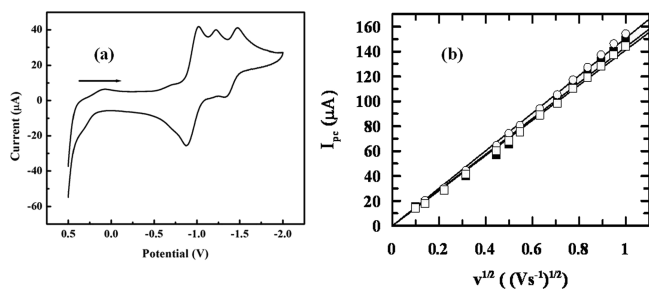
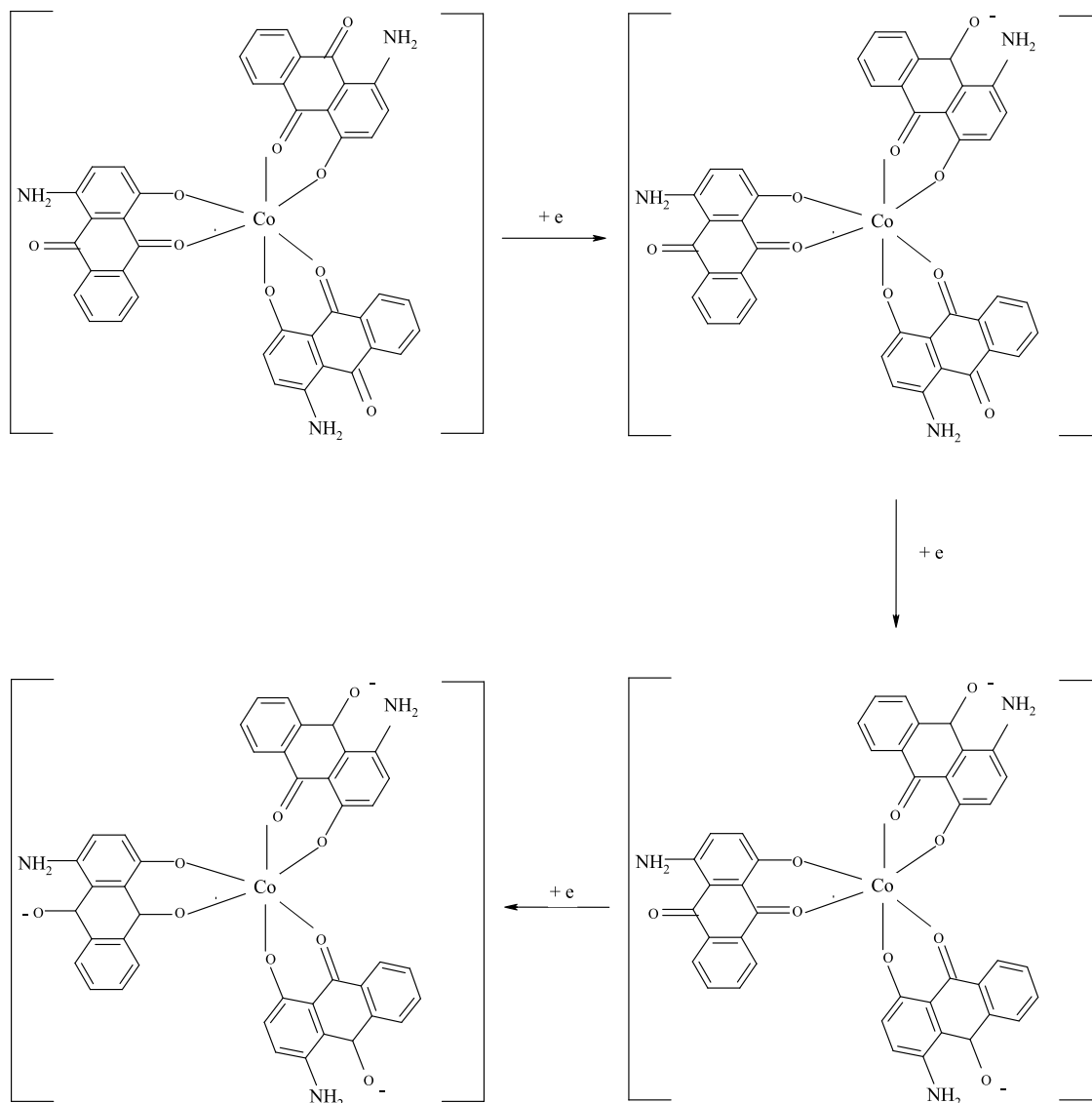
Scheme 3. Three Step One-Electron Reductions of CoQ₃ in Organic Polar Solvents Like DMSO and DMF

Figure 6. (a) Cyclic voltammogram of CoQ₃ in anhydrous DMF media. Scan rate: 0.10 Vs⁻¹. [CoQ₃] = 1 × 10⁻³ M, [TBAB] = 0.1 M, T = 298.15 K. (b) Plot of cathodic peak current vs square root of scan rate for first (open circles), second (open squares), and third reduction (solid squares) of CoQ₃ in anhydrous DMF.

2.8. Effect of CoQ₃ on Viability of MCF-7 Human Breast Cancer Cells by the MTT Assay. Using the MTT assay, the cytotoxic activity of CoQ₃ was analyzed against MCF-7 human breast cancer cells (Figure 7). It was estimated according to dose values of exposure of CoQ₃ required to reduce the survival to 50% (IC₅₀) in comparison to that of

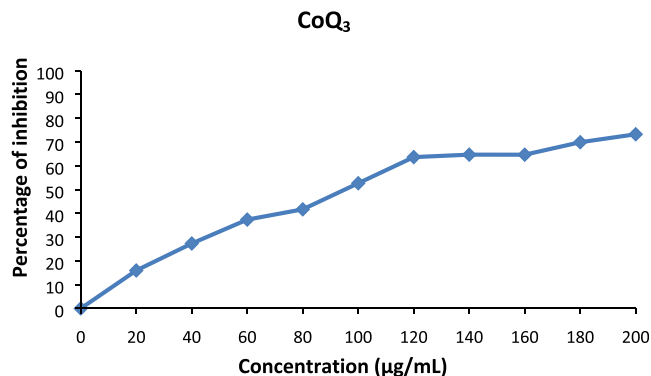


Figure 7. Cytotoxic effect of CoQ₃ on MCF-7 human breast cancer cells after exposure for 24 h.

untreated cells. The IC₅₀ value for 24 h was found to be (95 ± 0.05) µg/mL. This indicates that CoQ₃ is cytotoxic against MCF-7 breast cancer cells.

2.9. AO/EB Staining. Apoptosis is the hallmark of cell death and can be characterized by cellular morphological

changes observed during the process of cell death. The dual staining method of AO/EB detects such morphological changes. Figure 8 corresponds to AO/EB staining of

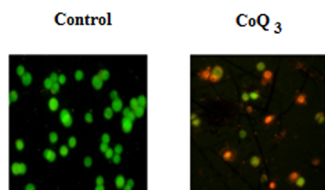


Figure 8. AO/EB staining of the control and CoQ₃-treated MCF-7 human breast cancer cells.

control/non-treated and CoQ₃-treated MCF7 breast cancer cells. Based on fluorescence emission and nucleus morphology, cells were distinguished to have viable, apoptotic, or necrotic characteristics. The viable cells were observed to have uniform green-colored nuclei with a typical cell morphology and intact membrane. On the other hand, apoptotic cells showed irregular cell morphologies with orange to red condensed chromatin and/or fragmented nuclei. Furthermore, the large orange to red fluorescent swollen cells with no fragmented nuclei were differentiated as necrotic cells. The results from AO/EB staining reveal that the control group contains more viable cells and a few apoptotic and necrotic cells. In contrast, CoQ₃-treated MCF7 breast cancer cells induced majority of cell death through the apoptosis mode and actually very few by necrosis. Furthermore, condensed and fragmented morphologies were mostly observed in the CoQ₃ treatment group. The results of calculating the percentage of apoptotic cell death induced by CoQ₃ and analyzed by fluorescent images of AO/EB staining revealed that AQS-treated cells induced a higher percentage of apoptotic cells and a lower percentage of necrotic cells than untreated cells (Figure 9). The graph depicts a percentage count of apoptotic normal and abnormal cells. The error bar represents the standard deviation across three replicates.

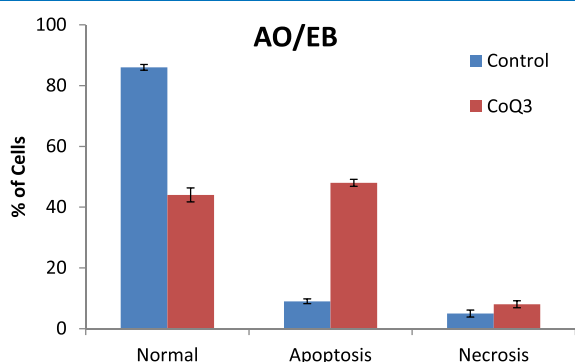


Figure 9. Comparison of percentage of cells in apoptotic death compared to healthy cells and necrotic death.

3. CONCLUSIONS

A Co(III) complex of 1-amino-4-hydroxy-9,10-anthraquinone (QH) with the molecular formula CoQ₃ was synthesized and characterized by different methods. The optimized molecular structure of CoQ₃ was estimated using computational methods. The HOMO and LUMO of CoQ₃ were also characterized by this method. Electrochemical properties of

CoQ₃ were studied in anhydrous DMSO and anhydrous DMF media using cyclic voltammetry, and the mechanism of reduction was established. It showed that different reduced anions of CoQ₃ are stabilized in a metal surrounding environment and that reductions would therefore be delayed. Polarity of the solvents also affects stability of the reduced anion. A significant modification of electrochemical properties of QH was also seen when it was bound to Co(III) in CoQ₃. The IC₅₀ value of CoQ₃ for 24 h of incubation corresponding to cytotoxicity of CoQ₃ on human breast cancer cells MCF-7 was evaluated as 95 ± 0.05 μg/mL. The study revealed that such cancer cells underwent both early and late apoptosis due to CoQ₃.

4. EXPERIMENTAL SECTION

4.1. Materials. 1-Amino-4-hydroxy-9, 10-anthraquinone (QH) (Scheme 1) (96%) purchased from Alfa Aesar, Germany was recrystallized from an ethanol–methanol mixture and characterized as mentioned earlier.^{6–9} The quinone moiety being sensitive to light, solutions were prepared either just before an experiment or very carefully stored in the dark. CoCl₂·6H₂O purchased from Merck, India was used to prepare the Co(III) complex. KCl and tetrabutyl ammonium bromide [TBAB] (both are AR grade, Spectrochem, India) were used as supporting electrolytes in aqueous and non-aqueous media, respectively.

Dimethyl sulfoxide (DMSO) (99.0%, Spectrochem, India) was first dried over fused CaCl₂ for 3–4 days, decanted, and then distilled under reduced pressure.⁵¹ The distilled sample was preserved in a well-stoppered Jena bottle in desiccators and redistilled again before use. *N,N*-Dimethyl formamide (DMF) (99.5%, Spectrochem, India) (LR, BDH) was purified⁵² first by distilling under reduced pressure in a N₂ atmosphere and then preserving the distillate over dry K₂CO₃ (Merck) for a week. Then, the DMF was decanted and allowed to mix with dry P₂O₅ (Riedel) and distilled again to be able to use it under anhydrous conditions. Anhydrous DMF and DMSO were used as solvents in electrochemistry experiments. All aqueous solutions were prepared in triple-distilled water.

4.2. Synthesis of CoQ₃. An aqueous solution of 0.5 mmol CoCl₂·6H₂O and a solution of 1.5 mmol QH in acetonitrile were mixed and stirred for about 6 h using a magnetic stirrer. Co(II) was oxidized to Co(III) by purging air into the reaction media. The solution was kept for 7 days in air to allow it to evaporate till it was almost 5 mL. A violet-colored complex was separated by filtration followed by washing with acetonitrile. The complex was recrystallized from a methanol–acetonitrile mixture and dried in air. Results of elemental analysis showed that it has the formula CoQ₃. Found: C, 65.09%; H, 3.08%; N, 5.51%. Calculated: C, 65.13%; H, 3.10%; N, 5.43%. In 25% aqueous ethanol solution, 0.1 mM CoQ₃ showed a conductance less than 5 μS/cm at 298.15 K, indicating that it is neutral.

4.3. Computational Studies. The structure of CoQ₃ was optimized using DFT with Ahlrich SV basis^{53,54} and B3LYP functional^{55–57} using the Orca program suite.⁵⁸ Electronic transitions were calculated by the time-dependent DFT method with the same basis set and functional using Orca. Pictures of molecular orbitals (MOs) were generated with the same basis set and functional using Gaussian 09W⁵⁹ and MaSK software.⁶⁰

4.4. Analytical Methods. With the help of a Perkin-Elmer 2400 II elemental analyzer, the carbon, hydrogen, and nitrogen

analyses were done. FTIR analysis was performed on a Perkin Elmer RX-I spectrophotometer. Spectra were obtained using KBr pellets in the range 4000–400 cm^{-1} . The mass spectrum was recorded on Micromass Q-Tofmicro, Waters Corporation. CoQ_3 was dissolved in an anhydrous acetonitrile solvent, and the MS data were recorded by using ESI positive mode. The instrument applies a focusing voltage to the electrospray probe to promote mobile phase evaporation as part of the ionization process. PXRD data was collected on a Bruker AXS D8 powder diffractometer using $\text{Cu K}\alpha$ radiation ($\lambda = 1.548 \text{ \AA}$) generated at 40 kV and 40 mA. UV–visible spectroscopy was done on a spectrophotometer (model: MECASYS OPTIZEN POP). Experiments related to cyclic voltammetry were performed using the conventional three-electrode system. The temperature was maintained at 25 $^\circ\text{C}$ with the help of a circulating water bath. The working electrode was glassy carbon, the surface area of which was 0.07065 cm^2 , the counter electrode was a platinum wire, and the reference electrode was Ag/AgCl in satd. KCl. Using a potentiostat (model DY2312, Digi-Ivy), all electrochemical studies were performed. The range of concentrations of different solutions was $5 \times 10^{-5} \text{ mol dm}^{-3}$ to $1.5 \times 10^{-3} \text{ mol dm}^{-3}$. Before the solutions were subjected to cyclic voltammetry, they were degassed for nearly 30 min using highly pure Ar.

4.5. Cell Culture. MCF7 human breast cancer cells were procured from National Center for Cell Science, Pune, India. Cells were cultured and maintained in DMEM high-glucose medium (Sigma-Aldrich, USA) supplemented by 10% fetal bovine serum (Gibco, Thermo Fisher, USA) and 20 mL of penicillin/streptomycin as antibiotics (Gibco, Thermo Fisher, USA), and incubated at 37 $^\circ\text{C}$ with 5% CO_2 in a CO_2 incubator (Thermo scientific, USA). All experiments were carried out using cells from the passage of 15 or less.

4.6. Cell Viability Assay. CoQ_3 was dissolved in DMSO and a stock solution was prepared. It was then diluted to obtain different concentrations of the compound in the range 0–200 $\mu\text{g}/\text{mL}$. Two hundred microliters of such solutions was added to wells containing 5×10^3 MCF-7 cells per well of a 96-well culture plate. DMSO was used as the control solvent. Twenty microliters of MTT solution (5 mg/mL in PBS) was transferred to each well following 24 h of incubation, and the plate was incubated at 37 $^\circ\text{C}$ for 4 h in the dark. To dissolve formazan crystals, 100 μL of DMSO was added to each well and the absorbance of the final solution was measured at 570 nm using a microplate reader (Bio-Rad, iMark, USA). Data was collected for three replicates each, and the respective mean was used in the following formula to calculate percentage inhibition:

$$\text{percentage inhibition} = \left(\frac{[\text{mean OD of untreated cells (control)} - \text{mean OD of treated cells (treated)}]}{[\text{mean OD of untreated cells (control)}]} \right) \times 100$$

4.7. Acridine Orange (AO) and Ethidium Bromide (EB) Staining. CoQ_3 -induced apoptosis was examined using the fluorescent-based dual staining method AO/EB as defined by Spector et al.⁶¹ with some modifications. In brief, cells treated for 24 h with the IC_{50} concentration of CoQ_3 were harvested and washed with cold PBS. Cell pellets were resuspended and diluted with PBS. The cell suspension (5000 in number) was mixed with AO/EB solution (3.8 μM AO and 2.5 μM EB in PBS) and transferred to a clean microscope slide. Morphological features of the cells were examined under a fluorescent microscope (Carl Zeiss, Axioscope2plus) with a UV filter (450–490 nm).

■ ASSOCIATED CONTENT

■ Supporting Information

The Supporting Information is available free of charge at <https://pubs.acs.org/doi/10.1021/acsomega.1c06125>.

(Figure S1) Mass Spectrum of CoQ_3 , (Figure S2) IR spectrum of QH and CoQ_3 , (Figure S3) energy level diagram of QH and CoQ_3 , (Figure S4) fluorescence spectra of QH and CoQ_3 in aqueous ethanol, and (Table S1) structural parameters of CoQ_3 (PDF)

■ AUTHOR INFORMATION

Corresponding Authors

Saurabh Das – Department of Chemistry, Jadavpur University, Kolkata 700032, India; orcid.org/0000-0002-0455-8760; Phone: +91 9123865911; Email: darsrv@yahoo.in, saurabh.das@jadavpuruniversity.in; Fax: +91 33 24146223

Asoke Prasun Chattopadhyay – Department of Chemistry, University of Kalyani, Nadia 741235 West Bengal, India; orcid.org/0000-0002-2411-1384; Phone: +919836156800; Email: asoke@klyuniv.ac.in; Fax: +91 33 2582 8282

Partha Sarathi Guin – Department of Chemistry, Shibpur Dinobundhoo Institution (College), Howrah 711102 West Bengal, India; orcid.org/0000-0001-9258-9227; Phone: +91 9330083036; Email: parthasg@gmail.com; Fax: +91 33 2688 0344

Authors

Somenath Banerjee – Department of Chemistry, Shibpur Dinobundhoo Institution (College), Howrah 711102 West Bengal, India; Department of Chemistry, Jadavpur University, Kolkata 700032, India

Sanjay Roy – Department of Chemistry, Netaji Subhas Open University, Nadia 741235, India; orcid.org/0000-0001-6841-4961

Dhanasekaran Dharumadurai – Department of Microbiology, School of Life Sciences, Bharathidasan University, Tiruchirappalli 620 024, India

Balaji Perumalsamy – National Centre for Alternatives to Animal Experiments, Bharathidasan University, Tiruchirappalli 620 024, India

Ramasamy Thirumurugan – National Centre for Alternatives to Animal Experiments, Bharathidasan University, Tiruchirappalli 620 024, India

Complete contact information is available at:

<https://pubs.acs.org/doi/10.1021/acsomega.1c06125>

Notes

The authors declare no competing financial interest.

■ ACKNOWLEDGMENTS

P.S.G. is grateful to UGC, New Delhi, India, for the financial support through the Major Research Project (file no. 41-225/2012(SR) dated 18 July 2012). S.D. gratefully acknowledges support received from UGC-DAE-CSR Collaborative Research Scheme for a project having sanction number UGC-DAE-CSR-KC/CRS/19/RC11/0985.

■ ABBREVIATIONS

QH, 1-amino-4-hydroxy-9,10-anthraquinone; CoQ_3 , Co(III) complex of 1-amino-4-hydroxy-9,10-anthraquinone; TBAB,

tetrabutyl ammonium bromide; DMSO, dimethyl sulfoxide; DMF, *N,N*-dimethyl formamide

REFERENCES

- (1) Hardman, J. -G.; Gilman, A.-G.; Limbird, L.-E. *Goodman and Gilman's The Pharmacological Basis of Therapeutics*, 9th ed.; McGraw-Hill Companies: New York, 1996.
- (2) Lim, K. H.; Kim, H. S.; Yang, Y. M.; Lee, S. D.; Kim, W. B.; Yang, J.; Park, J. G. Cellular uptake and antitumor activity of the new anthracycline analog DA-125 in human cancer cell lines. *Cancer Chemother. Pharmacol.* **1997**, *40*, 23–30.
- (3) Preobrazhenskaya, M. N.; Tevyashova, A. N.; Olsufyeva, E. N.; Huang, K.-F.; Huang, H.-S. Second generation drugs-derivatives of natural antitumor anthracycline antibiotics daunorubicin, doxorubicin and carminomycin. *J. Med. Sci.* **2006**, *26*, 119–128.
- (4) Hu, F. Q.; Liu, L. N.; Du, Y. Z.; Yuan, H. Synthesis and antitumor activity of doxorubicin conjugated stearic acid-g-chitosan oligosaccharide polymeric micelles. *Biomaterials* **2009**, *30*, 6955–6963.
- (5) Das, A.; Roy, S.; Mondal, P.; Datta, A.; Mahali, K.; Loganathan, G.; Dharumadurai, D.; Sengupta, P. S.; Akbarsha, M. A.; Guin, P. S. Studies on the interaction of 2-amino-3-hydroxy-anthraquinone with surfactant micelles reveal its nucleation in human MDA-MB-231 breast adenocarcinoma cell. *RSC Adv.* **2016**, *6*, 28200–28212.
- (6) Mondal, P.; Roy, S.; Loganathan, G.; Mandal, B.; Dharumadurai, D.; Akbarsha, M. A.; Sengupta, P. S.; Chattopadhyay, S.; Guin, P. S. 1-amino-4-hydroxy-9,10-anthraquinone - An analogue of anthracycline anticancer drugs, interacts with DNA and induces apoptosis in human MDA-MB-231 breast adenocarcinoma cells: Evaluation of structure-activity relationship using computational, spectroscopic and biochemical studies. *Biochem. Biophys. Res. Commun.* **2015**, *4*, 312–323.
- (7) Roy, S.; Mondal, P.; Sengupta, P. S.; Dhak, D.; Santra, R. C.; Das, S.; Guin, P. S. Spectroscopic, computational and electrochemical studies on the formation of the copper complex of 1-amino-4-hydroxy-9,10-anthraquinone and effect of it on superoxide formation by NADH dehydrogenase. *Dalton Trans.* **2015**, *44*, 5428–5440.
- (8) Roy, S.; Guin, P. S. Solvation of 1-amino-4-Hydroxy-9,10-anthraquinone governs its electrochemical behavior in non-aqueous and aqueous media: A cyclic voltammetry study. *J. Electrochem. Soc.* **2015**, *162*, H124–H131.
- (9) Roy, S.; Guin, P. S. Investigation on the interaction of 1-amino-4-hydroxy-9,10 anthraquinone with calf thymus DNA and CTAB micelles. *J. Mol. Liq.* **2015**, *211*, 846–853.
- (10) Guin, P. S.; Das, S.; Mandal, P. C. Studies on the formation of a complex of Cu(II) with sodium 1,4-dihydroxy-9,10-anthraquinone-2-sulphonate- An analogue of the core unit of anthracycline anticancer drugs and its interaction with calf thymus DNA. *J. Inorg. Biochem.* **2009**, *103*, 1702–1710.
- (11) Guin, P. S.; Mandal, P. C.; Das, S. The binding of a hydroxy-9,10-anthraquinone Cu^{II} complex to calf thymus DNA : Electrochemistry and UV/Vis Spectroscopy. *ChemPlusChem.* **2012**, *77*, 361–369.
- (12) Rossi, S.; Tabolacci, C.; Lentini, A.; Provenzano, B.; Carlomosti, F.; Frezzotti, S.; Beninati, S. Anthraquinones danthron and quinizarin exert antiproliferative and antimetastatic activity on murine B16-F10 melanoma cells. *Anticancer Res.* **2010**, *30*, 445–449.
- (13) Das, P.; Jain, C. K.; Dey, S. K.; Saha, R.; Chowdhury, A. D.; Roychoudhury, S.; Kumar, S.; Majumder, H. K.; Das, S. Synthesis, crystal structure, DNA interaction and *in vitro* anticancer activity of a Cu(II) complex of purpurin: Dual poison for human DNA topoisomerase I and II. *RSC Adv.* **2014**, *4*, 59344–59357.
- (14) Das, P.; Bhattacharya, D.; Karmakar, P.; Das, S. Influence of ionic strength on the interaction of THA and its Cu (II) complex with DNA helps to explain studies on various breast cancer cells. *RSC Adv.* **2015**, *5*, 73099–73111.
- (15) Das, P.; Guin, P. S.; Mandal, P. C.; Paul, M.; Paul, S.; Das, S. Cyclic voltammetric studies of 1,2,4-trihydroxy-9,10-anthraquinone, its interaction with calf thymus DNA and anti-leukemic activity on MOLT-4 cell lines: A comparison with anthracycline anticancer drugs. *J. Phys. Org. Chem.* **2011**, *24*, 774–785.
- (16) Mandal, B.; Singha, S.; Dey, S. K.; Mazumdar, S.; Mondal, T. K.; Karmakar, P.; Kumar, S.; Das, S. Synthesis, crystal structure from PXRD of a Mn^{II}(purp)₂ complex, interaction with DNA at different temperatures and pH and lack of stimulated ROS formation by the complex. *RSC Adv.* **2016**, *6*, 51520–51532.
- (17) Nakayama, T.; Okumura, N.; Uno, B. Complementary Effect of Intra- and Intermolecular Hydrogen Bonds on Electron Transfer in β -Hydroxy-Anthraquinone Derivatives. *J. Phys. Chem. B.* **2020**, *124*, 848–860.
- (18) Tian, W.; Wang, C.; Li, D.; Hou, H. Novel anthraquinone compounds as anticancer agents and their potential mechanism. *Future Med. Chem.* **2020**, 627.
- (19) Tikhomirov, A. S.; Shtil, A. A.; Shchekotikhin, A. E. Advances in the Discovery of Anthraquinone-Based Anticancer Agents. *Recent Pat. Anti-Cancer Drug Discovery* **2018**, *13*, 159–183.
- (20) Mukherjee Chatterjee, S.; Jain, C. K.; Singha, S.; Das, P.; Roychoudhury, S.; Majumder, H. K.; Das, S. Activity of Co^{II}-quinizarin: A novel analogue of anthracyclinebased anticancer agents targets human DNA topoisomerase, whereas quinizarin itself acts via formation of semiquinone on acute lymphoblastic leukemia MOLT-4 and HCT 116 cells. *ACS Omega* **2018**, *3*, 10255–10266.
- (21) Blasiak, J.; Gloc, E.; Warszawski, M. A comparison of the *in vitro* genotoxicity of anticancer drugs idarubicin and mitoxantrone. *Acta Biochim. Pol.* **2002**, *49*, 145–155.
- (22) Kapuscinski, J.; Daizynkiewicz, Z. Relationship between the pharmacological activity of antitumor drugs ametantrone and mitoxantrone (novatrone) and their ability to condense nucleic acids. *Proc. Natl. Acad. Sci. U. S. A.* **1986**, *83*, 6302–6306.
- (23) Ellis, A. L.; Randolph, J. K.; Conway, B. R.; Gewirtz, D. A. Biochemical lesions in DNA associated with the antiproliferative effects of mitoxantrone in the hepatoma cell. *Biochem. Pharmacol.* **2009**, *39*, 1549–1556.
- (24) Li, N.; Ma, Y.; Yang, C.; Guo, L.; Yang, X. Interaction of anticancer drug mitoxantrone with DNA analyzed by electrochemical and spectroscopic methods. *Biophys. Chem.* **2005**, *116*, 199–205.
- (25) Riah, S.; Reza Ganjali, M.; Dinarvand, R.; Karamdoust, S.; Bagherzadeh, K.; Norouzi, P. A theoretical study on interactions between mitoxantrone as an anticancer drug and DNA: application in drug design. *Chem. Biol. Drug. Des.* **2008**, *71*, 474–482.
- (26) Trachtenberg, B. H.; Landy, D. C.; Franco, V. I.; Henkel, J. M.; Pearson, E. J.; Miller, T. L.; Lipshultz, S. E. Anthracycline-associated cardiotoxicity in survivors of childhood cancer. *Pediatr. Cardiol.* **2011**, *32*, 342–353.
- (27) Shi, Y.; Moon, M.; Dawood, S.; McManus, B.; Liu, P. P. Mechanisms and management of doxorubicin cardiotoxicity. *Herz.* **2011**, *36*, 296–305.
- (28) Outomuro, D.; Grana, D. R.; Azzato, F.; Milei, J. Adriamycin-induced myocardial toxicity: New solutions for an old problem? *Int. J. Cardiol.* **2007**, *117*, 6–15.
- (29) Ferrans, V. J. Overview of cardiac pathology in relation to anthracycline cardiotoxicity. *Cancer Treat. Rep.* **1978**, *62*, 955–961.
- (30) Barasch, D.; Zipori, O.; Ringel, I.; Ginsburg, I.; Samuni, A.; Katzhendler, J. Novel anthraquinone derivatives with redox-active functional groups capable of producing free radicals by metabolism: are free radicals essential for cytotoxicity? *Eur. J. Med. Chem.* **1999**, *34*, 597.
- (31) Kumbhar, A.; Padhye, S.; Ross, D. Cytotoxic properties of iron-hydroxynaphthoquinone complex in rat hepatocytes. *BioMetals* **1996**, *9*, 235–240.
- (32) Bartoszek-Pączkowska, A. Metabolic activation of adriamycin by NADPH cytochrome P450 reductase; overview of its biological and biochemical effects. *Acta Biochim. Pol.* **2002**, *49*, 323–331.
- (33) Mandal, B.; Mondal, H. K.; Das, S. In situ reactivity of electrochemically generated semiquinone on emodin and its Cu^{II}/Mn^{II} complexes with pyrimidine based nucleic acid bases and calf thymus DNA: Insight into free radical induced cytotoxicity of anthracyclines. *Biochem. Biophys. Res. Commun.* **2019**, *515*, 505–509.

- (34) Das, S.; Saha, A.; Mandal, P. C. Radiation-induced double-strand modification in calf thymus DNA in the presence of 1,2-dihydroxy-9,10-anthraquinone and its Cu(II) complex. *J. Radioanal. Nucl. Chem.* **1996**, *196*, 57–63.
- (35) Feng, M.; Yang, Y.; He, P.; Fang, Y. Spectroscopic studies of copper(II) and iron(II) complexes of adriamycin. *Spectrochim. Acta* **2000**, *56*, 581–587.
- (36) Wang, H.; Hua, E.; Yang, P. The polarographic and voltammetric behaviour of the copper(II) mitoxantrone complex and its analytical application. *Talanta* **1995**, *42*, 1519–1524.
- (37) Yang, P.; Wang, H.; Gao, F.; Yang, B. Antitumor activity of the Cu(II)-mitoxantrone complex and its interaction with deoxyribonucleic acid. *J. Inorg. Biochem.* **1996**, *62*, 137–145.
- (38) Pereira, E.; Fiallo, M. M. L.; Garnier-Suillerot, A.; Kiss, T.; Kozłowski, H. Impact of aluminium ions on adriamycin-type ligands. *J. Chem. Soc., Dalton Trans.* **1993**, 455–459.
- (39) Italia, T.; Liegro, D. I.; Cestelli, A.; Matzanke, B. F.; Bill, E.; Trautwein, A. X. The interaction of Fe(III), adriamycin and daunomycin with nucleotides and DNA and their effects on cell growth of fibroblasts (NIH-3T3). *BioMetals* **1996**, *9*, 121–130.
- (40) Massoud, S. S.; Jordan, R. B. Kinetic and equilibrium studies of the complexation of aqueous iron(III) by daunomycin, quinizarin, and quinizarin-2-sulfonate. *Inorg. Chem.* **1991**, *30*, 4851–4856.
- (41) Maroney, M. J.; Day, R. O.; Psyris, T.; Fleury, L. M.; Whitehead, J. P. Structural model for the binding of iron by anthracycline drugs. *Inorg. Chem.* **1989**, *28*, 173–175.
- (42) Kolodziejczyk, P.; Garnier-Suillerot, A. Circular dichroism study of the interaction of mitoxantrone, ametantrone and their Pd(II) complexes with deoxyribonucleic acid. *Biochim. Biophys. Acta* **1987**, *926*, 249–257.
- (43) Kadarkaraisamy, M.; Mukjerjee, D.; Soh, C. C.; Sykes, A. G. Complexation, crystallography, and electrochemistry of new chelating nicotinylic and thiazolylanthraquinone ligands. *Polyhedron* **2007**, *26*, 4085–4092.
- (44) Di Vaira, M.; Orioli, P.; Piccioli, F.; Bruni, B.; Messori, L. Structure of a terbium(III)–quinizarine complex: The first crystallographic model for metalloanthracyclines. *Inorg. Chem.* **2003**, *42*, 3157–3159.
- (45) Jabłońska-Trypuć, A.; Świdorski, G.; Krętowski, R. K.; Lewandowski, W. Newly Synthesized Doxorubicin Complexes with Selected Metals—Synthesis, Structure and Anti-Breast Cancer Activity. *Molecules* **2017**, *22*, 1106.
- (46) Rumyantseva, T. A.; Alekseeva, A. A.; Tkachenko, M. A. Synthesis and Properties of Metal Phthalocyanines Containing Anthraquinone Chromophores. *Rus. J. Gen. Chem.* **2020**, *90*, 1660–1663.
- (47) Du, S.; Feng, J.; Lu, X.; Wang, G. The synthesis and characterizations of vanadium complexes with 1,2-dihydroxyanthraquinone and the structure-effect relationship in their in vitro anticancer activities. *Dalton Trans.* **2013**, *42*, 9699–9705.
- (48) Yuan, H.; Cheng, B.; Lei, J.; Jiang, L.; Han, Z. Promoting photocatalytic CO₂ reduction with a molecular copper purpurin chromophore. *Nat. Commun.* **2021**, *12*, 1835.
- (49) Fain, V. Y.; Zaitsev, B. E.; Ryabov, M. A. Tautomerism of the metal complexes with 1-amino-4-hydroxyanthraquinone. *Russ. J. Coord. Chem.* **2010**, *36*, 396–400.
- (50) Bard, A. J.; Faulkner, L. R. *Electrochemical Methods: Fundamentals and Applications*, 2nd ed.; John Wiley & Sons: New York, 1980.
- (51) Undre, P. B.; Khirade, P. W.; Rajenimbalkar, V. S.; Helambe, S. N.; Mehrotra, S. C. Dielectric Relaxation in Ethylene Glycol - Dimethyl Sulfoxide Mixtures as a Function of Composition and Temperature. *J. Korean Chem. Soc.* **2012**, *56*, 416–423.
- (52) Bose, K.; Kundu, K. Free energies of transfer of some single ions from ethylene glycol to its isodielectric mixtures with acetonitrile at 25°C. *Can. J. Chem.* **1978**, *57*, 2476.
- (53) Schäfer, A.; Horn, H.; Ahlrichs, R. Fully Optimized Contracted Gaussian Basis Sets for Atoms Li to Kr. *J. Chem. Phys.* **1992**, *97*, 2571–2577.
- (54) Schäfer, A.; Huber, C.; Ahlrichs, R. Fully optimized contracted Gaussian basis sets of triple zeta valence quality for atoms Li to Kr. *J. Chem. Phys.* **1994**, *100*, 5829–5835.
- (55) Becke, A. D. Perspective on Density functional thermochemistry. III. The role of exact exchange. *J. Chem. Phys.* **1993**, *98*, 5648–5652.
- (56) Becke, A. D. Density-functional exchange-energy approximation with correct asymptotic behavior. *Phys. Rev. A* **1988**, *38*, 3098–3100.
- (57) Lee, C.; Yang, W.; Parr, R. G. Development of the Colle-Salvetti correlation-energy formula into a functional of the electron density. *Phys. Rev. B* **1988**, *37*, 785–789.
- (58) Orca – an ab initio, DFT and Semi-empirical and SCFMO package, F. Neese, Max Planck Institute for Chemical Energy Conversion, Ruhr, Germany, version 3.0.1.
- (59) Gaussian 09, Revision A.02, Frisch, M. J. et al., Gaussian, Inc., Wallingford, CT, 2009.
- (60) Podolyan, Y.; Leszczynski, J. MaSK: A visualization tool for teaching and research in computational chemistry. *Int. J. Quantum Chem.* **2009**, *109*, 8–16.
- (61) Spector, D. L.; Goldman, R. D.; Leinwand, L. A., *Cell: A Laboratory Manual, Culture and Biochemical Analysis of Cells*, Cold Spring Harbor Laboratory Press: Cold Spring Harbor, CSHL Press: New York, 1998, pp.341–349.



ACS IN FOCUS

Cellular Agriculture
Lab-Grown
Dilek Erilliç, Corina Dorothea E.

Machine Learning in Chemistry
Jon Paul Janet & Heather J. Kulik

bacterials
Toria Cheng Jaramillo
William M. Wuest

ACS In Focus ebooks are digital publications that help readers of all levels accelerate their fundamental understanding of emerging topics and techniques from across the sciences.

pubs.acs.org/series/infocus

ACS Publications
Most Trusted. Most Cited. Most Read.

1436

<https://doi.org/10.1021/acsomega.1c06125>
ACS Omega 2022, 7, 1428–1436